National Library
of Canada

Acquisitions and
Bibliographic Services

395 Wellington Street
Ottawa ON K1A 0N4
Canada

Bibliothèque nationale
du Canada

Acquisitions et
services bibliographiques

395, rue Wellington
Ottawa ON K1A 0N4
Canada

Your file Votre référence

Our file Notre référence

The author has granted a non-exclusive licence allowing the National Library of Canada to reproduce, loan, distribute or sell copies of this thesis in microform, paper or electronic formats.

The author retains ownership of the copyright in this thesis. Neither the thesis nor substantial extracts from it may be printed or otherwise reproduced without the author's permission.

L'auteur a accordé une licence non exclusive permettant à la Bibliothèque nationale du Canada de reproduire, prêter, distribuer ou vendre des copies de cette thèse sous la forme de microfiche/film, de reproduction sur papier ou sur format électronique.

L'auteur conserve la propriété du droit d'auteur qui protège cette thèse. Ni la thèse ni des extraits substantiels de celle-ci ne doivent être imprimés ou autrement reproduits sans son autorisation.

0-612-46941-7

Canada

University of Alberta

Library Release Form

Name of Author:	Wei Yan Wang
Title of Thesis:	Rheological and Thermal Study of Triblock Copolymers
Degree:	Doctor of Philosophy
Year this Degree Granted:	1999

Permission is hereby granted to the University of Alberta Library to reproduce single copies of this thesis and to lend or sell copies for private, scholarly or scientific research purposes only.

The author reserves all other publication and other rights in association with the copyright in the thesis, and except as herein before provided, neither the thesis nor any substantial portion thereof may be printed or otherwise reproduced in any material form whatever without the author's prior written permission.

Wei Yan Wang
Apt. 521
609 Devenport Rd.
Waterloo, Ontario
N2L 6H9
Canada

Oct. 1, 1999
Date

University of Alberta

Faculty of Graduate Studies and Research

The undersigned certify that they have read, and recommend to the Faculty of Graduate Studies and Research for acceptance, a thesis entitled **Rheological and Thermal Study of Triblock Copolymers** submitted by **Wei Yan Wang** in partial fulfillment of the requirements for the degree of **Doctor of Philosophy** in Chemical Engineering.

Michael C. Williams

Dr. Michael C. Williams (Supervisor)

Dr. William McCaffrey

Dr. Liang Li

Dr. DongQing Li

Dr. Shijie Liu

Dr. Sirish Shah (Chair)
on behalf of Dr. R. Register (External)

Sept. 30, 1999

Date

Abstract

Several triblock copolymers of styrene-butadiene-styrene (SBS) and styrene-isoprene-styrene (SIS) were used in a study of the kinetics of the phase separation and structure ordering process. Here we report the results for an SIS copolymer with dispersed spherical polystyrene microdomains at temperatures below its microphase separation temperature (T_s). After the sample was quenched from $T > T_s$, dynamic mechanical measurements showed that the phase separation process just below T_s revealed a three-stage PS domain evolution process which was analogous to the nucleation and growth process of crystals. At temperatures far below T_s, $G'(t)$ growth lost the three-stage feature and become smoothly asymptotic. Surprisingly, at temperatures above T_s the $G'(t)$ also increased with time, which we propose was caused by compositional fluctuation induced by the shearing movement. At $T_s + 40$ °, frequency sweep tests (before and after the sample was annealed at $T < T_s$) suggested that the microstructures formed at temperatures below T_s did not disappear at higher temperatures.

Differential Scanning Calorimetry (DSC) was also used to study the microphase separation transition. When the block copolymers were cooled from above T_s two distinct exothermic peaks were found, which corresponded to the glass transition of the rubber block and the microphase-separation transition. The heat associated with the glass transition was consistent at all cooling rates, but the broadness of the peak was found rate-dependent. The heat produced by the microphase-separation transition was, however,

varied dramatically depending on the cooling rates. This phenomenon reflects the complication of the ordering mechanism. Although the microphase-separation occurs instantly upon cooling through T_s, the growth of the long-range microstructure depends very much on the speed of cooling.

Finally, the rheological behavior of several triblock copolymers were studied. The principle of time-temperature superposition was used. The master curves constructed reveals that the rheological behavior depends very much on the block copolymer morphologies. The activation energy at temperatures above and below the microphase separation transition was calculated and plotted as a function of compositions. The highest activation energy at $T < T_s$ was found at around 60% polystyrene content.

Acknowledgements

I would first like to thank Professor Michael C. Williams, who introduced me to polymer rheology and to the University of Alberta. Professor Williams is an excellent instructor, motivator and overseer of the whole project.

My colleagues of the Polymer and Rheology Laboratory are greatly thanked for their help over the years. To the list I must also add the staff at machine shop, DACS center, and instrument shop.

The block copolymer samples were provided by Dr. Kevin Mackay at DEXCO Polymer Ltd. (Plaquemine, LA, USA) and Dr. Bob Sammler at Dow Chemical (Midland, Michigan, USA). The financial support for this project was graciously provided through a research grant from the National Science and Engineering Research Council of Canada (NSERC).

Table of Contents

CHAPTER 1 INTRODUCTION 1

CHAPTER 2 INTRODUCTION TO POLYMER SCIENCE 6

2.1 Polymer Rheology 6
- 2.1.1 Chemical Nature of Polymeric Liquid 7
- 2.1.2 Maxwell Model 9
- 2.1.3 Non-Newtonian Viscosity (A Nonlinear Property) 11
- 2.1.4 Molecular Weight Dependence of Viscosity 13
- 2.1.5 Glass Transition 14
- 2.1.6 Small Amplitude Oscillatory Shear Flow (Linear Property) 15
- 2.1.7 Time-Temperature Superposition 18

2.2 Thermal Analysis of Two-Phase Polymer Systems 21
- 2.2.1 Thermodynamics and Phase Behavior 21
- 2.2.2 Miscibility Determination by T_g Measurement 24

CHAPTER 3 LITERATURE REVIEW 28

3.1 Thermodynamics of Phase Separation 30
- 3.1.1 Strong Segregation Limit (SSL) 34
  - 3.1.1.1 Two Phase Model 35
  - 3.1.1.2 Three Phase Model 36
  - 3.1.1.3 Interphase Free Energy Barrier 42
  - 3.1.1.4 Narrow Interface Theory 44
- 3.2.2. Weak Segregation Limit (WSL) 46

3.2. Experimental Aspects of Microphase Separation 53
- 3.2.1. Strong Segregation Limit (SSL) 53
- 3.2.2. Weak Segregation Limit 58

3.3. Rheology 64
3.3.1 Nonlinear Mechanical Properties 64
3.3.2 Effect of Molecular Architecture 67
3.3.3 Viscoelastic Behavior 70

CHAPTER 4 EQUIPMENT AND METHODS 75

4.1 Rheological Testing 75
4.1.3 Sensitivity 75
4.1.2 Modes of Operation 77
4.1.2.1 Dynamic Oscillatory Modes 78
4.1.2.2 Steady Mode 80
4.1.3 Auto-Zeroing of Motor 82
4.1.4 Alignment 82
4.1.5 Sample Gap 83
4.1.6 Auto-Tension 84
4.1.7 Internal Data Acquisition and Analysis 85
4.1.8 Sample Preparation 85
4.1.9 Temperature Control 87
4.1.10 Sample Loading 88

4.2 Differential Scanning Calorimeter (DSC) 89
4.2.1 DSC Calibration 91
4.2.2 Sample Preparation 92

CHAPTER 5 RHEOLOGICAL STUDY OF MICROSTRUCTURAL ORDERING MECHANISMS AND THE EFFECT OF ANNEALING, WITH AN SIS TRIBLOCK COPOLYMER 93

5.1. Introduction 93

5.2. Experimental 97
5.2.1 Material 97
5.2.2 Rheometry 98

5.3. Results and Discussion 101
  5.3.1 Determination of T_s by Rheology 101
  5.3.2 Microphase Ordering Mechanism 111
  5.3.3 The Effect of Annealing 141

5.4. Conclusions 149

CHAPTER 6 DSC STUDY OF HEAT EVOLUTION OF BLOCK COPOLYMERS DURING THEIR PHASE TRANSITION 152

6.1. Introduction 152

6.2. Experimental 154
  6.2.1 Samples 154
  6.2.2 Differential Scanning Calorimetry (DSC) 155
  6.2.3 Rheometry 156

6.3 Results and Discussion 157
  6.3.1 Determining T_s 157
  6.3.2 Thermal Stability of Block Copolymers 160
  6.3.3 The Heat Evolution of the Microphase-Separation Transition 165

6.3. Conclusions 185

CHAPTER 7 TIME-TEMPERATURE SUPERPOSITION OF DYNAMIC FUNCTIONS OF BLOCK COPOLYMERS 187

7.1. Introduction 187

7.2. Experimentals 191
  7.2.1 Sample Characterization and Preparation 191
  7.2.2 Equipment and Experimental Procedure 193

7.3. Results and Discussion 194

7.4. Conclusions 227

CHAPTER 8 THERMAL DEGRADATION OF BLOCK COPOLYMERS 228

8.1. Introduction 228

8.2. Materials and Equipment 229

8.3. Results and Discussion 231
  8.3.1 DSC Study of Thermal Degradation of TriblockCopolymers 231
  8.3.2 DSC and NMR Study of the Possible Degradation during Rheological Tests 237

8.4. Conclusions 242

CHAPTER 9 CONCLUSIONS 243

APPENDIX A CALIBRATIONS 247

A.1. Torque 247

A.2. Gap 250

A.3. Circulation Jacket 253

APPENDIX B EFFECT OF MOLD RELEASE AGENT ON THE RHEOLOGICAL TEST : SLIP EFFECTS 256

APPENDIX C DETERMINE THE CLOUD POINT AND POUR POINT TEMPERATURE OF CRUDE OIL BY RHEOLOGY 262

REFERENCES 270

List of Tables

Table 4.1 Staging Area Components of RMS-800 77

Table 5.1 SIS Polymer Characterization 98

Table 5.2 $G'(t)$ Time Characterizations of Ordering Process foe SIS-4111 124

Table 5.3 The Value of Exponent b for SIS-4111 128

Table 6.1 Sample Characterizations 155

Table 6.2 Characterizing Phase Transitions 180

Table 7.1 Sample Characterizations 192

Table 7.2 Characterizing T_s and Activation Energy E 216

Table 8.1 Sample Characterizations 229

Table A.1 Normal Torque Range Calibration 247

Table A.2 Low Torque Range Calibration 249

Table A.3 Tool Expansion Calibration 252

Table A.4 Circulation Jacket Temperature Calibration 254

List of Figures

Figure 1.1 Schematic of Diblock and Triblock Copolymers........................1

Figure 2.1 Maxwell Spring and Dashpot Model........................10

Figure 2.2 Typical Viscosity of Polymer Melt........................11

Figure 2.3 Parallel Plates Rheometer........................15

Figure 2.4 Phase Diagram of Polymer Blends........................23

Figure 3.1 Schematic Illustration of $(AB)_n$ Type Block Copolymer Architecture.....29

Figure 3.2 One-Dimensional Composition Profiles of Weak- and Strong-Segregation Limits........................33

Figure 3.3 Model of Phase-Separated Microstructure........................38

Figure 3.4 Composition Profile across Mixed Interphase........................43

Figure 3.5 Theoretical Phase Diagram for Diblock Copolymer in Weak Segregation Limit........................48

Figure 3.6 Instantaneous Real-Space Composition Patterns in Weak Segregation Limit........................51

Figure 3.7 Strong Segregation Limit Morphologies........................54

Figure 4.1 RMS-800 System........................76

Figure 4.2 Compression Mold........................87

Figure 4.3 Schematic Representation of a Heat-Flux DSC Cell........................90

Figure 5.1 DSC Scan of SIS-4111........................102

Figure 5.2 Isothermal Frequency Sweep for SIS-4111........................104

Figure 5.3 Tan δ Master Curve for SIS-4111........................105

Figure 5.4 η' and η'' at $\omega = 0.1$ rad/s for SIS-4111..107

Figure 5.5 η' *vs* Temperature for SIS-4111..110

Figure 5.6 Temporal Evolution of G' at $\omega = 1$ rad/s for SIS-4111........................113

Figure 5.7 Temporal Evolution of G''at $\omega = 1$ rad/s for SIS-4111........................114

Figure 5.8 G' *vs* Temperature at $\omega = 1$ rad/s for SIS-4111..............................115

Figure 5.9 3-D Plot of G' *vs* Temperature at $\omega = 1$ rad/s for SIS-4111....................116

Figure 5.10 Temporal Evolution of G' at $\omega = 0.1$ rad/s for SIS-4111......................117

Figure 5.11 Temporal Evolution of G''at $\omega = 0.1$ rad/s for SIS-4111......................118

Figure 5.12 $t_{1/2}$ and t_∞ *vs* Temperatures for SIS-4111..125

Figure 5.13 Effect of Sampling Interval on G' at 164 °C..126

Figure 5.14 Temporal Evolution of G' at $\omega = 1$ rad/s for SIS-4111, at 1-minute time interval..131

Figure 5.15 Temporal Evolution of G' at 160 and 164 °C..134

Figure 5.16 Temporal Evolution of $G'$and G''at 164 °C with (a) $\omega = 0.1$ rad/s and (b) $\omega = 0.1$ rad/s..139

Figure 5.17 Temporal Evolution of $G'$and G''at 190 °C with (a) $\omega = 0.1$ rad/s and (b) $\omega = 0.1$ rad/s..140

Figure 5.18 Annealing Effect at 170 °C ($T > T_s$) for SIS-4111..............................143

Figure 5.19 Annealing Effect at 140 °C ($T < T_s$) for SIS-4111..............................146

Figure 5.20 Annealing Effect at 100 °C ($T < T_s$) for SIS-4111..............................147

Figure 5.21 Effect of Annealing at Different Temperatures, for SIS-4111..............150

Figure 6.1 Temperature Sweep Test for SIS-4111..158

Figure 6.2 Temperature Sweep Test for SBS-8508..159

Figure 6.3 DSC Scan for SIS-4111, in Air and N_2..163

Figure 6.4 DSC Scan of SBS-8508, in Air and N_2..164

Figure 6.5(a) Typical DSC Run for SBS Sample..166

Figure 6.5(b) Typical DSC Run for SIS Sample..167

Figure 6.6 DSC Cooling for SBS-8508, at Different Rates..170

Figure 6.7 DSC Cooling for SBS-8508, at 1 °C/min 171

Figure 6.8 DSC Cooling for SBS-8508, at 5 °C/min..172

Figure 6.9 DSC Cooling for SBS-8508, at 7.5 °C/min..173

Figure 6.10 DSC Cooling for SBS-8508, at 10 °C/min..174

Figure 6.11 DSC Cooling for SIS-4111, at Different Rates..175

Figure 6.12 DSC Cooling for SIS-4111, at 1 °C/min..176

Figure 6.13 DSC Cooling for SIS-4111, at 5 °C/min..177

Figure 6.14 DSC Cooling for SIS-4111, at 10 °C/min..178

Figure 6.15 Illustration of Heat of Phase Transitions under DSC Curve..183

Figure 7.1 Reduced Plot of tan δ for SIS-4111..196

Figure 7.2 Reduced Plot of tan δ for SBS-8508..197

Figure 7.3 Reduced Plot of tan δ for SIS-4211..198

Figure 7.4 Reduced Plot of tan δ for SIS-4411-D..199

Figure 7.5 Reduced Plot of tan δ for SBS-6241-D..200

Figure 7.6 Frequency Sweep Test For SBS-8508..202

Figure 7.7 Frequency Sweep Test For SBS-6241-D, η^* *vs* ω..210

Figure 7.8 Frequency Sweep Test For SBS-6241-D, η' *vs* T..211

Figure 7.9 Master Curve of $\eta^* b_T \sim \omega a_T$, for SBS-6241-D 213

Figure 7.10 Shift Factor a_T and b_T for SBS-6241-D 215

Figure 7.11 Master Curves ($\eta^* b_T \sim \omega a_T$) for Five Copolymers 217

Figure 7.12 Shift Factors a_T for Five Copolymer Samples 218

Figure 7.13 Activation Energy E vs PS Composition 222

Figure 8.1 T_g^{PS} vs DSC Scan Rates, for SIS-4111 230

Figure 8.2 DSC Heating Scan of SIS-4111, at 5 °C/min 232

Figure 8.3 DSC Heating Scan of SBS-8508, at 5 °C/min 233

Figure 8.4 DSC Heating Scan of SIS-4411-D, at 5 °C/min 234

Figure 8.5 DSC Heating Scan of Homopolystyrene, at 5 °C/min 235

Figure 8.6 DSC Scan of SIS-4111, after Sample Tested in RMS-800 239

Figure 8.7 NMR Trace of Fresh SIS-4111 240

Figure 8.8 NMR Trace of SIS-4111 Sample Tested in RMS-800 241

Figure A.1 RMS-800 Transducer Calibration Set-up 248

Figure A.2 Tool Expansion Calibration 251

Figure A.3 Circulation Oven Temperature Calibration 255

Figure B.1 Frequency Sweep $\eta' \sim \omega$ for HDPE, with Mold Release Agent 257

Figure B.2 Frequency Sweep $\eta' \sim \omega$ for HDPE, with Aluminum Foil 259

Figure B.3 Steady-Shear Test $\eta \sim \dot{\gamma}$ for HDPE 261

Figure C.1 DSC Scan of Oil Sample No.1 264

Figure C.2 Dynamic Test $\eta' \sim T$ for Oil Sample No.1 265

Figure C.3 DSC Scan of Oil Sample No.2 267

Figure C.4 Dynamic Test $\eta' \sim T$ for Oil Sample No.2 268

Nomenclature

a_T	shift factor for frequency
B	subscript or superscript denotes polybutadiene
b_T	shift factor for rheological functions
E	energy, or activation energy (J/mol or kcal/mol)
E_1	activation energy at $T < T_s$ (microphase separation temperature)
E_2	activation energy at $T > T_s$
E'	storage modulus in tension (Pa)
E''	loss modulus in tension (Pa)
E^*	complex modulus in tension (Pa)
f	overall fraction of interphase
G	shear modulus (Pa), or Gibbs free energy (J/mol)
G'	storage modulus in shear (Pa)
G_0'	storage modulus in shear (Pa) at time zero
G_∞'	steady state value of storage modulus (Pa) at very lone time
$\Delta G'$	$\equiv G_\infty' - G_0'$
G''	loss modulus in shear (Pa)
G^*	complex modulus in shear (Pa)
G_r	relaxation modulus in shear (Pa)
ΔG	free energy difference (J/mol)
H	height (gap spacing) (mm)
ΔH	enthalpy difference (J/mol)
I	subscript or superscript denotes polyisoprene
K	Kelvin degree
M_c	critical molecular weight for entanglement onset, or molecular weight between crosslinks (g/mol)
MW	Molecular weight (g/mol)
M_w	weight average molecular weight (g/mol)
M_n	number average mlecular weight (g/mol)

PB	polybutadiene
PI	polyisoprene
PS	polystyrene
R	radius of platens
ΔR	interphase thickness
S	subscript or superscript denotes polystyrene
SB	styrene-butadiene diblock copolymer
SBR	random copolymer of styrene and butadiene
SBS	sytrene-butadiene-styrene triblock copolymer
SI	styrene-isoprene diblock copolymer
SIS	styrene-isoprene-styrene triblock copolymer
$SEBS$	styrene-(ethylene/butylene)-styrene triblock copolymer
ΔS	entropy difference (J/mol.K)
t	time
$t_{1/2}$	time for $G'$to reaches half of G_{∞}'
t_{∞}	time for $G'$to reaches G_{∞}'
T	temprature (°C or K)
T_g	glass transition temperature (°C or K)
T_g^{PB}	glass transition temperature of polybutadiene (°C or K)
T_g^{PI}	glass transition temperature of polyisoprene (°C or K)
T_g^{PS}	glass transition temperature of polystyrene (°C or K)
T_s	microphase separation temperature (°C or K)
ΔT	interphase thickness (A)
V_m	molar volume (m^3/mol)

Greek Letters

γ	shear strain (%)
γ_N	commanded (steady) shear strain (%)
$\dot{\gamma}$	strain rate, or shear rate (1/s)
γ^{0}	dynamic (shear) strain amplitude (%)

γ_N°	commanded dynamic (shear) strain amplitude
δ	phase angle (degree)
δ_i	solubility parameter of component *i* $(cal/cm^3)^{1/2}$
$\Delta\delta$	solubility parameter difference, $\delta_i - \delta_j$, $(cal/cm^3)^{1/2}$
ε	tensile strain
ε_E	engineering tensile strain
η	viscosity (Pa.s)
η_o	zero shear rate limiting Newtonian viscosity (Pa.s)
η'	dynamic viscosity (Pa.s)
η''	..................(Pa.s)
η^*	complex viscosity, $= \eta' - i\eta''$ (Pa.s)
θ	angle of rotation (rad)
λ	relaxation time (s)
μ	Newtonian viscosity (Pa.s)
μ_i	chemical potential, $= (\partial G / \partial N_i)_{N_j, T, P}$ (J/mol)
ρ	density (kg/m^3)
σ	stress (Pa)
σ_y	yield stress (Pa)
ϕ_i	volume fraction of component *I*
ϕ_I	overall volume fraction of interphase
τ	shear stress (Pa)
ω	frequency (rad/s)
χ	interaction parameter between two polymers

Chapter 1 Introduction

Block copolymers consist of long sequences of monomer A connected to long sequences of monomer B. Two typical block copolymers: diblock copolymer and triblock copolymer are depicted in Figure 1.1.

AAAA....AAAABBBB....BBBB

AAAA....AAAABBBB....BBBBAAAA....AAAA

Figure 1.1: Schematic of Diblock and Triblock Copolymers. In this case, the triblock copolymer has two identical end blocks.

The production of block copolymers was first announced by the Shell Chemical Company in 1965 [Encyclopedias of Polymer, 1992]. Since then they have found applications in many commercial products such as shoe soles, blend compatabilizers and adhesives. Of the various types of block copolymers, those based on triblock copolymers of polystyrene and polydiene are the largest (in terms of commercial production) and one of the earliest to be investigated.

The block copolymers in Figure 1.1 are known as the AB type diblock copolymer and ABA type triblock copolymer. One of the blocks is usually a "soft" component with low glass transition temperature (e.g. $T_{room} > T_g^B$, which means the block is soft and rubbery at room temperature), and the other is usually a "hard" component with high glass transition temperature (e.g. $T_{room} < T_g^A$, which means the block is glassy at room temperature). The two chemically incompatible blocks are covalently bonded together by anionic polymerization techniques. The preparation of triblock copolymers may be classified by four different approaches, depending on the initiator chosen: (1) Difunctional initiator process: Use of a dicarbanion or dicarbanion forming species (e.g. sodium naphthalene) in either a one-stage process or a two-stage sequential addition process. (2) Three-stage sequential addition process: Use of monofunctional initiators (e.g. alkyllithiums) with three sequential monomer additions. (3) Coupling process: Use of a two-stage process to prepare a diblock polymer that is "coupled" (e.g. with phosgene or alkyl dihalides) to form the A-B-A. (4) Tapered blocks process: Polymerization (partial or complete) of the initial styrene block followed by copolymerization of a mixture of styrene and diene. In the second step, the diene is preferentially polymerized first (in hydrocarbon solvents) to produce a predominantly A-B-A sturcutre directly [Noshay and McGrath 1977]. The result of this polymerization is that the blocks contain no sections of randomly polymerized A and B monomers (random copolymer) and that each block has a narrow molecular weight distribution, or called mono-disperse.

Block copolymers demonstrate a number of unique properties as a result of morphological features that are unique to such systems. The unique features are the result of phase separation of the incompatible block components being restricted to a microscopic size scale. The resulting "microphases" have dimensions on the order of the dimensions of the constituent polymer blocks, and the microphases often develop into highly organized domain morphologies.

For the triblock copolymer of the ABA type, as depicted in Figure 1.1, having a rubbery center block and glassy end blocks at room temperature, the resulting material is often known as "thermoplastic elastomer" and it behaves more like a crosslinked rubbery solid. The elastomeric character similar to that of chemically crosslinked elastomer is due to the network structure of these polymers. The glassy domains that contain end blocks act as multi-junction crosslink points among the rubbery center blocks phase. These multi-junction points and the entanglements in the rubbery center blocks enhance the strength of the rubbery phase and also prevent them from slipping off the network structure. This gives the material most of the useful physical properties of vulcanized rubbers: high resilience, high tensile strength, highly reversible elongation and high abrasion resistance.

All of these properties are achieved without chemical crosslinking. Above the microphase-separation temperature T_s, where the two-phase system disappears and the material becomes homogeneous, this block copolymer will flow under stresses like any polymer melts, so that these materials can be formed into useful products using conventional polymer processing technology. Upon cooling through T_s, microphase separation occurs and the network structure is reformed. This is unlike conventional vulcanizates which are thermosets, which cannot be melted and returned to the liquid state upon reheating and thus cannot be reformed. The temperature reversibility of the network structure leads to the "thermoplastic" in the name.

The microphase separation is the single most important phase transition for block copolymers. The two-phase system will become unstable and disappear (given enough time) upon heating through T_s and the material becomes a homogeneous liquid. This makes block copolymers easier for processing. When cooled through T_s the two components of the block copolymer become phase-separated again. The final morphology, however, will depend on both the weight fraction of the components and on the cooling rate. The weight fraction of the components determines the kind of morphology the sample should have at equilibrium, but the actual microstructure is controlled by the cooling rate, relative to the speed of forming that particular morphology. Therefore, understanding the ordering mechanism at T_s and below largely determines how well we can control the final properties of the products.

The rheology of these multi-phase materials has also been an area of active research since their discovery and has presented many interesting questions to researchers. It can be used as a probe of the microstructure and the ordering of microstructure, right down to molecular dimensions. It can also be used to investigate the relationship between stress, strain and structure as well as the role of strain as a thermodynamic variable.

The rheology clearly has an important role to play in understanding the processing of these materials. The utility of polymers in the market place stems largely from our ability to tailor the properties to our applications. While control over these properties is not absolute, processing history joins chemical structure as an important factor in determining end properties. With highly structured materials which display marked shear history dependence such as block copolymers it is possible to choose the shear history to achieve a wide range of properties. The complex features of the rheology of these materials are also important to the processing characteristics and final properties. These include the yield stress, strongly non-Newtonian viscosity, high melt elasticity, and temperature-induced as well as shear-induced phase transitions [Jackson *et al* 1995,Balsara *et al* 1994a and 1994b].

Chapter 2 Introduction to Polymer Science

2.1 Polymer Rheology

A few definitions should be covered before discussing the rheology of polymers.

Rheology The study of the deformation of matter.

Flow Deformation without a limit imposed by the material.

Solid A material which will not flow, i.e. the molecular character or microstructure of a solid material imposes a limit on deformation.

Liquid Any material which will flow (gases excepted).

Polymeric fluids are sometimes called **viscoelastic fluids**. This means that the fluids have both viscous and "elastic" properties.

In science and industry it is important to establish control over the macroscopic behavior of materials to a sufficient degree so that one can manufacture the particular materials best suited for a given purpose, design for it appropriate machinery for manufacture and processing, and choose the rate of production, temperature, pressure etc. The best results have been achieved by combining theory and experiment in subjects such as rheology.

For the purpose considered here the macroscopic behavior will be described in an approximation with statistical averages. This allows a great simplification in that one can represent the material with its intricate discontinuous constitution of structural components of colloidal, molecular, atomic and subatomic size, as a continuous medium which maintains its continuity under all applied mechanical actions.

In this thesis the mechanical properties of materials we are interested will be confined to the shear properties only, which connected with the changes in form [Weissenberg 1966].

2.1.1 Chemical Nature of Polymeric Liquid

A macromolecule (or polymer) is a large molecule composed of many small simple chemical units, generally called structural units. Polymer molecules differ from the small molecules in many important ways:

a). *Great Diversity in Possible Molecular Structure*. There are many ways in which the structural units can be assembled to create different "architectures", each being a different type of polymer materials: straight chain polymers, branched polymers, block copolymers, closed-ring polymers, and so on.

b). *Molecular Weight Distributions* (*MWD*). When polymers are synthesized, the molecules in the sample do not all have the same length or weight (not " monodisperse"), but instead they are of varying length ("polydisperse" and the macroscopic sample must be characterized by a distribution of mole weights). The *MWD* has an enormous effect on the macroscopic properties; small amounts of very high molecular-weight components can alter the rheological properties significantly [Ferry 1980].

c). *Large Number of Internal Degrees of Freedom.* Since many polymeric materials contain molecules with molecular weights in the millions, each molecule in the material is capable of existing in a huge number of configurations. When the constituent molecule is stretching, rotating and deforming, the force transmitted along the chain backbones of the molecules in these various configurations has a great effect on the stress tensor, the central object of study in rheology.

Because of these three features of polymeric liquids, the molecular modeling of polymeric liquids will be considerably different from the analogous topics of simple liquids. Two models have been used extensively. The earliest is the entanglement model. Polymer molecules are thought to loop around each other and hinder each other in moving. Therefore, to move any single polymer molecule it is necessary to move several others because of the restricting entanglements.

The other model envisions a polymer molecule in the melt state as being surrounded by segments of all its neighboring polymer chains, which form a series of barriers to motion so that the central polymer is confined in a kind of conduit or tube. The creeping flow of a polymer in the melt, termed "reptation" (moving like a reptile), is easier along the tube formed by these neighbors than it is sideways, where its progress would be impeded by the presence of surrounding chains. Regardless of direction, the net displacement of the chain center of mass requires the simultaneous cooperative motion of many segments. The small probability of cooperative motion in such long chains is the source of the high viscosity of polymers. This "reptation" model overcomes some fundamental objections to the entanglement model, since polymer molecules are not flexible enough to loop tightly around each other in a manner usually depicted in conceptual diagrams (like a knot in a shoelace). However, the reptation model has yet to prove its utility in a quantitative way to the extent that the entanglement model has [Bird *et al* 1987].

2.1.2 Maxwell Model

The first attempt to obtain a viscoelastic constitutive equation appears to have been that of Maxwell [Bird *et al* 1987], who over a century ago developed a model for viscoelasticity, because he thought that gases might be viscoelastic. He proposed that fluids with both viscosity and elasticity could be described by a Hookean spring (with modulus G) and a dashpot (containing a Newtonian viscous liquid with viscosity η) coupled in series as depicted in Figure 2.1.

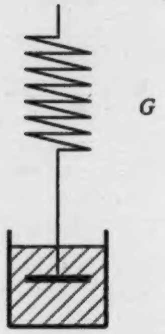

Figure 2.1: Maxwell Spring and Dashpot Model

Which leads to a differential equation relating stress (τ) and strain (γ):

$$\tau + \frac{\eta}{G}\frac{\partial \tau}{\partial t} = -\eta \frac{\partial \gamma}{\partial t} = -\eta \dot{\gamma} \qquad (2.1-1)$$

where η/G is sometimes replaced by λ, a time constant called "relaxation time".

For steady-state motions this equation simplifies to the Newtonian fluid with viscosity η. For sudden changes in stress, the time derivative term dominates the left side of the equation, and then integration with respect to time gives the Hookean solid with elastic modulus G. The Maxwell model is the simplest expression for the shear stress for a fluid that is both viscous and elastic.

The Maxwell model cannot successfully be used for fitting data on polymers, mainly because it contains only one relaxation time while real polymers would have a spectrum of relaxation times because each polymer chain has many relaxation modes and any polydispersity would broaden the spectrum even further. However, the Maxwell model is qualitatively correct and more complex models of linear viscoelasticity (such as "Jefferys Model", which has two time constants, "relaxation time" and "retardation time" [Bird *et al* 1987]) will not be discussed here.

2.1.3 Non-Newtonian Viscosity (A Nonlinear Property)

Probably the single most important characteristic of polymeric liquids is the fact that they have a "shear-rate dependent" or "non-Newtonian" viscosity. A typical plot of $\eta(\dot{\gamma})$ or $\eta^*(\omega)$ is given in Figure 2.2.

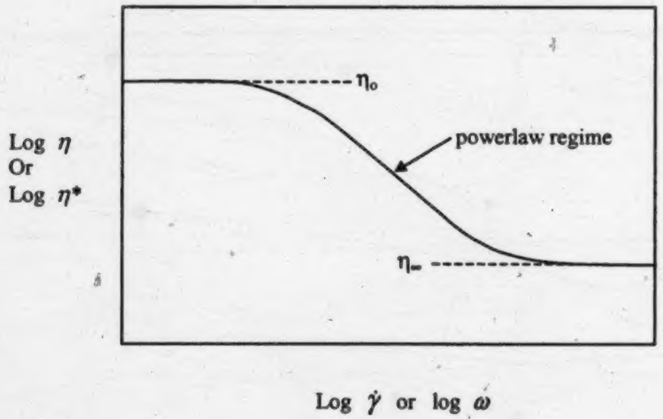

Figure 2.2: Typical shear-rate or frequency dependent viscosity of polymer melt

The high initial plateau is known as the low shear limiting viscosity, or Newtonian limit (η_o). And the low plateau at high shear rate is known as the infinite-shear-rate viscosity (η_∞). For concentrated solutions and melts, η_∞ is not usually measurable since polymer degradation becomes a serious problem before sufficiently high shear rates can be obtained. In the middle range of shear rate, the curve exhibits a pronounced linear region that can persist over several decades of decreasing viscosity. This linear section is called "power-law" region ($\tau = m \times \dot{\gamma}^n$ or $\eta = m \times \dot{\gamma}^{n-1}$). The range of shear rate or frequency over which the transition from η_o to the power law region occurs is fairly small for narrow molecular weight distributions. As the molecular weight distribution of the polymer is broadened, the transition region is also broadened and the onset shifted to lower shear rates.

The viscosity curve can perhaps best be understood by first considering the case of steady shear flow. The limiting Newtonian viscosity is a manifestation of the hindered motion of the polymer chains due to entanglements, requiring high shear stress to pull them apart. In the transition region where viscosity drops off with increasing shear rates, the entanglement network is gradually disrupted. It this region the process of disentanglement and re-entanglement occur simultaneously, but as the shear rate increases disentanglement dominates to an increasing degree. At high shear rates the entanglement network is disrupted to its largest degree and the shear stress once again becomes proportional to shear rate so that the viscosity is constant.

In small amplitude oscillatory shear testing a similar relationship is seen between dynamic viscosity η^* and frequency ω. Low frequency (or long-wavelength) shear deformations are a probe of long range structure because they correspond to the longest relaxation times that are related to long range cooperative motions. Long-range motions in a polymer melt are difficult because of the hindrance of surrounding chains. Cooperation between many segments of a chain must occur for motion of the center of mass of the chain to occur and thus $|\eta^*|$ (the complex viscosity) is high at low frequencies. At higher frequencies shorter-range motions are detected corresponding to movements of smaller segments of a chain that is easier and thus $|\eta^*|$ is lower. At high frequencies a point is reached at which the relaxation time corresponding to the movement of a single subunit of the chain is being detected. This is the shortest range motion of the chain, requiring the least time and least cooperation and thus the $|\eta^*|$ again levels off with frequency.

2.1.4 Molecular Weight Dependence of Viscosity

It is found that the limiting viscosity η_o of polymer melts, when plotted logarithmically against molecular weight $\overline{M}_w$, increases linearly with a slope of 1 until a critical molecular weight M_c at which point the slope changes abruptly to a steeper linear relationship. The slope of the curve above M_c has been measured quite universally to be approximately 3.4 indicating that $\eta_o \propto \overline{M}_w^{3.4}$ in this regime. M_c is interpreted as the molecular weight at which a long-range entanglement network is established, due to the probability that there could exist at least two entanglements per polymer chain when the chains become this long.

2.1.5 Glass Transition

The glass transition temperature is the main characteristic temperature of the amorphous solid and liquid states. Amorphous polymer molecules in the molten state change position by thermally activated segmental jumps. Upon cooling, the amount of free volume decreases and these jumps occur less frequently due to less space available to receive the jumping segment [Ferry 1980]. The microscopic process involved is the freezing of large-scale molecular motion without change in structure. When a temperature is reached at or below which there is a limiting free volume fraction, below which segmental jumps cease almost entirely for practical purposes. This temperature is called the glass transition temperature (T_g), and it is similar to a thermodynamic second-order transition. The freezing of molecular motion is, however, time dependent, so that the glass transition occurs at a recognizable "transition temperature" because of a rather large temperature dependence of the relaxation time for large-scale molecular motion in the glass transition region.

The most precise determination of the glass transition temperature is done by cooling an equilibrium melt at a specified rate and finding the temperature of half-freezing as it can be measured, for example, by heat capacity or expansivity measurement. This temperature is close to the inflection point of the thermal analysis curves. If one plots the integral quantities such as volume, enthalpy, or entropy, this temperature is close to the break in these curves. Experiments at faster or slower cooling rates will give higher or lower glass transition temperatures, respectively.

2.1.6 Small Amplitude Oscillatory Shear Flow (Linear Property)

In a concentric disk rheometer, a sample is subjected to an oscillatory shear strain as illustrated in Figure 2.3.

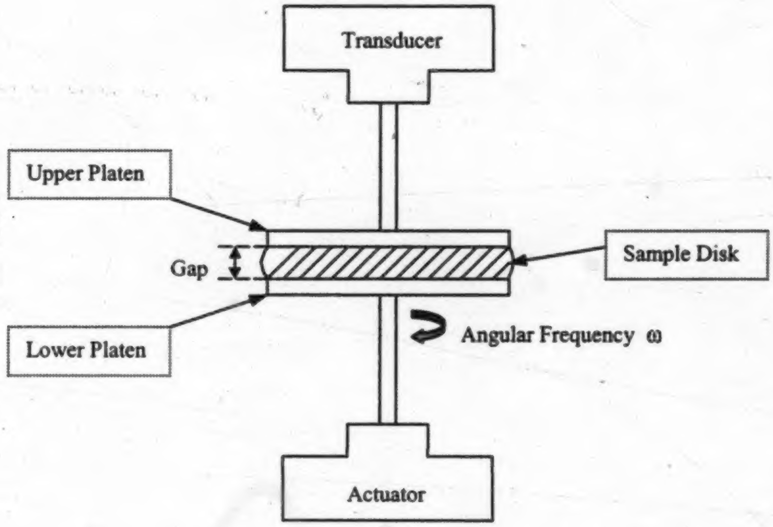
Transducer
Upper Platen
Sample Disk
Gap
Angular Frequency ω
Lower Platen
Actuator

Figure 2.3: Parallel Plates Rheometer

The bottom platen oscillates with strain:

$$\gamma = \gamma^{\circ} \sin \omega t \qquad (2.1.-2)$$

while the top platen transmits torque to a transducer which measures the sample stress output. A perfect elastic solid (the Hookean spring) would respond to a sinusoidal strain input with an in-phase sinusoidal stress output that could be used to define the elastic shear modulus G:

$$\tau = G\gamma(t) = G\gamma^{o}\sin\omega t \qquad (2.1-3)$$

An inelastic Newtonian fluid that obeys Newton's law of viscosity would, if subjected to the same sinusoidal strain input, respond with an out-of –phase sinusoidal stress output:

$$\tau = \eta\dot{\gamma} \equiv \eta\frac{d\gamma}{dt} = \eta\gamma^{o}\omega\sin(\omega t + \frac{\pi}{2}) \qquad (2.1-4)$$

with a 90° phase lag between stress and strain.

A viscoelastic fluid, however, will respond with a phase lag somewhere between 0° and 90°. An oscillatory strain input of angular frequency ω (Eq. 2.1-2) results in a sinusoidal stress output which leads the strain by a phase angle δ:

$$\tau = \tau^{\circ}\sin(\omega t + \delta) \qquad (2.1.-5)$$

rewriting Eq. 2.1-5 by means of trigonometric identity [$sin(\alpha+\beta)$ = $sin\alpha cos\beta$ + $cos\alpha sin\beta$] we obtain:

$$\tau = (\tau^{\circ}\cos\delta)\sin\omega t + (\tau^{\circ}\sin\delta)\cos\omega t \qquad (2.1-6)$$

the stress consists of two components: one in phase with strain ($\tau^{o}cos\delta$) and the other 90° out of phase ($\tau^{o}sin\delta$). Both τ^{o} and δ are functions of ω.

Two equivalent sets of linear viscoelastic material functions can be defined. One set involves the framework of the modulus G' and G'':

Storage modulus (in phase), related to energy stored elastically:

$$G' \equiv \frac{\tau^{\circ}}{\gamma^{\circ}} \cos\delta$$

Loss modulus (out of phase), characterizing energy lost by viscous processes:

$$G'' \equiv \frac{\tau^{\circ}}{\gamma^{\circ}} \sin\delta$$

so that

$$\tau = \gamma^{\circ}[G' \sin\omega t + G'' \cos\omega t] \qquad (2.1-7)$$

The other set of viscoelastic material functions employs the viscosity framework:

$$\eta' \equiv \frac{G''}{\omega} = \frac{\tau^{\circ}}{\gamma^{\circ}\omega} \sin\delta$$

$$\eta'' \equiv \frac{G'}{\omega} = \frac{\tau^{\circ}}{\gamma^{\circ}\omega} \cos\delta$$

where η', also called dynamic viscosity, measures the energy lost during test and η'' relates the energy stored in the material during test.

The complex modulus and complex viscosity are as follows:

$$G^{*} = G' + iG'' \qquad (2.1.-8)$$

$$\eta^{*} = \eta' - i\eta'' \qquad (2.1-9)$$

where

$$|\eta^{*}| = [(\eta')^{2} + (\eta'')^{2}]^{1/2}$$

and

$$|G^{*}| = \omega|\eta^{*}|$$

The modulus and viscosity functions are measured at various strain amplitudes to determine the range of strains at which the measured properties do not change with the strain amplitude. This is known as the linear region in which by definition the microstructure of the tested material is not affected by the test. Properties measured in the linear region are called "linear viscoelastic properties".

2.1.7 Time-Temperature Superposition

Time-temperature superposition is a procedure whereby viscoelastic property data, such as the nonlinear $\eta(\dot{\gamma})$ or linear $\eta'(\omega)$, $G''(\omega)$, etc or time-dependent properties such as creep compliance $J(t)$ or stress relaxation modulus $G_r(t)$, taken as a function of $\dot{\gamma}$ or ω or t at various temperatures are superposed to incorporate the temperature dependence into the time scale (or $\dot{\gamma}$ or ω scales) . The resulting response curves cover an expanded time (or $\dot{\gamma}$ or ω) window, which can be useful for approximating the behavior of a material at times or frequencies inaccessible with the instrument used to obtain the original data. The resulting curve is called a "master curve", referred to a specific reference temperature T_R (representing how the material would respond at that temperature over many orders of magnitude of the independent variables). The most important practical feature of time-temperature superposition is that it permits us to condense our full knowledge of the viscoelastic properties-e.g $G'(\omega,T)$ of a given polymer over a wide temperature/frequency range into two curves: a master curve

$G'(a_T\omega, T_R)$ corresponding to the reference temperature T_R and a curve for shift factor $a_T(T)$ versus temperature (See also Chapter 7).

Although empirical in its origins, time-temperature superposition has had rigorous theoretical justification, mainly by Ferry and his co-workers [Ferry 1980]. According to their point of view, temperature can be regarded as a volume-increasing variable similar to a negative isotropic pressure. The increase in free volume facilitates molecular movement and results in a multiplicative shift in all relaxation processes. It is this shift that is needed for the superposition of data obtained at two different temperatures.

The ability to superpose viscoelastic data, also referred to as thermorheological simplicity, has been demonstrated for a wide variety of single-phase polymers. Lack of the ability to superpose is often a strong indication of two-phase polymers or a phase change brought about by the changing temperature. Chemical changes can also interfere with superposition.

The criteria for applying the time-temperature superposition are (a) exact matching of the shapes of adjacent curves (curves at adjacent temperatures), (b) the same values of shift factor a_T must superpose all types of viscoelastic functions, (c) the temperature dependence of a_T must have a reasonable form consistent with experience.

The temperature dependence of the shift factor has been most often compared with the prediction of the Williams-Landel-Ferry (WLF) [Williams *et al* 1955] empirical equation:

$$\log \mathrm{a_T} \equiv \log \frac{\eta_o(T)}{\eta_o(T_g)} = \log \frac{\lambda(T)}{\lambda(T_g)} = -\frac{C_1(T-T_g)}{C_2+(T-T_g)} \qquad (2.1-10)$$

where a_T is the shift factor required to superpose data taken at temperature T onto data taken at the glass transition temperature T_g, while C_1 and C_2 are parameters related to the free volume of any polymer (i.e., universal constants). The WLF equation has been most successful when applied to shift factors for data in the temperature range $T_g < T < T_g +$ 100^o. Kaelble [1985] suggested a modification to extend this range below T_g:

$$\log a_T = -\frac{C_1^g(T-T_g)}{C_2^g+|T-T_g|} \qquad (2.1-11)$$

For temperatures higher than T_g + 100^o, better results are obtained with the Arrhenius equation:

$$\log a_T = b_1(\frac{1}{T}-\frac{1}{T_R}) \qquad (2.1-12)$$

$$b_1 = \frac{E}{R}$$

or the Fox [Fox and Loshaek 1955] equation:

$$\log a_T = b_1(\frac{1}{T^{b_2}}-\frac{1}{T_R^{\,b_2}}) \qquad (2.1-13)$$

where E is the activation energy and T_R is a reference temperature to which the shifts of data at temperature T are made and b_1 and b_2 are constants.

The modulus data are often normalized for density $\rho(T)$ and temperature as suggested by the Rouse [1953] theory and the kinetic theory of rubber elasticity [Tobolsky and Andrews 1943]. The result is a modulus that would be expected if the temperature were, in fact, at the reference temperature. Foe example, for the stress relaxation modulus $G_r(T,t)$:

$$G(T_R,t)=\frac{T_R}{T}\frac{\rho(T_R)}{\rho(T)}G(T,\frac{t}{a_T}) \qquad (2.1-14)$$

And for the dynamic modulus $G'(T,\omega)$:

$$G'(T_R,\omega)=\frac{T_R}{T}\frac{\rho(T_R)}{\rho(T)}G'(T,\omega a_T) \qquad (2.1-15)$$

If both components of the complex modulus form master curves by being shifted with identical values of a_T, tan δ (= G''/G') should also reduce to a master curve. Concentrating on tan δ instead of a dimensional modulus means no density or temperature adjustment should be required.

2.2 Thermal Analysis of Two-Phase Polymer Systems

2.2.1 Thermodynamics and Phase Behavior

The fact that two polymers might be miscible at a given temperature and composition does not mean they are miscible at other temperatures and compositions. Most polymer pairs are immiscible. The necessary conditions for a binary system being miscible at a particular temperature and composition are [Paul and Barlow 1982, MacKnight and Karasz 1989]:

$$\Delta G_m < 0, \qquad \left(\frac{\partial^2 \Delta G_m}{\partial \phi_2^{\,2}}\right)_{T,P} > 0 \qquad (2.2-1)$$

where ΔG_m ($= \Delta H_m - T\Delta S_m$) is the free energy of mixing per unit volume and ϕ_2 is the volume fraction of component 2. If ΔG_m is positive over the entire composition range at a given temperature, the two polymers will separate into phases that are compositionally pure in either component providing that a state of thermodynamic equilibrium has been reached.

The low entropy of mixing (ΔS_m) of two polymers implies that the miscibility is determined mainly by the enthalpy of mixing, which according to the Flory-Huggins model is given by:

$$\Delta H_m = NRT\chi_{12}\phi_1\phi_2 \qquad (2.2-2)$$

where N is the number of moles of segments in the system, R is the gas constant, T is the absolute temperature, and χ_{12} is the interaction parameter [Flory 1942, Huggins 1941].

The relation of enthalpic and entropic contributions to the miscibility of polymer pairs can be viewed through the general form of the free energy expression:

$$\Delta G_m = RT[(\frac{\phi_1}{\overline{V}_1})\ln\phi_1 + (\frac{\phi_2}{\overline{V}_2})\ln\phi_2] + \chi_{12}\phi_1\phi_2 \qquad (2.2-3)$$

Where $\overline{V}_1$ and $\overline{V}_2$ are the molar volumes of the polymers in the binary mixture, and χ_{12} is the Flory-Huggins interaction parameter. The term in the brackets represents the combinational entropy of mixing while the second term that includes the interaction parameter contains the enthalpic contribution to the free energy of mixing. χ_{12} can be estimated through the use of Hildebrand solubility parameters (δ)of the two polymers:

$$\chi_{12} \propto (\delta_1 - \delta_2)^2 \qquad (2.2-4)$$

and miscibility can be achieved by matching polymers whose solubility parameters are equal.

The phase behavior of polymers and polymer blends at different temperatures and compositions can be graphically represented in phase diagrams. Most polymer blends have phase behaviors that fall in either of two categories: upper critical solution temperature (UCST) or lower critical solution temperature (LCST).

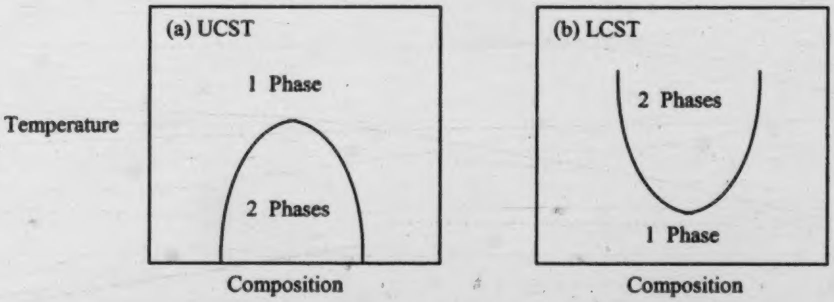

Figure 2.4: Phase diagrams of polymer blends. (a) Upper critical solution temperature (UCST); (b) lower critical solution temperature (LCST).

Figure 2.4(a) illustrates the case of systems showing an upper critical solution temperature. These systems are miscible at all compositions at temperatures above the UCST, but they will phase separate at some compositions if cooled below the UCST. There are also systems that present the opposite behavior (Figure 2.4b): they are miscible at all compositions at temperatures below the LCST, but they will phase separate at some compositions if heated above LCST. The unmodified Flory-Huggins theory can explain only UCST behavior. But one can understand the LCST behavior from a physical point of view if it is kept in mind that miscibility in polymer blends is usually due to the components being held together by binary interactions (e.g. hydrogen bonding) which may "dissociate" at higher temperatures because of increased thermal motions.

2.2.2 Miscibility Determination by T_g Measurement

Many techniques described in the literature have been used to determine the miscibility of polymer blends. The most widely used criterion relies on the measurement of the glass transition temperature, T_g. The detection of a single glass transition temperature whose value falls somewhere between the T_g's of the component polymers is an indication of a miscible system. Conversely, a non-miscible system will show two T_g's corresponding to the T_g's of the individual components that retain their physical identity in the blend (e.g. in the same sense as in the dispersed and continuous phases of an emulsion). It should be noted, however, that it is accepted that a single T_g does not imply miscibility at the monomer level (≤ 10 Å).

The measurement of T_g for pure or blended polymer components in most of the literature was performed by differential scanning calorimetry (DSC). The glass transition temperature is detected by the DSC as a step change in the ordinate (heat flow), which arises because the heat capacity of that polymer undergoes a step change at T_g (C_p for glass > C_p for elastomer or melt). The value typically reported is the temperature at which the ordinate reaches the midpoint between extrapolated baselines before and after the transition. Some advantages of DSC over other methods of measuring T_g include temperature uniformity in the sample, temperature accuracy, possibility of controlled fast heating/cooling rates, ease of sample preparation, and small sample size. In addition, DSC can measure the T_g of some microphases with dimensions of as small as 100 A, or even smaller, as long as the total mass of material composing that phase is sufficiently large to produce a signal that can be detected.

Numerous attempts have been made to relate the T_g of a miscible blend to blend composition, as is often done with random copolymers. Among them, the simplest one is the rule of mixtures:

$$T_g = w_1 T_{g1} + w_2 T_{g2} \qquad (2.2-5)$$

where w_1 and w_2 represent the mass fractions of the components and T_g, T_{g1}, and T_{g2} are the T_g's of the blend, component 1, and component 2, respectively. Another simple prediction is provided by the Fox equation [Fox 1956]:

$$\frac{1}{T_g} = \frac{w_1}{T_{g1}} + \frac{w_2}{T_{g2}} \qquad (2.2-6)$$

However, most miscible blends do not conform to either of the preceding equations. The most commonly used equation is the Gordon-Taylor [Gordon and Taylor 1952] equation, which was originally derived for random copolymers:

$$T_g = \frac{w_1 T_{g1} + k w_2 T_{g2}}{w_1 + k w_2} \qquad (2.2-7)$$

where

$$k = \frac{\Delta\alpha_2 V_2}{\Delta\alpha_1 V_1}$$

$\Delta\alpha_i$ is the change in volume expansion coefficient of the *i*th component at its glass transition temperature, and V_i is its specific volume at T_g. In most instances k is used as an adjustable parameter.

Another commonly used equation for miscible blends is that derived by Couchman [1980] and Karasz [Couchman and Karasz 1978]:

$$\ln T_g = \frac{\sum_i w_i \Delta C_{pi} \ln T_{gi}}{\sum_i w_i \Delta C_{pi}} \qquad (2.2-8)$$

where ΔC_{pi} is the difference between two components heat capacity in specific heat of the *i*th component at T_g. However, because of the experimental difficulty of measuring accurate values of ΔC_p, many researchers have obtained better fits by taking the ΔC_{pi} of the two components of a binary blend as an adjustable parameter.

There are also equations that are used to model polymer blends with strong intermolecular interactions. But the equations mentioned above serve us better because they all have been used to describe the glass transition of random copolymers in terms of the glass transitions of the component homopolymers.

Chapter 3 Literature Review

Block copolymers are macromolecules composed of sequences, or blocks, of chemically distinct repeat units. The development of this field originated with the discovery of termination-free anionic polymerization, which made possible the sequential addition of monomers to various carbanion-terminated ("living") linear polymer chains. Polymerization of just two distinct monomer types (e.g. styrene and isoprene) leads to a class of materials referred to as $(AB)_n$ block copolymers. The simplest combination, obtained by the two-step anionic polymerization of A and B monomers, is an (A-B) diblock copolymer. A three-step reaction provides for the preparation of (A-B-A) or (B-A-B) triblock copolymers. As a consequence of the "living" nature of these reactions, the resulting block and overall molecular weight distributions are nearly ideal, i.e. $1.0 < \frac{\overline{M_w}}{\overline{M_n}} < 1.1$, where $\overline{M_w}$ and $\overline{M_n}$ represent the weight and number-average molecular weight, respectively.

Since the original studies of anionic block copolymerization in the 1950s [Szwarc *et al* 1956, Schlick and Levy 1960] a variety of new polymerization methods (e.g. condensation, Ziegler-Natta, etc.) have contributed to an expanding number of block copolymer classes (e.g. ABC) and novel architectures (e.g. graft-block). Although some of the developments have resulted in important new materials (e.g. polyurethanes), anionic polymerization remains the only viable method for producing monodisperse block copolymers with well-defined architectures. Because current theories deal almost exclusively with model $(AB)_n$ type materials, we have restricted our attention in this review to studies based solely on this class of anionically polymerized block copolymers (see Figure 3.1).

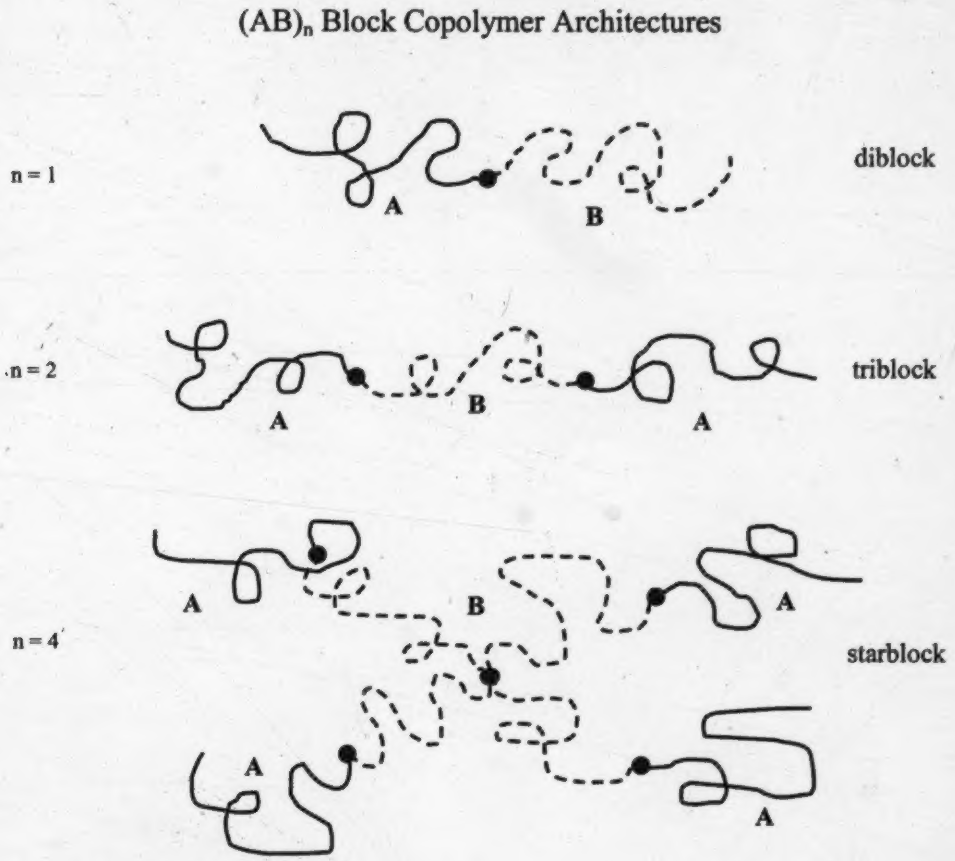
(AB)n Block Copolymer Architectures
n = 1
A
B
diblock
n = 2
A
B
A
triblock
n = 4
A
B
A
starblock
A
A

Figure 3.1: Schematic illustration of several $(AB)_n$ type block copolymer architectures. Solid and dashed lines represent A and B block chains, respectively. The $n = 1$ and $n = 2$ architectures are commonly referred to as diblock and triblock copolymers, while $n \geq 3$ are denoted starblock copolymers.

The preparation of model (undiluted) block copolymers for the purpose of studying the microphase separation transition (*MST*) [also referred to as the order-disorder transition (*ODT*)] is complicated by the limited range of experimentally accessible temperatures. In order to overcome this difficulty, researchers often add modest amounts of a neutral solvent to the bulk material, thereby diluting the A-B contacts. Here a neutral solvent is defined as one that shows no preference for either block type. In general, such concentrated solutions behave much like the bulk materials, with χ (Flory-Huggins interaction parameter between polymers) replaced by an effective interaction parameter that is proportional to the copolymer concentration. Thus, we have included this restricted group of block copolymer solution studies in the present review; semidilute and dilute copolymer solutions fall outside the scope of our review. We have also focused primarily on the significant developments that have occurred within roughly the past two decades. Prior advances in block copolymers are documented in earlier reviews [Goodman 1982 and 1985, Meier 1983, Allport and Jones 1973, Aggarwal 1970, Burke and Weiss 1973].

3.1 Thermodynamics of Phase Separation

It is essential to understand the thermodynamics of block copolymers in order to understand their microstructure as well as their mechanical and rheological behavior. Chemical incompatibility between block segments A and B of an AB or ABA block copolymer causes segments of like chemical structure to coalesce (A segments with A segments and B segments with B segments), causing microphase separation (aggregated block A segments form dispersed microphases amid the continuous matrix of the block B segments). These microphases, while distinct, are covalently bonded through the segment junctions. Therefore, adhesion between these distinct phases in block copolymers is unlike the adhesion in any other multi-phase system. Stresses are easily transferred from the matrix, whether it be composed of the A or B segments, to the dispersed phase; however, enthalpic forces oppose stresses which tend towards remixing of the blocks, *i.e.* domain destruction. It is easy to see then how the thermodynamics of phase separation dominates the mechanical and rheological properties of these materials.

The phase behavior of undiluted (bulk) $(A\text{-}B)_n$ block copolymers is determined by three experimentally controllable factors: the overall degree of polymerization N, architectural constraints characterized by n and the composition f (overall volume fraction of the A component), and the A-B segment-segment (Flory-Huggins) interaction parameter χ. [Here, we use the terms monomer and segment interchangeably to imply statistical segment] The first two factors are regulated through the polymerization stoichiometry and influence the translational and configurational entropy, whereas the magnitude of (the largely enthalpic) χ is determined by the selection of the A-B pair. We note that for all the materials considered in this review, the interaction parameter has the temperature dependence $\chi \approx \alpha T^{-1} + \beta$, where $\alpha > 0$ and β are constants for given values of f and n, and the chemistry of segments A and B. Since the $n = 1$ (diblock) and $n = 2$ (triblock) cases have received the most comprehensive theoretical treatments, our introductory remarks focus on diblock and triblock copolymers.

At equilibrium, a dense collection of monodisperse copolymer chains will be arranged in minimum free energy configurations. Increasing the energy parameter χ (e.g. lowering the temperature) favors a reduction in A-B monomer contacts. If N is sufficiently large, this may be accomplished by local compositional ordering as shown in Figure 3.2 (with some loss of translational and configurational entropy). (Here we note that block crystallization, which can also occur, lies outside the scope of this review. We consider only amorphous copolymers). Such local segregation is often referred to as *microphase separation*; macroscopic phase separation is impossible in a single-component block copolymer (means that since the segment A and B are covalently bonded into one single molecule, it is impossible for A and B blocks to be separated macroscopically). Alternatively, if either χ or N is decreased enough, the entropy will lead the copolymer to form a compositionally disordered (homogeneous) phase. Since the entropic and enthalpic contributions to the free energy density scale as N^{-1} and χ, respectively [Leibler 1980], it is the product χN that dictates the block copolymer phase state. For $f = 0.5$, the transition between the ordered and disordered states occurs when $\chi N \sim 10$, for a diblock copolymer.

Two limiting regimes (weak and strong segregation) exist in the block copolymer, as illustrated in Figure3.2. For $\chi N \ll 1$, a copolymer melt is disordered $(\phi_A(x) \equiv f \equiv \text{constant})$ and A-B interactions sufficiently weak that the statistics of individual copolymer chains are unperturbed (i.e. Gaussian). The connectivity of the two blocks and the incompressibility of the melt, however, lead to a correlation hole [deGennes 1979, Leibler 1980] that is manifested in light scattering measurements as a peak corresponding to a fluctuation length scale $D \sim R_g$. (Here R_g is the copolymer radius of gyration). As χN is increased to be order of 10 ($\chi N \sim 10$), a delicate balance between energetic and entropic factors produces a disorder-to-order phase transition (the microphase separation transition). It has been suggested [Leibler 1980] that in the vicinity of this transition, the A-B interactions are sufficiently weak that the individual copolymers remain largely unperturbed, and the ordered composition profile is approximately sinusoidal with position. We shall refer to such a regime as the *weak segregation limit* (WSL, and $\chi N \sim 10$). Current order-disorder transition (ODT) theories are based on this WSL assumption because it greatly simplifies the calculations, although strict adherence of experimental systems to the WSL postulates is still not completely established.

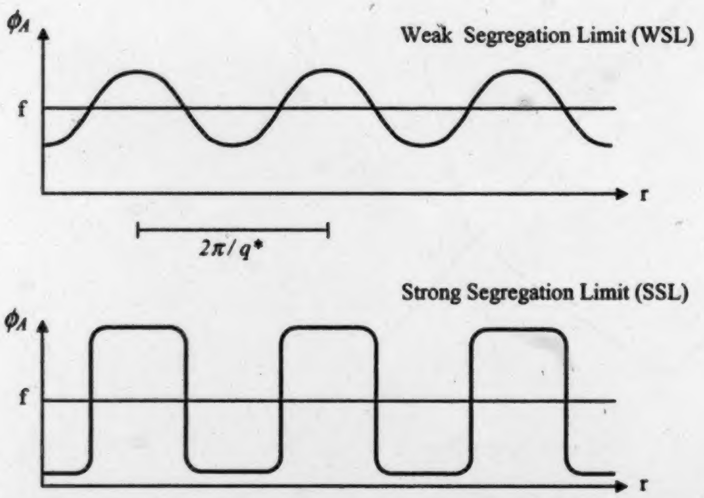

Figure 3.2: Composition of the one-dimensional composition profiles characterizing the weak (WSL) and strong (SSL) segregation limits. ϕ_A and f refer to the local and stoichiometric (i.e. macroscopic) A-block volume fractions, respectively.

The second limiting regime of phase behavior is referred to as the *strong segregation limit* (SSL) and corresponds to the situation of $\chi N >> 10$. In this regime, an interphase of finite width with mixed A and B segments [Leary and Williams 1970, 1973 and 1974] separates the pure A and B microdomains. The interaction energy associated with A-B contacts is localized in these interphase regions; the system would like to minimize the total volume of such interphase, but must do so under the constraint of incompressibility and with the entropic penalty of extended chain configurations.

Since most theories and experiments dealing with block copolymer phase behavior can be categorized as either WSL or SSL, we have organized this review under these general headings.

3.1.1 Strong Segregation Limit (SSL)

By the middle of the 1970s, the physical principles that govern the microphase separation in the SSL had been well-established by pioneering studies of Meier [1969], Leary and Williams [1970, 1973 and 1974] and Helfand & Wasserman [1975,1976 and 1982].

Early thermodynamic models [Meier 1969, Krause 1969, Bianchi *et al* 1969, Marker 1969, LeGrand 1970 and Inoue *et al* 1969] proposed a two-phase structure in these materials. A major advancement was the realization that a third, mixed phase of significant dimension exists in the microstructure [Leary and Williams 1970, 1973, Helfand 1977, Meier 1977]. The importance of this mixed phase, or interphase, in interpreting the rheological and mechanical properties of these materials will become evident as we review the literature.

3.1.1.1 Two Phase Model

Meier [1969] developed a model for phase separation in block copolymers assuming the existence of spherical domains of A in a continuous matrix of B with a well-defined surface between the phases. The criterion for phase separation was that the Gibbs free energy difference ΔG between the random mixture of block copolymer segments and the domain system be negative.

This ΔG was separated into several entropic and enthalpic contributions. The first was the "placement entropy" ΔS_p. This was a decrease in the entropy relative to the random reference state caused by forcing the A-B junction to lie at the interface. S_p was evaluated from a lattice model. The "restricted volume" entropy difference ΔS_v, evaluated by chain statistics, arose from the restriction of the A and B segments to the inside and outside of the domains respectively. The "elastic entropy" difference ΔS_{el} arose from the perturbation of chain dimensions in the domain system from their random-flight values.

The enthalpy difference ΔH between the domain and random systems was evaluated as the heat of demixing of a simple mixture of A and B segments, despite the fact that the component blocks are joined together. The residual interaction of the A and B segments at the domain surface was treated as a surface free energy G_s and characterized by an interfacial tension. Using this model Meier proceeded to define a criterion for phase separation in terms of a critical molecular weight (M_c) at a given composition. Although it is true that $M_c = M_c\ (T, f)$, Meier made no mention of a temperature correlation in this initial work. The incorporation of a temperature correlation was an innovation of the model of Leary and Williams [1973].

3.1.1.2 Three Phase Model

A major advance in the understanding of block copolymer thermodynamics in the early 70's was the recognition by Leary and Williams [1970, 1973] that the model must incorporate a third (mixed) region which they termed the "interphase". This region is of significant dimensions and influences the properties profoundly.

The model of Leary and Williams, like that of Meier, began with a random mixture of A and B polymer segments as the reference state. However, Leary and Williams considered triblock copolymers and did not restrict the model to spherical geometries. Rather, one of five geometries could be chosen and the change in the Gibbs free energy between the reference state and the phase separated state was calculated. All five of the geometries considered, spherical or cylindrical domains of A in matrix of B; lamella domains of A and B; and spherical or cylindrical domains of B in matrix of A, had been experimentally observed. The phase-separated morphologies of spherical, cylindrical and lamella of A in B matrix are shown in Figure 3.3.

In Figure 3.3, ϕ_A represents the local volume fraction of A blocks as a function of distance. The model first [Leary and Williams 1970] assumed a step change in ϕ_A with the interphase having a 50-50 composition. In order for the phase separated structure to exist, the change in Gibbs free energy:

$$\Delta G = \Delta H - T\Delta S \qquad (3.1-1)$$

from the reference state would have to be negative, and the equilibrium structure would be that with the largest negative ΔG.

The enthalpy of demixing was obtained from Scatchard-Hildebrand regular solution theory:

$$\Delta H = -V_m \phi_A \phi_B (\delta_A - \delta_B)^2 + f_{\text{interphase}} V_m \overline{\phi'_A \phi'_B} (\delta_A - \delta_B)^2 \qquad (3.1-2)$$

where the first term represents complete demixing and the second term corrects for that exaggeration in terms of the mixed interphase. Here $\overline{\phi'_A \phi'_B}$ is the volume averaged product of the volume fractions of A and B in the interphase and $f_{interphase}$ is the overall volume fraction of the interphase*. V_m is the molar volume of the copolymer molecule and δ_i is the

---

* This $f_{interphase}$ differs from f defined earlier.

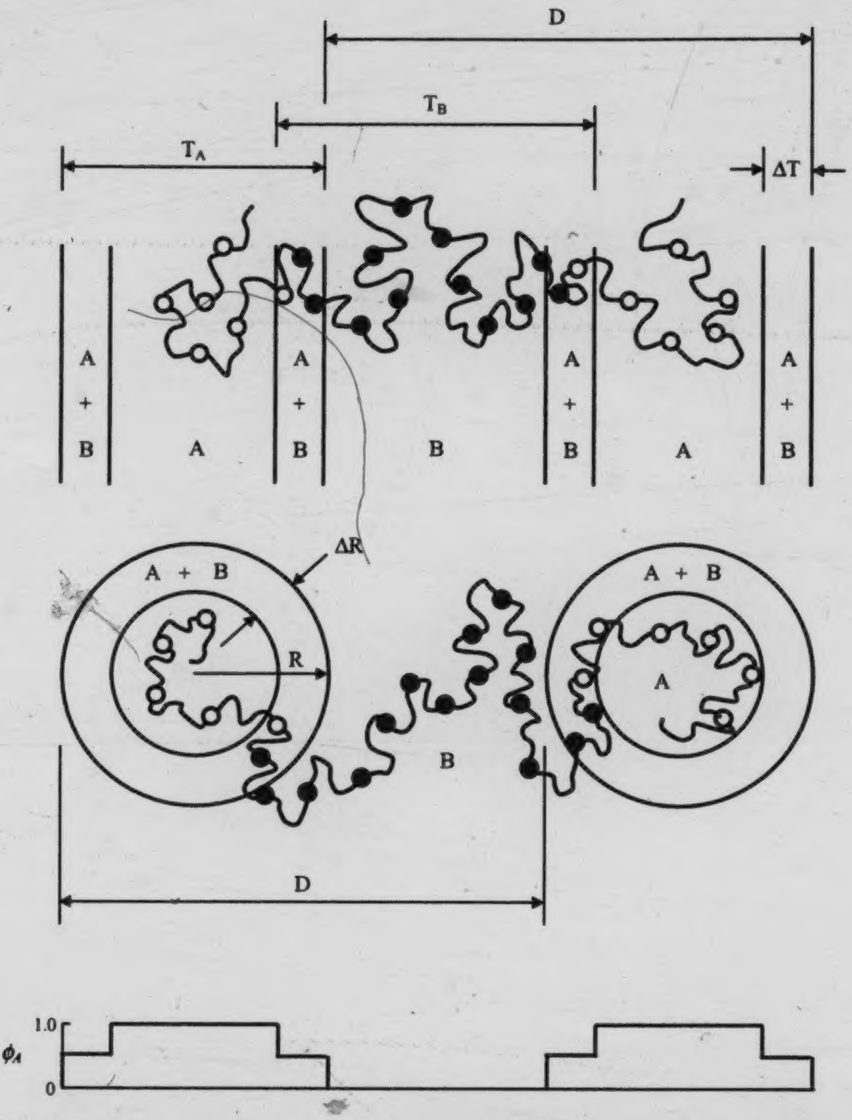

Figure 3.3: Model of phase-separated microstructure for lamellar domains (top) and normal spherical or cylindrical domains (middle), showing the composition profile of minor component A (bottom) assuming a step change to 50% in the interphase . ΔT (or ΔR for cylindrical and spherical morphology) is the interphase thickness and D is the repeat-distance spacing. ϕ_A is the compositional profile of component A.

solubility parameter of component *i*. This model did not require any knowledge of the domain surface free energy (used in Meier's model) which would be unknown and unmeasurable.

The entropy of phase separation was thought of as arising from three contributions:

$$\Delta S_{total} = \Delta S_{I} + \Delta S_{A} + \Delta S_{B} \qquad (3.1-3)$$

where ΔS_I was considered as the entropy change resulting from one of the A-B junctions of a polymer molecule being forcing to reside in the mixed region while ΔS_A and ΔS_B resulted from forcing A and B segments respectively to reside either in a pure A or pure B domain or in the mixed region. These terms could be generated from chain statistics; however, the mathematical details are beyond the purview of the present work.

Since the transition from a randomly mixed state to a phase-separated state is a first order transition, a critical temperature for domain formation could be determined by letting $\Delta G = 0$, so that from Equation 3.1-1:

$$T_{critical} = \left.\frac{\Delta H}{\Delta S}\right|_{\Delta G=0} \qquad (3.1-4)$$

Leary and Williams then coined the phrase "separation temperature" or T_s. This designation will be used for the order-disorder transition temperature in much of this work, regardless of whether the transition under consideration is from a disordered to an ordered state or the other way around, in which case it might more accurately be described as the "homogenization temperature".

The model predicted that T_s is directly proportional to the square of the solubility parameter difference $(\delta_A - \delta_B)^2$ as well as to the molecular weight (*i.e.* to V_m)and the product of the volume fractions of the A and B components. Model predictions of T_s were compared to experimental values [Leary and Williams 1974] obtained from differential scanning calorimeter (DSC) and laser light transmittance as well as electron microscopy and mechanical properties. It was found to be qualitatively correct in every case and in several cases to be accurate to within 10 degrees.

The model also permitted calculation of ΔT, the interphase thickness, and planar repeat distance D for lamella structures. Henderson and Williams [1985] applied the model to planar morphologies and found that ΔT generally increases with increasing ϕ_A, although at very large and very small ϕ_A there is no phase separation. D was found to increase with increasing weight as $M^{0.50}$ to $M^{0.75}$.

The influence of various interphase composition profiles $\phi_A(x)$, where x is dimensionless distance through the interphase, was also considered [Henderson and Williams 1985]. The step change in composition used for simplicity in the Leary-Williams model was rather unrealistic. As mentioned earlier, the second term in equation 3.1-2 is dependent on the volume average product of the volume fractions of A and B in the interphase. This is where the choice of interphase composition profile influences the model. That choice was predicted to have significant effect on the separation temperature as well as on the interphase thickness. The model was also extended to consider incomplete demixing of A and B components within the homogeneous domains (since data suggested some dilution in the glassy phase) as well as asymmetric interphase composition profile [Henderson and Williams 1985]. It was shown that no conditions led to a true equilibrium with any mixing within the domains (implying that data represented a state of kinetically controlled entrapment of *B* within *A*, as *A* vitrified upon cooling), and also that an interphase slightly rich in the end block component *A* was preferred, as experimental evidence showed [Henderson and Williams 1985].

It should be noted that the Leary-Henderson-Williams model predicts that such physical properties as T_s and ΔT are dependent on molecular weight. Model predictions can be calculated for any given molecular weight; however, comparison with experiment may be difficult because all real polymer samples have some finite polydispersity ($PD \equiv \frac{\overline{M}_w}{\overline{M}_n}$) and thus represent a continuous spectrum of molecular weights. Since T_s is proportional to molecular weight, a *PD* of 1.1 for a polymer having a predicted T_s of 400 K would result in a 40 K transition range. This led Spontek and Williams [1990] to use continuous thermodynamics to investigate the effects of PD on microstructures of block copolymers. It was found that $T_s = T_s(PD) = T_s(1)$ + linear increase with *PD*. Direct application of the model is sometimes complicated by the fact that it predicts equilibrium properties, while the microstructure of a given experimental sample may not be at equilibrium due to kinetic effects or solvent effects or sample strain history.

3.1.1.3 Interphase Free Energy Barrier

Theoretical predictions of the influence of the interphase on block copolymer properties were first expounded by Henderson and Williams [1979]. An explanation of these mechanical properties rightly belongs in a discussion of block copolymer thermodynamics. We begin by considering a triblock copolymer (ABA) which is phase separated, *i.e.* $T < T_s$. Figure 3.4 shows a mixed interphase separating a pure A domain and a pure B matrix. The composition profile across the interphase is shown in Figure 3.4 (a) as $\phi_A(r)$.

If some macroscopic force is imposed on the sample then individual chains will also experience some local stress field which in general would be difficult to predict from the macroscopic stress. However, we need only consider the force on a single chain for now. The total force on a chain will be the sum of frictional as well as interphase thermodynamics forces, $F = F^f + F^i$. Four terms contribute to the friction: drag on B segments moving through B matrix (F_{BB}^f), drag on A segments through A domain (F_{AA}^f), drag on A segments moving through B matrix (F_{AB}^f) and drag on each type of segment in the interphase with varying composition (F^{fi}). These are all represented in Figure 3.4(c).

The composition profile in Figure 3.4(a) corresponds to a chemical potential variation $\mu_A(r)$. An interphase barrier force therefore exists which is the negative gradient of the chemical potential:

$$F_A^i(r) = -\nabla \mu_A \qquad (3.1-5)$$

which is shown in Figure 3.4(b). Each of the A-chain units (k = 1,2,...,n) in the interphase feels a local force $F_{Ak}^{i} = -\nabla\mu_{Ak}$ so that the local barrier force is:

$$F_A^i = \sum_k^n F_{Ak}^i \qquad (3.1-6)$$

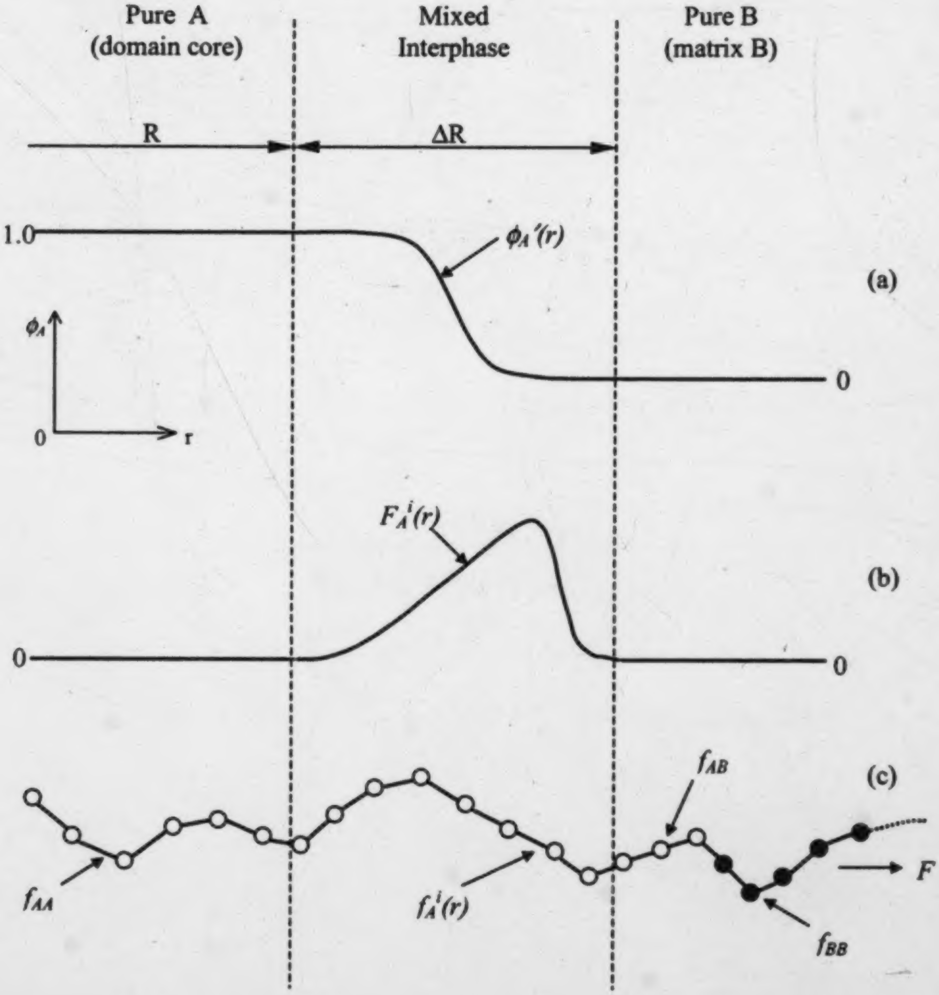
Pure A
(domain core)
Mixed
Interphase
Pure B
(matrix B)
R
ΔR
1.0
$\phi_A'(r)$
(a)
ϕ_A
0
r
0
$F_A^i(r)$
(b)
0
0
f_{AB}
(c)
f_{AA}
$f_A^i(r)$
F
f_{BB}

Figure 3.4 (a) Composition profile across the mixed interphase of thickness ΔR. The profile may be asymmetric, as shown. (b) Thermodynamic force profile corresponding to composition profile. The total barrier force F_A^i described in the text is the sum of the F_{Ak}^i acting on all units in the interphase. (c) Withdrawal of A block from domain core into matrix of B. Friction coefficients of four different types are indicated.

If the external force on the chain is less than F_A^i then block pull-out will not be possible and then no flow can occur, which would explain the absence of a limiting viscosity η_o at low $\dot{\gamma}$ and establishes the theoretical basis for a liquid yield stress σ_y.

Two more points should be noted: (1) the shape of the interphase composition profile is predicted to have a major influence on the rheology. (2) The chemical potential μ_A can be expressed in terms of the solubility parameter difference δ_A - δ_B and therefore rheological properties should be strongly dependent on δ_A - δ_B.

3.1.1.4 Narrow Interface Theory

Helfand and Wasserman [1975, 1976 and 1982] developed a self-consistent field theory that permits quantitative calculations of free energies, composition profiles, and chain conformations. They identified the three principal contributions to the free energy in the regime $\chi N >> 10$: (1) contact enthalpy in the narrow interfaces between nearly pure A and B microdomains. (2) entropy loss associated with extended chain configurations to ensure incompressibility (i.e. stretching free energy), and (3) confinement entropy due to localization of the block copolymer joints (covalent bonding sites between blocks) to the interfacial regions. They showed that these narrow interfaces have characteristic thickness $\sim\chi^{1/2}$. Helfand and Wasserman also developed numerical techniques for calculating the phase diagram in the SSL, and located the (virtually temperature independent) compositions that delimit the thermodynamic stability of spheres, cylinders and lamellae. These compositions are in good agreement with experimental determinations of the phase boundaries.

Although the Helfand-Wasserman theory is believed to contain all proper physical ingredients necessary to describe the SSL, its practical application has been hindered because of the requirement of rather difficult numerical analysis. The theoretical advances of the past two decades have been focused on developing analytical methods for estimating the free energy in the asymptotic limit $\chi N \rightarrow \infty$. Probably the most influential of these modern studies was a paper by Semenov [1985], which addressed a diblock copolymer melt in the SSL. Semenov argued that because the copolymers are strongly stretched in this regime, the required configurational integrals are dominated by the classical extremum of the energy functional (Hamiltonian). The extremum path corresponds to the most probable configuration of a copolymer block as it extends from an interphase into a microdomain and experiences the chemical potential field produced by the surrounding molecules. Moreover, Semenov showed that the differential equation describing this path (which resembles the equation of motion of a classical particle) is analytically solvable, even when the chemical potential is determined self-consistently to maintain constant density of copolymer segments. This solution indicates that the copolymers are stretched non-uniformly (along their contours) as they enter into the microdomains and predicts that the chain ends are distributed at excess in the domain interiors. The classical mechanical analogy identified by Semenov has been further clarified by Milner, Witten and Cates [Milner *et al* 1988(a), 1988(b) and 1988(c)] and was extensively exploited by these authors to treat related problems of grafted polymer brushes and surfactant interfaces. To appreciate the reduction in complexity afforded by this method, we note that the Helfand-Wasserman approach corresponds to the solution of a time-dpendent problem in quantum mechanics, whereas the Semenov-Milner-Witten-Cates approach requires only the solution to the classical limit of this problem. Of course, the latter approach is only legitimate under conditions of strong chain stretching.

It is somewhat surprising that in spite of the significant chain deformations predicted for the SSL, the domain (stretching) contribution to the free energy per chain was found by Semenov to have the same scaling as for a Gaussian chain. And finally, we note that Semenov's theory also provides estimates of the compositions that delimit the various ordered phases. As with the Helfand-Wasserman theory, these compositions are predicted to be temperature-independent.

3.2.2. Weak Segregation Limit (WSL)

Whereas the theoretical advances in the SSL were catalyzed by pioneering experiments involving the synthesis and characterization of model copolymers, developments in the WSL were strongly influenced by a seminal theoretical paper by Leibler [1980]. Leibler considered the case of a monodisperse A-B diblock copolymer melt with degree of polymerization *N*, composition *f*, and equal monomer volumes and statistical segment lengths. For such a system, Leibler constructed a free energy expansion (Landau type) which proved to be useful in the vicinity of a second-order or weak first-order phase transition. Indeed, the *MST* of symmetric ($f = 0.5$) or weakly asymmetric block copolymers is such a transition. Leibler's mean-field calculation was particularly helpful, because he proved the only relevant parameters related to the *MST* are the product χN, and the copolymer composition f [Leary-Williams theory [1970, 1972 and 1974] predicted that T_s was controlled by the analogous parameters in that theory: $(\delta_A - \delta_B)^2 \tilde{V}_m$) and $\bar{\phi}_A$].

Leibler was, thus, able to map out the phase diagram of a diblock copolymer melt near the *MST*. The phase diagram so obtained, in the parameter space of χN and f, is shown in Figure 3.5(a). The theory predicts a critical point at $(\chi N)_c = 10.5, f_c = 0.5$, where a compositionally symmetric diblock melt is expected to undergo a second-order phase transition from the disordered to the lamellar phase. At such a transition, the amplitude of the lamellar pattern grows continously from zero on lowering the temperature (*i.e.* increasing χN). The lattice constant (period) of the lamellar phase is predicted to be $D \approx 3.23R_g \sim N^{1/2}$ at the symmetric *MST*, consistent with the WSL assumption that the copolymers are only weakly perturbed by the inhomogeneous composition field. For asymmetric diblock copolymers, $f \neq 0.5$, the Landau theory [Leibler 1980] predicts a weak first-order transition from the disordered phase to the BCC (Body-centered-cubic) spherical phase. In contrast to the situation in the SSL, it is important to note that the Landau theory predicts a first-order transition between solid phases that can be accessed by changing temperature.

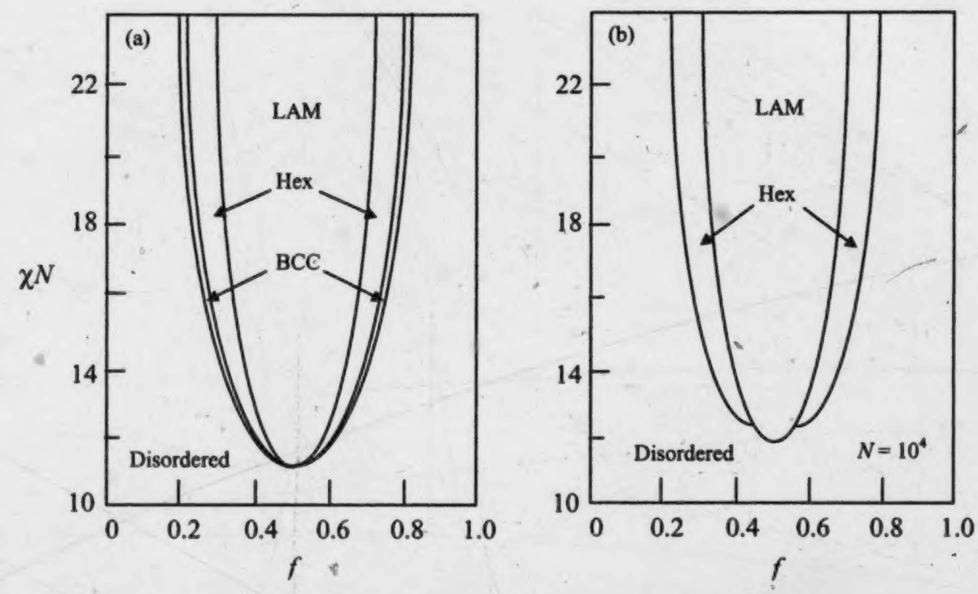

Figure 3.5: Theoretical phase diagrams for diblock copolymers in the weak segregation limit: (a) mean-field theory [Leibler 1980] (b) fluctuation theory with $N = 10^4$ [Fredrickson and Helfand 1987]. LAM, Hex and BCC correspond to lamellar, hexagonal (cylindrical morphology) and body-centered-cubic (spherical morphology) symmetries. (figure reproduced from Ref. [Bates *et. al* 1990(b)]

It was recognized by Leibler [1980] that the Landau type theory, which predicts mean-field critical behavior [Ma 1976], is inadequate in the vicinity of the $f = 0.5$ critical point discussed above. Brazovskii [1975] had previously demonstrated that such critical points, predicted by mean-field theories for systems exhibiting transitions between isotropic and striped (i.e. lamellar) phases, are suppressed by large-amplitude order parameter fluctuations. By means of a self-consistent Hartree approximation, Brazovskii showed that the mean-field critical point is replaced by a weak first-order phase transition, induced by fluctuations. It should be emphasized that such *fluctuation-induced first-order phase transitions* [Binder 1987] have been predicted to occur in a variety of other physical systems, such as liquid crystals and driven (nonequilibrium) fluids. Experiments to test these predictions, however, have been quite limited.

Fredrickson and Helfand [1987] extended Brazovskii's Hartree method of analysis to the A-B diblock copolymer melt considered by Leibler. They found that the fluctuation corrections are controlled by a Ginzburg parameter N [Ma 1976], proportional to the copolymer molecular weight. For fixed incompatibility χN, but $N \to \infty$, Fredrickson and Helfand found that Leibler's mean-field predictions are asymptotically approached. For finite N, however, the fluctuation corrections impose both qualitative and quantitative changes in the phase diagram (Figure 3.5(b)). In particular, it leads to a suppression of the symmetric critical point at $(\chi N)_c = 10.5$, which is replaced by a weak first-order transition at (a low temperature) $(\chi N)_{ODT} = 10.5 + 41 \times N^{-1/3}$. Because N is of order $10^3 - 10^4$ for the typical experimental sample, these fluctuation corrections can be substantial. The changes in the phase diagram for asymmetric diblocks are even more dramatic, as is indicated in Figure 3.5(b) for $N = 10^4$. An important distinction from the mean-field diagram (Figure 3.5a) is that the lamellar and the hexagonal phases are accessible at the *MST* in the Hartree approximation for $f \neq 0.5$. However, the mean-field prediction of first-order transitions between ordered phases that can be accessed by changing temperature is preserved in the Hartree approximation [Fredrickson and Helfand 1987].

The Hartree approximation leads to an interesting physical picture of a symmetric diblock copolymer melt in the vicinity of the *MST* [Bates et al 1990]. Whereas the Landau theory gives statistical weight only to the extremum composition field configurations in the ordered and disordered phases, namely the uniform and perfectly ordered configurations shown in Figure 3.6a, the Hartree approximation also weights configurations like those shown in Figure 3.6b. The latter configurations have superimposed upon the extremum configurations isotropic composition fluctuations that have a preferred wavelength, $2\pi/q^*$, but random directions and phases. The Fredrickson-Helfand theory [1987] suggests that the root-mean-squared amplitude of these fluctuations is comparable to the amplitude of the long-range-ordered lamellar component. It is interesting to note that the typical equilibrium composition field configurations in a disordered diblock melt (which fluctuate in time) are reminiscent of the transient non-equilibrium patterns encountered during the intermediate and late stages of spinodal decomposition [Gunton et al 1983].

(a) Mean-field Picture (f = ½)

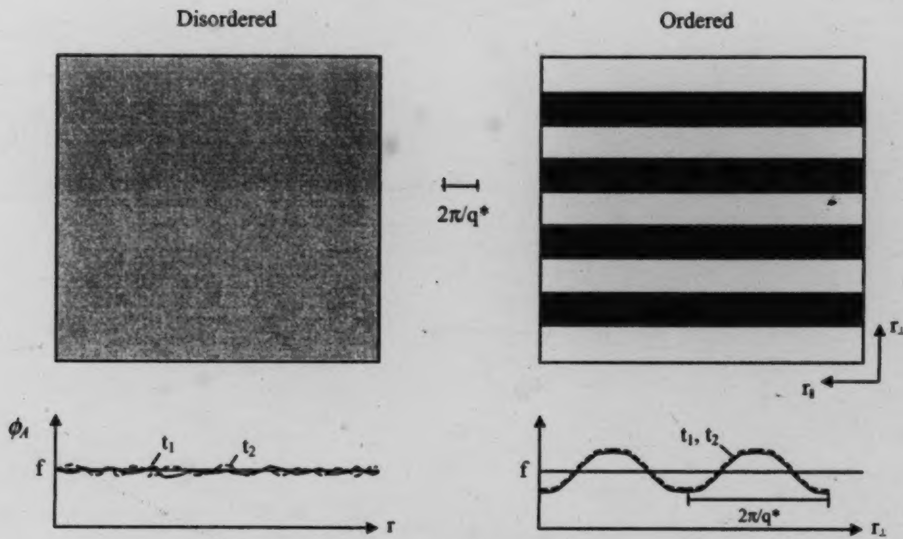
Disordered
Ordered
2π/q*
r⊥
r∥
ϕA
f
t1
t2
r
f
t1, t2
2π/q*
r⊥

(b) Fluctuation Picture (f = ½)

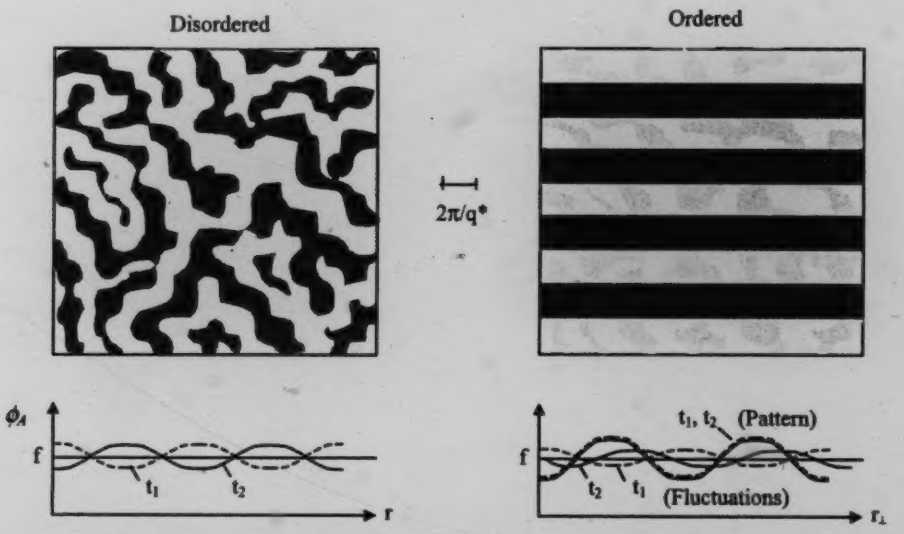
Disordered
Ordered
2π/q*
ϕA
f
t1
t2
r
t1, t2 (Pattern)
f
t2
t1 (Fluctuations)
r⊥

Figure 3.6: Instantaneous real-space composition patterns in the weak segregation limit: (a) mean-field theory, and (b) fluctuation theory. ϕ_A versus *r* depicts the expected time dependence ($t_1 \neq t_2$) of each morphology, where ϕ_A is the local volume fraction of A segments. $2\pi/q^*$ is the wave length (reproduced from Ref. [Bates *et al* 1990(b)]

A recent theoretical study by Semenov [1989] suggests that the asymmetric wings of the phase diagram, i. e. $f << 0.5$ and $f >> 0.5$, could be much more complicated by the Landau or Hartree theories. By using techniques discussed above for the SSL, Semenov [1985] argues that the free energy of formation of spherical micelles changes sign at an incompatibility $(\chi N)_M$ that is lower than the Landau or Hartree theories $(\chi N)_{ODT}$. Such micelles are localized, large amplitude fluctuations in an (otherwise disordered) asymmetric diblock copolymer melt that are not accessible by the perturbative WSL approach described in the present section. Due to the favorable energetics of micelles formation near $(\chi N)_M$, Semenov postulates the existence of a phase containing spherical micelles that becomes more concentrated in micelles as χN is increased. By computing the interaction energy between two micelles, he further predicts a phase transition at which the micelles order into a macrolattice with fcc symmetry. If Semenov's arguments are correct, this transition constitutes the *MST* for asymmetric copolymers. Subsequent first order structural transitions into hexagonal and bcc phases are also predicted by the theory.

The Hartree approximation has been explored for triblock copolymers [Mayes *et al* 1989]. The extension to concentrated and semidilute diblock copolymer solutions with a neutral (nonselective) solvent has been carried out [Fredrickson 1989, *de la* Cruz 1989]. It has frequently been assumed [Hashimoto *et al* 1983] that copolymer solutions have a uniform distribution of the non-selective solvent in the ordered microphases. This suggests that in the concentrated regime, where swelling effects are absent, the phase diagram of a copolymer solution is simply obtained by re-scaling χ to $\phi\chi$ in the melt phase diagram, where ϕ is the copolymer volume fraction (in the solution). Fredrickson and Leibler [1989] have shown that this "dilution approximation" method [Hashimoto *et al* 1989, Hong *et al* 1983] neglects several aspects of the physics of such solutions. In particular, these authors demonstrated that even in the WSL there is a tendency for a neutral, good solvent to accumulate at the interfaces of the microdomains. The non-uniform placement of the solvent screens the unfavorable A-B monomer contacts, but does so with an entropy price. Screening occurs until that entropy cost exactly compensates the loss of contact enthalpy. For a good solvent, this compensation produces a periodic solvent composition profile with amplitude that is N^{1} smaller than the amplitude of the A-B composition profile. As the solvent quality decreases, the two order parameter fields have comparable amplitudes in the weakly ordered microphases and a tricritical point is encountered [Fredrickson *et al* 1989]. Another aspect of neutral copolymer solutions that distinguishes them from molten copolymers, is that the *MST* is associated with a two-phase region in which disordered solvent-rich and ordered solvent-poor phases coexist. This region is very narrow for good solvents, but broadens as the solvent quality is decreased.

3.2. Experimental Aspects of Microphase Separation

3.2.1. Strong Segregation Limit (SSL)

Until roughly two decades ago transmission electron microscopy (TEM) was the preeminent experimental technique for studying block copolymer structure. The combination of relatively large monodisperse microstructures and efficient heavy-metal staining techniques (e.g. osmium tetraoxide) produced truly spectacular electron micrographs of ordered phases in polystyrene-polydiene block copolymers [Hasegawa *et al* 1996]. Five ordered phases were identified in the strong segregation limit. Two types of spherical, cylindrical and lamellar microstructures, as well as a Ordered-Bicontinuous-Double-Diamond (OBDD) morphology (Figure 3.7), were shown to exist within well-defined composition ranges in close agreements with theoretical predictions [Leary and Williams 1972, Helfand *et al* 1982]. During the past two decades, analytical capabilities have been greatly enhanced by the development of small-angle scattering techniques that complement advances in TEM and provide access to new thermodynamic and fluctuation quantities. The topics in this section reflect these recent developments.

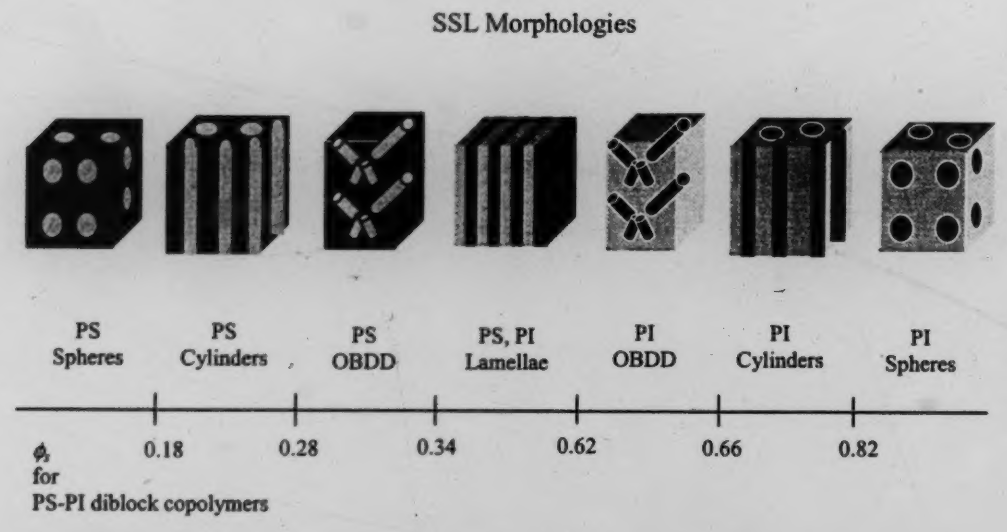
SSL Morphologies
PS Spheres
PS Cylinders
PS OBDD
PS, PI Lamellae
PI OBDD
PI Cylinders
PI Spheres
0.18
0.28
0.34
0.62
0.66
0.82
ϕ_s for PS-PI diblock copolymers

Figure 3.7: Strong segregation limit (SSL) equilibrium morphologies for $(A\text{-}B)_n$ type block copolymers. The microphase separation transition compositions shown apply to polystyrene-polyisoprene diblock copolymers (slightly different for triblock copolymers) where ϕ_s corresponds to the polystyrene volume fraction. White regions represent PS and black regions represent PI.

In a seminal series of publication, Hashimoto and co-workers [Hashimoto *et al* 1974, 1977, 1980(a) and 1980(b), Todo *et al* 1977, Fujimura *et al* 1981] explored microdomain size and packing, and interfacial mixing in a model set of polystyrene-polyisoprene diblock copolymers by SAXS and TEM. The quantitative measurement of the interphase thickness between microphases represented an important development, particularly in the light of theoretical predictions by Leary and Williams [1970, 1973 and 1974], Henderson and Williams [1985a and 1985b], and Helfand and Wasserman [1982] regarding this characteristic. They evaluated the large scattering wave-vector region of their SAXS data and determined an interphase thickness $t = 20 \pm 5$ Å, independent of microstructure (lamellar or spherical) and molecular weight. A subsequent small-angle-neutron-scattering (SANS) study of polystyrene-polybutadiene diblock copolymers by Bates *et al.* [1983] produced essentially the same conclusions regarding interphase thickness. (These authors also determined body-centered-cubic packing of spherical polybutadiene domains [Bates *et al.* 1982] in agreement with the weak segregation prediction of Leibler). In independent SAXS measurements on polystyrene-polybutadiene diblock and triblock copolymers, Roe *et al.* [1981] found $10 \le t \le 17$ Å. These authors also reported interphase thickness measurements for $T > T_{MST}$ (which we define as being in the WSL) suggesting the presence of microdomain structure within the disordered state. All these small-angle scattering results for polystyrene-polydiene block copolymers are in reasonably good agreement with the prediction of Helfand and Wasserman [1982]: $t \approx \sqrt{2/3}a\chi^{-1/2} \cong 23$ Å, where a is the statistical segment length.

Although small-angle scattering experiments are capable of establishing a precise characteristic interphase thickness, they are not able to discriminate between different mathematical expressions for the interphase profiles due to limitations set by background and domain scattering. Spontak *et al* [1988c] have attempted to address this deficiency by measuring the interphase composition profile directly by TEM. This method requires use of extremely thin osmium-stained sections, which raises questions regarding stain-induced local segregation and swelling. Nevertheless, Spontak *et al.* reported interfacial composition profiles with characteristic thickness, $t \approx 26\,\text{Å}$, slightly greater than were found by the small-angle scattering. The interphase composition profile was found to be slightly richer with end blocks (which were PS) than the middle block segments (which were PB) [Spontak *et al* 1988c].

One of the most exciting discoveries with the strong segregation regime in the last decade is the ordered bicontinuous double diamond (OBDD) morphology, depicted in Figure 3.7 along with the five originally recognized equilibrium morphologies. The earliest published TEM picture of the OBDD phase was obtained from a polystyrene-polydiene star-block copolymer and reported by Aggarwal [1976] as the "wagon wheel" morphology. Later Thomas and co-workers [1986] identified the now well-known OBDD phase, consisting of two continuous interpenetrating diamond (tetragonally coordinated) networks of polystyrene rods embedded in a continuous polyisoprene matrix. Evidence for this structure was provided by the combined use of SAXS and TEM. Small-angle scattering reflections from the ordered lattice were instrumental in identifying the exact lattice type and space group, which was then correlated with numerous tilted TEM images based on computer generated two-dimensional crystallographic projections.

Following these publications on star-block copolymers, Hasegawa *et al* [1987] reported an equivalent ordered phase, denoted the "tetrapod-network structure" in polystyrene-polyisoprene diblock copolymers, thus demonstrating the occurrence of the OBDD phase in simple linear block architectures.

Central to the theory of strong segregation in block copolymers is the concept of an extended block conformation, made necessary by the combined constraints of block joint localization at a narrow interphase and overall uniform density. The effects of extended chain conformation are most readily observed in the molecular weight dependence of the periodic lattice spacing and domain dimensions. With the advent of SANS, the direct experimental determination of block chain statistics is now possible.

Richards and Thomas [1981] reported the first SANS measurements on mixtures of partially labeled and unlabeled polystyrene-polyisoprene diblock copolymers. The SANS pattern contained two scattering contributions, one deriving from single-block scattering from within the polystyrene spherical domains (containing 4% deuterated polystyrene blocks) and a second associated with domain scattering. Richards and Thomas estimated the domain scattering based on the SANS pattern obtained from an unlabeled sample, and subtracted it from the total scattering intensity to arrive at an estimate for the polystyrene block dimension within the spherical domains.

Unfortunately, this subtraction method is extremely sensitive to small differences in molecular weight and composition between the labeled and unlabeled polymers, and this sensitivity limits the practical application of the method. Hadziioannou *et al.* [1982b] published the first SANS study of block chain dimensions in a lamellar microstructure. By mixing small amounts of partially deuterated polystyrene-polyisoprene block copolymer (per- deuterated polystyrene block) with an equal molecular weight of unlabeled material, these researchers created scattering contrast within the polystyrene domains that could be used to determine the average block conformation within the lamellar. They measured the chain dimensions parallel to the lamella, though the perpendicular dimensions could not be measured. Their study indicated a significant lateral contraction of the block chain dimensions parallel to the lamella, relative to the unconstrained size.

3.2.2. Weak Segregation Limit

As discussed in the previous section, bulk block copolymers can be brought into the weak segregation regime by decreasing either χ or N. The former is generally accomplished by selecting structurally similar monomers. For example, diblock copolymers ($f \sim ½$) prepared from styrene and α-methyl-styrene remain disordered (i.e. homogeneous) at around 180 °C for $\overline{M}_w \leq 5 \cdot 10^5$ g/mol [Baer 1964, Robeson *et al* 1974, Krause *et al* 1977]. In contrast, symmetric polystyrene-polydiene diblock copolymers exhibit a microphase separation transition at about this temperature when $10^4 \leq \overline{M}_w \leq 2 \cdot 10^4$ g/mol, depending upon the polydiene type (e.g. polybutadiene or polyisoprene) and microstructure [Mori *et al* 1985, Owens *et al* 1989]. Since these first reports, only a handful of block copolymers have been investigated in the WSL.

Within the weak segregation regime the most significant feature is the microphase separation transition (*MST*). Identification of the MST temperature, denoted T_s, is often complicated by the weak first-order character of this phase transition and the presence of significant composition fluctuations above and below T_s. Earlier studies established the existence of phase separation based on the calorimetric or dynamic mechanical evaluation of the glass transition. A single glass transition is indicative of homogeneity (i.e. disordered), whereas two glass transitions (say, T_g^A and T_g^B) signal microphase separation (i.e. ordered) [Baer 1964, Robeson *et al* 1974, Krause *et al* 1977, Owens *et al* 1989, Ramos *et al* 1977, Cohen *et al* 1979 and 1982]. Although these techniques (DSC) remain useful screening methods, sometimes it is difficult to use them to identify T_s quantitatively.

The ordering of a block copolymer is accompanied by gross changes in the low frequency rheological properties as first shown by Chung *et al* [1976 and 1978] and Pico & Williams [1976] for a poly(styrene-butadiene-styrene) (SBS) triblock copolymer, and plasticized SBS, respectively. This behavior is characterized by the transition from a terminal dynamic mechanical response for $T > T_s$ (e.g. $G' \sim \omega^2$ and $G'' \sim \omega$ for $\omega \rightarrow 0$ where G' and G'' are dynamic elastic and loss moduli, respectively [Ferry 1980]) to a non-terminal response for $T < T_s$. At sufficiently low frequencies, G', and to a lesser extent G'', drop discontinuously as the temperature is raised through the first-order *MST*.

This discontinuity provides a quantitative means of identifying T_s; typical rheometer temperature control affords approximately 1 °C precision in the determination of T_s. This technique has been demonstrated and exploited by several research groups studying both diblock [Rosedale *et al* 1990, Bates 1984] and triblock [Han *et al* 1987, 1989 and 1990, Widmaier *et al* 1980, Gouinlock *et al* 1977] copolymers. And, in judgement, represents the most efficient and accurate method for establishing T_s.

In addition to these abrupt changes in the limiting low frequency ($\omega \rightarrow 0$) rheological properties at the *MST*, composition fluctuations near the phase transition lead to significant departures from thermo-rheological simplicity. The details of this dynamic behavior will be discussed later. Nevertheless, the continuous development of thermo-rheological complexity, particularly in the disordered state, is a direct manifestation of the fluctuation effects discussed previously and described below, and should not be confused with the discontinuous changes that mark the *MST*.

As with the strong segregation limit, SAXS and SANS are very powerful and important experimental tools for investigating block copolymers in the weak segregation limit. The choice between using X-rays or neutrons as incident radiation is dictated primarily by the choice of polymers, which determine the contrast factor. Non-polar systems governed by relatively large χ parameters such as polystyrene-polydiene generally exhibit a sizeable electron density difference between components, which provides good X-ray contrast. Accordingly, these materials are frequently studied by SAXS. Increasing block compatibility by selecting structurally similar polymers such as isomers [Cohen *et al* 1982, Bates *et al* 1984] greatly reduces χ and eliminates X-ray contrast, making the use of SAXS either difficult or impossible. In this situation, deuterium labeling (e.g. deuterating one block) provides strong neutron contrast, thus making SANS the experimental method of choice. These considerations are particularly important in the WSL. An intrinsically weak contrast factor {i.e. similar pure component electron densities (for SAXS) or neutron scattering densities (for SANS)} will be sensitive to small changes in the local specific volume. Therefore, any inhomogeneously distributed (i.e. composition dependent) excess volume of mixing will modify this factor. If the local composition pattern changes with temperature, the contrast factor will vary with temperature. This effect will be most severe when the composition profile is most temperature dependent, i.e. near the *MST*. Such spurious temperature dependence of the scattering intensity (I) would preclude the quantitative evaluation of theory.

As discussed in the previous section, Fredrickson and Helfand have recently incorporated fluctuation effects into Leibler's original weak segregation mean-field theory, arriving at the phase diagram illustrated in Figure 3.5(b) ($N = 10^4$). Several experimentally testable differences between the mean-field and fluctuation theories can be identified. As the *MST* is approached in the disordered phase, both theories anticipate a rapid increase in the peak scattering intensity $I(q^*)$. However, for the general case in which $\chi = \alpha T^{-1} + \beta$ the mean-field and fluctuation theories differ significantly in the predicted temperature dependence of $I(q^*)$; the former predicts $I^{-1}(q^*)$ to be linear with T^{-1}, whereas fluctuation effects produce a nonlinear relationship between $I^{-1}(q^*)$ and T^{-1} parameters.

Beginning with Roe and co-workers [1981], the *MST* has been examined by SAXS for a variety of polystyrene-polydiene diblock copolymers [Roe *et al.* 1981, Romas *et al.* 1977, Hashimoto *et al.* 1988], triblock [Han *et al.* 1990]. These studies have relied on SAXS data obtained as a function of temperature for determining T_s. In general, the *MST* has been correlated with the temperature at which a deviation from linearity in a plot of $I^{-1}(q^*)$ versus T^{-1} is observed, as predicted by mean-field behavior. In all these SAXS studies the *MST* appears as a continuous transition as evidenced by an unbroken $I(q^*, T)$, contrary to the prediction of a first-order transition by both mean-field ($f \neq 1/2$) and fluctuation theory. None of these publications corroborate the assignment of T_s with rheological evidence of the phase transition.

Bates and co-workers [1989(a)] reported the preparation of fully saturated hydrocarbon diblock copolymers in the WSL. A series of monodisperse, $f \cong 0.55$, poly(ethylene-propylene)-poly(ethylethylene) (PEP-PEE) samples were studied rheologically [Rosedale *et al* 1990] and by SANS [Bates *et al* 1988 and 1990]. A full evaluation of the PEP-PEE SANS results revealed the first clear evidence of composition fluctuation near the *MST*. In the high temperature disordered state, the principle scattering reflection could be quantitatively fit with the theoretical structure factor. In addition, a shoulder (in SANS plot of $I^{-1}(q^*)$ *vs* T^{-1}) was apparent and became more prominent as the temperature was lowered towards T_s. This feature is not accounted for by current theory and suggested that the disordered phase may possess more "structure" (i.e. large composition gradients) than has previously been assumed. Overall, the disordered state

SANS structure factor closely resembles the structure factor characterizing the final stage of spinodal-decomposition in a symmetric ($f = 0.5$) binary polymer mixture [Bates *et al* 1989(b)], which is the basis for the real-space morphology of the fluctuating disordered phase depicted in Figure 3.6. In their SANS result, $I^{-1}(q^*)$ is clearly nonlinear in T^{-1} over the entire temperature range examined, which extends 56 °C above T_s. A quantitative comparison of the mean-field and fluctuation theory confirms the predicted significance of fluctuation effects in the disordered state near the *MST* and rules out the use of the mean-field assumption in these regions of the block copolymer phase diagram.

Bates *et al* [1990(b)] also investigated the ordered state of a PEP-PEE specimen by using SANS. In order to facilitate these measurements, a sample was shear-oriented. Scattering experiment revealed a lamellar morphology that persisted up to T_s, confirming the fluctuation theory prediction that for slightly asymmetric composition (here $f = 0.55$) the lamellar ordered phase should lead directly to the disordered phase (see Figure3.5b), while mean-field theory predicts a lamellar-hexagonal-(body-centered-cubic)-disordered sequence of phase transitions (Figure 3.5a).

Near the *MST*, the ordered and disordered states differ primarily in the extent of coherence of compositional order. Although this difference would be immediately apparent in direct images (see Figure 3.6b), the associated small-angle scattering patterns barely reflect the phase transition. Such long-range morphological features are best studied by direct methods such as transmission electron microscopy (TEM). Unfortunately, most model systems in the WSL are not readily studied by this technique.

All the block copolymers considered in this review require staining prior to quantitative TEM analysis. Near the MST, selective staining may seriously influence phase behavior, obviating use of the method. Samples that have chemically similar blocks such as PEP-PEE, are difficult if not impossible to stain selectively. Polystyrene-polydiene block copolymers are easily selectively stained and thus represent the most attractive candidates for TEM analysis (SSL experiments). In fact, several provocative electron micrographs obtained from polystyrene-polyisoprene-polystyrene triblock copolymers quenched from near the *MST* (T_s was well above the polystyrene glass transition temperature) to room temperature seem to exhibit disordered morphologies similar to that shown in Figure 3.6b [Widmaier *et al* 1980, Hadziioannou *et al* 1982a]. The segregation of a glassy component probably reduces the effects of strain-induced changes in miscibility. However, it is difficult to assess the impact of such large temperature changes above T_g on the non-equilibrium state of the sample. This method might be improved by placing T_s slightly above T_g for polystyrene, through adjustment of *N*, which would dramatically increase the system response time relative to the temperature quench time. Under such conditions, a quantitative analysis of demonstrably "frozen" structures could be conducted.

3.3. Rheology

3.3.1 Nonlinear Mechanical Properties

Bishop *et al* [1969] and Bishop & Davidson [1969], studying SBS and SIS triblock copolymers, proposed a two-phase structure in these materials with the middle block phase constituting a continuous three dimensional matrix and dispersed end blocks serving as multi-junction linkage points. They demonstrated that the elastic modulus G could be accurately predicted from classical rubber elasticity theory if the middle block is a rubbery polymer such as polybutadiene (PB) or polyisoprene (PI) and the end block is a glassy thermoplastic.

The classical rubber elasticity theory predicts [Rodriguez 1989]:

$$G = \frac{\rho RT}{M_c} \qquad (3.3-1)$$

where M_c is the molecular weight between crosslinks. While the junctions between chains in block copolymers are not chemically crosslinked, it is found that if the network is considered as a classical rubber then from both elastic modulus and solvent swelling data Equation 3.3-1 predicts an M_c which is the same as the molecular weight between entanglements of the homopolymer center block rather than the total molecular weight of the center block. Because the ends of the chains are trapped in the glassy domains, these entanglements can slide along the center blocks but cannot slip off, thus forming functionally effective crosslinks.

The effect of the glassy microdomains was accounted for by modeling the material as a rubber containing hard filler particles. Because the bonding between the "filler" and the matrix is highly effective, the result is an increase in tensile strength. Bishop *et al* [1969] further pointed out that because the entanglements which form the crosslinks can slide along the chain the result is a more equitable distribution of stresses which also contributes to the high tensile strength of the materials. As a result the tensile strengths of SBS and SIS block copolymers were shown to be much higher than either of their respective homopolymers of similar covalent crosslinking density. However, as also shown by Bishop *et al.* [1969], a triblock copolymer having rubbery end blocks, namely BSB, has low tensile strength unless it is chemically vulcanized. They also demonstrated that at higher temperatures (which we interpret as $T > T_g^{PS}$) the PS domains in SBS or SIS become fluid and can be disrupted by applied stress, but upon cooling they become hard again, once again immobilizing the ends of the PB middle section.

Brunwin *et al.* [1969] obtained tensile properties for an SBS with $\phi_s = 0.40$ and proposed that the high Young's modulus indicates that at low extension the PS domains cannot move independently of each other. Therefore, the PS domains must interact with each other to form a loosely bound continuous phase of PS (lamellar). Both stress and extension at break were shown to decrease with increasing temperature which they attributed to the softening of the PS domains. Diamant *et al.* [Diamant *et al.* 1988, Diamant and Williams 1989(a), 1989(b)] performed uniaxial tensile tests on solvent cast SBS triblock copolymers with different PS compositions. They found the first-cycle moduli E_1 was highly sensitive to composition or domain microstructure, which in turn reflected both thermodynamic effects and the kinetic effects of processing. Solvent effects were also important in cast specimens. But, the second-cycle moduli E_2 they found were typical of rubbers filled with different amounts of randomly dispersed hard domains. The original effects of solvent and processing were nearly completely eliminated. They also found a plastic-to-rubber transition that was due to simultaneously breaking down of the PS continuity across the entire cross-section of the test specimen.

Manthis *et al.* [1977] studied the effects of morphology on the tensile mechanical properties of SIS copolymers with cylindrical morphology. They found when the cylinders were oriented perpendicular to the stress, the sample deformed elastically (the glassy cylinders simply were carried apart when the elastic matrix was stretched). With the stress parallel to the cylinders, the structure was destroyed rapidly (since the stress was transferred to the glassy network which then snapped). Yamaoka and Kimura [1993] also found that SBS copolymers with oriented lamellae showed excellent impact strength and large elongation. Those with wavy lamellae, on the other hand, showed enhanced rigidity and heat resistance.

3.3.2 Effect of Molecular Architecture

It is well understood that the A-B or A-B-A block copolymers based on styrene and dienes are called thermoplastic elastomers and that they can be melt processed like thermoplastics. However, rheological investigations of these two-phase systems show their melt behavior to be much more complicated than that of their corresponding homopolymers or random copolymers [Kraus *et al* 1967(b) and 1971, Holden *et al* 1967 and 1969, Arnold *et al* 1970, Kotaka *et al* 1974, Minor *et al* 1970].

McGrath [1967] noted the effect of styrene block molecular weight on compression moldability. Styrene-isoprene-styrene copolymers having block molecular weights of 100,000-400,000-100,000 could not be successfully molded. It was speculated that chain entanglements in the hard segment were important. Holden *et al.* [1969] reported that melt viscosity (at $T > T_s$) was very sensitive to molecular weight changes, particularly at low shear rates. The behavior was not Newtonian at low shear rates and thus could not be examined by the well-known equation that states that the zero shear viscosity is proportional to molecular weight raised to the power 3.4. At the relatively low shear rate of 10^{-1} seconds, the exponent was approximately 5.5 for block copolymers. The melt viscosity of styrene-butadiene-styrene block copolymers is greater than either of the homopolymers at the same molecular weight. It was suggested [Holden *et al* 1967 and 1969, Kraus *et al.* 1971] that the high viscosities result from the fact that the two-phase structure still exists in the melt ($T > T_g^S$). At high temperatures, the polystyrene domains are fluid and flow is possible. The microphase separation, however, requires the polystyrene domains to flow through the polydiene matrix. An additional energy term is needed to describe this feature, which shows up as a higher melt viscosity [Holden *et al.* 1969].

The effect of block sequence (e.g. styrene-butadiene-styrene or butadiene-styrene-butadiene), molecular weight and branching on steady flow and dynamic viscosity was investigated [Kraus *et al* 1971]. At constant molecular weight and total styrene content, viscosities were greater for polymers terminating in styrene blocks. The effect was more important than the degree of branching. Branching did decrease the viscosity of either butadiene-styrene-butadiene or styrene-butadiene-styrene at a constant M_w. The length of the terminal block was also shown to be more important than the total molecular weight. The styrene domains in butadiene-styrene-butadiene should not be affected to any great extent when the polymer flows. In contrast, the styrene-butadiene-styrene system can not flow without disruption of the styrene domain.

The dynamic viscosities of styrene-butadiene-styrene have also been studied as a function of frequency and temperature using a Weissenberg rheogoniometer [Arnold *et al* 1970]. This technique has advantages over the capillary method in the low shear rate range. The viscous and elastic responses are independent of deformation amplitude and may be analyzed using linear viscoelastic theory. The data confirm a domain-type structure at low frequencies and a thermoplastic behavior in the high frequencies range. It is not possible to obtain a zero shear viscosity value for the styrene-butadiene-styrene. Further experiments by these investigaters [Arnold *et al* 1970] showed that the viscoelastic properties of styrene-butadiene-styrene were not amenable to simple thermoplastic characterization. It was proposed that styrene-butadiene-styrene can exist in three distinct states depending upon the rate of deformation. At low frequencies, the molecular network is intact and a very high viscosity is observed. At intermediate regions of shear stress, the domains are disturbed and a viscosity higher than expected is still observed. Finally, at very high shear stresses the domains are largely separated and a typical thermoplastic response is displayed. It is also interesting to note that two vastly different flow activation energies ($T_g < T < T_s$) were observed for different values of *f*. Above or below ~31% (volume) styrene, the values were 38 and 19 Kcal/mol, respectively. It was suggested that the higher value resulted from disrupting a semi-continuous polystyrene phase as would be consistent with a lamellar morphology. These investigators also found that the response in the low-frequency region was much more dependent upon the length of the styrene end block than on the polybutadiene segment.

The effects of center block structure on the rheological properties were studied by Futamura and Meinecke [1977]. The chemical structure of the center block was found to have a pronounced effect on the rheological properties of the ABA block copolymer melts. The long-range relaxation times of these block copolymer melts increased with increasing incompatibility between the styrene block and the center block. However, the rheological properties of the block copolymers were not influenced significantly by the glass transition or the entanglement molecular weight of the center block. (Note: these center blocks were always rubbery, so that $T_g^B << T_g^S < T_s$)

3.3.3 Viscoelastic Behavior

The two-phase nature of diene-styrene block copolymers has been described by Angelo *et al.* [1965], Ikeda *et al.* [1970], Kraus *et al.* [1967(a)], Tobolsky and co-workers [Cooper *et al.* 1966], and many others [McGrath 1967, Canter 1968, Meier 1969, Leary and Williams 1974 etc.]. The dynamic properties and glass transition temperatures of both random and styrene-butadiene-styrene block copolymers were discussed by Kraus *et al.* [1967(a)]. The moduli of the block polymers at temperatures above the diene T_g are higher than those of the random copolymers and are proportional to the styrene content.

This may be due to the "filler" effect. It was shown that the width as well as the ω-position of the dynamic loss $G''(\omega)$ peak was useful in characterizing these systems. Uniformly random copolymers in which the comonomers follow each other in a statistically well-defined way (i.e. composition does not vary along the chain and all molecules have the same composition) showed the narrowest loss peak. More heterogenous (e.g. longer sequence distributions) random copolymers also showed only one loss peak, but it was considerably broadened. The position and width of the block copolymer peaks were dependent upon the block length and compositional purity.

It cannot be overemphasized that morphology governs the viscoelastic and mechanical behavior of these systems. Thus, in addition to block purity, sequence length and ratio of components, the method of sample preparation can be critical. The nature of the casting solvent, evaporation rate, drying conditions and molding times and temperatures can have enormous effects. Of course, additives such as plasticizers and cross-linking agents have an additional bearing on the viscoelastic response. Dependence of mechanical properties on morphology has been discussed by Kaelble *et al.* [1971 and 1973].

The variations in the properties of solvent-cast films, which are possible merely by changing the nature of the casting solvents, have intrigued a number of investigators. The principal role of the solvent is often to cause a given phase to become more continuous or more discrete. Alternatively, solvent can be chosen to encourage phase separation or phase blending. The mechanism is a development of the technique due to

Merrett [1954] wherein "good" or "poor" solvents, respectively, can expand or collapse a chain and predetermine the resultant morphology after solvent evaporation.

Block copolymers fabricated from the melt are often vastly different from solution-cast films. The most important reason for the different behavior is the characteristic high melt viscosity. Morphological studies described earlier show that the unoriented melt-fabricated specimens do not develop the same degree of order as carefully prepared cast film. Furthermore, Juliano [1968] observed unusually large effects of molding time and temperature on melt-molded specimens. It was also demonstrated by Canter [1968] that the upper transition (T_g^S) can be quite diffuse, unless the molded film is first submitted to stress relaxation at high elongations. This treatment is believed to improve the degree of phase separation. Several other phenomena that are related to thermal history have been reviewed elsewhere [Estes *et al.* 1970].

The stress relaxation rate of the molded styrene-butadiene-styrene has been studied [Smith *et al.* 1969]. The values were derived from constant extension rate data and were found to be about 8% per decade of time at temperatures from –40 °C to +40 °C and at extensions from about 20% up to 400%. A modified Rouse-Bueche-Zimm theory was used by Shen *et al.* [1977] to predict the maximum relaxation time of homogeneous ($T > T_s$) block copolymers.

An unusual relationship between tensile modulus E' and shear modulus G' for molded SBS film has been reported [Kraus *et al* 1971 and 1972]. Ratios of $E'/3G'$ as high as twelve have been observed with 40% styrene materials. By contrast, films solution-cast from toluene had the expected value of about unity (as expected also for incompressible elastic bodies in general). It was suggested [Kraus *et al.* 1971] that the disparity resulted from the formation of interconnected polystyrene domains in the molded specimens. Further work [Kraus *et al.* 1972] confirmed this picture. The loss tangent in tension ($\tan\delta = E''/E'$) is heavily weighted by mechanical losses in the polystyrene phase, whereas the corresponding shear value ($\tan\delta = G''/G'$) is only moderately affected.

The effects of sample preparation and flow geometry on the melt rheological behavior and morphology of SBS and SIS block copolymers were studied [Han *et al.* 1995]. For compression-moulded specimens the shear viscosities obtained using a cone-and-plate rheometer did not overlap those obtained using a capillary rheometer, while for solvent-cast specimens there was a reasonably good agreement between the two. The viscosities of solvent-cast specimens were much lower than those of compression-moulded specimens. The steady shear flow was found to affect greatly the morphology with PS cylindrical morphology, whereas it had little effect on the PS spherical microdomains.

Winey *et al.* [1993] also addressed this problem by studying a SI diblock copolymer with well-aligned lamellar morphology. They found the oscillatory shear within the linear regime did not effectively align the block copolymer morphology and the onset of non-linear viscoelastic effects occurred at small strain (~1%). The well-aligned samples were disrupted by steady shear flow.

Chapter 4 Equipment and Methods

4.1 Rheological Testing

The Rheometrics Mechanical Spectrometer 800 (RMS-800) was used to characterize the melt rheological properties. This characterization is accomplished by using dynamic (oscillatory) and steady shear tests under conditions of controlled temperature, strain and frequency (or shear rate). The RMS-800 is essentially a rotational rheometer, which can be operated with various test geometries for shearing the fluid; for this project, 25-mm diameter parallel plates were used to deform a disk of polymer held between them. The bottom plate, or platen, is connected to a motor that is capable of a range of displacements with different time dependencies, which will be described below. The top platen is connected to a force rebalance transducer (FRT) capable of measuring both torque and normal force. A labeled diagram of the staging area in the rheometer is given in Figure 4.1 showing the transducer, thermocouple and oven. An explanation of the parts is given in Table 4.1.

4.1.3 Sensitivity

The manufacturer's quoted torque range for the mid-range transducer (used exclusively in this project) is between 2 and 2000 g·cm. However, it was found that torque lower than 2 g·cm could be reliably measured. Torque as low as 1 g·cm could be

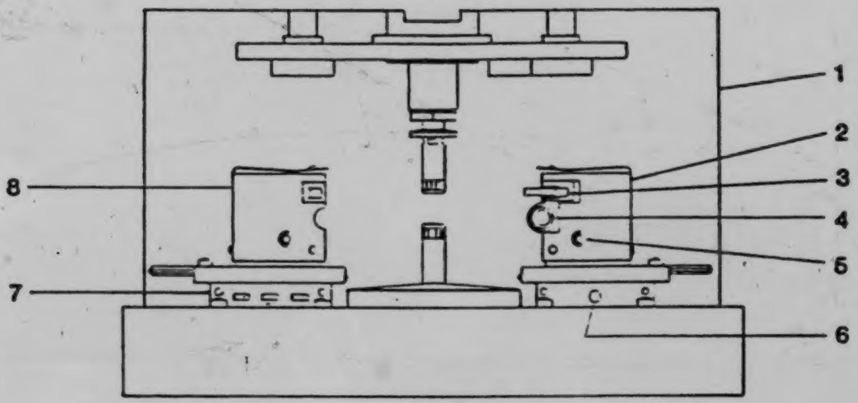

LEGEND

1. Test station upper frame assembly
2. Oven, right half
3. Locking latch
4. Sample viewing port
5. Handle
6. Light switch
7. Thermocouple-to-computer coupling connector panel
8. Oven, left half

Figure 4-1. Environmental System (Oven)

accurately measured while torque down to 0.3 g·cm could be statistically differentiated from zero, but not accurately measured. This was determined by a calibration using known weights. The method and results are described in Appendix A.

Table 4.1: Staging Area Components.

1	Transducer.
2	Transducer anvil on which upper platen is mounted.
3,9	Right and left halves of oven.
3	Oven light.
4	Motor.
6,7,8	Thermocouple receptacles.
10	Motor Anvil on which lower platen is mounted.
11	Tool Thermocouple.
12	Heater gun.
13	Platform or quill which houses the transducer and can be raised or lowered by the stepper motor.

4.1.2 Modes of Operation

The modes used in this experimental program are described below. The equations used in different test modes and geometry are listed in Appendix A.

4.1.2.1 Dynamic Oscillatory Modes

The bottom platen can be displaced torsionally in a sinusoidal pattern at frequencies ranging from 10^{-3} to 10^{2} radian/second, with displacements from 1.25×10^{-5} up to 0.5 radian. Stress and strain are both measurable signals. In dynamic oscillatory mode several sweeps (such as strain sweep, time sweep, ... etc.) can be performed as described below.

A. Single Mode

This position is used primarily in designing a new experiment or in rapidly determining the extreme range of response of a new material. The mode executes a single test at a specific frequency, strain amplitude and temperature. One and a half strain cycles are performed before the input (strain) and output (stress) waves are fitted to a sinusoid, thereby generating the amplitude ratio and phase lag. These quantities are then used to calculate automatically the rheological functions, such as η', η'', G', G'', tan δ etc. At the end of the test the motor automatically returns to the same torsional zero position.

B. Strain Sweep Mode

The strain sweep test mode is an automatic test used to determine the material characteristics across a range of dynamic strain amplitude (γ°), at a fixed temperature T and a fixed frequency ω (often 1 Hz, for convenience). This test permits strain sweeps with data recorded at strain intervals spaced evenly on either a linear or logarithmic scale.

The test is implemented by incrementing the angle of rotation in a dynamic test using step increases in strain between user-selected limits. This test is usually run first, giving properties such as $\eta'(\gamma^{\circ})$ (at constant ω and T), which are useful for determining the strain at which the sample material can be considered to be in a linear viscoelastic region. Typically, nonlinearities are manifested by a drop-off in the η' value when γ° becomes too large. The strain amplitude is calculated using

$$\gamma^{o} = \frac{\theta R}{H} \times 100\% \qquad (4.1-1)$$

where γ° is strain, θ is angular displacement in radians, R is platen radius and H is sample thickness (platen separation or sample gap). In the parallel plate geometry, Equation 4.1-1 gives the strain at the outer boundary of the disk (hereafter designated as γ_R^{*}), which is also the maximum strain. The sample between the plates is experiencing non-homogeneous strain which approaches zero at the centerline. Despite the nonhomogeneity of the strain field, the value of γ_R^{*}, Equation 4.1-1 is normally identified as the measure of the strain magnitude in all dynamic testing.

C. Frequency Sweep Mode

The frequency sweep test mode is used to determine the dependence of material properties across a range of frequencies (e.g.: $\eta'(\omega)$) at a fixed temperature and fixed strain amplitude. The oscillatory frequency is sequentially increased (or decreased) between user-selected limits. In automatic rate sweep, the equilibration and measurement time is selected as part of the test parameters and will be controlled by the computer.

D. Temperature Sweep Mode

Temperature sweep test mode is an automatic test used to determine the dependence of a material property on temperature across a range of temperatures (e.g.: $\eta'(T)$) at a fixed ω and γ°. In this mode, temperature is automatically stepped up or down from selectable end points for up to four temperature ranges (zones) at programmed increments. A selected thermal soak time at the onset of each new temperature ensures temperature stability prior to measurement. A single measurement is made at each temperature at fixed γ° and ω. In a parallel plate test, a gap correction in micron/°C corrects (manually) the initial sample gap for thermal expansion or contraction of the test fixtures. This allows the strain amplitude (γ°) applied to the sample be a function of true sample gap.

E. Time Sweep Mode

In a time sweep test, repeated measurements are taken at constant temperature, ω and γ° at an operator-selected time interval. This provides a means of measuring property time-dependence which may reflect the buildup or breakdown of network structure.

4.1.2.2 Steady Mode

The bottom platen connected to the motor can be rotated at a constant rate ranging from 10^{-3} to 10^{2} radian/second in either the clockwise or counter-clockwise direction. Steady torque and normal force, instead of oscillating torque and phase lag in dynamic mode, are the measurable signals in steady mode.

In the parallel plate geometry, a simple shear flow is given by the velocity field:

$$V_\phi = \dot{\gamma}_{\phi z} Z; \qquad V_z = 0; \qquad V_r = 0 \qquad (4.1\text{-}2)$$

in which the velocity gradient $\dot{\gamma}_{\phi z}(= dV_\phi / dz)$ can be a function of time. The absolute value of $\dot{\gamma}_{\phi z}$ is called the shear rate $\dot{\gamma}$. The purpose of such tests (steady shear) is to measure the dependence of the properties (e.g.: viscosity η) on $\dot{\gamma}$. Thus, at sufficiently large $\dot{\gamma}_R$ (shear rate at the rim, $\dot{\gamma}_R = \frac{\Omega R}{h}$, [Bird 1986]) the value of $\eta(\dot{\gamma}_R)$ drops, signaling the onset of the property known as non-Newtonian viscosity.

A. Single Mode

The single test mode is used primarily to design a new experiment or rapidly determine the extreme range of response of a new material.

B. Rate Sweep Mode

The rate sweep test mode is used to determine various properties of a material across a range of steady shear rates at fixed temperature. The most useful example is $\eta(\dot{\gamma})$. The shear rate is sequentially increased (or decreased) between user-selected limits.

4.1.3 Auto-Zeroing of Motor

In dynamic oscillatory mode the motor to which the bottom platen is connected has a fixed zero position. Each time the motor is turned on or a test is ended (even between tests in a sweep) the motor returns to this zero position. In steady mode there is no fixed zero, but rather the motor chooses a zero point each time the motor is turned on and moves to this zero point. The zero is always in close proximity to the position of the motor when it was off.

In dynamic oscillatory mode each test begins in the direction of rotation opposite to that of the previous test. For example, in a strain sweep from 1% to 5% in 1% intervals, 1%, 3% and 5% tests would be started in the clockwise direction while 2% and 4% tests would be started in the counter-clockwise direction. The same would be true of isolated single tests provided that the rheometer was not turned off between tests, or the computer control unit was not reset. In dynamic mode and steady mode the user may select the direction of rotation.

4.1.4 Alignment

In a parallel plate rheometer it is important that the bottom and top platens be aligned very precisely. This is because the stress is calculated from the geometry and torque. The greatest stress contribution is from the outer edges of the platens. The effects of a small error in either parallelism (commonly referred to as flatness), or concentricity of the platens would be greatest near the edges, where they would cause the greatest error in the stress calculation, and also lead to fluid torque differing from the ideal case. The following alignment specifications are given in the RMS-800 manual. The flatness of the platens should be within ± 0.0003 inches from zero, that is, total error must not exceed 0.0003 inches from high to low point. Similarly the platens should be concentric to within ± 0.001 inches. In the present work, the flatness and concentricity alignment were secured within 0.0001 and 0.0005 inches, respectively.

4.1.5 Sample Gap

Because precise knowledge of the platen separation (commonly referred to as the “gap”) is essential for γ^{o} and γ calculation that corresponds to the measured torque, it is important that it be known accurately. The platform assembly holding the transducer, to which the upper platen is attached, can be raised and lowered automatically by a stepper motor. All components are so well machined that alignment of the platens does not change significantly with the elevation of the platform. A metal block on the platform pushes against the armature of a dial gauge which is marked in 2 micron (2×10^{-6} m) increments. Position of the platform can therefore be measured accurately to within 1 micron.

The gap is measured relative to a zero position (h=0) which is achieved by lowering the platen until a very small positive normal force is registered on an analogue meter, indicating that the upper platen has touched the lower platen.

Due to thermal expansion of the platens, the gap is not constant with temperature. This can be compensated for in two ways.

1. The gap can be zeroed at the planned test temperature.
2. If the sample is to be tested at several temperatures, then the gap can be corrected by employing the thermal expansion of the platens. In an automatic temperature sweep the auto-tension mode can be used so that the upper platen moves up and down with changing temperature. The rheometer control computer senses the change in the gap by a magnetic indicator on the dial gauge. For manual temperature sweeps a calibration of gap change with temperature is done by zeroing the gap at a range of temperatures. This calibration is given in Appendix A.

4.1.6 Auto-Tension

The auto-tension mode maintains a constant normal force on the transducer within a user-defined window (the auto-tension window, given in percent of full scale). Positive normal forces, that is in the upward direction, are relieved by raising the platform and hence the upper platen. Negative normal forces are relieved by lowering the platform. This is particularly useful in temperature sweep tests to ensure that the transducer is not forced off scale in the normal direction, as well as maintain the sample covering the whole platen area (not more and not less).

4.1.7 Internal Data Acquisition and Analysis

The RMS-800 Mechanical Spectrometer is interfaced with a dedicated electronics console/computer controller. The electronics are proprietary, but it is known that this unit contains an analogue-to-digital converter capable of converting the ± 10V full scale signals from the transducer (both normal force and torque) and from the motor (displacement) into a signal in bits. In dynamic oscillatory mode, input (strain, γ^0) and output (stress, τ) signals are fitted to sinusoidal functions by proprietary software. In dynamic transient mode, the data is collected at 512 equally spaced (in time) points in each of four time zones of user-selected duration between 1 second and 130,000 seconds. Typically the first zone is the shortest when the most rapid fluid relaxation is occurring. For example, zone 1 may extend from 0 to 1 second, zone 2 from 1 to 11 seconds, followed by zones of 100 and 3,600 seconds.

4.1.8 Sample Preparation

"Solid" polymer samples were compression molded into disks 25 millimeters in diameter and roughly 2 millimeters in thickness using a mold fabricated in-house. The mold is simply three square sheets of stainless steel about 2 millimeters thick (as illustrated in Figure 4.2). The middle sheet has 9 circular holes 25 millimeters in diameter to hold the polymer pellets. To facilitate sample removal, aluminum foils (very thin sheets) were placed between middle and upper sheets, as well as between middle and lower sheets. A heated press was used to compress these three metal sheets under a force of 7 tons, during which the polymer pellets (then melted) were also compressed and forced to assume the dimensions of the circular disk holes. All samples were molded around 170 °C; the molding time was never allowed to exceed about 5 minutes, to avoid thermal damage (An investigation of thermal and oxidative degradation of the samples used here at high temperatures is given in Chapter 8). The stress buildup in the sample was not removed by annealing in the mold, but was later released in the rheometer at higher temperature prior to the rheological test. Previously a teflon-based mold release agent (Crown 66075 Dry Film Lubricant & Mold Release Agent) was used, instead of aluminum sheet. It was sprayed onto the steel surfaces prior to the molding to prevent polymer sticking to the mold. This was found to lead to subsequent measurement artifacts, since the mold release agent formed a thin layer on the sample surface, and this caused slipping between the sample and the rheometer platen surface while testing. Details on rheological measurement artifacts during slip are given in Appendix B, as well as evidence for removal of the artifacts with the aluminum sheet technique. The discovery of this problem associated with the mold release agent was important, since most rheological laboratories in industry and academia use similar mold release agents in their work, and the literature may therefore contain much data which is not valid.

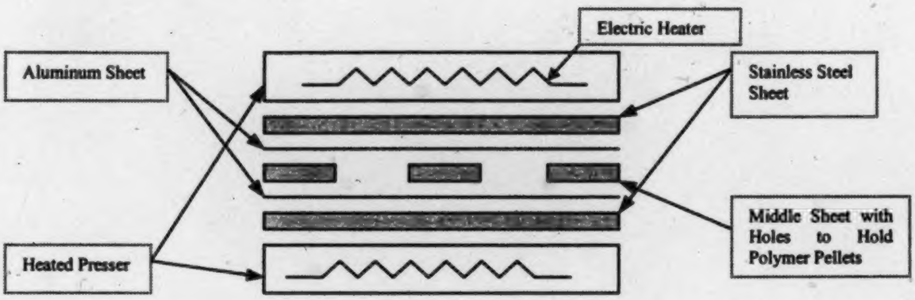

Figure 4.2: Compression Mold

4.1.9 Temperature Control

A gun heater protrudes inward from the back of the rheometer to within one or two centimeters of the platens. An insulated jacket closes around the platens and the gun heater. The heater operates by compressed air or nitrogen if provided (in this project only nitrogen was used). The temperature range of this convection oven is from ambient to 500 °C. The temperature feedback is taken from a platinum resistance thermometer (PRT) located in the gas and positioned just beneath the lower surface of the bottom platen (tests showed that the PRT temperature was always within half a degree of the platen temperature itself). The control scheme is proportional and integral plus derivative (PID). The manufacturer's quoted stability is ± 0.5 °C when equilibrated. In practice it was found to be stable to within 0.1 to 0.2 °C. Measurement of sample temperature [illegible] possible from a thermocouple located next to the PRT, which protrudes through the center shaft of the lower platen and rests in a pivot at the center of the bottom platen. This thermocouple is known as the "tool thermocouple" and the temperature so measured is known as the "tool temperature". Because of the high thermal conductivity and heat capacity of the metal platen, its temperature and that of the polymer sample contacting it are virtually identical.

To achieve subambient temperatures, the convection oven must be replaced with a liquid circulation jacket. The gun heater and high temperature jacket are removed and the circulation jacket installed to close around the platens. Silicone oil is circulated through the jacket halves by a Haake F3 circulator/heater and refrigeration unit with temperature range of –30 to +105 °C, which results in a range of –25 to +100 °C at the platens. A calibration of sample temperature vs. tool temperature using the circulation jacket is given in Appendix A.

4.1.10 Sample Loading

The molded sample disk was loaded into the rheometer by the following procedure. The disk was placed on the lower platen at room temperature and the upper platen was lowered to contact the sample until the normal force was approximately 10% of full scale. The oven was then closed and heated to 180~190 °C, thus softening (liquefying) the sample. The upper platen was slowly lowered further, compressing the sample until the gap was reduced to around 1 millimeter. While in auto-tension mode, the oven was then cooled to 160 °C and opened, and the excess polymer sample outside the platen's edge was cleaned away by a special razor-blade-like tool. The sample was subsequently heated up to 200 °C (or any other temperatures above the microphase-separation temperature T_s of that specific polymer sample, where the polymer was in a homogeneous melt state). This was done in auto-tension mode and under zero normal force so as to let the sample fully relax. The time for sample to stay at this high temperature varied from a couple minutes to 20 minutes. The sample was then cooled to the testing temperature and equilibrated thermally for a few minutes to allow the sample temperature to stabilize before testing.

4.2 Differential Scanning Calorimeter (DSC)

The Differential Scanning Calorimeter (DSC) (*TA Instrument DSC 2910*) determines the temperature and heat flow associated with material transition as a function of time and temperature. It also provides quantitative and qualitative data on endothermic (heat absorption) and exothermic (heat evolution) processes of materials during physical transition. A schematic representation of a DSC cell is given in Figure 4.3. A heat-flux type DSC relies on the measurement of a difference in heat flux fed to or extracted from a sample pan and a reference pan. It utilizes a pair of matched temperature sensors, generally thermocouples, one in contact with the sample pan and the other in contact with the reference pan. As the specimen is heated or cooled in a controlled manner, its temperature will depart from the normal rate as it undergoes a reaction or transformation. Two individual heaters under the sample and the reference pans then will increase or reduce the heat flow so to maintain the temperatures of these two pans the same.

Consider the simple thermal analysis of the heating curve. If the event is endothermic (e.g.: melting), then the sample will slow its rate of heating while undergoing the particular process. As a result, the DSC will subsequently input more heat to the sample pan to maintain the temperature difference between two pans to be zero ($\Delta T = 0$). Similarly, if the event is exothermic (e.g.: crosslinking or thermal degradation), then the sample's temperature will increase at a more rapid rate during that period and the DSC then has to reduce the heat supply to the sample pan. The output of the differential heat flux is amplified and fed to the recorder or data acquisition system. And ΔQ (heat flux difference) is generally plotted as a function of the actual sample temperature, or time. A change in the thermal conductivity or heat capacity of the sample (during a phase transition) will give an upward or downward step and then a change in slope on the DSC curves (ΔQ *vs*. T), as well as a peak (exo- or endothermic) related to ΔH of the transition event itself.

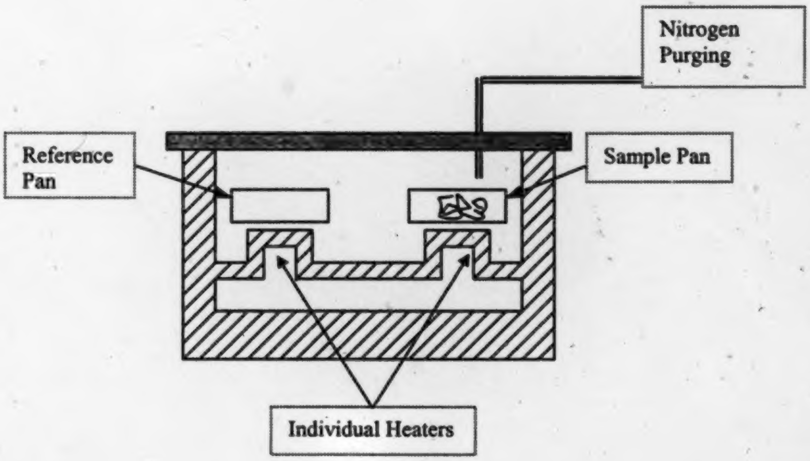

Figure 4.3 : A schematic representation of a heat-flux DSC cell

4.2.1 DSC Calibration

To obtain accurate experimental results, the DSC must be calibrated periodically. The calibration usually covers the temperature range intended for use in experiments.

A. Baseline Slope Calibration

The baseline slope calibration needs to be performed separately for each cell. This calibration involves heating the cell through the entire temperature range in which it is expected to operate. Ideally the heat flow (ΔQ) should be zero, when there is no sample in the cell. The baseline slope calibration measures the amount by which the heat flow curve deviates from zero so that this deviation can be taken into account by the DSC Calibration program. The DSC Calibration program (computer software supplied by the DSC manufacturer) then uses this baseline slope calibration file to adjust the baseline so that it will be flat in the selected experimental region. For precise experimental results, a new baseline calibration is needed once the following parameters are changed:

- Ramp rate, $T(t)$
- Purge gas or its flow rate
- Cooling Technique
- Pressure
- Cell

B. Cell Constant and Temperature Calibration

The cell constant determination and temperature calibration are both based on a run in which a known sample (usually indium) is heated through its transition temperature (usually its melting point). A separate run is required for each cell.

4.2.2 Sample Preparation

A small specimen (10 ~ 20 mg) cut from a polymer pellet is weighed and placed in an aluminum sample pan (only non-hermetic pans were used in this project). The sample pan is then closed by an encapsulating press. An empty pan is also prepared as a reference. Both sample and reference pans are then placed in the DSC cell which is filled up with nitrogen as purging gas.

Chapter 5 Rheological Study of Microstructural Ordering Mechanisms and the Effect of Annealing, with an SIS Triblock Copolymer

5.1. Introduction

The block copolymer has long been known as a phase-separated material at temperatures below its microphase-separation temperature (T_s). The resulting microphases have dimensions on the order of the dimensions of the constituent polymer blocks. The morphologies often develop into one of the following: alternating lamellae, cylinders or spheres; which of these particular structures is the case depends primarily upon the relative block molecular weights (i.e., the weight-fraction composition of the polymer) with secondary influences related to sample preparation. Above its T_s the material is generally spatially homogeneous. Sometimes the microphase separation transition (*MST*) is also referred to as the order-disorder transition (*ODT*).

The *MST* is characterized as a weak first order transition [Leary and Williams 1974] and induced by concentration fluctuations [Leibler 1980]. It has been thought to be a gradual transition [Hasegawa and Hashimoto 1996]. Much research has been dedicated to the rheological properties near the *MST*, but the ordering mechanism below *MST* (in the important practical temperature regime), i.e. whether or not it involves spinodal decomposition or nucleation and growth and how those mechanisms might affect the properties of the block copolymers at those temperatures, is by and large unknown. Since processing of block copolymers, is mostly conducted at temperatures above the *MST* and then cooled to below the *MST* for practical use, it is critical to understand the ordering mechanisms in both these temperature regimes.

Spontak and Williams [Spontak *et al* 1988, Spontak and Williams 1988] first applied a filtered back-projection reconstruction method to a set of transmission electron microscope (TEM) pictures and achieved a three-dimensional view of a SBS polymer of cylindrical morphology. They found some globules of PS in a clearly non-equilibrium state, which they suggested was due to the SBS molecules' limitation in diffusional mobility during the phase-transformation process. Further annealing of initially non-equilibrated SBS sample caused increasing ordering of styrene domains.

Rosedale and Bates [1990] studied poly(ethylenepropylene)-poly(ethylethylene) (PEP-PEE) diblock copolymers. By monitoring the $G'(t)$ evolution following the sample quenched from above the *MST*, they concluded that the ordering process near T_s was governed by heterogeneous (secondary) nucleation. Collin *et al* [1992] used atomic force microscopy (AFM) to study the surface of a spin-cast thin film of poly(styrene-*b*-*n*-butylmethacrylate), P(S-*b*-BMA), diblock copolymer. The AFM pictures show the evolution of islands and holes on the sample free surface. Schuler and Stuhn [1993] used time-resolved small-angle X-ray scattering to investigate the time dependence of structure formation at the ordering transition in bulk diblock copolymers. Two relaxation processes were found in the ordered state on well-separated time scales. They attributed the first step to formation of concentration fluctuations and the second to the diffusion of the center of mass (of the congregated blocks) to form the macrolattice.

Winter *et al* [1993] studied an SIS triblock copolymer with hexagonally packed cylinders using rheology and SAXS. The microphase separation, they found, occurred rapidly upon cooling below the *MST* (within the first 20 minutes) while the growth of large-scale spatial order (~ 1-μm scale) needed long annealing time (~ 11 hours). The slow part of the structuring process gave sufficient time for flow alignment of microphase-separated domains during their growth phase. Perahia *et al* [1994] applied SAXS to SI diblock copolymers, and found that the signature of the microphase separation transition depended crucially on the ordering process, which, in turn, is governed by annealing history. They had been able to measure the *MST* for samples that had been annealed at room temperature for 3 months, but were unable to detect T_s for the samples that had been annealed for only 1 hour. (They cooled the sample below the *MST* and annealed for certain time, then heated it up to above the *MST* to see if they could identify the *MST*)

Vogt *et al* [1994] found the poly (ethymethysiloxane-block-dimethysiloxane), EM, diblock copolymers melts at temperatures above the *MST* displayed significant dynamic light scattering due to fast density and composition fluctuations. By fast solution casting, Takenaka *et al* [1995] studied a poly(styrene-b-tert-butylstyrene) diblock copolymer while it changed from a frozen "disordered" state to an "ordered" state. (quench the sample below *MST*, then observed the frozen disordered sample ordering)

The SAXS scattering intensity (at $T < T_s$) grew with time exponentially. Adams *et al* [1996] investigated the mesophase order in compositionally asymmetric SI diblock copolymers (13% wt PS), as well as in an SIS triblock copolymer (13% PS), by time-resolved small-angle X-ray scattering and dynamic oscillatory rheological measurements. They found the ordering kinetics of both types were significantly slower than those observed for nearly symmetric (~50% PS) polymers of similar T_s, and the evolution of storage modulus $G'(t)$ measured at constant frequency displayed a two-step increase after a quench from above the *MST*. They concluded the long-time (final) step corresponded to the development of a body-centered-cubic (bcc) lattice of spherical microdomains (the ordering process), while the first step resulted from the finite time required for large-amplitude composition fluctuations to develop fully (the microphase separation). Floudas and co-workers [1996] studied four-arm star diblock copolymer melts by rheology and SAXS. The phase-separation kinetics and ordering process showed a dramatic slowing as compared to the symmetric and asymmetric linear diblock copolymers. This seems reasonable in view of the difficulty of moving the star center-of-mass with all arms developing hindrances by independent phase separations.

While those workers (cited above) have focused on the bulk polymer melts, other researchers also explored the ordering kinetics in the copolymer thin films [Shull *et al* 1991, Russell *et al* 1993, Mutter and Stuhn 1995, Wang *et al* 1996], copolymer solutions [Jian *et al* 1994] and block copolymer-homopolymer blends [Tanaka and Hashimoto 1988]. However, most effort has been directed at the process of microstructure formation as temperature drops to below T_s; few reports have ever investigated the structure changes at temperatures rises from below T_s to above T_s.

Virtually all studies of the kinetics of microphase separation and ordering have used diblock copolymers as their subjects, even though these are of very limited practical use. The triblock copolymers, of primary industrial importance, have received minimal attention. In this work, I used an asymmetric styrene-isoprene-styrene (SIS) copolymer to study, by rheology, the ordering mechanism in triblock copolymers at temperatures both above and below the *MST*, with emphasis on the rheological effects of annealing at different temperatures around T_s.

5.2. Experimental

5.2.1 Material

One poly(styrene-*block*-isoprene-*block*-styrene) (SIS) sample was synthesized and characterized by DEXCO Polymers (Plaquemine, LA). It has M_w = 125,000 g/mol, polystyrene content (ϕ_{PS}) = 18 % (wt%), and polydispersity $\overline{M}_w / \overline{M}_n \leq 1.06$, measured by gel permeation chromatography (GPC) at DEXCO Polymers. The isoprene was high (93% - 95%) in 1,4-content. The equilibrium ordered morphology of this SIS at temperatures below its T_s was a body-centered-cubic (bcc) lattice of spherical polystyrene (PS) microdomains in a polyisoprene (PI) matrix, and T_s was measured to be 165 ~ 169 °C by rheology (details in Section 5.3.1). The glass transition temperatures of both polystyrene domains (T_g^{PS}) and polyisoprene matrix (T_g^{PI}) were detected by differential scanning calorimetry (DSC). The sample characterization is listed in Table 5.1.

Table 5.1: SIS Polymer Characterization

Polymer	M_w * (g/mol)	ϕ_{PS} * (wt %)	M_w / M_n *	T_g^{PI} (°C)$^+$	T_g^{PS} (°C)$^+$	T_s (°C)$^+$
	GPC		GPC	DSC	DSC	Rheology
SIS-4111	125,000	18	≤1.06	-58±2	73±4	167 ± 2

* By supplier DEXCO
$^+$ This work, details in section 5.3.1

5.2.2 Rheometry

Dynamic mechanical properties were measured on a Rheometrics Mechanical Spectrometer (RMS-800) with parallel plate geometry (25 mm diameter). Temperatures were controlled by a convection oven, with nitrogen as purging gas to minimize the oxidative degradation. The RMS-800 temperature control is accurate to ±1 °C. Small-amplitude sinusoidal strain, $\gamma(t) = \gamma^0 \sin\omega$ (γ^0= 1%),, was chosen in all oscillatory tests to keep the sample properties well within the linear viscoelastic range. Three different types of dynamic measurements were used to measure T_s and study the microdomain ordering process around T_s: (1) temperature sweep at constant frequency (ω = 0.1 rad/s or 1 rad/s) and constant strain (γ^0 = 1%), (2) isothermal time sweep at constant frequency (ω = 0.1 rad/s or 1 rad/s) and constant strain (γ^0 = 1%), and (3) isothermal frequency sweep (ω = 0.01 rad/s to 100 rad/s) at constant strain (γ^0 = 1%), at a sequence of times during microstructural evolution.

SIS-4111 pellets were first pressed into discs 25 mm in diameter and 2 mm in thickness in a compression molding device at a temperature around 170 °C. The molding time was controlled to be within 2~3 minutes to avoid possible thermal damage. The sample disc was then further compressed in RMS-800 at about 180 °C (when the sample was soft and semi-liquid) and the final gap between the parallel plates was set at around 1 mm.

For the ordering mechanism study, the sample loaded between the RMS platens was first heated up to 200 °C ($T \cong T_s + 35$ °C) and held there for about 10 minutes to make sure that the material was in a homogeneous state, with all ordered microstructure dissipated, and to release the stress that built up during the compression molding. Then it was quenched (cooled at about 10 °C per minute) to the specific testing temperatures below T_s. Approximately 2 ~3 minutes was required for the rheometer oven temperature to stabilize. The time, at which the rheometer oven temperature stabilized and when the rheometer was commanded to start the isothermal time sweep, was designated as the zero time for the ordering mechanism measurements. Since the RMS-800 rheometer used oven temperature as feedback in its control system, the sample temperature would not be identical to the oven temperature but the difference was within ± 0.5 °C (see discussion in Appendix A). The sample would then be sheared at constant frequency and constant strain amplitude. The temporal evolution of $G'(t)$ and $G''(t)$ was monitored for various lengths of time (usually long enough to let $G'(t)$ and $G''(t)$ to reach steady values). After the isothermal time sweep was terminated, at a specific point in the microstructure development (at constant T), an isothermal frequency sweep on the same specimen was conducted and the results were used for comparison (compared with the result of frequency sweep test on a different sample that did not go through the isothermal time sweep test, which will be discussed in the following sections).

One potential problem that received much attention was the possibility of thermal degradation, due to the high temperatures I worked with (about 70 to 210 °C). Adams *et al* [1996] reported that by using GPC analysis following rheological or X-ray measurements that lasted several days at 150 °C they found only minor amounts (< 10%) of chain scission and branching for SI diblock and SIS triblock copolymers. But no indication was given whether the sample was in air or under nitrogen blanket. Unfortunately we found almost no literature report on thermal degradation for SI or SIS block copolymers other than that, and only a few on SB diblock copolymers [Abu-Zeid *et al* 1986, McNeill and Stevenson 1985, 1985]. For the individual elements of the SIS block copolymer (polystyrene and polyisoprene), Maecker and Armentrout [1989] reported that in the absence of oxygen, polystyrene usually begins to exhibit significant weight loss (gas species produced) at about 300 °C due to thermal degradation. However, molecular weight reductions (without weight loss) by random chain scissions were observed at much lower temperatures (around 250 °C). The polyisoprene chain undergoes random scission along the main chain at temperatures above 200 °C under inert gas or *in vacuo* [Tamura *et al* 1983, Yano 1980].

I used DSC to study (Chapter 8) the SIS thermal degradation both in air and in nitrogen and found no detectable thermal change up to 230 °C under a nitrogen blanket, but in air the sample underwent thermal degradation starting at 185 °C and gave an endothermic peak at around 220 °C (Figure 5.1), even though the SIS sample we used is a commercial product and contains some antioxidant additives. The sample disc looked liquid-like after being tested rheologically at 200 ° C and 210 °C for 200 to 300 minutes (in N_2), indicating that no major crosslinking happened throughout the sample (in a later DSC study of block copolymers, we found the crosslinking occurs at around 300 to 350 °C, in N_2).

5.3. Results and Discussion

5.3.1 Determination of T_s by Rheology

Intuitively, passing T_s is expected to be accompanied by a dramatic change in rheological properties, resulting from drastically different diffusion mechanisms in the disordered (homogeneous) and ordered (phase-separated) states. The diffusion mechanism in the homogeneous block copolymer melt ($T > T_s$) would be similar to that found in homopolymers and random copolymers (by reptation), while the thermodynamic barrier imposed by microphase separation should eliminate flow at temperatures below the *MST* [Leary and Williams 1974, Bates 1984].

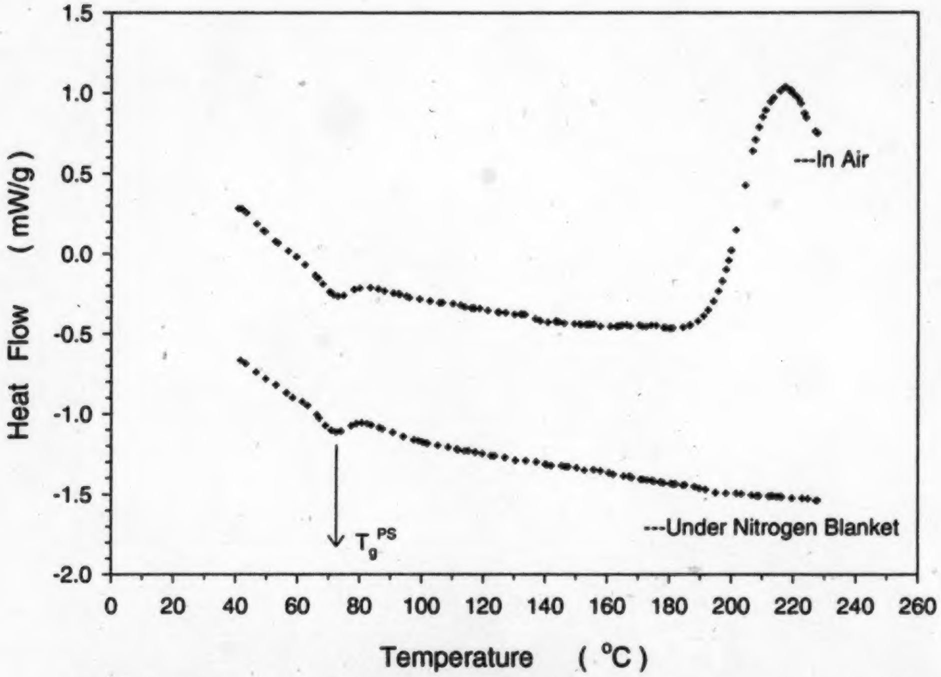

Figure 5.1: DSC scan of SIS-4111 at 10 °C/min, in air and under nitrogen blanket. The glass transition temperature of polystyrene domain is measured to be around 73 °C, which is rate dependent. The broad endothermic peak at around 220 °C (in air) is due to thermal-oxidative degradation. No detectable thermal change was observed for the sample under nitrogen blanket in the same temperature range (around 220 °C). The heat flow curve for a sample under nitrogen blanket has been shifted to a lower value (ΔH = -1 W/g), to avoid the two curves overlapping in the figure.

Several groups of researchers [Chung and Gale 1976, Gouinlock and Porter 1977, Pico and Williams 1976 and 1977] reported an elevated temperature transition in the viscoelastic properties of styrene-butadiene-styrene (SBS) triblock copolymer. They observed a transition of dynamic properties from solid-like character (i.e., large value of $\eta'(\omega)$ or G'' or η at low ω) to a moderate-valued or Newtonian viscosity (η_o) above a critical temperature. They suggested that phase miscibility above this temperature could account for this observation and the temperature at which this transition occurs is T_s.

In Figure 5.2, the results of isothermal dynamic frequency-sweep tests (with strain amplitude $\gamma^o = 1$ %) show non-Newtonian responses (η' follows a power-law behavior) at temperatures below 160 °C, while above 170 °C the dynamic viscosity η' approaches a constant Newtonian limit at low frequency ($\omega \rightarrow 0$). Attempts to superimpose the isothermal $\eta'(\omega)$ curves to create a single master curve according to the time-temperature superposition principle fail at temperatures around 160~170 °C. The resulting master curve of η' (as a function of ωa_T, where a_T is the shift factor) has two branches, one containing data below 160 °C and another containing data above 170 °C (plots will be shown in Section 7.3.1). Figure 5.3 shows plots of the loss tangent (tan δ = G''/G'). The reduced frequency plot (tan δ *vs* ωa_T) shows two distinct curves, one for data at $T \leq 160$ °C and another for $T \geq 170$ °C. At low frequency end, tan δ (= G''/G') above 170 °C tends to go to larger values, which indicates the sample is approaching a liquid state with small G' (and η'') and large G'' (and η') (a homogeneous disordered state). Because at low frequencies ($\omega \rightarrow 0$), tan δ is large for all the uncross-linked polymers and in fact becomes inversely proportional to the frequency [Ferry 1980].

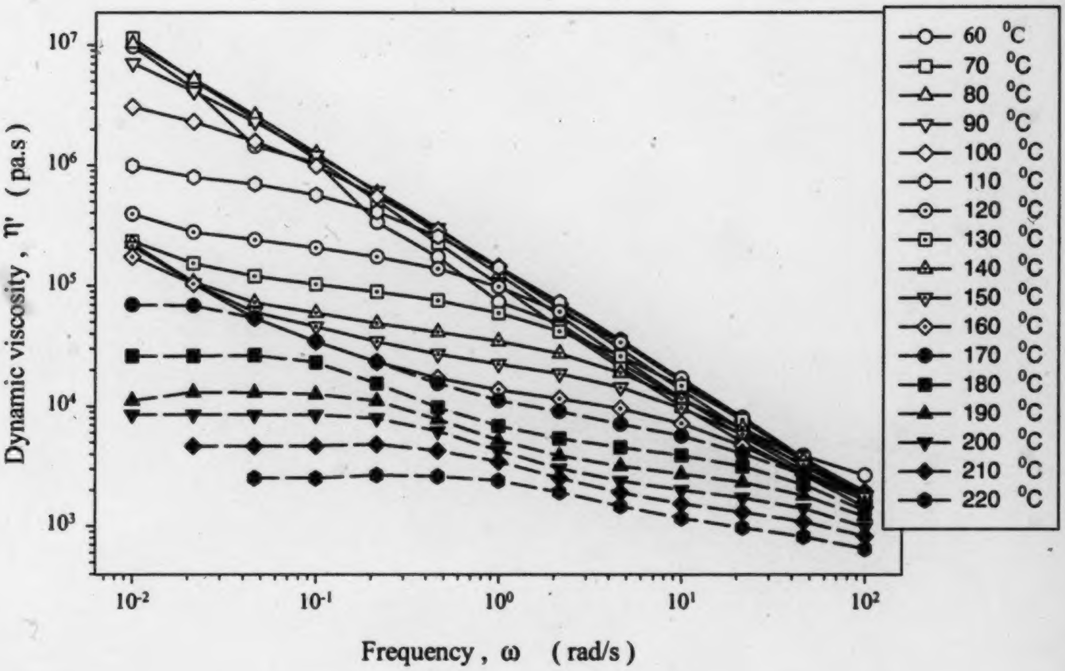

Figure 5.2: Isothermal frequency sweep for sample SIS-4111. Open symbols represent data at $T \leq 160$ °C, while the filled symbols represent data at $T \geq 170$ °C.

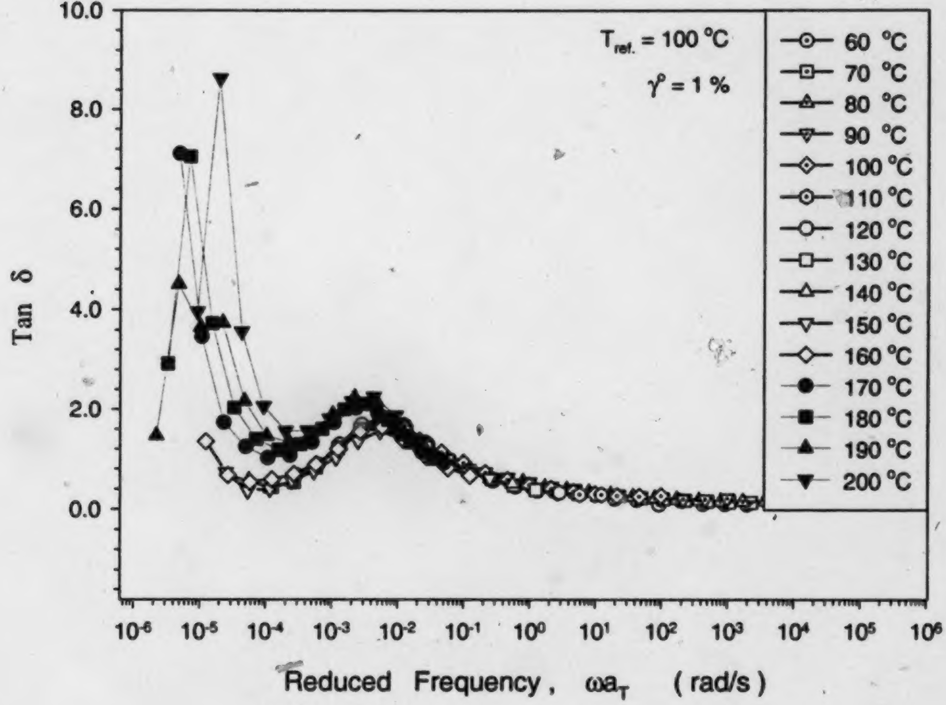

Figure 5.3: Tan δ plots at reduced frequency, for sample SIS-4111. Open symbols are data at temperatures below 160 °C, and the filled symbols at temperatures above 170 °C.

In the terminal zone ($\omega \to 0$), G'' is proportional to ω and G' to ω^2, so from G''/G' it is clear that tan δ is proportional to ω^{-1}. This (G'' is proportional to ω and G' to ω^2) is also used by some researchers [Rosedale and Bates 1990, Han and Kim 1993] as a criterion to identify T_s for the block copolymers. The fact that in Figure 5.3 the tan δ master curve splits into two branches (filled symbols and open symbols) at low ω and the data on those two curves show different tendencies separated by $T \cong 160 \sim 170$ °C (data at $T \geq 170$ °C [filled symbols] have much larger values than data at $T \leq 160$ °C [open symbols]) indicates that a phase transition occurs at $T_s \cong 160$ to 170 °C.

Some authors [Rosedale and Bates 1990, Winter *et al* 1993] also suggested that at the *MST*, $G'(\omega)$ [or $\eta''(\omega)$] showed a discontinuous drop especially evident at low frequency where rheology is very sensitive to microstructure. In Figure 5.4 we show $\eta'(T)$ and $\eta''(T)$ data at constant frequency ($\omega = 0.1$ rad/s) and strain amplitude ($\gamma^0 = 1\%$). During cooling from 230 °C (above T_s) at the rate of 5 °C/min, η'' rises three orders of magnitude and levels off at $T \leq 160$ °C. Winter *et al* [1993] showed a similar plot of $G'(T)$ and $G''(T)$ on a heating run. They found the *MST* transition happened at the temperature at which the two properties (G' and G'') cross over, in agreement with some other experimental evidences. In Figure 5.4, the η' curve crosses over η'' at around 167 °C, suggesting $T_s \cong 167^{\circ}C$ in SIS-4111.

Bates [1984] also showed that frequency had a great effect on the dynamic properties measured by rheology. At the low frequency, $G'(T)$ dropped by 2-3 orders of

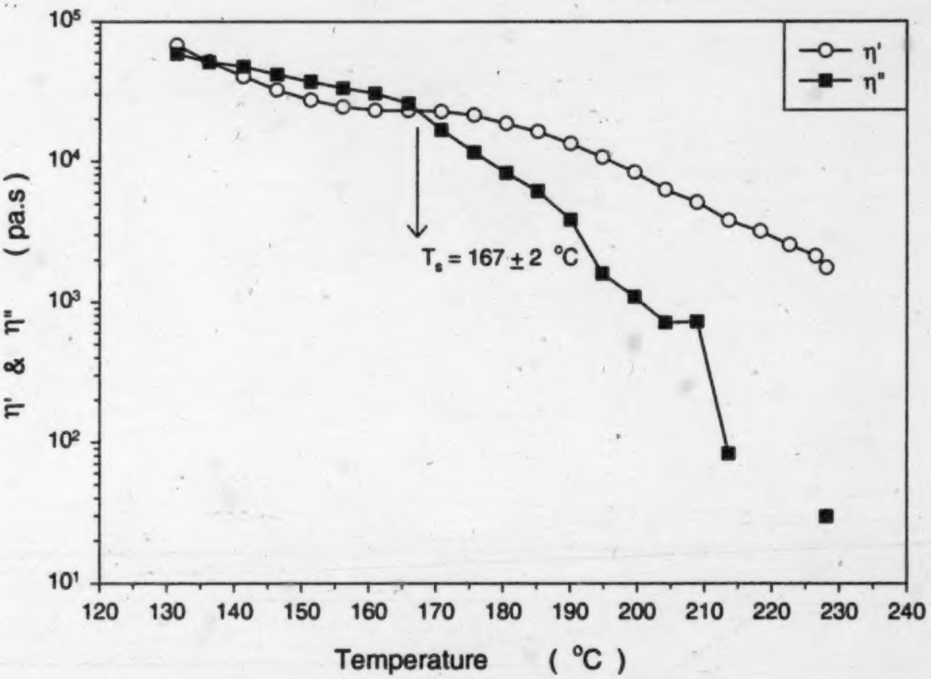

Figure 5.4: SIS-4111, η' and η'' cooling curves at $\omega = 0.1$ rad/s and $\gamma^{\circ} = 1$ %. Cooling at the rate about 5 °C/min from 230 °C. η' crosses over η'' at around 167 °C.

magnitude when temperature exceeded T_s, which agrees with Figure 5.4 (η'' or G') between 167° and 210 °C at $\omega = 0.1$ rad/s. When the Bates [1984] data was in the high frequency regime, it showed no abrupt drop above T_s. In Figure 5.5, our $\eta'(\omega)$ data at low frequency ($\omega = 0.01$ rad/s) from isothermal frequency-sweep tests shows three distinctive transitions on the $\eta'(T)$ curve. The first one is at around 80 °C, which corresponds to the glass transition temperature of the polystyrene domain containing short PS blocks, which was also measured by DSC ($T_g^{PS} = 73 \pm 4$ °C, depending on the DSC scanning rate). The second transition occurs at 160 °C $\le T \le$ 170 °C where η' drops again. Combined with the previous plots, it is a good assessment to say that this is where the *MST* is and $T_s \equiv 167 \pm 2$ °C. This temperature is also in good agreement with the result predicted by some theoretical calculations using modified Leary-Williams model [Leary and Williams 1974, Henderson and Williams 1977] (detailed calculation is in Chapter 7).

One more transition also occurs in Figure 5.5, at 210 °C. On Figure 5.4, $\eta''(T)$ is seen to drop suddenly at 210 °C as well. The η'' data points scattered all around zero at $T > 210$ °C (Figure 5-4) and a couple points were not even measurable (the η'' points recorded at 220 and 225 °C were below the lower sensibility of the RMS rheometer and thus given a value of zero, which can not be shown on a logarithmic scale such as the ordinate in Figure 5.4). A possible explanation is that the sample undergoes severe thermal degradation above 200 °C. Some studies [Tamura *et al* 1983, Yano 1980] reported that G' (or η'') would be decreased if a scission reaction occurred in the main chain and increased if a crosslinking reaction occurred during the degradation of elastomers. Polyisoprene does undergo random scission along the main chain above 473

K (200 °C) under inert gas or *in vacuo* [Tamura *et al* 1983]. But thermal degradation is not consistent with the fact that, when cooled from 230 °C to 130 °C (Figure 5.4), the sample still underwent a microphase separation transition. If the sample had been already degraded at 230 °C (which means, if the sample is thermally crosslinked or the main molecule chain has broken above 210 °C), the *MST* transition should not be observed when cooled through T_s. Thus we believe that this is a transition from the composition fluctuation state to the homogeneous state (see detailed discussion in the later sections of this chapter). The η'' function has a small value when the sample is in either the composition fluctuation ($T_s < T < 210^\circ C$) or the homogeneous state ($T > 210^\circ C$), compared to the η'' in the ordered state (at $T < T_s$ in Figure 5.4). When the composition fluctuation in the block copolymer sample disappeared, the material became homogeneous and η'' fell dramatically. But the dynamic viscosity η' did not change much at this temperature (~210 °C). Whether in the composition fluctuation or the homogeneous state, the sample is a polymer melt (this temperature range is 50 °C above the *MST* transition). The only indication of the transition (from composition fluctuation to homogeneous state, not exactly a phase transition) is the η'' changes (drop) above 210 °C.

Sakamoto *et. al.* [1997] reported some TEM pictures on the same copolymer sample. The TEM of the quenched sample (from 220 to 0 °C) shows a smeared picture I believe was caused by quick phase separation during the quench. The TEM of the sample (from 200 to 0 °C) also looks like a frozen composition fluctuation plus some quick phase separation. Some researchers [Hale and Bair, 1981] have shown that in order to achieve a TEM picture of homogeneous block copolymer, a very thin film of sample has to be quenched in the liquid nitrogen. Otherwise, phase separation will always happen. Thus, excluding the possible early-stage phase separation, the TEM picture [Sakamoto *et. al.* 1997] agrees with our conclusion (fluctuation to homogeneous at 210 °C).

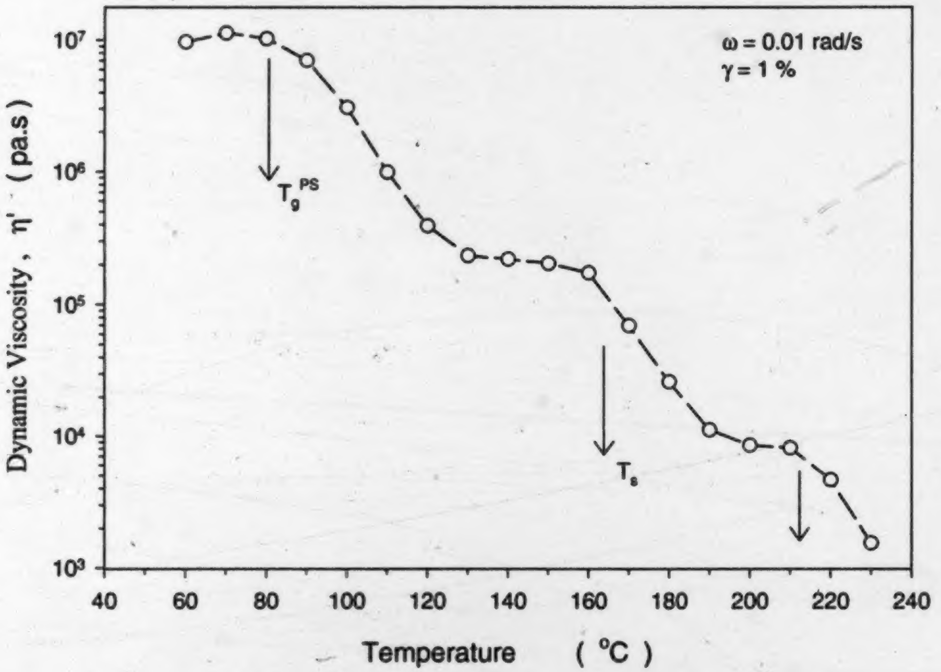

Figure 5.5: SIS-4111, dynamic viscosity η' vs. temperature at $\omega = 0.01$ rad/s. $T_g^{PS} \cong 80$ °C and $T_s \cong 167 \pm 2$ °C.

5.3.2 Microphase Ordering Mechanism

The uniqueness of a block copolymer is mainly due to its microphase separation. Below T_s, the block copolymers will form one of many intricate microstructures (namely spherical, cylindrical and lamella). When heated to above T_s, the microstructure will dissolve and the block copolymers become homogeneous again. This unique transition makes the block copolymers easy to recycle by heating it above T_s, and reprocessing as a melt. The properties of block copolymers at $T < T_s$ are, however, largely dependent on the microstructures, which in turn are controlled not only by the composition, but also by the process of the microstructure formation. Thus, to understand how the microstructure forms, or in other words the ordering mechanism, we can better control the properties of the block copolymers.

Among the many ways to study the block copolymer ordering mechanism, rheology is the most frequently used one. By monitoring the temporal evolution of $G'(t)$ and $G''(t)$ at constant frequency and strain amplitude, we can qualitatively investigate the ordering kinetics at some fixed temperatures below the *MST*. The isochronal frequency we used here meets two requirements: (1) it should be low enough that the mesophase structure dominates the rheological response and (2) it should be high enough to provide adequate time resolution. Since the temperature we work with spans almost 100 degrees (from 120 °C to 210 °C) and the sample structure undergoes several transitional changes, we choose both 1 rad/s and 0.1 rad/s frequency in this study primarily for probing the structure evolution below and above the *MST*. Similar criteria also apply to the strain amplitude, both lower enough to keep rheological response within the linear viscoelastic range and high enough to give measurable torque signals. From our preliminary study we found $\gamma^{\circ} = 1$ % fit for both frequencies (1 rad/s and 0.1 rad/s).

The block copolymer sample was first heated from room temperature to 200 °C, in a convection oven with N_2 purging. After the sample was thermally soaked at 200 °C for 10 minutes (to allow the sample's microstructure to disappear), it was quickly cooled to the testing temperature at the rate of 10~15 °C/min (quench process), except for the testing at 200 and 210 °C. A time-sweep test was subsequently conducted to monitor the $G'(t)$ and $G''(t)$ evolution. The results are shown in Figure 5.6 to Figure 5.11.

In Figure 5.6 the storage modulus, $G'(t)$, of copolymer sample SIS-4111 is plotted *vs* time, at constant ω and γ°. All $G'(t)$ curves increase with time and decrease when the testing temperature increases. This shows that as the temperature rises, the block copolymer becomes softer especially when the temperature surpasses T_s at which the sample liquifies.

Three distinct groups of $G'(t)$ curves are observed in Figure 5.6. The first group is at $T < T_s$ (filled symbols in Figure 5.6). At $T = 164$ °C (quench depth $\Delta T \equiv T_s - T_{testing} \cong 3$ °C), $G'(t)$ rises quickly with a sigmoidal shape within the first 50 minutes and then gradually approaches its final equilibrium value asymptotically (in about 760 minutes). At deeper quench depths ($T = 140$ and 150 °C, $\Delta T \cong 30$ to 50 °C), $G'(t)$ curves lose the early-time S-shape and become simply asymptotic.

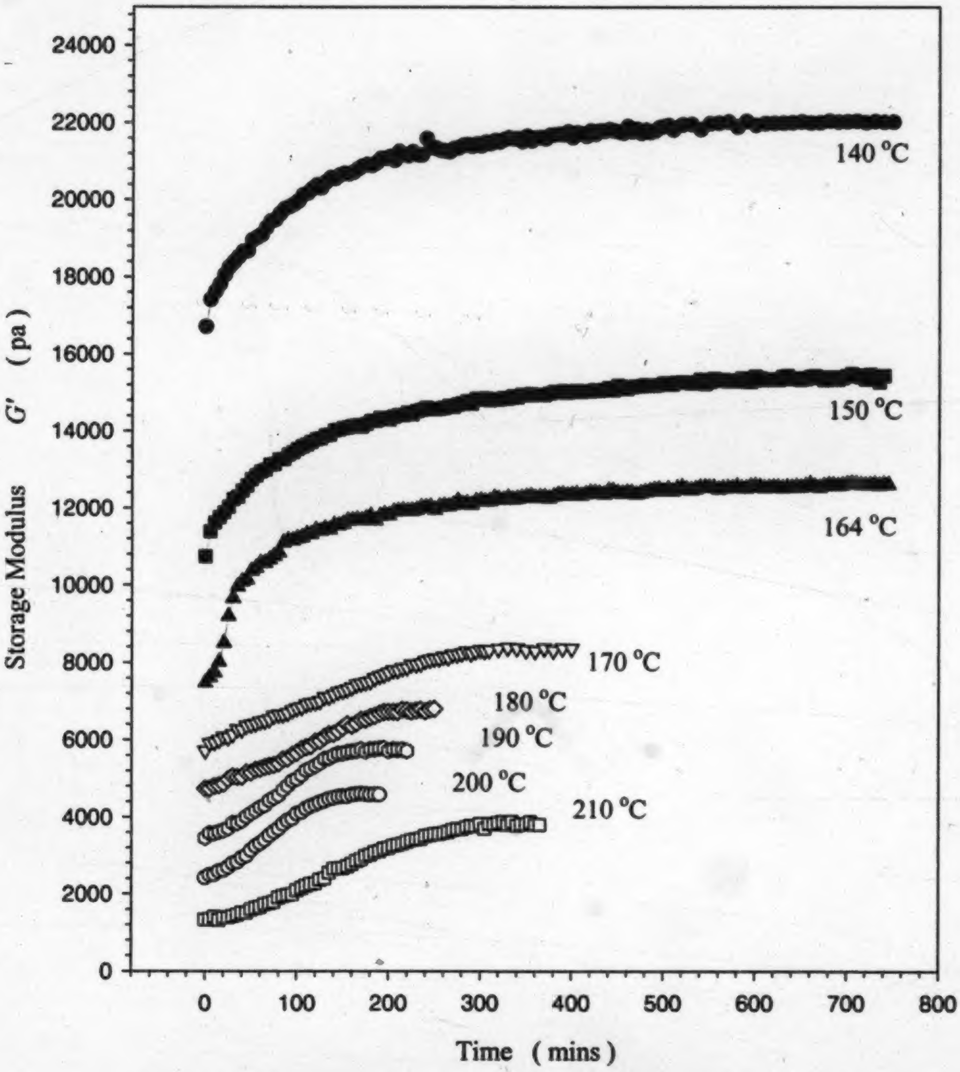

Figure 5.6: Temporal evolution of G' for sample SIS-4111, at $\omega = 1$ rad/s and $\gamma^\circ = 1$ %. Measuring at 5-minute time interval. Note that the shape of the curves changes around T_s ($T_s = 167$ °C) and between $T = 200$ °C and $T = 210$ °C. Symbols in black represent data at $T < T_s$. Open symbols represent G' at $T > T_s$. The data were taken at 5 minutes interval.

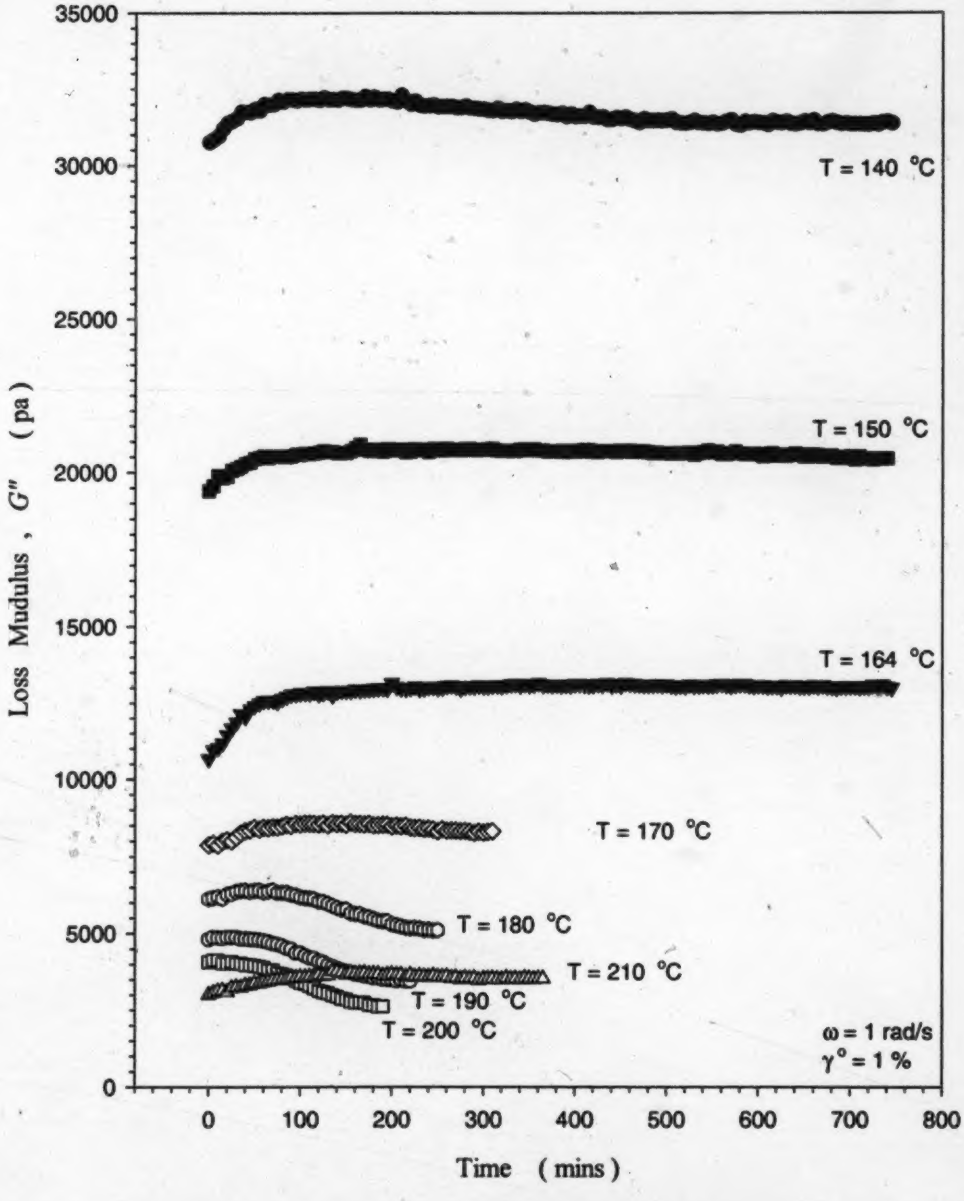

Figure 5.7: Temporal evolution of *G″* for sample SIS-4111, at $\omega = 1$ rad/s and $\gamma^{o} = 1$ %. Measuring at 5-minute time interval.

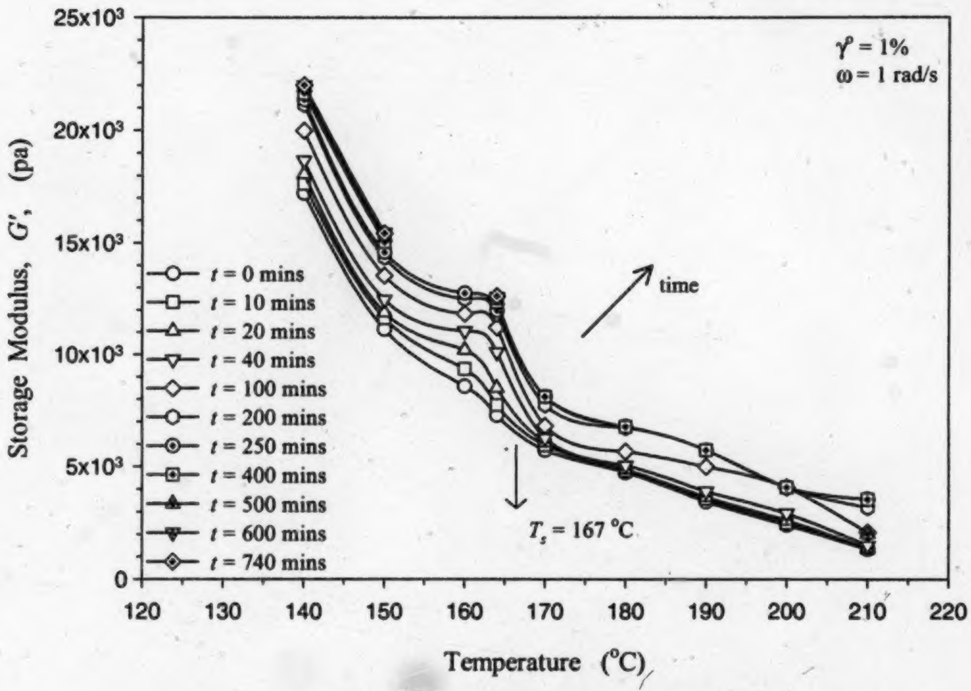

Figure 5.8: Storage modulus *vs* temperatures for sample SIS-4111, at $\omega = 1$ rad/s and $\gamma^\circ = 1\%$. As time progressing, the difference of G' at below and above T_s becomes more obvious. The total increments, $\Delta G'$, at $T < T_s$ are twice the $\Delta G'$ at $T > T_s$.

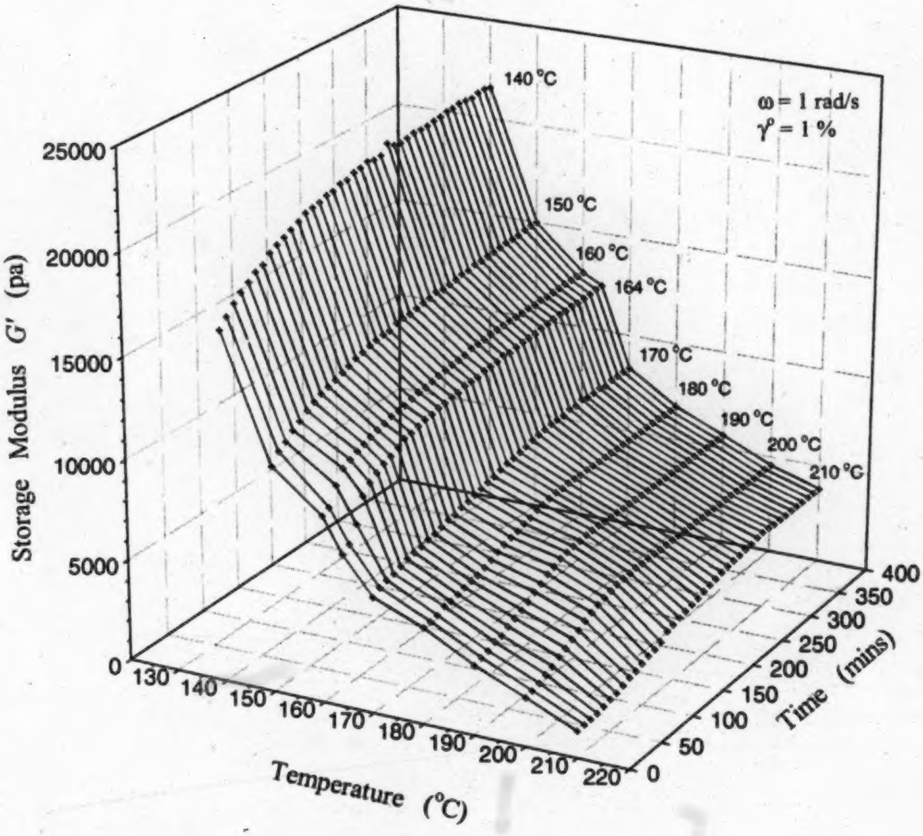

Figure 5.9: 3-D plot of storage modulus for sample SIS-4111, at $\omega = 1$ rad/s and $\gamma^{\circ} = 1\%$.

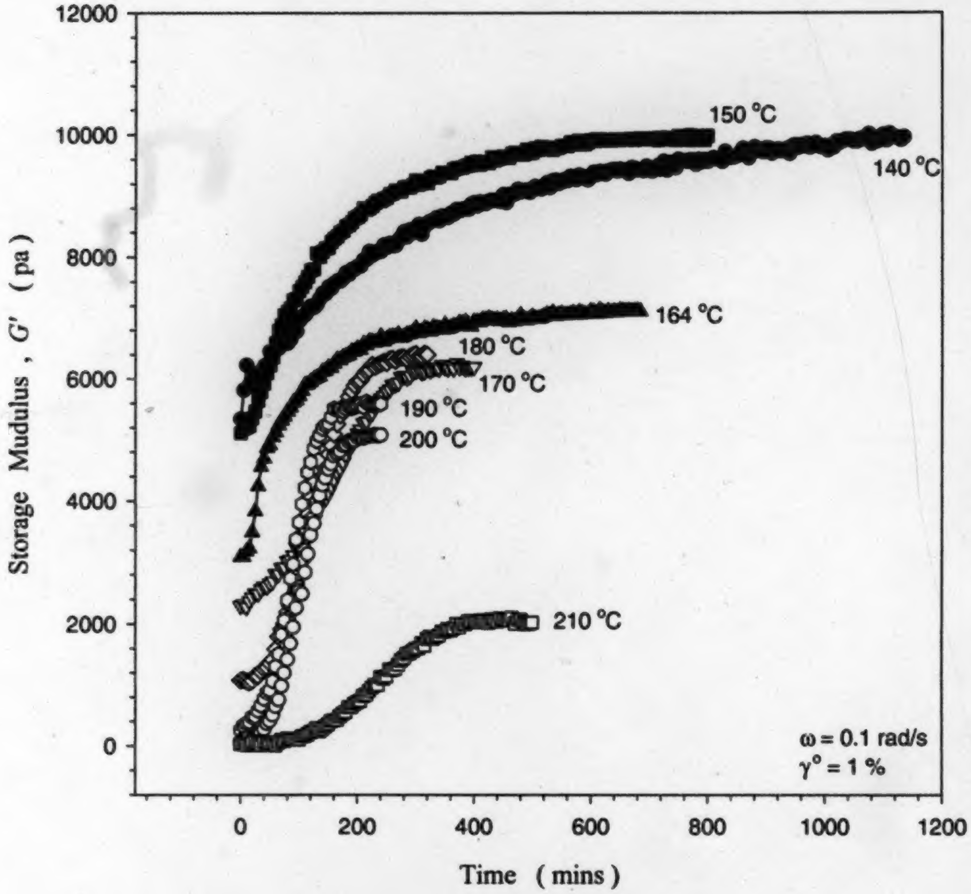

Figure 5.10: Temporal evolution of G' for sample SIS-4111 at $\omega = 0.1$ rad/s and $\gamma^{o} = 1$ %. Measuring at 5-minute time interval.

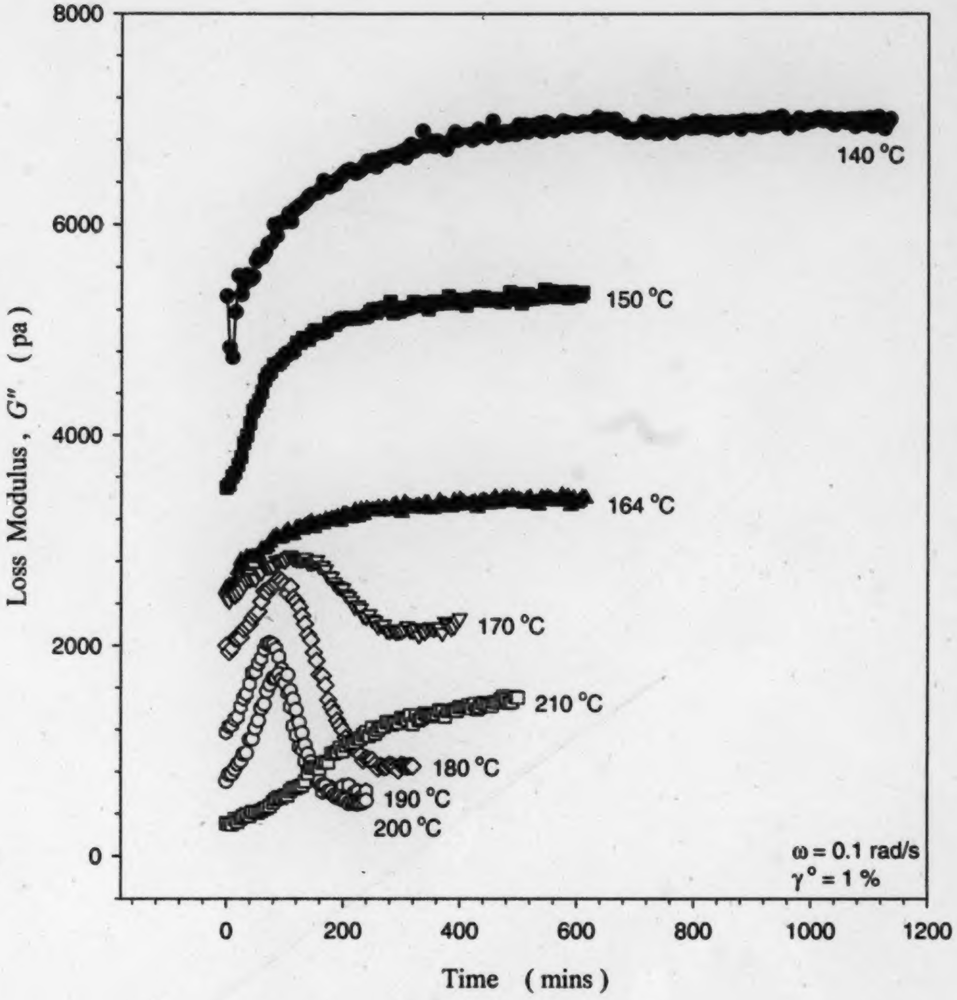

Figure 5.11: Temporal evolution of G'' for sample SIS-4111 at $\omega = 0.1$ rad/s and $\gamma^{\circ} = 1$ %. Measuring at 5-minute time interval. Note the shape changes between 164 °C and 170 °C, 200 °C and 210 °C.

The second group of $G'(t)$ curves is at $T > T_s$ (open symbols in Figure 5.6). $G'(t)$ increases with time but reaches the final equilibrium value in a much shorter time than the other group. This group of curves does not have the steep increase of $G'(t)$ (as the $G'(t)$ curve at 164 °C does in the first 50 minutes). This group of $G'(t)$ curves represents a surprise; by intuition, we expected $G'(t)$ would not be a function of time at temperatures above T_s since the sample is believed universally to be in the homogeneous state (in which the sample should have a constant viscosity and modulus). The third group of curves (actually one curve only) is at 210 °C. The $G'(t)$ increases with time but has a distinct difference from the curves at $T \leq 200$ °C. The time for latter group to reach a steady value decreases with increasing temperatures (from 170 to 200 °C), but at 210 °C the time increases again. The difference is also obvious for G'' functions in Figure 5.7.

Figure 5.7 shows the loss modulus $G''(t)$ as a function of time at $\omega = 1$ rad/s (relatively high ω) and $\gamma^0 = 1$ % (which is the complement of the G' functions in Figure 5.6). The two functions, $G'(t)$ and $G''(t)$ differ in their T-dependence, reflecting their different dependence on microstructure and its growth kinetics. The storage modulus G' is related to energy stored elastically and used to characterize the solid behavior of the material (structural etc). On the other hand, the loss modulus G'' is related to the energy lost by viscous processes and used to characterize the liquid behavior of the sample (such as viscosity $\eta' = G''/\omega$). While both G'(t) and $G''(t)$ decrease with increasing temperature, the $G''(t)$ in Figure 5.7 shows a mild maximum at some temperatures (140, 170, 180, 190 and 210 °C). At other temperatures it increases with time monotonically (at 150, 164 °C).

The $G''(t)$ curves also seem to group into three different sets which are separated by T_s and 200~210 °C. This agrees with the G' curves in Figure 5.6.

The G' data in Figure 5.6 are also plotted in Figure 5.8 and Figure 5.9 as simultaneous functions of temperature and time. At time zero (t = 0) log G' decays approximately exponentially with temperature (Figure 5.8). But as the time progresses, the G' curves deviate from exponential decay around T_s. G' drops at T_s. In Figure 5.9, the data were plotted 3-dimensionally, $G'(T,t)$. The changes at *MST* are prominent (Figure 5.8). The existence of a narrow temperature regime is obvious right below T_s, where as time progresses the G' changes most dramatically. Within this temperature range (3 to 10 degrees below T_s in Figure 5.8), the thermodynamic force that drives the copolymers from homogeneous state to phase separated state is large and the block copolymer molecules still have high mobility. Thus the microstructure changes most dramatically in this temperature window, which makes it the ideal temperature frame (160 ~ 167 °C) to study the microstuctural ordering process.

Figure 5.10 and Figure 5.11 show the temporal evolution of G' and G'' at lower frequency (ω = 0.1 rad/s). Generally the modulus has a lower value at lower frequency [compare G' growing from 0 to 10000 Pa in Figure 5.10 (ω = 0.1 rad/s) and from 2000 to 22000 Pa in Figure 5.6 (ω = 1 rad/s)]. The G' curves in Figure 5.10 look a little different from those in Figure 5.6 (ω = 1 rad/s).

At 164 °C ($\Delta T = T_s - T \cong 3^{o}C$), G' increases rapidly within the first 100 minutes and then approaches a steady state value. At 140 and 150 °C, the storage modulus simply grow with time gradually. However, though $G'_{t=0}$ has a lower value at 150 °C than at 140 °C, the G' increases faster at 150 °C than it does at 140 °C in the early 300 minutes. Though slow in the early stage, the modulus at 140 °C keeps growing even after 20 hours. At $T > T_s$, a similar trend persists. G' at high temperatures increases faster than that at lower T. The G' reaches steady-state values much faster at $T > T_s$ than at $T < T_s$.

The $G'(t)$ increment from time zero to its final steady state value varies with temperature and frequency. Consider first the low-ω case (ω = 0.1 rad/s): the G' increment at $T > T_s$ is the same as at $T < T_s$. G' grows as much as 4000 to 5000 at both $T > T_s$ and $T < T_s$ (Figure 5.10). However, at high frequency (ω= 1 rad/s), the G' increment at $T < T_s$ is much larger than those at $T > T_s$. At $T < T_s$, $G'(t)$ increases about 4200 to 5000 Pa ($\Delta G' = G'_{t=\infty} - G'_{t=0}$), while at $T > T_s$ $\Delta G' \cong 2200$ Pa (Figure 5.6). The modulus increment is more than doubled upon heating, relative to when sample was cooled by the same ΔT over the T_s. This cooling below T_s reflects the solidifying process that takes place at *MST*. The block copolymer changes from the disordered (homogeneous) state to an ordered state (phase separated).

Figure 5.11 shows the $G''(t)$ at ω = 0.1 rad/s. Again three groups of curves are evident. The loss modulus curves at $T < T_s$ increase with time monotonically. The second group is in the temperature window $T_s < T \leq 200$ °C, where G'' all show a maximum at the time frame of about 80 to 120 minutes. Comparison of G'' and G' (at $\omega = 0.1$ rad/s and $T > T_s$ in Figure 5.10) shows that the time frame within which G'' shows maximums coincides exactly with the time at which G' curves are at their fastest growing speed (the slope of G' is the greatest at 80 to 120 minutes in Figure 5-10). The third type of $G''(t)$ behavior in Figure 5.11 is at 210 °C. The difference between curves at $T \leq 200$ °C and 210 °C is more apparent at lower frequency (in Figure 5.10 and 5.11), which indicates the sensitivity of the structure to the mechanical movement at high temperature (higher frequency may suppress the rheological response of the structural changes such as at $\omega =$ 1 rad/s).

Rosedale and Bates [1990] used the crystallization process in crystalline polymers as an analogy to represent the ordering kinetics in block copolymers. They proposed that $G'(t)$ could be modeled by the Avrami Equation [Avrami 1939 and 1940] for the dimensionless parameter $X(t)$.

$$X(t) = 1 - e^{-kt^n} \qquad (5.3-1)$$

where

$$X(t) = \frac{G'(t) - G'(t_0)}{G'(t_\infty) - G'(t_0)} \qquad (5.3-2)$$

which varies from 0 to 1.0.

Here $G'(t_0)$ is the initial storage modulus at time $t = 0$ and $G'(t_\infty)$ is the equilibrium value achieved at long times. It is also useful to define $t_{1/2}$ and t_∞ as the times at which G' reaches the half ($X = 1/2$) and full ($X = 1$) increments. t_∞ was taken as the time at which

G' increment was less than 30 Pa within the hour that followed. The reason which justifies the use of $t_{1/2}$ is that some curves rise quickly at the early stage and then take very a long time to reach a steady state value. Using t_∞ only would be misleading in some cases. Both $t_{1/2}$ and t_∞ at different temperatures are listed in Table 5.2, at $\omega = 0.1$ and 1 rad/s, so that the effect of ω can be assessed.

In Table 5.2, $t_{1/2}$ and t_∞ at $\omega = 0.1$ rad/s are longer than at $\omega = 1$ rads/s, which indicates the degree of assistance or interference of frequency in the ordering process. Higher frequency exerts more movements on the polymer molecules and helps the diffusion of both single molecules and PS domains (hence, shorter $t_{1/2}$ and t_∞). At $T > T_s$, t_∞ is approximately double $t_{1/2}$. But at $T < T_s$, t_∞ is almost ten-times of $t_{1/2}$. For example, at 164 °C (just below T_s = 167 °C), the $G'(t)$ curves take 595 and 680 minutes to reach t_∞ at $\omega = 1$ rad/s and $\omega = 0.1$ rad/s respectively, while $t_{1/2}$ value are much shorter (35 and 60 minutes respectively).

The $t_{1/2}$ and t_∞ in Table 5.2 are also plotted in Figure 5.12. At $T > T_s$, $t_\infty \cong 2 \times t_{1/2}$. But below the *MST*, $t_\infty >> t_{1/2}$ ($t_\infty \cong 6 \times t_{1/2}$). $t_{1/2}$ drops when cooled through T_s, while t_∞ increases dramatically. The abrupt change of $t_{1/2}$ and t_∞ at T_s reveals the fundamental difference between the structures formed in these two temperature regimes (above and below T_s). Below *MST*, the process of transforming the sample from homogeneous material to microphase separated material is quick in the early stage but takes very long to complete. The change of G' at $T > T_s$ is less dramatic and at relatively constant speeds

Table 5.2: $G'(t)$ Time Characterizations of Ordering Process for SIS-4111*

T (°C)	$\Delta T = T_s - T$ (°C)	$t_{1/2}$ (mins)	t_∞ (mins)	$t_{1/2}$ (mins)	t_∞ (mins)
	± 2	at ω = 1 rad/s		at ω = 0.1 rad/s	
140	37	98	660	≅ 200	>1200**
150	27	80	595	105	800
164	3	35	510	60	680
$T_s \cong 167$ °C	0	--	--	--	--
170	-3	135	295	155	340
180	-13	105	190	127	280
190	-23	83	165	90	215
200	-33	68	150	105	195
210	-43	145	300	230	390

* Where $t_{1/2}$ is the time when G' reaches its half increment, and t_∞ is when G' reaches its final staedy-state value.

** After 20 hours $G'(t)$ still has a strong tendency to grow, so we assume t_∞ is too long for practical experiment.

In Figure 5.13, the storage modulus values measured at two different sampling time intervals are plotted (both at 164 °C), which illustrates how the mechanical movement of the rheometer has affected the ordering process. At ω = 1 rad/s, the two G' curves were measured at two sampling time intervals. One group of data was collected at 5-minute intervals (filled diamond symbols in Figure 5.13), and another group at 1-minute intervals (open circular symbols). The G' measured at 1-minute intervals will reach a steady state value much faster than those measured at 5-minute intervals. Apparently the shearing movement that the rotating platen exerts on the copolymer helps the sample to achieve its stable microstructure, whatever the microstructure might be. When these two curves reach their steady-state values, the microstructures they

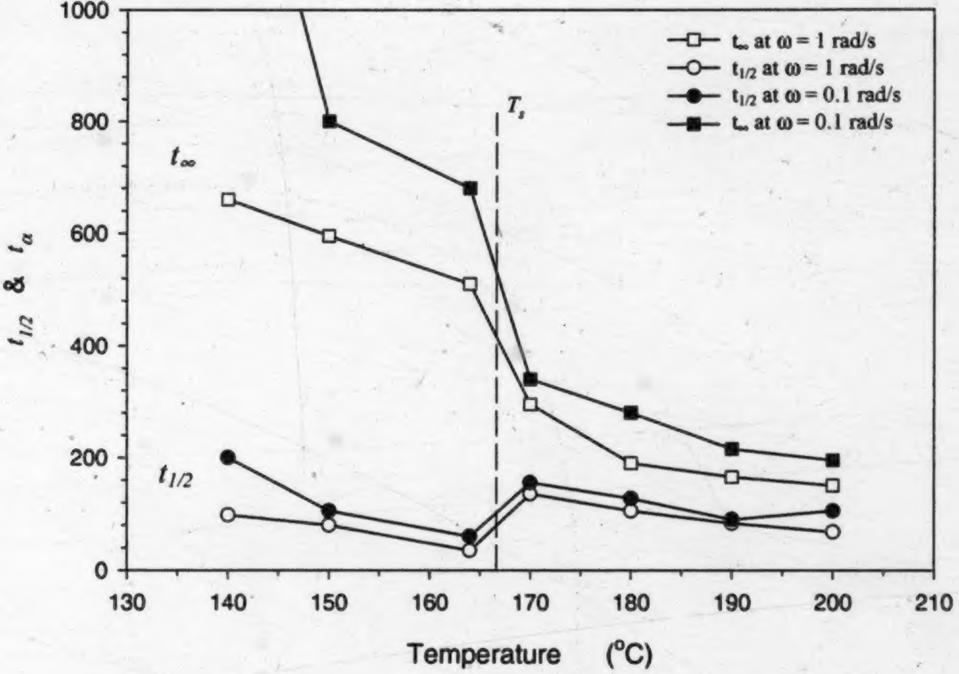

Figure 5.12: Plot of $t_{1/2}$ and t_∞ for sample SIS-4111, at two different frequencies.

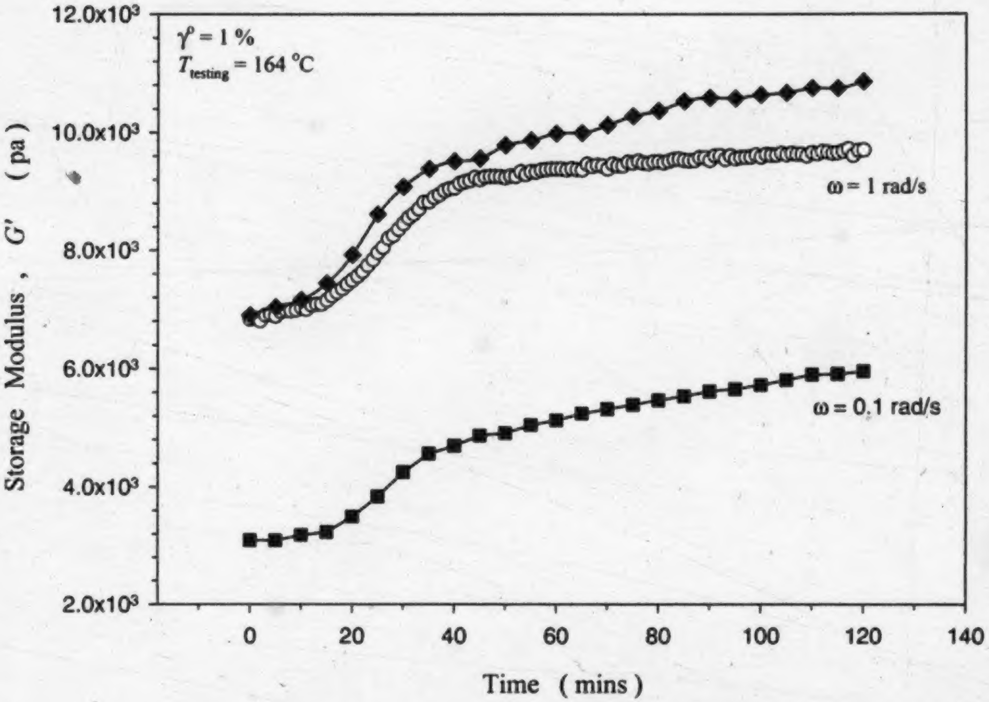

Figure 5.13: The effect of sampling time interval on temporal evolution of G' of SIS-4111, at T = 164 °C. The filled symbols represent the data taken at 5-minute time interval, and open symbols represent data measured at 1-minute time interval.

represent may be different. (The total increment of G' at different measuring intervals are different in Figure 5.13; since the evolution of G' is a measurement of the structure forming process, different $\Delta G'$ values indicate different degrees of ordering).

The G' curves, measured at 5-minutes interval at two different frequencies, have the same growing speeds. Since, between the 5-minutes (or 1-minutes for that matter) time interval, the sample is virtually stationary between platens, it is obvious that shearing the copolymer sample more often produces higher speed of structural formation. Shearing a sample at two different frequencies but at both at 5-minutes interval produces the same speed of forming the microstructure, even though the two microstructures are different.

The $G'(t)$ curves in Figure 5-13 are also curve-fitted by an empirical equation:

$$y = y_0 + \frac{a}{1 + (\frac{x}{x_0})^{-b}} \qquad (5.3\text{-}3)$$

where $y = G'$, $y_0 = G'_{t=0}$, $a = \Delta G' = (G'_{t\to\infty} - G'_{t=0})$, $x = t, x_0 = t_{1/2}$ and $b = 2$ for data taken at 5-minute time interval and $b = 3.57$ when G' were measured at 1-minute time interval, where $G'_{t=0}$ is the initial G' value at $t = 0$ and $G'_{t\to\infty}$ is the steady state value at very long time. The $t_{1/2}$ is the same as defined in Table 5.2. The value of exponent b ($\equiv 2$ and 3.57) are calculated only based on the data in Figure 5.13 (up to 120 minutes and G' is far from reaching the steady value). Thus a completed curve-fitting was performed for data in Figure 5.6 and 5.10 (t up to 700 minutes). The b values are listed in Table 5.3.

Table 5.3: The Value of Exponent b for SIS-4111 (Figures 5.6 & 5.10)*

T-regime	$\omega = 0.1$ rad/s	$\omega = 1$ rad/s
$T < T_s$	$b \cong 1$	$b \cong 1$
$T > T_s$	$b \cong 3.9$	$b \cong 2.4$

* at 5- minute time intervals. See page 5.35.

Thus, Equation 5.3-3 becomes:

at $T < T_s$ (both ω)

$$G' = G_0' + \frac{G_\infty' - G_0'}{1 + (\frac{t}{t_{1/2}})^{-1}} \qquad (5.3\text{-}4)$$

at $T > T_s$ (two ω)

$$G' = G_0' + \frac{G_\infty' - G_0'}{1 + (\frac{t}{t_{1/2}})^{-2.4 or -3.9}} \qquad (5.3\text{-}5)$$

Equations 5.3-4 and 5.3-5, I found, are better both in terms of curve fitting and expressing the physical meaning of the ordering process than Equation 5.3-1 and 5.3-2, particularly within the temperature range right below the *MST* transition (at 160 and 164 °C). Outside of this narrow temperature window, however, Equation 5.3-1 may be better suited (after all, this form of equations such as Equation 5.3-3 are specifically used for sigmoidal curves). Equation 5.3-2 uses two parameters that are related to the speed of the microstructure formation: k and n (disregarding G_0' and G_∞', which are related only to the initial and final states of the material). Both parameters characterize the ordering process in their own way and balance each other. So it is hard to use either one of them solely (we have found that, with changing temperatures, one parameter increased and the other decreased, or visa versa). In Equation 5.3-3, however, only one parameter (*b*) is used. Thus, it can be used as the sole indicator of the speed of structure formation. With increasing *b*, the speed of G' to reach G'_∞ increases.

From Figure 5.13, it is obvious that the more often the sample was sheared (high ω) the higher value of the exponent *b*, which in turn indicates a higher speed of structure formation. The frequent mechanical shearing movement accelerates the migration of the PS domains. The mechanical energy imported helps to ease up the friction between the PS domain and PI matrix and overcomes the energy barrier.

From Equation 5.3-4, it is clear that for $T < T_s$ frequency affects *b* a little (the exponent *b* at $\omega = 1$ rad/s is slightly larger than 1). However, $\Delta G' (\equiv G'_\infty - G'_0)$ is about the same for both frequencies ($\cong$ 5000 pa). This means that, given the same $\Delta G'$ or the same initial and final state of the sample, the microstructure does grow a little faster at $\omega = 1$ rad/s than at $\omega = 0.1$ rad/s. This is also manifested in Table 5.2, where for $T < T_s$ t_∞ is 510 and 680 minutes, at $\omega = 1$ rad/s and $\omega = 0.1$ rad/s respectively. This (ω affects *b* little at $T < T_s$) is, though, not 100 % correct at lower temperatures (such as 140 °C). Part of this may due to the unsuitability of applying the empirical equation to the curves at lower temperatures.

Equation 5.3-5 shows that, at $T > T_s$ however, the exponent b is larger at lower frequency ($b_{\omega=0.1} \cong 1.6 \times b_{\omega=1}$). But $\Delta G'(\equiv G'_\infty - G'_0)$ is, on the other hand, also larger ($\Delta G'_{\omega=0.1} \cong 2 \times \Delta G'_{\omega=1}$). This produces a result hard to interpret. At $\omega = 0.1$ rad/s, the speed for G' to grow from G'_0 to G'_∞ is faster, but the difference between G'_0 and G'_∞ is also greater. The speed of the mechanical shearing movement not only affects the speed of the structure formation (or composition fluctuation), but also affects the final state of the material.

Apparently, below the *MST* transition ($T < T_s$) the mechanical shearing does not change the final state of the microstructure much, but does accelerate the structure formation a little with higher frequency. Above the *MST* transition ($T > T_s$), however, the changes of the microstructure, as well as the speed of the changes are greatly affected by the mechanical shearing that the rheometer imposes.

Figure 5.14 shows the temporal evolution of G' at 160 and 164 °C, representing quench depth ΔT =7 and 3 °C respectively. By measuring at 1-minute time intervals, we carefully expand the region where the ordering process initially takes place, namely, at the early 40 to 100 minutes. (The data points wouldn't be enough to show a complete curve if measured at 5-minute intervals). The $G'(t)$ curve at 164 °C clearly shows a three-stage increase pattern. The curve at T = 160 °C shows a similar pattern except the first stage is shorter.

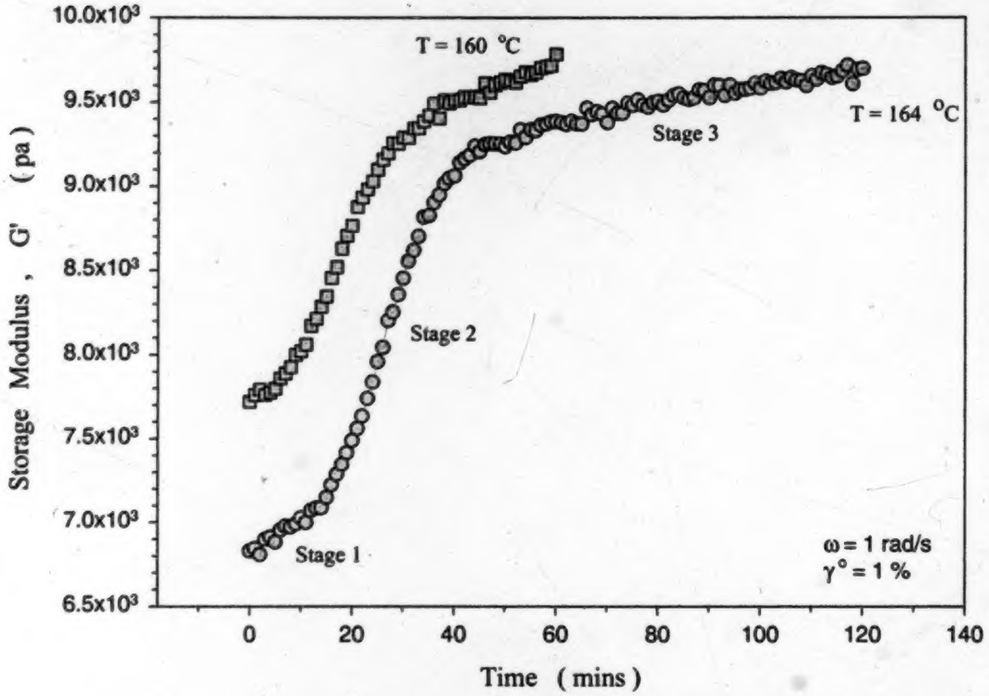

Figure 5.14 :Temporal evolution of *G′* at $\omega = 1$ rad/s and $\gamma^{\circ} = 1$ %. Measuring at 1-minute time interval. At T = 164 °C, $G'(t)$ curve displays a distinctive three-stage shape. At lower temperature (*e.g.* at T = 160 °C), the first stage is shortened. At lower temperatures (140 and 150 °C), $G'(t)$ curves lose this distinctive shape.

The mean-field treatment of order and disorder in block copolymers by Leibler [1980] predicts a stability limit just below the *MST*, and a critical point for $f = ½$ (f is the overall composition of one component in the block copolymer). On the basis of this theory, Hashimoto [1987] proposed a time-dependent Ginzburg-Landau treatment for the ordering process in block copolymers following a temperature quench from the disordered state. This approach closely resembles traditional spinodal decomposition theory [Cahn 1965]]

Fredrickson and Helfand [1987] have demonstrated that the introduction of fluctuation corrections to Leibler's theory completely suppresses the stability line, thus eliminating the second-order (i.e. continuous) critical point. Therefore, we do not expect Hashimoto's approach (giving SD-like behavior) to describe the ordering kinetics correctly since, within the context of fluctuation theory, there is no stability limit. Instead, we anticipate a nucleation and growth mechanism, as is commonly encountered for systems undergoing a first-degree transition.

Fredrickson and Binder [1990] developed a homogeneous nucleation and growth theory for nearly symmetric diblock copolymers based on the previously described fluctuation picture. These authors predicted a narrow temperature region of slow ordering kinetics just below the *MST*, consistent with our experimental findings. Unfortunately, no theoretical work of this sort on triblock copolymers has been found.

Rosedale and Bates [1990] studied a series of poly(ethylenepropylene)-poly(ethylethylene) diblock copolymers. By carefully comparing their experimental data with the prediction of the Fredrickson and Binder theory, they believed that homogeneous (primary) nucleation is not the controlling mechanism. This is well known in homopolymer (such as polyethylene) crystallization where secondary nucleation determines the crystallization kinetics at moderate undercoolings. Thus they concluded that a heterogeneous (secondary) nucleation governs the ordering process near the *MST*.

When passing through *MST* (cooling through *MST*), the block copolymer goes through a drastic change. The near-homogeneous liquid material forms a microphase separated solid material (with microphases interconnected with each other, the block copolymer behaves much like a crosslinked polymer). Accompanying this transformation, the rheological functions, such as G', G'', η' and η'', will all have dramatic increases (generally, these functions have higher values for solids than for liquids). This has been shown in Figure 5.6 through Figure 5.12 (at $T < T_s$). The way the storage and loss modulus changed after the sample was cooled through T_s reveals the ordering process that the sample has gone through. It is to study these changes that we investigate the mechanism of the microphase forming.

In Figure 5.14, the storage modulus is plotted at 160 and 164 °C. The curves are labeled stage 1, stage 2 and stage 3 to correspond to the three different growth stages. The ordering process, we propose, follows a procedure like nucleation and growth, as schematically illustrated in Figure 5.15. In the first stage ($t = 0 \sim 15$ mins., at $T = 164$ °C)

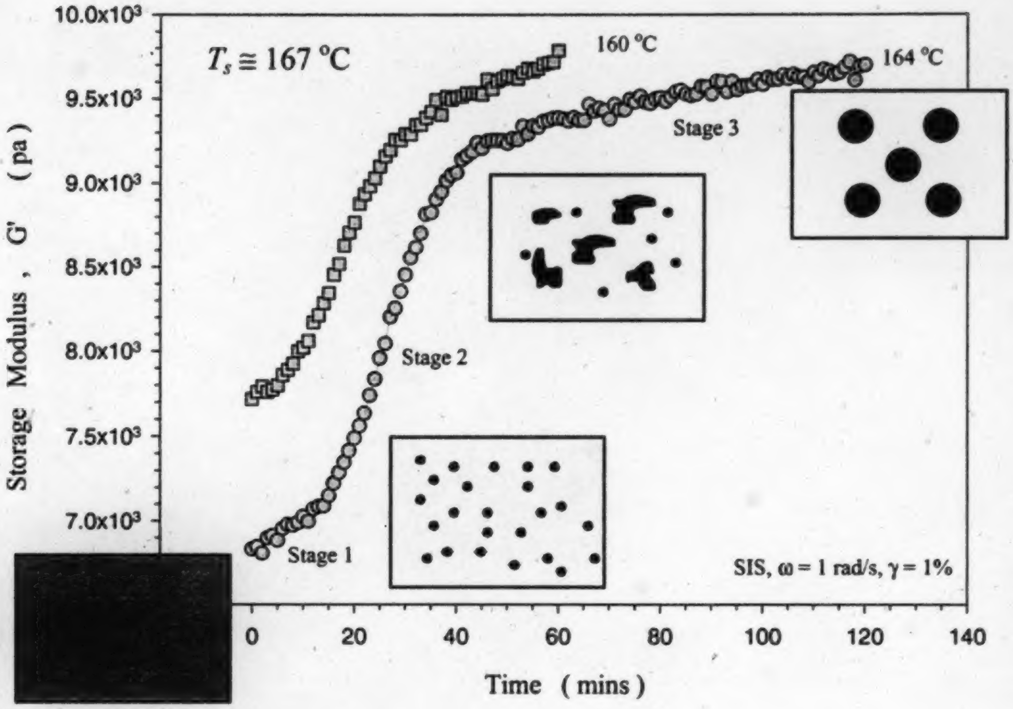

Figure 5.15: Temporal evolution of G' at T = 160 and 164 °C, which are 7 and 3 degrees below T_s, respectively. At 164 °C, the microstructure evolves from homogeneous (disordered) state (t = 0) to particle-filled system ($t \cong 15$ mins) and then a two-phase state ($t \cong 40$ mins), and finally to a body-centered-cubic lattice structure (t

the copolymer molecules and associated S-blocks diffuse through a homogeneous medium to form small S-particles scattered throughout the sample (nucleation). G' increases nearly linearly with time. The microphase separation, however, is almost completed in this stage. The time required for microphase-separation agrees well with what was reported by Winter *et al* [1993] (~20 minutes).

In the second stage (t = 15 to 40 mins. at T = 164 °C), those small PS particles migrate through PI matrix to aggregate and form large PS domains (growth), a process that transforms a particle-filled homogeneous matrix material into a two-phase heterogeneous material. In responding to this phase change, $G'(t)$ takes a jump of 2200 pa (from 6900 to 7100 pa) in a short time (25 minutes). In stage 3, the PS domains gradually move onto a body-center-cubic (bcc) lattice of PS microdomains. The latter procedure takes almost 10-times longer than the first two stages, due to the low diffusion coefficient for PS domains. At this stage, the network structure is nearly complete. The PS domains, with the center PI blocks of their molecules mingled and entangled with other PI blocks in the PI medium, will have tremendous thermodynamic barriers to overcome. This process is extremely slow and difficult. Thus, t_∞ is very long (indeed, there is no end to the 3rd stage process observed on the time scale of Figure 5.10, at 140 °C for example). The time scale for this stage also agrees well with that reported by Winter *et al.* [1993] (11 hrs.).

At 160 °C, a similar shape of curve indicates a similar ordering process (except that the first stage is shorter). This is because at greater quench depth, the nucleation process will be faster with a higher thermodynamic driving force (because the sample is a little supercooled). Part of the nucleation process might even be complete during the quench procedure. Such is the situation at 140 and 150 °C (in Figure 5.6 and 5.10). The first stage of ordering (nucleation) at these temperatures is either completed during the quench process, or the molecules are simply being frozen into some intermediate stage that could not complete the nucleation process (due to slow-down of kinetic processes at lower temperatures). The *G′* curves lose the three-stage character and grow monotonically. This is more evident at low frequency (in Figure 5.10). The storage modulus at 140 °C grows much slower than that at 150 °C, and takes a much longer time to reach the final equilibrium state (if it will ever reach such an state).

The 2nd stages of the *G′* curves (at 160 °C and at 164 °C in Figure 5.15) look similar, except the transitions from the 1st stage to the 2nd stage and from the 2nd stage to the 3rd stage are a little smoother. Both grow at the same speeds and take the same time to finish (about 25 minutes). The growth stages at these two temperatures are not much affected by the 4 degrees of temperature difference, except the transient from stage to stage is not as distinct at lower temperature, due to less molecular mobility. The 3rd stages again are very similar (in Figures 5.15 and 5.6).

By comparing the *G′* curves at 160 and 164 °C, it is clear that the quench process plays an important role in the microstructure formation. At right below T_s (164 °C) and 4 degrees lower (160 °C), the quenching only affects the 1st stage, namely accelerating the nucleation process and making the transition between stages a little smoother. But at lower temperatures (140 and 150 °C in Figure 5.6 and 5.10), the super-fast cooling clearly changes all of the ordering process. It may no longer be nucleation and growth. And to anneal the sample at the right temperatures to achieve the most desirable microstructures becomes important (this will be discussed in Section 5.3.3).

At $T > T_s$, however, the rheological functions are expected not to be functions of time; at these temperature ranges, the block copolymer samples are supposed to be in a homogeneous (disordered) state at which the rheological functions are constant with time (only functions of temperature). Surprisingly, both G' and G'' appear to be changing with time too (in Figures 5.6 to 5.11).

Some other workers have also reported that such properties change with time above *MST*. By using SANS [Morrison *et al* 1990] and rheology [Rosedale and Bates 1990, Xie *et al* 1994], these changes have been tracked, in some cases [Rosedale and Bates 1990] as high as 50 degrees above T_s. They [Rosedale and Bates 1990] have attributed this to the composition fluctuation effects. According to Leibler's theory [1980], the *MST* transition is induced by the local composition fluctuation. As the temperature approaches the T_s (from above T_s) the composition fluctuation increases its magnitude and eventually causes microphase separation. These composition fluctuations could occur at temperatures above T_s, especially if accompanied by certain mechanical shearing movement. In our cases, the oscillatory shearing movement of the platen causes the copolymer molecules to congregate locally (composition fluctuation). This change in local composition will cause the storage modulus to increase. The G'' function, however, increases and then decreases with time, reaching a maximum at the same time that G' has the fastest speed of growth. G'' is also an indication of the viscosity (since $G'' = \eta'\omega$, where ω is a constant in this case). When the local molecules reconfigure and fluctuate at the full speed, the viscosity increases and reaches a maximum. But when this fluctuation reaches an equilibrium state, where the material is still in a liquid state, the viscosity drops (Figure 5.11).

In Figure 5.16 the storage and loss modulus were measured at $T = 164$ °C (quench depth $\Delta T \cong 3$ °C) with $\omega = 0.1$ rad/s and 1 rad/s. The $G'(t)$ curves have the similar S-shape at both high and low frequencies. But at low frequency ($\omega = 0.1$ rad/s), $G'(t) > G''(t)$ (Figure 5.16a). However, at high frequency ($\omega = 1$ rad/s), $G'(t) < G''(t)$, with the tendency for the two functions to cross over each other at a certain time (Figure 5.16b). High frequency clearly has suppressed the response of microstructure. In Figure 5.16a, the sample shows a solid-like response from time zero ($G'(t) >> G''(t)$, which means the the rheological function characterizing the solid-like properties (G'') has a greater value than that characterizing the liquid-like properties (G')). At high frequency (Figure 5.16b) the response of microstructure has a tendency of transforming from liquid-like to solid-like (from $G'(t) < G''(t)$ to $G'(t) > G''(t)$). Figure 5.17 shows the $G'(t)$ and $G''(t)$ curves at $T = 190$ °C ($T - T_s \cong 23$ °C). At both high and low frequency, $G''(t) > G'(t)$ initially and then crosses over. The transition from liquid-like to solid-like behavior occurs at around 75 ~ 80 minutes, at both frequencies. The $G'(t)$ at low frequency (Figure 5.17a) shows the

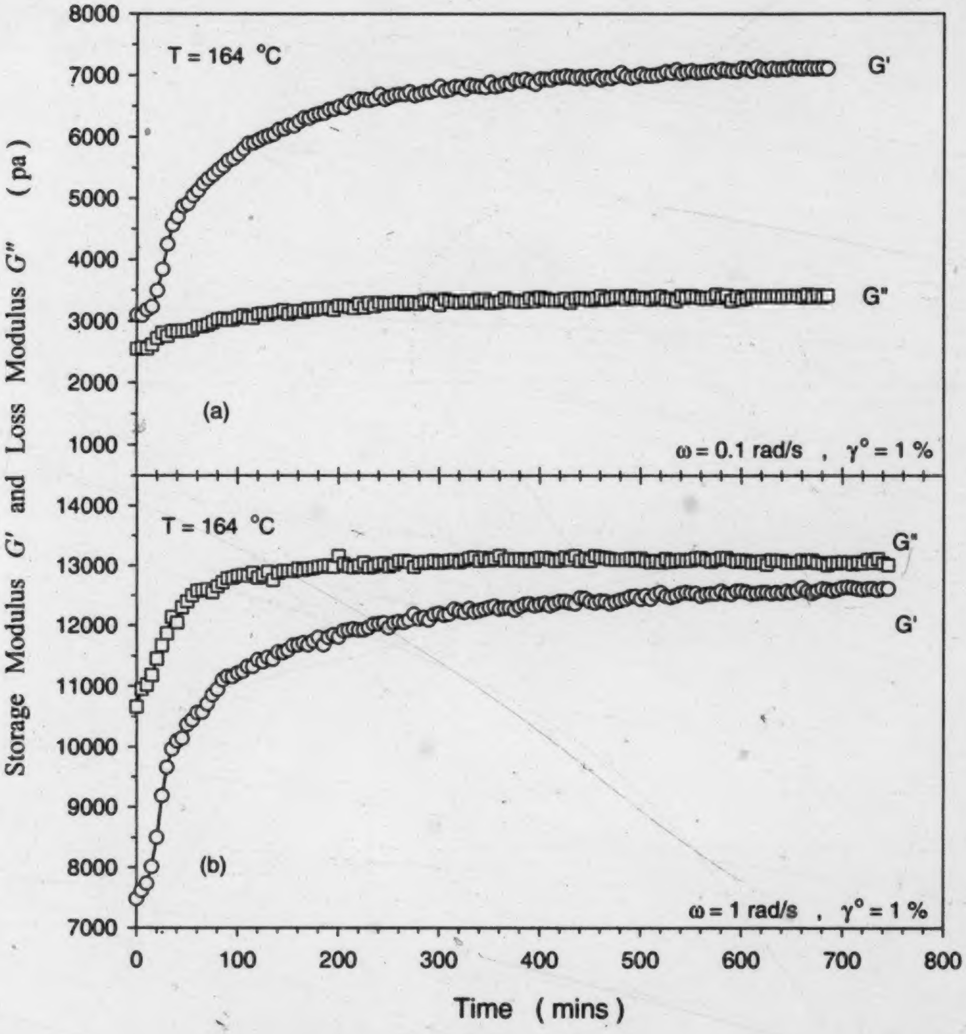

Figure 5.16: Temporal evolution of G' and G'', of sample SIS-4111, measured at 164 °C (quench depth $\Delta T \cong 3$ °C), with (a) $\omega = 0.1$ rad/s and (b) $\omega = 1$ rad/s. Strain amplitude is 1 % in both cases. In 5-16(a) $G'(t) > G''(t)$, while in 16(b) $G'(t) < G''(t)$ with a tendency to cross over at long times.

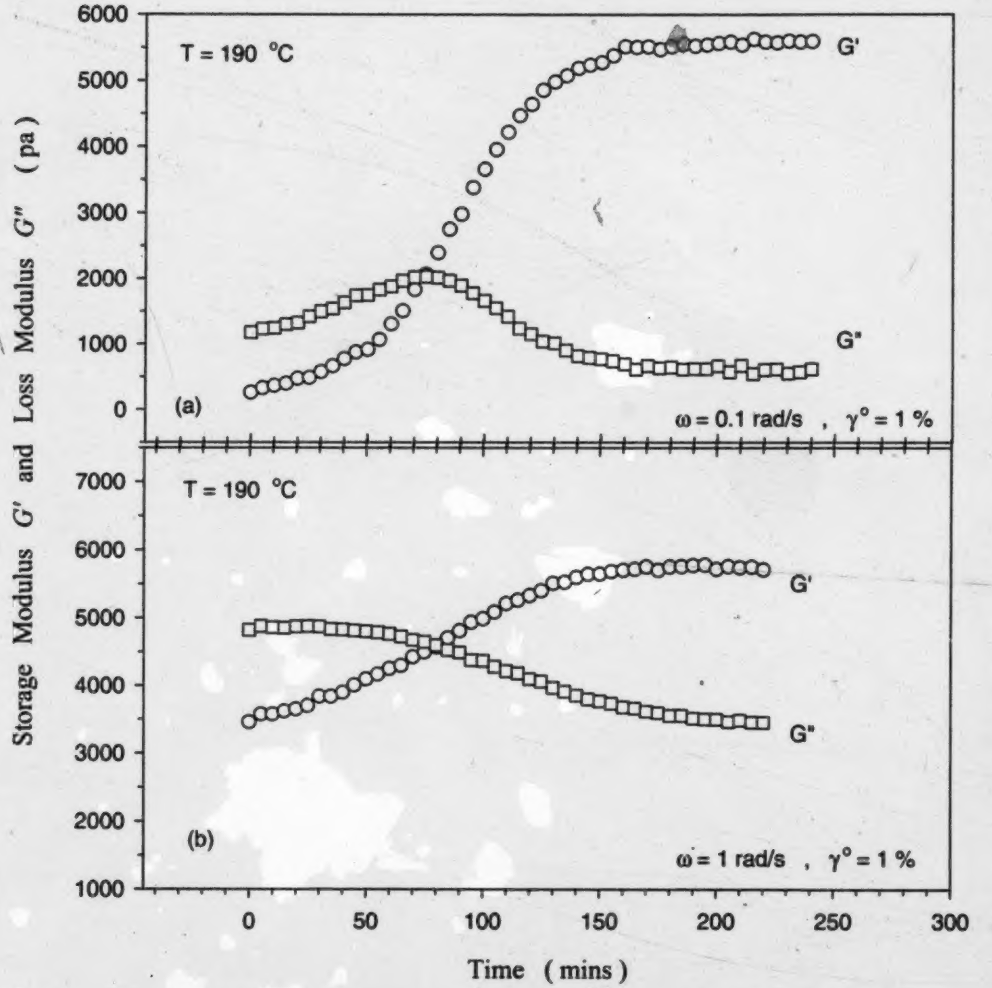

Figure 5.17: Temporal evolution of G' and G'', of sample SIS-4111, measured at 190 °C ($T - T_s \cong 23$ °C), at $\omega = 0.1$ rad/s (17a) and $\omega = 1$ rad/s (17b).

same S-shape as in Figure 5.14, though loses the S-shape details at high frequency (Figure 5.17b).

Comparing the storage and loss modulus measured at $T > T_s$ and $T < T_s$, it is clear that the microphase structures are very sensitive to frequency. In Figure 5.16, the sample behaves like solid throughout the test at lower frequency ($\omega = 0.1$ rad/s, in Figure 5.16a), while at higher frequency G'' always has a higher value than G' although after 200 minutes these two functions are almost equal. High frequency clearly suppresses the solid behavior in the sample, even though at this temperature (164 °C) the material is phase-separated. In Figure 5.17, however, the difference caused by frequency is diminished. The different behavior of these functions below and above T_s reveals a subtle difference between the structure formed below and above the *MST*. The microphase-separated structure developed below T_s is essentially a weak solid structure. Low frequency tests reveal the solid character but the high frequency test very much disturbs the structure and shows the predominant liquid properties. At $T > T_s$ (Figure 5.17), the sample behaves liquid-like at time zero, no matter what frequencies, and transforms into solid-like material within the same time frame. The $G'(t)$ and $G''(t)$ curves at other temperatures (either above or below T_s) all indicate similar results.

5.3.3 The Effect of Annealing

It is both interesting and important to understand the effect of annealing on the block copolymers and how to achieve certain desired microstructures and properties by annealing the samples at some proper temperatures. As we have discussed in the previous sections, the cooling procedure plays a very important role in the microstructure formation, which in term dictates the properties of the block copolymers. How fast to cool the sample and cool to what temperature for annealing will alter the ordering process greatly. In this section, we try to answer these questions by annealing the block copolymer sample at certain temperatures and then comparing the rheological properties measured to those without being annealed.

The block copolymer sample is first heated to a higher temperature ($T > T_s$, usually 200 °C) to ensure homogeneity. The sample is then quenched to the testing temperature. The $\eta'(\omega)$ and $\eta''(\omega)$ functions are measured immediately after the quench for one sample, while another sample goes through an isothermal time-sweep (here we call it "annealing") at constant ω and γ° before the $\eta'(\omega)$ and $\eta''(\omega)$ are measured. In other cases, one sample was annealed at a temperature right below T_s and then cooled to the testing temperature.

First, we examine the effect of annealing at temperatures above *MST*. Figure 5.18 shows a typical result for $T > T_s$ (T = 170 °C in this case). Both $\eta'(\omega)$ and $\eta''(\omega)$ are measured at 1% strain amplitude with one sample being first annealed (isothermal time sweep) at 170 °C for 500 minutes. Both η' and η'' show a strong power-law behavior (at $\omega \leq 1$ rad/s) after sample being annealed, while those functions of the sample without annealing show maximum and turn down as $\omega \to 0$ and much smaller values for η'' than for η'.

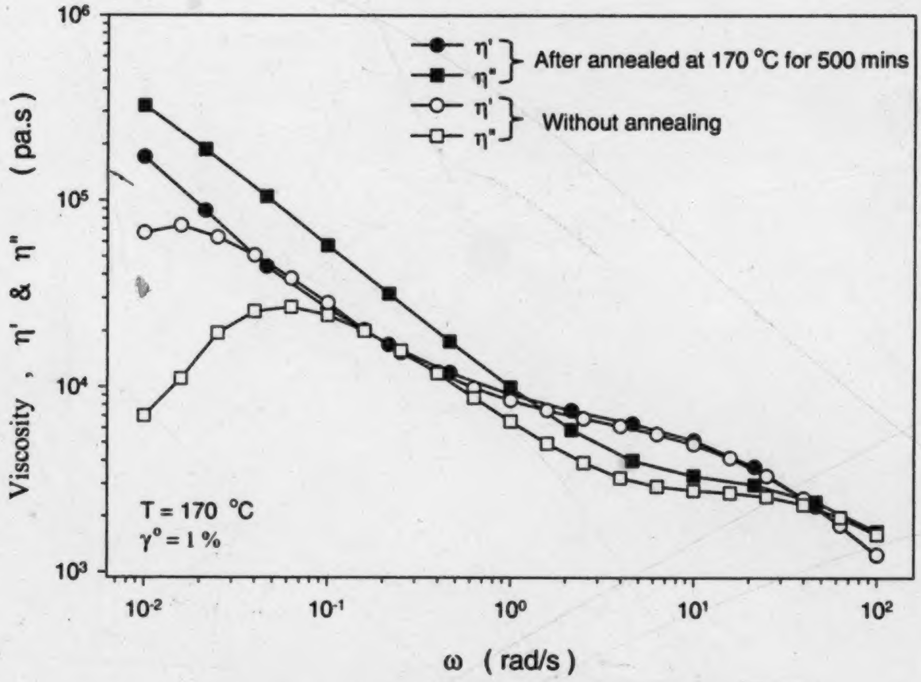

Figure 5.18: Annealing effect of sample SIS-4111 at $T > T_s$. Frequency-sweep test at 170 °C, before (open symbols) and after (filled symbols) being annealed at 170 °C for 500 minutes. Circular symbols represent η' and square symbols represent η''.

Notice the annealed and non-annealed η' functions are almost identical for $\omega \geq \omega_c = 0.04$ rad/s in this case. The η'' function of the sample with annealing is always larger than the η'' function of sample without annealing (except at very high frequency, $\omega = 100$ rad/s). The frequency ω_c increases with increasing temperatures, as we found from similar plots for $T = 180 \sim 200$ °C (not shown here).

At different frequencies the sample responses that the rheometer measures are different. At high frequency, rheology tests the short relaxation-time response of the sample, namely the short-distant (or local) molecular movements in the block copolymer sample. On the other hand, the low frequency test measures the long-range molecular movements (long relaxation time response) as well as the long-range microstructure.

In Figure 5.18, both η' and η'' have the same high-ω value with or without annealing. This indicates that the local molecular movements, short range movements such as the vibration of the segments or small domains, are the same for a sample that has or hasn't been annealed. But the long-range movements measured (at low frequency end) are drastically different. The annealed sample shows a solid-like ($\eta'' > \eta'$) behavior that reveals the existence of long-range microstructure (such as composition fluctuation), which hinders any large molecular movements. The behavior of unannealed sample is more liquid-like ($\eta' > \eta''$). Annealing clearly transfers the block copolymer sample from liquid behavior towards more solid-like.

In Figure 5.19 is shown the typical viscosity functions measured at $T < T_s$ (T = 140 °C in this case). One sample has been annealed at 140 °C for 1140 minutes. Both η' and η'' functions have the same power-law behavior at the low frequency end for samples with or without annealing, while at the high frequency end the functions merge for both annealed and unannealed sample. The viscosity functions have a substantially larger value for the sample that has been annealed ($\eta'_{annealed} \cong 2 \times \eta'_{without\ annealing}$ at $\omega = 0.01$ rad/s). Though the rheological functions measured indicate both samples (with or without annealing) are in solid state, the annealed sample clearly has a stronger structure than the unannealed one. Annealing even at $T < T_s$ gives the block copolymer molecules and microdomains more time to maneuver around to form more equilibrium microstructure. Such movement is physically possible as long as $T > T_g^{PS}$.

But 140 °C is not an ideal temperature for annealing, as we have discussed in the previous section. The temperature is too low and close to the glass transition temperature of the PS domain. On the other hand, we have found that at the temperature right below the *MST*, there is a narrow range of temperatures in which the block copolymer molecules have both thermal driving force and enough mobility to allow the microstructures to grow fully. Thus we chose 164 °C to anneal the next sample. The results are shown in Figure 5.20.

In Figure 5.20, the viscosity is measured at 100 °C, with one sample being annealed at 164 °C for 740 minutes and one without any annealing. The testing

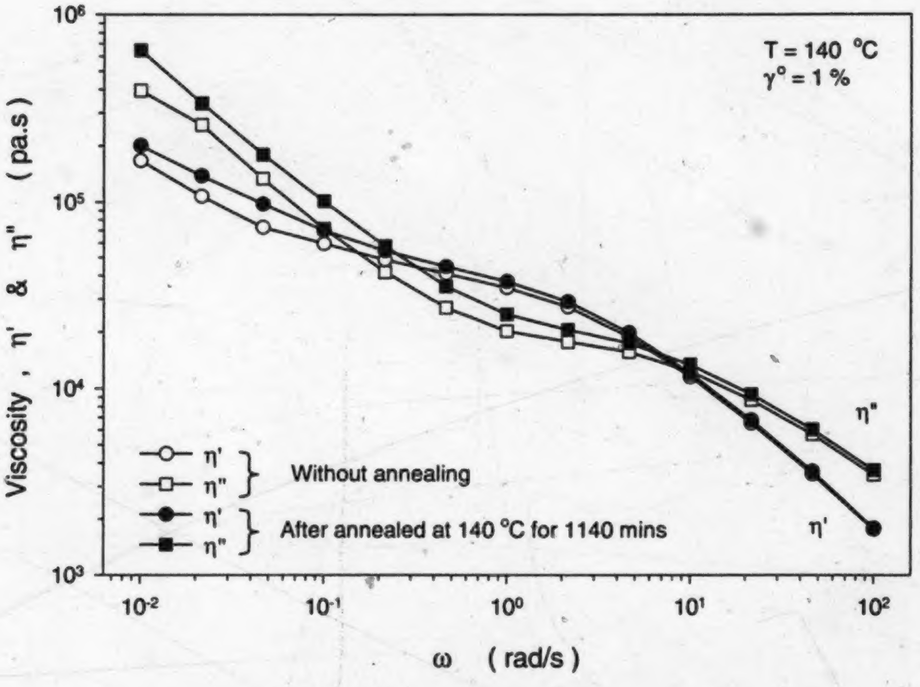

Figure 5.19: Annealing effect of sample SIS-4111. Frequency-sweep test at 140 °C before (open symbols) and after (filled symbols) being annealed at 140 °C for 1140 minutes. Circular symbols are *η′* and square symbols are *η″*.

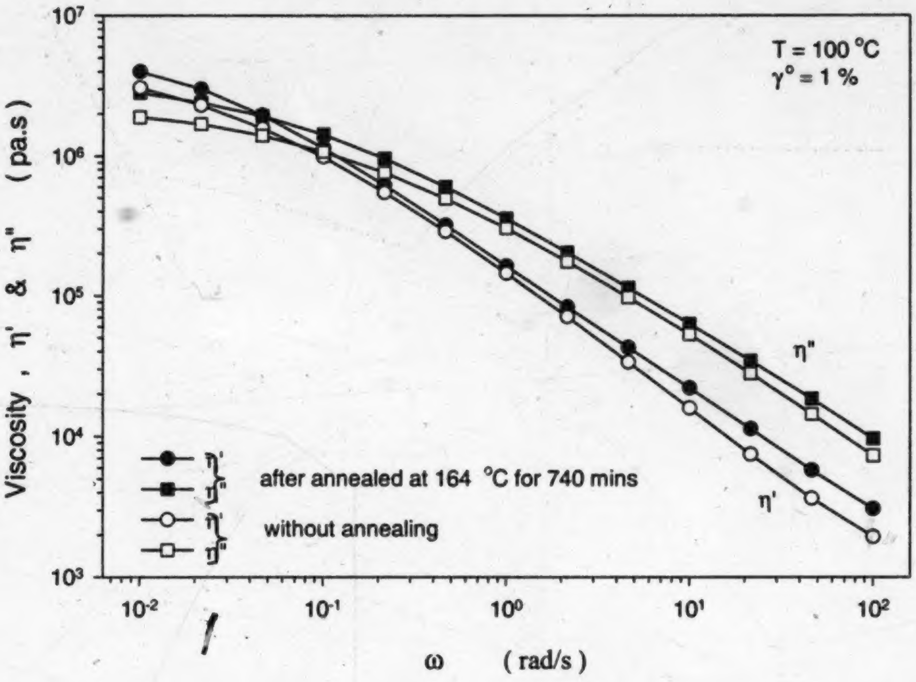

Figure 5.20: Frequency-sweep test at 100 °C, with (filled symbols) and without (open symbols) being annealed at 164 °C for 700 minutes. Circular symbols are η' and square symbols are η''.

temperature is relatively low and close to the T_g of the PS domain (we measured at around 70 °C). Though having the same shape, both η' and η'' functions of the annealed sample have much larger value (20~60 % higher) in the entire frequency range. As for viscosity at temperatures around T_s (140 °C and 170 °C in Figures 5.18 and 5.19, for example), the η' and η'' will always have the same values at the high frequency end for samples either with or without annealing. But in Figure 5.20, the viscosity functions of the annealed sample are always larger than those of the unannealed sample. This means that, in the case of annealing at the testing temperatures (in Figure 5.19 at 140 °C for example), the short-range (or local) structures are the same though the long-range structures are different after annealing. This is understandable because the short-range structures are formed during the quench and soon after the sample reaches the testing temperature, while the long-range structures take much longer time to develop.

Since the samples (in Figure 5.19) reach the testing temperature through the same quench process, the viscosities are the same at the high frequency end, but differ substantially at the low frequency end after one sample has been annealed. In the case of annealing at the temperatures right below the *MST*, at which even the short-range (or small local structures) structures have enough time to develop fully, as well as the long-range structure such as the body-centered-cubic structures, the viscosities of the annealed sample are always larger (Figure 5.20). Thus annealing at the right temperatures seems to be crucial for forming the final equilibrium structures, in our study of the body-centered-cubic lattice.

Figure 5.21 demonstrates the difference when a sample has been annealed at the temperature right below T_s ($T = 164$ °C and quench depth $\Delta T \cong 3$ °C). The annealing time is chosen to be 40 minutes, for the reason as being illustrated in Figure 5.21(a)--the nucleation and growth process is complete within the first 40 minutes. In Figure 5.21(b)-(d), the samples which were annealed at 164 °C show a big difference. The G' curves of annealed samples are larger and grow much more slowly than those of samples without annealing. Without annealing, the sample undergoes microphase separation gradually in supercooled condition, as shown in Figure 5.21 by the filled symbols. The lower the temperature, the more gentle the slope as G' growing. As for the annealed samples, the PS domains have less mobility to move around and develop into the bcc lattice at 130-160 °C, since the nucleation and growth procedure is completed during annealing. Thus the slope of G' grows is insignificant.

5.4. Conclusions

In this report I present a rheological investigation of the ordering phenomena of an asymmetric styrene-isoprene-styrene triblock copolymer around the microphase-separation temperature. A narrow temperature range right below the *MST* was found within which the ordering process could be carefully studied. A three-stage growth pattern of storage modulus $G'(t)$ has been observed, which resembles a nucleation and growth process. The ordering process is much slower at low temperature than those at temperatures near T_s. The frequency of rheological dynamic testing has been found to have the effect of accelerating the ordering. The process of forming the lattice structure

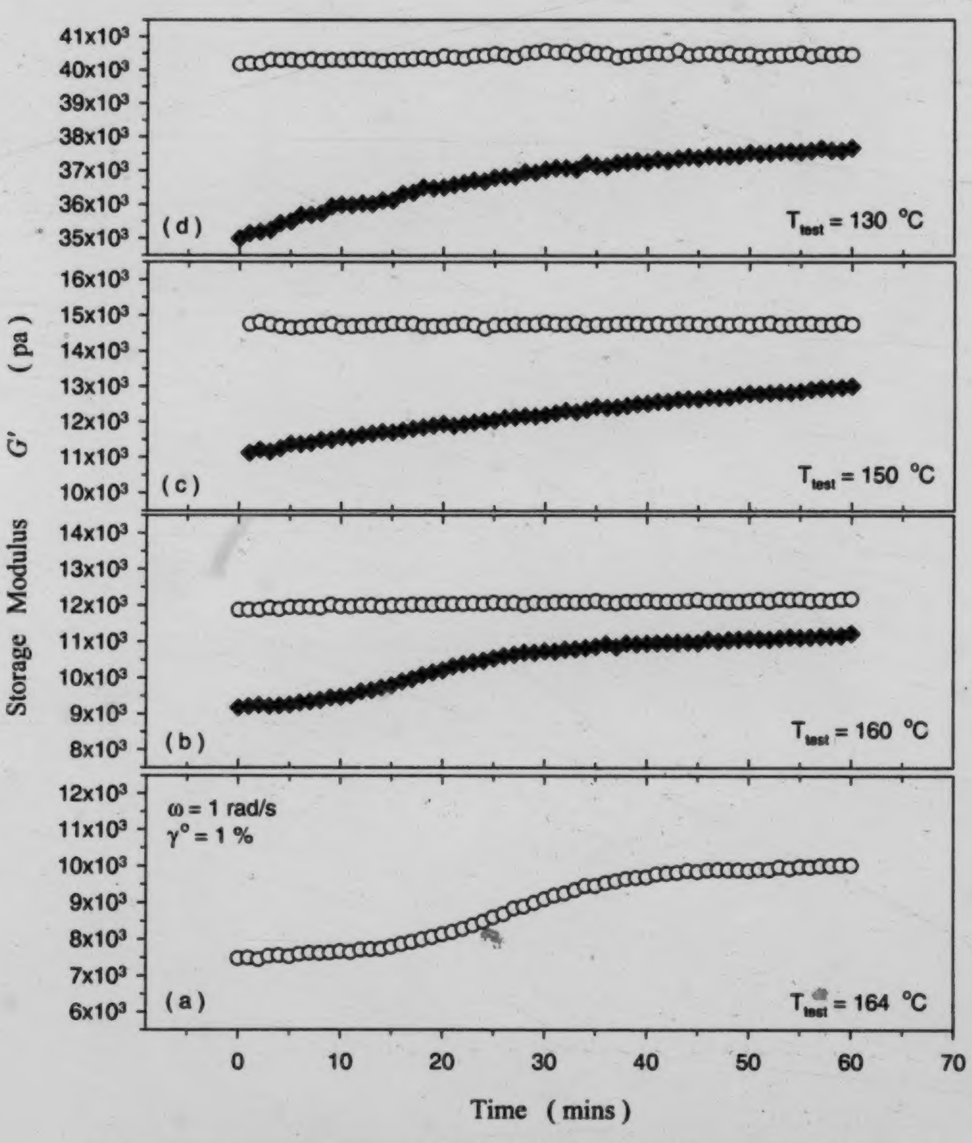

Figure 5.21: The effect of annealing., for SIS-4111. Figure 5.21(a) shows the sample being annealed at 164 °C for 40 minutes. Figures 5.21(b)-(d) show comparisons of samples that have not been annealed (filled symbols) with samples that have been annealed at 164 °C for 40 minutes (open symbols, sample has gone through the process in Figure 5.21(a) before being further cooled to the testing temperatures).

takes the majority of the time. The oscillatory shearing movement in dynamic testing is believed to cause composition fluctuation above T_s. For the two frequencies used in this study, the microstructure formation below the *MST* is relatively insensitive to the frequency. But the composition fluctuation developed above the *MST* is very sensitive to the frequency. The effect of annealing has been also studied. Annealing the sample at right below T_s has substantially shortened the ordering process relative to annealing at lower temperatures and the sample also shows higher values of rheological properties, which in turn indicates larger degree of ordering.

Chapter 6 DSC Study of Heat Evolution of Block Copolymers during their Phase Transition

6.1. Introduction

The properties that make block copolymers unique are determined by the microphase separation. Therefore, it is important from an application standpoint to be able to understand and control the degree of microphase separation and its relation to morphology. Thermal analysis, such as by differential scanning calorimetry (DSC), is an invaluable tool in assessing the extent of phase mixing or phase segregation.

A microphase-separated block copolymer will display several thermal transition temperatures corresponding to those of the homopolymers, such as two glass transition temperatures, each corresponding to one of the major phase, T_g^A and T_g^B for copolymers of block structure AB, ABA, etc. They are generally close to T_g of homopolymers A and B of similar molecular weights. This behavior is different from random copolymers, which usually exhibit only a single T_g at somewhere between T_g^A and T_g^B. Ikeda *et al* [1970] reported two distinct glass transition temperatures for SBS triblock copolymers in their DSC data, one corresponding to the polybutadiene phase and the other to the polystyrene phase. Meyer and Widmaier [1982] used DSC to study SIS triblock copolymers and found a third T_g, besides the two distinctive T_g's that correspond to the PS and PI domains. They interpreted this third T_g in terms of the existence of an interphase. Miyamoto *et al* [1970] also found a change of slope for DSC thermograms at −14 °C, a temperature between T_g^B and T_g^S of a SBS copolymer. They attributed this to a third phase composed of mixed PS and PB caused by incomplete phase separation. Spaans and Williams[1999] observed a region of broad nonlinear curvature, in DSC trace of a SBS block copolymer, between the glass transition temperatures of the two principal microphases. They attributed this curvature to a smoothly varying composition profile through the interfacial region lying between microphases.

Leary and Williams [1974] studied SBS block copolymers and found the microphase-separation temperature (T_s) measured by DSC consistent with their theory prediction. Iskandar and Krause [Iskandar and Krause 1981] used DSC to detect the ODT of a SBS block copolymer. Their approach was to heat the sample above T_{ODT} to make it homogeneous, quench it in liquid nitrogen, and then scan it in DSC heating to verify whether only one intermediate T_g is present (homogeneous) or two T_g's can be detected (phase-separated). All their samples revealed a sharp butadiene microphase T_g as well as a diffuse styrene T_g. They concluded that a two-phase structure still exists after heating and quenching. In principle, if a homogeneous block copolymer is quenched fast enough to a temperature below T_g, it should stay "trapped" in its homogeneous state. If the rate of cooling is not fast enough, phase separation will occur at temperatures below T_{ODT}. Bair [1994] has illustrated this behavior in the case of polyethylenepropylene-polyethylethylene block copolymers. When this system is quenched from room temperature to −100 °C at a rate of 250 °C/min, the copolymer displays only one T_g upon heating. At slow cooling rates, phase separation occurs during cooling, and subsequent heating displays two T_g's. Leung and Koberstein [1986] did succeed in observing a single T_g after heating a polyurethane block copolymer sample that had been quenched from the homogeneous melt state; upon heating above T_g, these quenched homogeneous samples spontaneously microphase-separated, showing an exotherm in the DSC. They also showed that the polyurethanes displayed multiple endothermic behaviors in DSC, and they attributed the intermediate temperature endotherm to the order-disorder transition or the onset of microphase mixing. Koberstein and Russell [1986] studied the same polyurethane sample by simultaneous SAXS and DSC. They found that the onset of microphase mixing upon heating, as reflected by the dramatic decrease of the total integrated X-ray scattering intensity, coincided with the DSC endotherm attributed to the order-disorder transition.

In this project, extensive DSC measurements were done to study qualitatively the phase transitions of triblock copolymers, as well as the heat evolution associated with the phase transition during cooling from above T_s.

6.2. Experimental

6.2.1 Samples

One styrene-butadiene-styrene (SBS) copolymer and one styrene-isoprene-styrene (SIS) copolymer were used in this study. The SBS and SIS samples were provided and characterized by DEXCO Polymers. The SBS had a total molecular weight ($\overline{M}_w$) of 70,000 g/m[illegible] and polystyrene content (ϕ_{PS}) of 29 %, which gives a cylindrical morphology under microphase-separation (polystyrene cylinders surrounded by a polybutadiene matrix). The SIS had $\overline{M}_w$ = 125,000 g/mol and styrene content (ϕ_{PS}) of 18 % with spherical polystyrene microdomains at temperatures below its T_s. The molecular weight and composition were measured by GPC and NMR at DEXCO. The T_s of both samples were measured in our lab by rheology. The details of sample characterizations are listed in Table 6.1.

Table 6.1: Sample Characterizations

Polymer	$\overline{M}_w$	ϕ_{PS}	M_{PS}	$\overline{M}_w / \overline{M}_n$	T_g^{PI}	T_g^{PB}	T_g^{PS}	T_s
	(g/mol)	(wt%)	(g/mol)		(°C)	(°C)	(°C)	(°C)
SBS	70,000	29	10,150	≤ 1.06		-90	69	244±2
SIS	125,000	18	11,250	≤ 1.06	-59		69	167±2
PS*					--		100~105	--
PB*						-100	--	--
PI*					-70		--	--

* Data taken from literature [18], for high-$\overline{M}_w$ homopolymers.

6.2.2 Differential Scanning Calorimetry (DSC)

The calorimeter used in this study was the TA Instruments Differential Scanning Calorimeter (DSC) 2910. It replies on the measurement of a difference in temperature between the sample and a reference (an empty sample pan). The polymer pellets were weighed and used to fill a non-hermetic aluminum pan. Multiple DSC scanning rates were used, from 1 °C/min up to 40 °C/min for both cooling and heating depending on the particular experimental schemes. Typically a double cycle of testing was used, with heating followed by cooling and then another heating /cooling. The sample weights averaged 15~20 mg. For each measurement at least three tests were carried out for accuracy. Indium and sapphire (Al_2O_3) were used to calibrate the apparatus (Indium has a well-known melting temperature which appears on the DSC curve as a very sharp peak. This was used to calibrate the temperatures. Sapphire was used to calibrate the baseline since its heat capacity was measured accurately by the DSC manufacturer, over a broad range of temperatures). Nitrogen was used as the purging gas during most tests.

6.2.3 Rheometry

First, rheological tests over a range of temperatures were done on a Rheometrics Mechanical Spectrometer 800 (RMS-800) to locate the T_s. Polymer pellets were first compression molded at T = 170 °C into a disk of 25 mm in diameter and 2 mm in thickness. Parallel plate geometry (plates of 25 mm diameter) was used. Sample gap was set at around 1 mm. Temperature was controlled by a convection oven, with nitrogen as purging gas to minimize oxidative degradation. Small-amplitude strain (γ° = 1 %) was chosen in all oscillatory tests to keep the sample properties well within the linear viscoelastic range. Both temperature sweep and isothermal frequency sweep were used to measure T_s.

6.3 Results and Discussion

6.3.1 Determining T_s

Passing the sample through T_s is expected to be accompanied by a dramatic change in viscoelastic properties, resulting from different diffusion mechanisms in the disordered and ordered state. Many researches have proved this. Rosedale and Bates [1990] suggested that the most precise and practical method of establishing T_s be by the discontinuity in $G'(T)$ at low frequencies. Winter [1993] found the *MST* occurred at the temperature where $G'(T)$ and $G''(T)$ crossed over. Figures 6.1 and 6.2 show the viscosity η', η'' and shear modulus G', G'' of SIS and SBS samples, respectively. In Figure 6.1, η' and η'' of sample SIS were measured at $\omega = 0.1$ rad/s and $\gamma^o = 1\%$, and they cross over at about 167 °C. η'' drops three decades at $T > 167$ °C, but is relatively level for $T < 167$ °C. Superposing tan δ data results in a master curve which separates into two branches at 167 °C (plot shown in Chapter 5, Figure 5.3). It is a good assessment to say that for the SIS sample, the microphase separation happens at 167 °C. Figure 6.2 shows that for the SBS sample, T_s = 240 °C. The microphase-separation temperatures for both SIS and SBS samples are also in good agreement with the results predicted by some theoretical calculations [Leary and Williams 1974, Winter *et al* 1993].

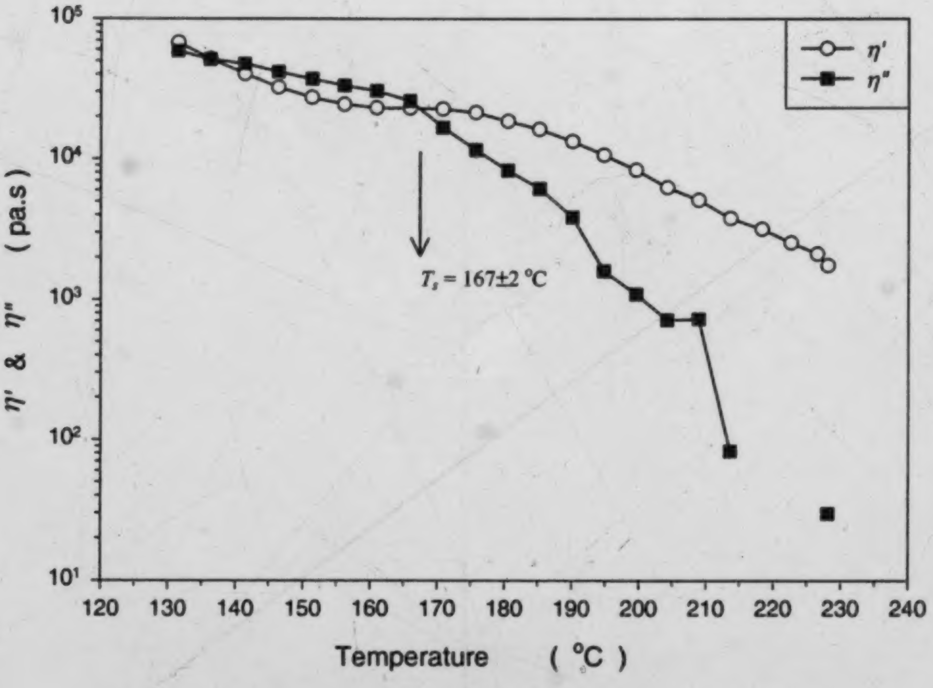

Figure 6.1: Temperature sweep for SIS sample, at $\omega = 0.1$ rad/s and $\gamma^\circ =$ 1 %. Microphase separation occurs at 167 °C where η'' drops abruptly and where η' and η'' cross over each other.

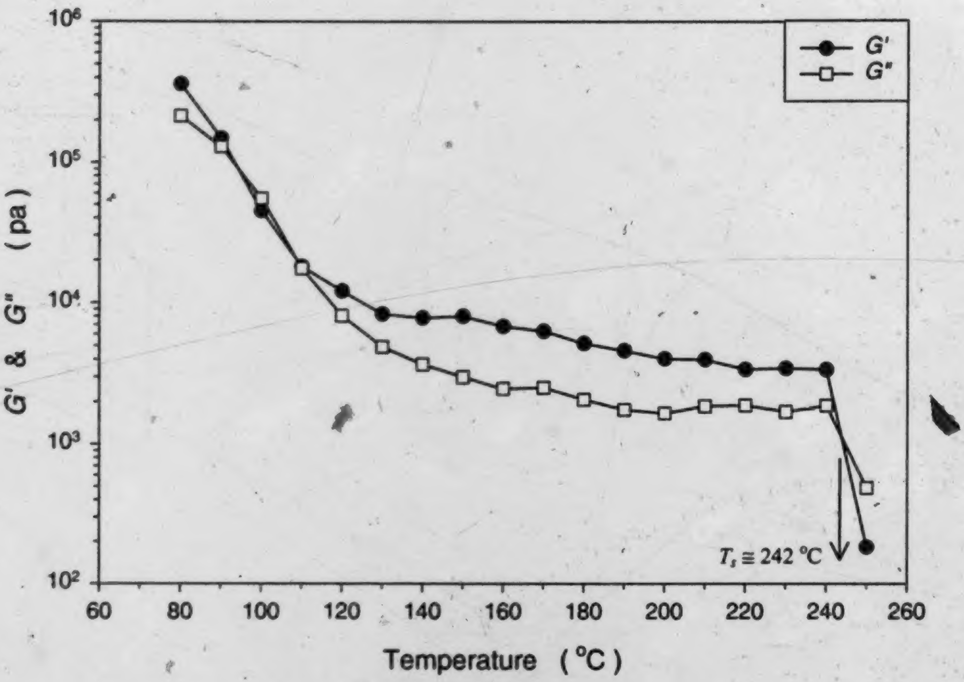

Figure 6.2: Temperature sweep for SBS sample, at $\omega = 0.02154$ rad/s and $\gamma^o = 1$ %. Microphase separation occurs at 242 °C where G' and G'' drop abruptly and cross over each other.

6.3.2 Thermal Stability of Block Copolymers

The study of thermal oxidative degradation of linear macromolecules is of great interest, because it can in many cases determine the upper temperature limit of the use for a material. The actual chemical reactions occurring in these processes are often rather involved and not known in detail because of the many reactions that are simultaneously possible on pyrolysis of the carbon-carbon bond. Only in rare cases are the decomposition reactions the reverse of the polymerization.

Thermal degradation of elastomers (e.g. PB and PI) is known to involve chain scission and/or crosslinking. If the scission or the crosslinking reaction occurs in the mainchain molecules, the mechanical properties such as strength, elongation, and modulus must be affected. McNeill and Stevenson [1985] studied the thermal degradation of styrene-butadiene diblock copolymer (with ≅ 50% wt composition) and compared it with the characteristics of the degradation of homopolystyrene (PS) and homopolybutadiene (PB) and a 1:1 by weight blend of the homopolymers. In DSC measurements under programmed heating conditions with nitrogen blanket, they found the SB diblock copolymer showed an exothermic peak and immediately followed by an endothermic peak. The exothermic peak started at 300 °C, with a maximum at 375 °C and the peak ended around 415 °C where the endotherm started. The endothermic peak had a maximum at around 450 °C. The exothermic peak was attributed to cyclisation in the PB sections of the chains, with no volatile products produced. Upon further heating, volatile by-products 1,3-Butadiene (one of the block B monomers) and 4-Vinylcyclohexene were produced. This reaction corresponded to the endothermic peak in the DSC curve. In the case of SB block copolymer, great amounts of PS and PB chain structures can persist to higher degradation temperatures compared to PB homopolymer and PB + PS blend, mainly because of the stabilization effect of the PS sections. Unfortunately we have not found any report on the degradation of SI or SIS block copolymers. However, Adams *et al* [1996] mentioned in one paper that by using GPC analysis following rheological or X-ray measurements, they found only minor amounts (< 10%) of chain scission and branching for SI diblock and SIS triblock copolymers after exposure to 150 °C for several days (no mention of whether in air or in nitrogen).

Due to the temperature range (-150 ~ +280 °C) we work with in this project, we are particularly concerned with the possibility of thermal degradation. Several DSC runs were carried out in both nitrogen and air. Figure 6.3 shows the DSC traces of the SIS sample. Tested in air, the DSC curve shows an exothermic peak at around 220 °C, while under nitrogen blanket the DSC trace shows no peak. This indicates that though the polyisoprene chains undergo oxygen-induced degradation in air, the SIS sample is virtually intact under the nitrogen blanket up to 230 °C. Similar tests are shown in Figure 6.4 for the SBS sample. Heated at 5 °C/min in air, the SBS sample shows two exotherms. One starts at 220 °C and ends around 400 °C. The tail of the first exothermic peak is overlapped with the second. Similar to polyisoprene chains, the polybutadiene chains start to react at around 220 °C in the presence of oxygen. With or without the presence of oxygen, the polybutadiene chains undergo a chemical reaction (crosslinking or cyclisation) at around 350 °C, as evidenced by the second exotherm at 350 °C in both curves. In the DSC trace tested in nitrogen, the second exotherm and the following endotherm are exactly same as those measured by McNeill and Stevenson [1985]. The mechanisms of polybutadiene chains cyclisation at 350 °C are similar either in air or in nitrogen, at least it seems so by judging from the DSC curves. The shape and area under the exothermic peaks are same for both curves (in air or nitrogen). But the decompositions at 450 °C are obviously different. Though both samples were completely burned above 450 °C, (no sample remains were left in the pan after tested in N_2, only carbon black left after tested in air) the sample tested in air doesn't complete the second half of the endothermic peak while the sample tested in nitrogen shows a full endothermic peak. Understandably the samples burn out in oxygen, but break down to some volatile products in nitrogen.

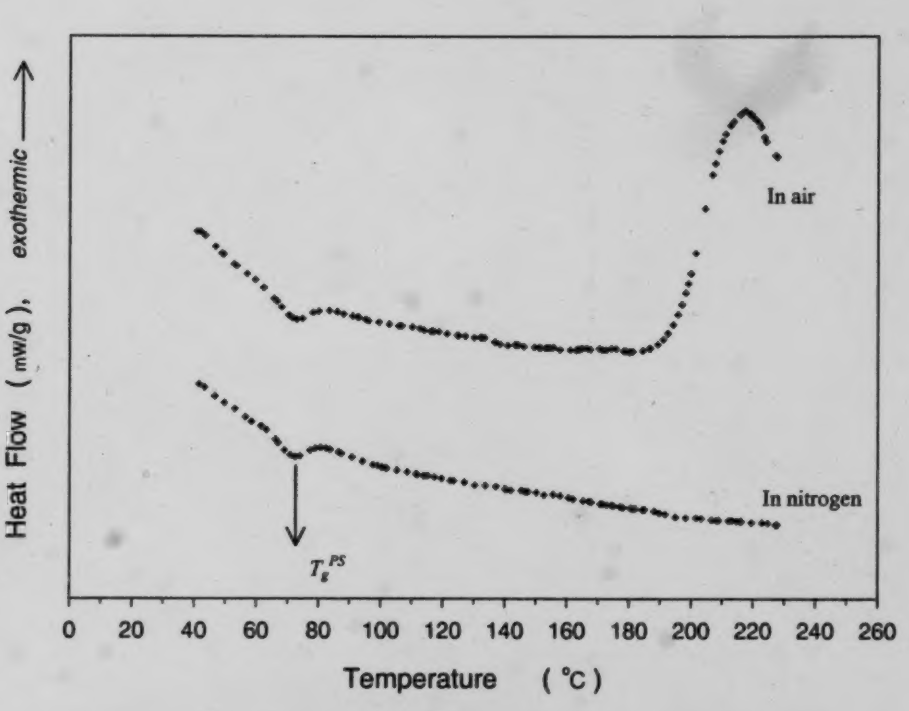

Figure 6.3: DSC scan of SIS sample at 5 °C/min heating rate. The sample tested in air gave an exothermic peak around 220 °C, due to the oxygen-induced thermal degradation along the polyisoprene chains. Nitrogen purging eliminates this problem. A small endothermic peak at 70 °C is the glass transition of the polystyrene block. (these two curves have been moved vertically to avoid overlap)

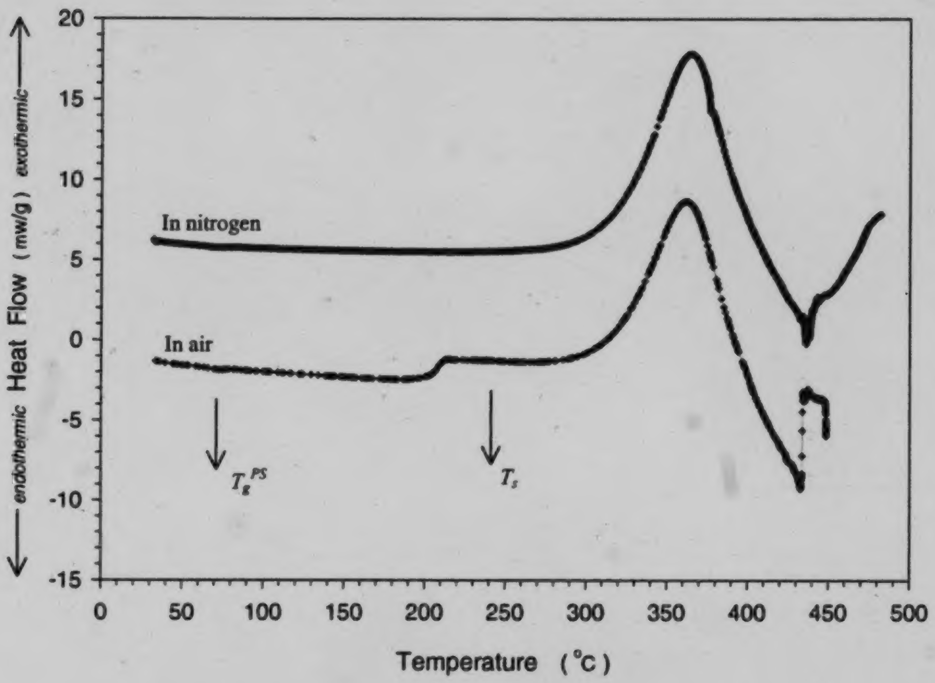

Figure 6.4: DSC scan of SBS sample at 5 °C/min heating rate. The sample tested in air gave two exothermic peaks followed by an endothermic peak. The first exothermic peak, at 220 °C, is the crosslinking of polybutadiene chains induced by the presence of oxygen in the air. The second exothermic peak at 350 °C is probably mainly caused by the cyclisation of polybutadiene chains. The endothermic peak starting at 400 °C is the decomposition of the sample. The SBS sample tested in nitrogen only has one exothermic peak (at 350 °C), probably caused by the cyclisation of the polybutadiene chains, and the same endothemic peak at 430 °C as in air. Glass transition of the polystyrene block is found to be around 70 °C. (The two curves have been moved vertically to avoid overlap) The position of T_s is marked, for reference, but on this scale the heating traces cannot detect the weak heat effects at this transition. Recently, Spaans *et al* [1999] were able to capture T_s for one SBS with DSC.

6.3.3 The Heat Evolution of the Microphase-Separation Transition

Differential scanning calorimetry has been proven to be an excellent analytical technique for determining multiple glass transitions of block copolymers. The existence of two distinct T_g regions is clearly shown in the DSC thermograms, as illustrated by typical DSC runs for SBS and SIS samples in Figures 6.5a and 6.5b respectively. Starting at room temperature (30 °C usually), the sample is heated up to above T_s at a specific scan rate (arrow 1 in Figure 6.5). Although higher temperature is more desirable because it can create a longer baseline for the subsequent calculation of the heat associated to the phase transition, the prime concern here is the thermal stability of block copolymer samples. The upper temperatures are usually set just 30~40 degrees above T_s (270 °C for SBS and 200 °C for SIS). As soon as it hits the upper temperature, the sample is cooled at the same scan rate to -100 or -150 °C (arrow 2 in Figure 6.5), then heated up to room temperature again (arrow 3 in Figure 6.5).

In the literature, there are many ways of characterizing glass transitions. In this project the glass transition temperature of the polybutadiene phase or polyisoprene phase is taken as the temperature at which the DSC trace reaches its local maximum on the cooling run. In Figure 6.5, $T_g^{PB} \cong -90$ °C and $T_g^{PI} \cong -60$ °C. These temperatures also correspond to the midpoints of the step changes on the heating runs. Spaans *et al* [1999] demonstrated how to identify the midpoint between two extrapolated baselines before and after the transition when measuring the glass transition. The glass transition temperature of polystyrene block is taken as the temperature at which the DSC

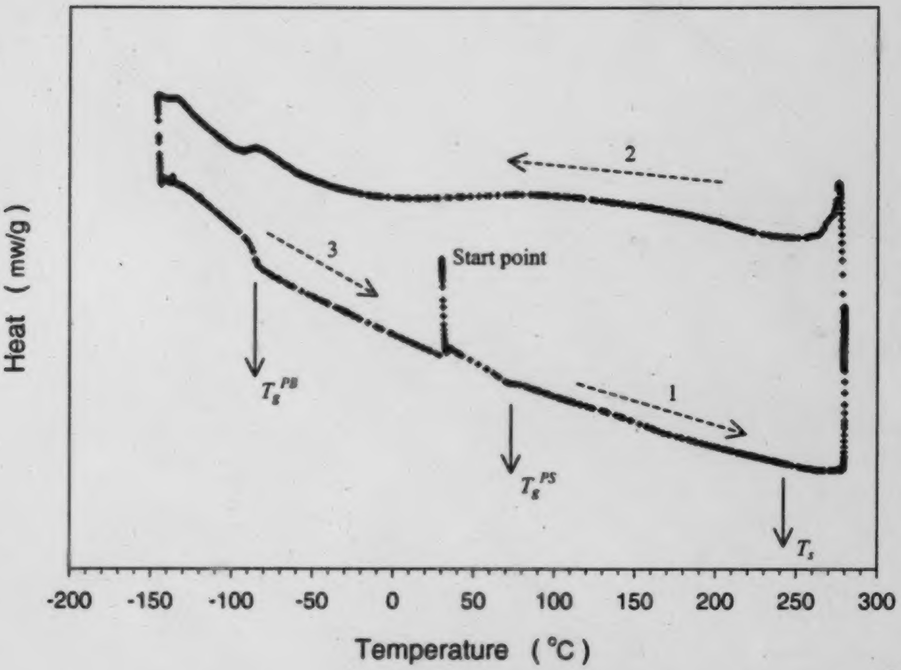

Figure 6.5(a): Typical DSC runs for SBS. The numbered arrows represent the scanning sequences. The temperature at which the heating curve changes slope is taken as the glass transition temperature of polystyrene block ($T_g^{PS} \cong$ 70 °C) and where the cooling curve reaches its local maximum is taken as the glass transition temperature of the polybutadiene ($T_g^{PB} \cong$ -85 °C) block.

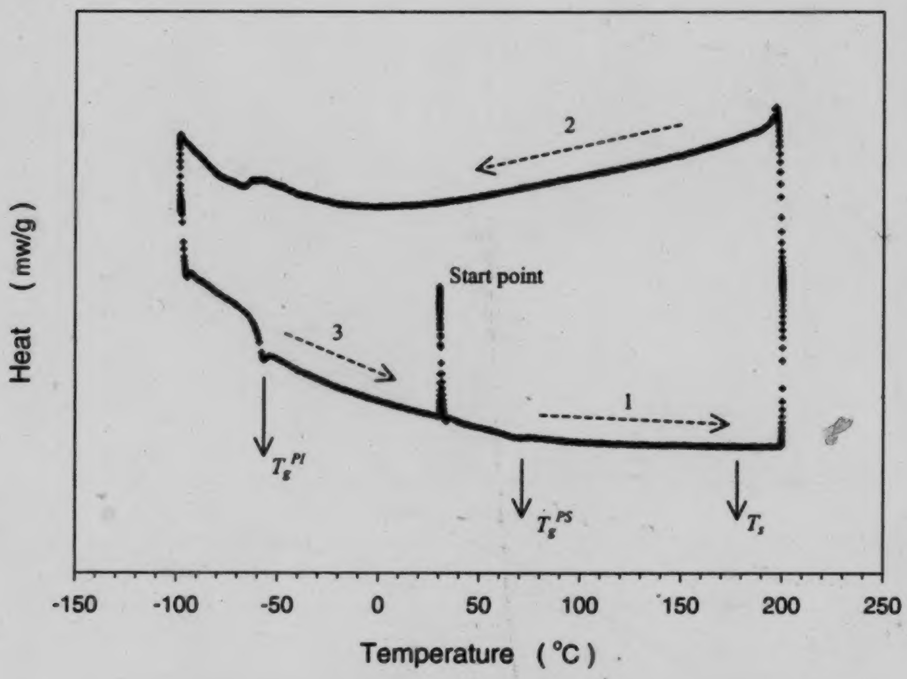

Figure 6.5(b): Typical DSC runs for SIS samples. The numbered arrows represent the scanning sequences. The temperature at which the heating curve changes slope is taken as the glass transition temperature of polystyrene block ($T_g^{PS} \cong 70$ °C) and where the cooling curve reaches its local maximum is taken as the glass transition temperature of the polyisoprene ($T_g^{PI} \equiv -60$ °C) block.

trace changes its slope on the heating run. In Figure 6.5, $T_g^{PS} \cong 70$ °C. On the cooling run we were never able to detect the glass transition temperature of polystyrene. All T_g 's measured in this work are rate-dependent. Usually the faster the scan-rate, the higher the T_g.

The two distinct T_g's corresponding to those of the parent polymers indicate microphase separation. The glass transition temperatures of PB and PI blocks are substantially higher than those of their corresponding homopolymers, as well as T_g of PS block is lower than its homopolymer (Table 6.1). The apparent lowering of the PS block T_g and the elevating of the rubber block T_g is probably due to the existence of a third phase between the rubber and polystyrene phase, called interphase by Leary and Williams [1970]. The mixing of PS blocks and PI or PB blocks in the interphase makes the T_g's of the two blocks shift towards each other. The low T_g^{PS} for the blocks here could also be due to their low molecular weight.

The small endothermic peak on the heating curve at polyisoprene T_g (Figure 6.5b) is called the hysteresis peak. It is the result of the coupling of slow cooling with fast heating. When the equilibrium melt cannot be attained at the temperature where the system froze on cooling, the superheated glass drifts quickly toward equilibrium as soon as the changing time scale of heating permits. In heat flow or heat capacity, this behavior is characterized by an endothermic minimum, and is called hysteresis or enthalpy relaxation behavior and it can be used to obtain information on the thermal history.

Interestingly though, the thermal histories are identical because the heating and cooling rates in this experiment are same.

Another distinctive feature of the DSC curve (in Figure 6.5a) is the broad convex curvature on the cooling run. This curvature covers a temperature range of 240 degrees from 230 °C to −10 °C. The cooling curves of the SBS sample at different cooling rates are shown in Figure 6.6. All curves show similar convex curvatures, but the onset temperatures are shifted toward lower temperature as the cooling gets faster. At 1 °C/min cooling, the curvature starts around 250 °C (Figure 6.7). Figure 6.8, 6.9 and 6.10 show that at 5, 7.5 and 10 °C/min cooling rate, the curvatures start at temperatures 240, 210 and 190 °C, respectively. The baseline curves are constructed by connecting the data at above T_s with data between T_g^{PS} and T_g^{PB} then with the data at below T_g^{PB}, so that the whole baseline should have a more natural concave curvature, like most cooling curves do. The curve-fitting was done by a computer program. Although we can not get much of the baseline at $T > T_s$ due to the possibility of thermal degradation, when the cooling gets faster and faster, such as at 10 °C/min, eventually the baseline at above T_s covers as much as 70 degrees of temperature (Figure 6.10). Similarly, it is difficult to say what the baseline should look like around T_g^{PB}. At higher cooling rates (Figures 6.9, 6.10), the baseline around T_g^{PB} becomes much more clear than at lower cooling rates (Figures 6.7, 6.8). At 1 °C/min cooling, the low-temperature baseline is almost a straight line, except for a small exothermic peak corresponding to the polybutadiene glass transition.

Similar plots for the SIS sample are shown in Figure 6.11 to Figure 6.14. Same convex curvature for *MST* is clear in Figure 6.12 when cooled at 1 °C/min. A very small convex curvature can also be observed in Figure 6.13 with cooling at 5 °C/min. But it is difficult to identify the same curvature in Figure 6.14. It appears to be general that the

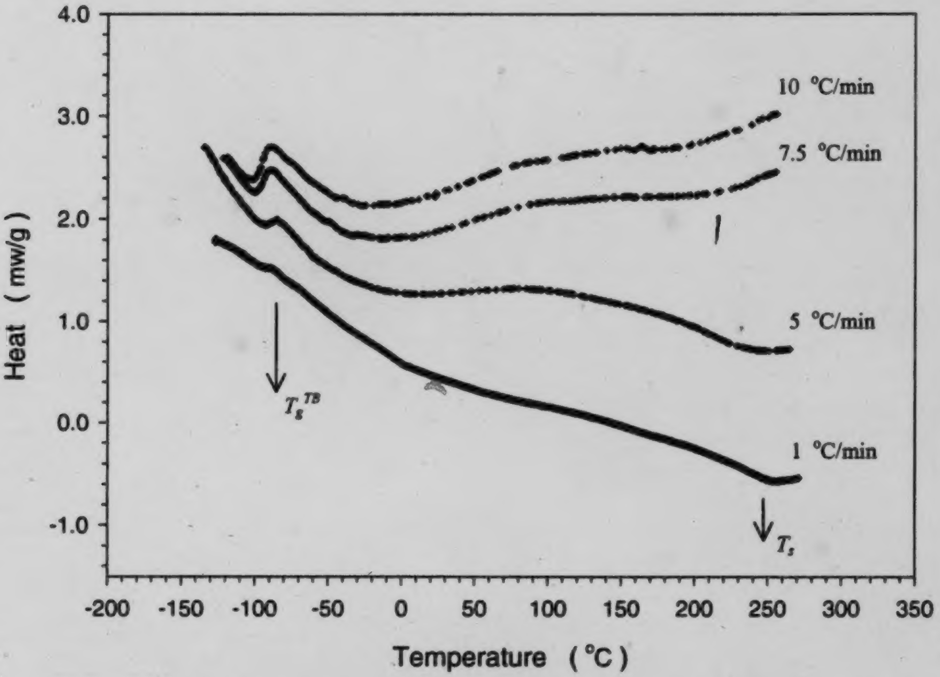

Figure 6.6: The SBS samples cooled from above T_s at different scan rates, where $T_s \cong 242$ °C. The common features of these curves are the convex curvatures below T_s. The shapes and the broadness of the T_g^{PB} exothermic peaks are rate dependent, although the heat measured are more or less the same. $T_g^{PB} \cong -89$ °C.

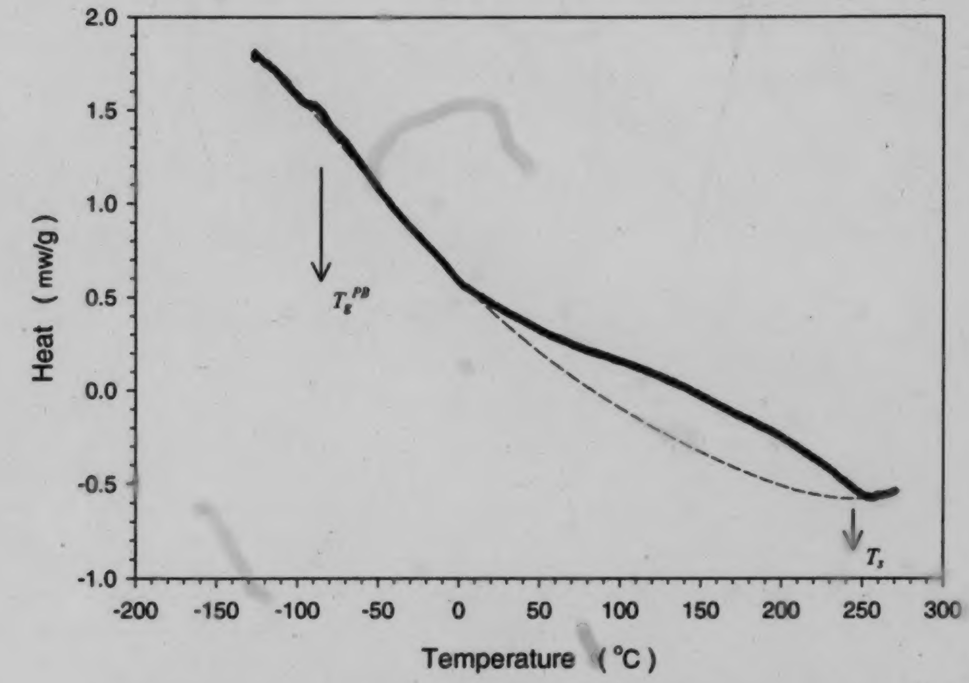

Figure 6.7: SBS sample cooled at 1 °C/min. The solid line represents the DSC trace, and the dash line represents the computer-generated baseline.

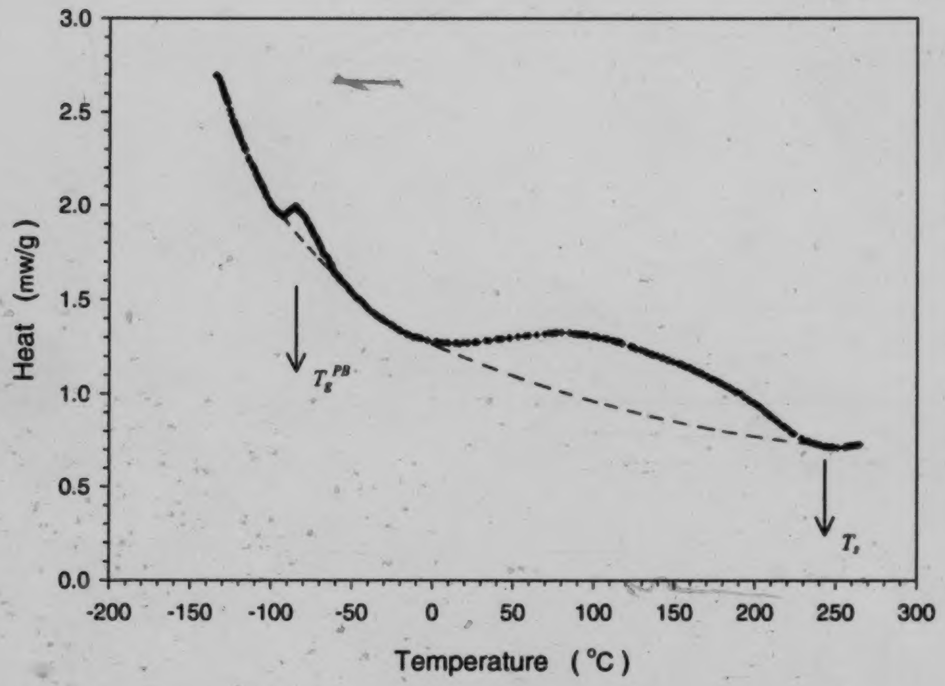

Figure 6.8: SBS sample cooled at 5 °C/min. Solid line represents the DSC trace, and the dash line represents the computer-generated baseline.

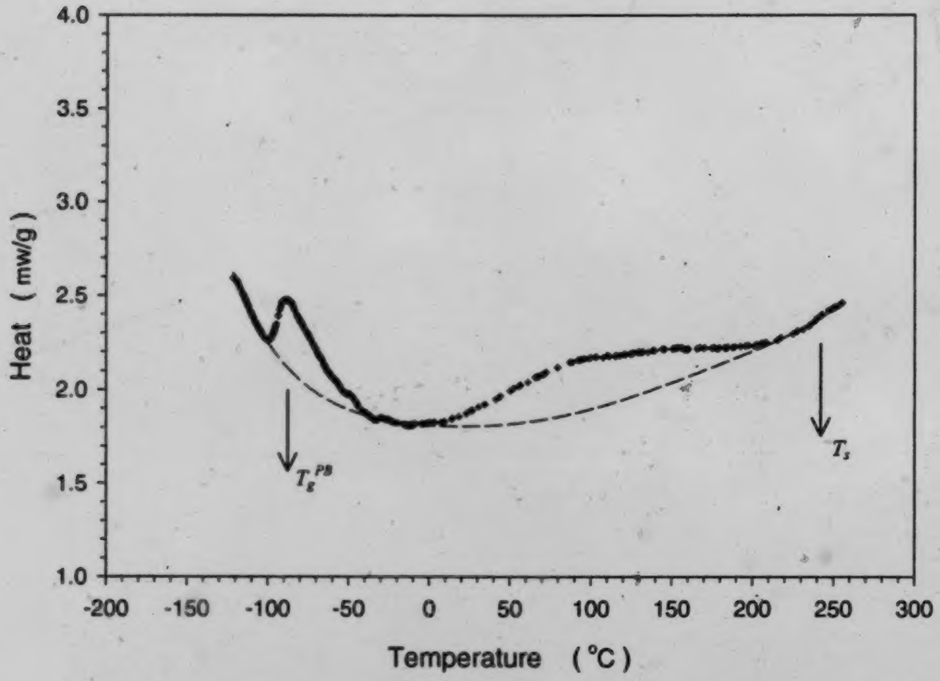

Figure 6.9: SBS sample cooled at 7.5 °C/min. Solid line represents the DSC trace, and the dash line represents the computer-generated baseline. The temperature covers about 50 degrees at T_s where the DSC trace matches the baseline.

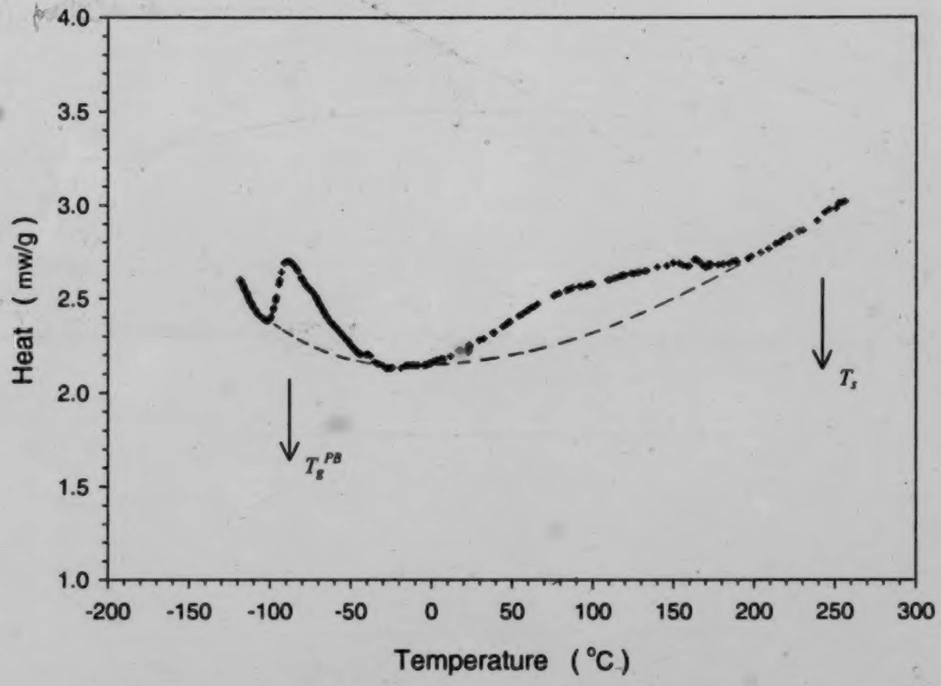

Figure 6.10: SBS sample cooled at 10 C/min. Solid line represents the DSC trace, and the dash line represents the computer-generated base line. The temperature at T_s covers about 70 degrees where the DSC trace matches the baseline.

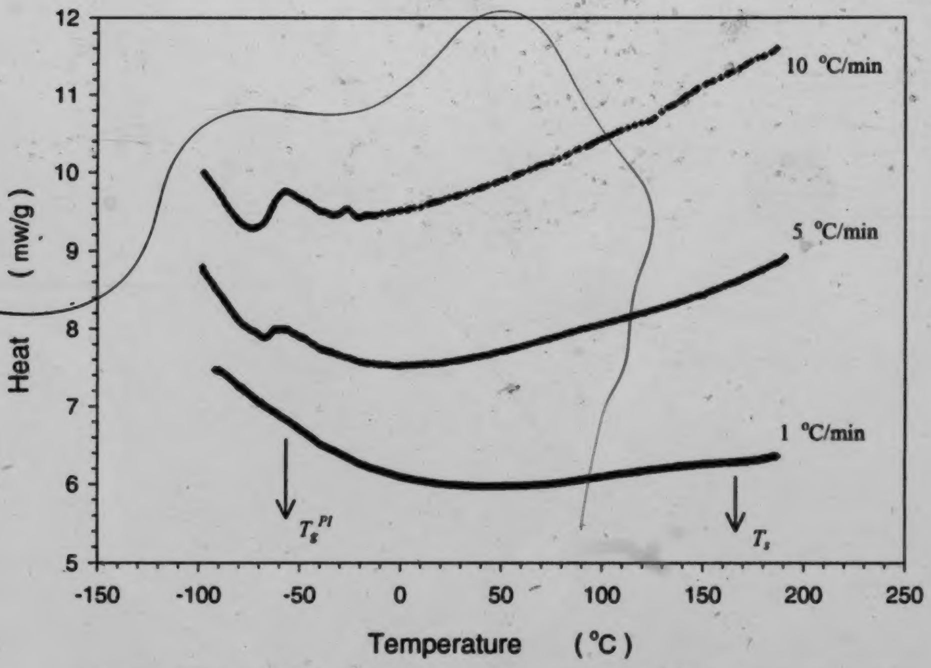

Figure 6.11: SIS samples cooled from above T_s at different scan rates, where $T_s \cong 167 \pm 2$ °C. The convex curvature is not so obvious at higher cooling rates. $T_g^{PI} \cong -59$ °C.

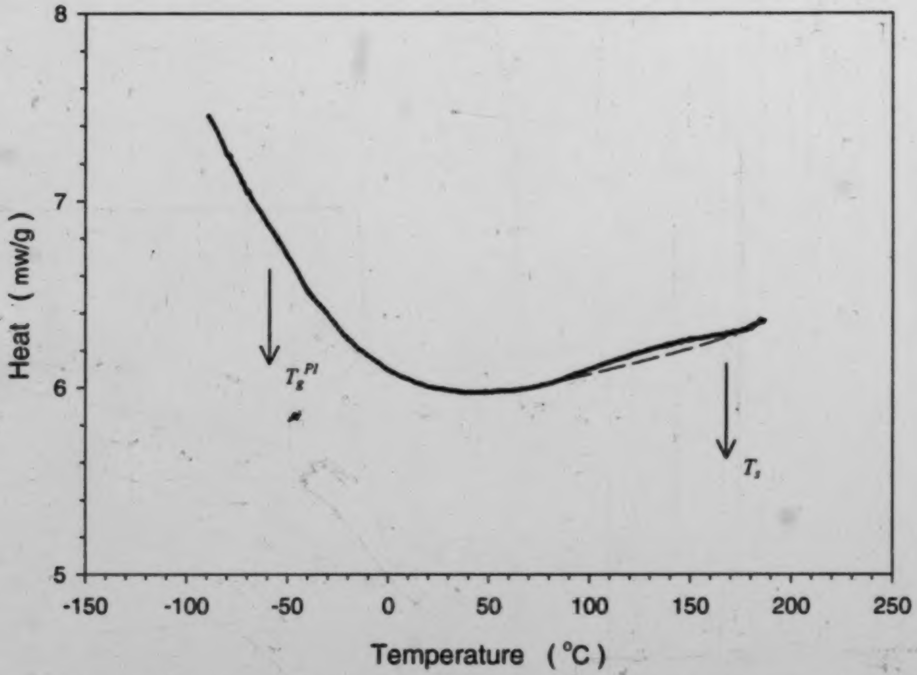

Figure 6.12: SIS sample cooled at 1 °C/min. The solid line represents the DSC trace, and the dash line represents the computer-generated baseline.

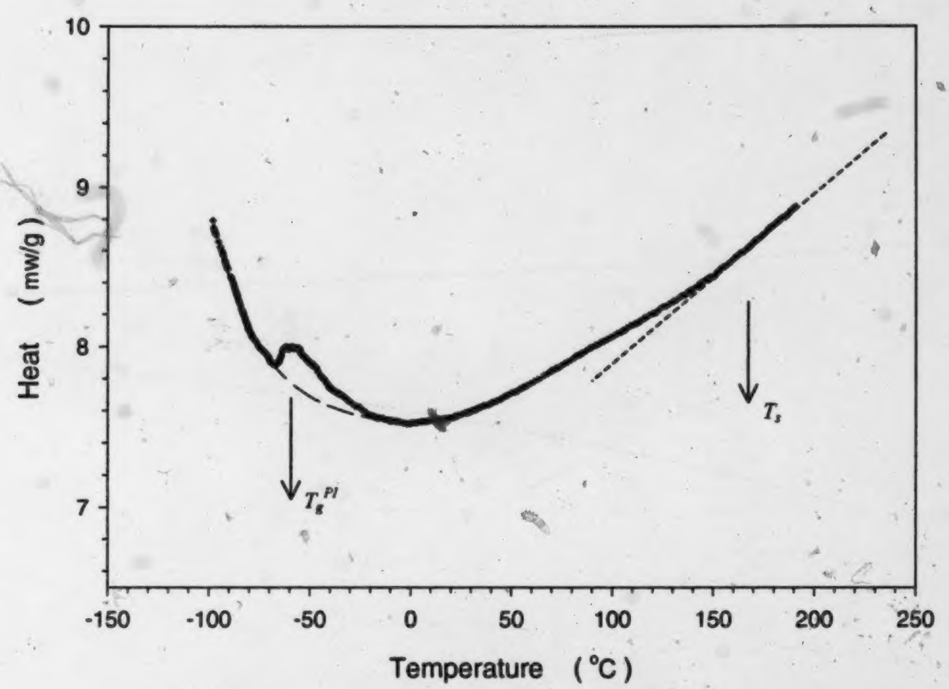

Figure 6.13: SIS sample cooled at 5 °C/min. The solid line represents the DSC trace, and the dash line represents the computer-generated baseline. The DSC trace shows a small convex curvature starts at about 150 °C.

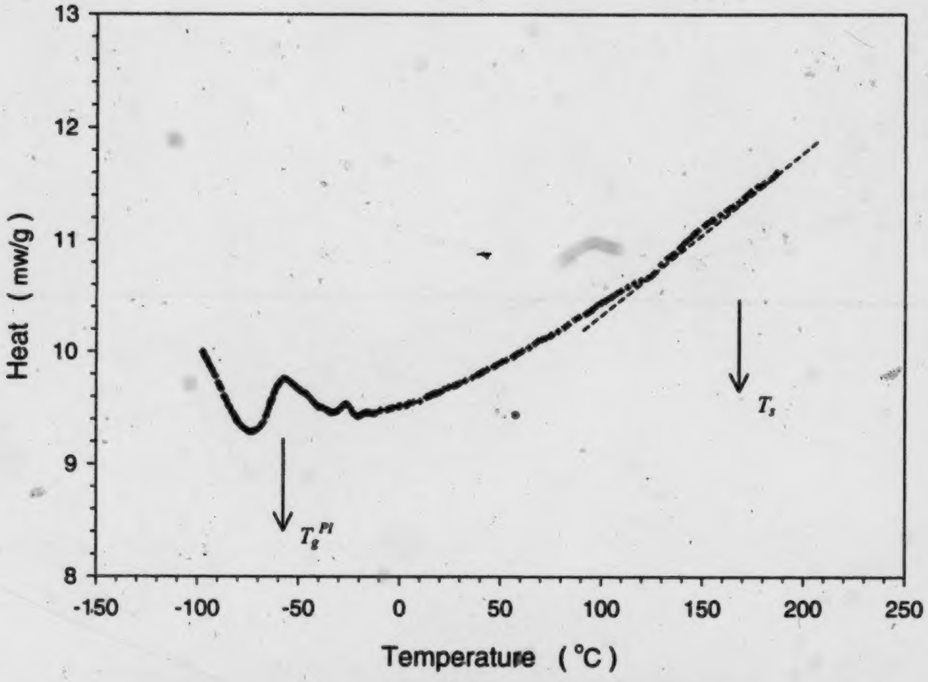

Figure 6.14: SIS sample cooled at 10 °C/min. The solid line represents the DSC trace, and the dash line represents the computer-generated baseline. The little exothermic peak around -30 °C is reproducible, but never be observed on other cooling rates and other samples. The exothermic peak at T_g^{PI} is somewhat altered by this little peak around –30 °C.

Convexity begins to appear shortly after T_s is passed (i.e., when $T < T_s$), and also that the faster the cooling, the smaller the convex curvature becomes. It has been reported [Henderson and Williams 1985, Adams et al 1996, Spontak and Williams 1988 and 1988, Wang and Williams 1998] that at T just below T_s, the block copolymer microstructure will take a long time to become fully grown. When the samples were quenched from above T_s to certain quench depths ΔT ($\Delta T = T_s - T$), the storage modulus G' grew asymptotically and reached its final equilibrium value at a time scale from couple hundred to several thousand minutes. The dispersed phase was observed to evolve from nucleation and growth to organizing the long-range structures (sphere, cylinder and lamella etc.). We have also reported [Wang and Williams 1998] that for a given SIS sample used in this project, the lower the temperature T ($T < T_s$), the slower the ordering process.

Though the actual ordering mechanism is much more complicated and beyond the scope of this project, it is obvious that the ordering kinetics greatly affect the DSC measurement. The ordering process at one particular temperature T ($T < T_s$) is so slow that in the DSC experiments the block copolymers are always under supercooled condition, as evidenced by the factor that the faster the cooling, the lower the onset temperatures of the *MST* transitional peak (details listed in Table 6.2). Cooling at 10 °C/min is equivalent to a semi-quench process. Long before the sample achieves some equilibrium configuration, it has been locked into a lower energy level and certain microstructures has been frozen and preserved into lower temperatures. The fine-tuning of microstructures will never happen when the cooling is too fast. This could probably explain the observation that the heat associated with the *MST* transition decreases dramatically as the cooling gets faster (Table 6.2). But for relatively simpler transitions, such as the glass transition of polybutadiene and polyisoprene, the heat is more or less the same (Table 6.2). The near-independence of scan speed for the heat associated with PB and PI glass transitions also gives us more confidence in drawing the baselines.

Table 6.2: Characterizing Phase Transitions

		$T_g^{PB\ or\ PI}$				*MST*			
	Cooling Rate (°C/min)	Onset Temp. (°C)	End Point (°C)	Broadness (degree)	$\Delta H \times 10^3$ (cal/g)	Onset Temp. (°C)	End Point (°C)	Broadness (degree)	$\Delta H \times 10^3$ (cal/g)
SBS	1	-80	-97	17	1.74	252	0	252	57.7
	5	-60	-96	36	1.77	243	-10	253	19.4
	7.5	-38	-100	62	1.83	210	-10	220	5.38
	10	-27	-103	76	1.96	190	-10	200	3.30
SIS	1	--	--	--	--	170	82	88	42.7
	5	-13	-67	54	1.41	145	--	--	--
	10	--	--	--	--	120	--	--	--

Theoretically, though, there should be no heat associated with a second-order phase transition, such as the glass transition (as demonstrated in Figure 6.12). The exothermic peaks we have measured are most likely related to supercooling. When temperature approaches T_g, the process of shrinkage of free space within the block copolymer sample involves simultaneous movements of many adjacent molecules. This is significantly slower than the process of cooling. Under the supercooled condition, the molecules have to move more quickly to catch up with the rapidly decreasing temperature, which makes the heat flow detected by the DSC give a small exotherm that resembles a first-order phase transition. At fast cooling such as 10 °C/min (Figure 6.10 and Table 6.2), the SBS sample starts to sense the supercooling at as high as –27 °C, while at slow cooling (Figure 6.7 and Table 6.2), the onset temperature is closer to the transition point. In the case of SIS there is no detectable change on the cooling curve (Figure 6.12). The heat associated with these time-lag phenomena at the T_g^{PB} transition also slightly increase when samples are cooled at faster rates. It is important to remember the morphology differences between the SBS and SIS samples. The SBS sample, with 29% of PS, has a semi-infinite cylindrical PS phase reside in the PB matrix. The SIS sample, on the other hand, with only 18% of PS has finite spherical PS domains dispersed among the PI matrix. Understandably the shrinkage of rubbery PI matrix with small PS spheres will be much easier than the shrinkage of rubbery PB matrix with the infinitely long PS cylinders connected from one end of the sample to the other. This could account for the fact that at 1 °C/min cooling, the SBS sample still shows a small exotherm while none is observed for the SIS sample.

The broadness of the *MST* peaks is also rate-dependent (Figures 6.7, 6.8, 6.9, 6.10 and Table 6.2). Contrarily to the glass transition, the onset temperatures get lower for the *MST* transition at faster cooling. At the slowest cooling (1 °C/min), the onset temperature of the *MST* transition is slightly higher than T_s, for both SBS and SIS block copolymers. However, at medium scan rates (5 °C/min) the onset temperature coincides with T_s, and it is significantly lower for faster cooling (such as 10 °C/min). Similar to the T_g^{PB} transition, the endpoint temperatures are more or less the same for all cooling rates. The whole *MST* peak thus shifts to lower temperature T ($T < T_s$) as cooling-rate increases. The heat of

SBS microphase-separation was reported [Leary and Williams 1974] to be only 0.05~0.10 cal/g theoretically. This is, however, the heat generated when the equilibrium morphology is reached, such as polystyrene and polybutadiene microphases at their equilibrium state. The actual phase-separation happens rather rapidly at early stage compared to the subsequent growing of long-range equilibrium structures. In our experience, cooling at 40 °C/min from above T_s, the SBS sample still shows a distinctive T_g^{PB} transition on both cooling and heating curves, which is a manifestation of the microphase-separation. In general though, the DSC is not a good instrument to detect this small amount of heat. The broad exotherms we identified on the heat-flow curves are the heat associated with this early stage phase separation (non-equilibrium morphology). Spontak and Williams [1988, 1988] showed, by three-dimensional transmission electron microscope (TEM) pictures, that a SBS block copolymer required thermodynamically to have cylindrical morphology was clearly in a non-equilibrium state, with some non-cylindrical globules of PS after being quenched from the homogeneous state ($T > T_s$). Further annealing of the initially non-equilibrium SBS sample caused increasing ordering of styrene domains. The non-equilibrium state is obviously cooling-rate dependent. The faster the cooling, the less time the block copolymer molecules have for reconfiguration at one particular temperature, and farther is the microstructure from the equilibrium. In terms of the *MST* peak, it shifts further away from T_s at higher cooling rates. The microphase-separation may still occur at T_s, but the mass movement of many small PS domains (such as the "globules of PS") to form long-range structures (such as near-infinite one-dimensional "PS cylinders") will most likely have no time to occur at or near T_s. Instead, it will happen at much lower temperatures, and will become more and more difficult with the ever-growing PS clusters having less and less mobility. This is why most of the quenched samples are in non-equilibrium state.

The heat of exothermic peaks for both T_g and *MST* transitions were calculated by integrating the heat flow curve along the time scale as illustrated in Figure 6.15. The

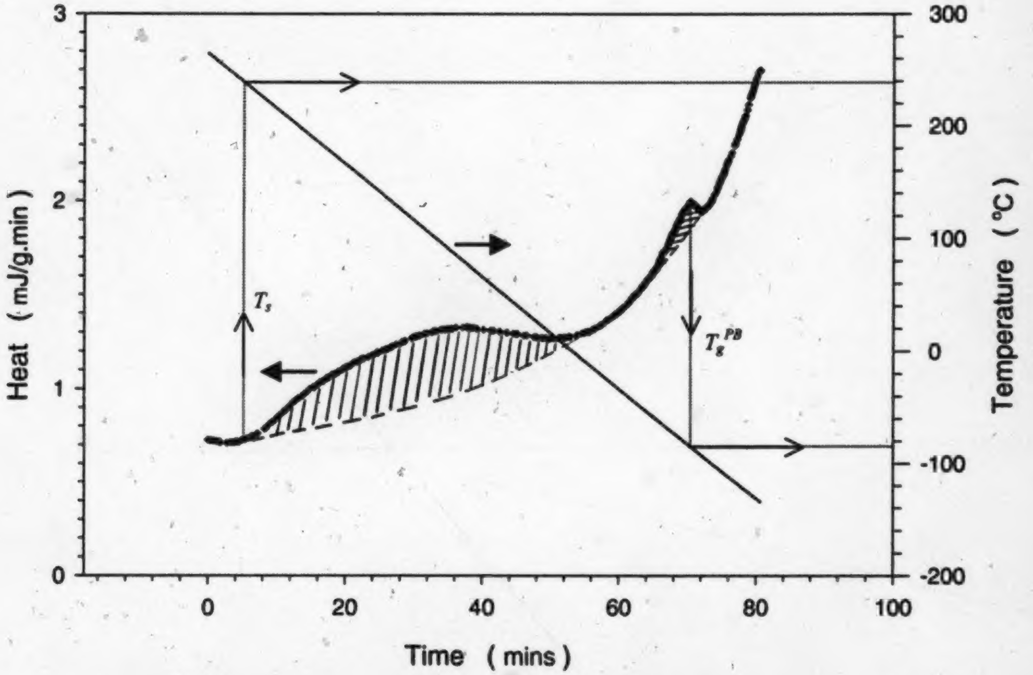

Figure 6.15: Illustration of how the heat at *MST* and T_g^{PB} transition is calculated curing a cooling scan from above T_s for the SBS sample. The solid curve represents the DSC trace, and the dash line represents the computer-generated baseline. The crosshatched regions between the DSC exothermal and the baseline represent the transition heats. Thus, the heat was calculated by integrating the crosshatched area along the time axis. The diagonal line is used to convert the time reading (abscissa) to the sample temperature (right-hand ordinate) at that instant, for the given DSC scan rate.

crosshatched area represents the actual heat given out in that particular transition. In Table 6.2, I listed the values of the heat measured at different cooling rates. Since the *MST* exotherm also covers the polystyrene glass transition temperature on the cooling curve, the heat associated with *MST*-transition should thus also include the pseudo-heat of the T_g^{PS}-transition produced, regardless how trivial it might be.

For SBS samples, the heat associated with *MST*-transition decreases dramatically as cooling rate increases. At 1 °C/min cooling, the heat generated is almost 20 times the amount being produced at 10 °C/min cooling. This indicates that the fast cooling has enormous effect on the growth of long-range microstructures. At 10 °C/min cooling, this microstructure growth is virtually impossible. As have reported elsewhere (Chapter 5), at the temperature right below T_s where the block copolymer molecules should have the greatest mobility, the half-time ($t_{1/2}$) for the storage modulus G' to reach its equilibrium value was about 35 minutes. It tripled to 98 minutes at 25 degrees below T_s. Even cooling at 1 °C/min is too quick for the microstructure to be fully-grown.

Although the heat associated with the SIS *MST*-transition at 1 °C/min cooling is of the same magnitude as that of the SBS sample, it appears to be very difficult to calculate the heat at higher cooling rates. In Figure 6.13 and Figure 6.14, only slight convexity could be spotted on the cooling curves. This difference between the cooling curves of SBS and SIS samples could be attributed to the different morphologies of the two polymers. The SBS sample (with 29% PS) has unbound-length one-dimensional cylindrical PS domains among PB matrix, while the SIS sample (with 18% PS) has only small spherical PS phases dispersed in the PI matrix. Thus, the heat produced during the growth of the lone-range structures will differ greatly for the two polymers. While the SBS is building the PS cylinders throughout the sample, the PS spheres inside the SIS sample only need to grow and readjust the shapes at the local level to lower the total free energy. Subsequently, the heat produced by the SIS sample will be less than that of the SBS sample. It is even harder for the DSC to detect at higher cooling rates, as illustrated by Figure 6.13 and Figure 6.14.

6.3. Conclusions

Two triblock copolymers have been studied by Differential Scanning Calorimeter (DSC). In the presence of oxygen, the SBS and SIS samples were found to be reacting-believed to be crosslinking at around 220 °C, but this did not occur under nitrogen. Upon further heating, the cyclisation of the polybutadiene chains occurred at 350 °C regardless with or without oxygen. The SBS samples eventually burned out at about 450 °C in oxygen or broke down to volatile products in nitrogen. When the block copolymers were cooled from above T_s two distinct exothermic peaks were found, which corresponded to the glass transition of the rubber block and the microphase-separation transition. The heat associated with the glass transition was consistent at all cooling rates, but the broadness of the peak was found to be rate-dependent. The heat produced by the microphase-separation transition, however, varied dramatically between slow and fast cooling. This behavior, in turn, reflects the complication of the ordering mechanism. The microphase-separation occurs instantly upon cooling through T_s. But the growth of the long-range microstructure depends very much on the speed of cooling.

Chapter 7 Time-Temperature Superposition of Dynamic Functions of Block Copolymers

7.1. Introduction

Time-temperature superposition has long been used for polymer systems to obtain master curves of steady-shear rheological properties (e.g., η) over an extremely wide range of dynamic variable (e.g., $\dot{\gamma}$) at a fixed temperature by shifting values of η obtained at various temperatures along the $\dot{\gamma}$ axis or by shifting values of dynamic modulus (G' & G'') and /or dynamic viscosities (η' & η'') along the frequency (ω) axis. Here, one chooses a reference temperature and shifts the rheological properties of interest, which were obtained at other temperatures, to the corresponding values at the reference temperature. There is a shift factor, a_T, which is a function of temperature, that enables one to obtain these master curves in terms of "reduced" variables (i.e. log η_r *versus* log $\dot{\gamma}a_T$, log G'_r versus log ωa_T, and log η'_r versus log ωa_T plots, where $\eta_r = \eta\rho_o T_o/\rho T$, $G'_r = G'\rho_o T_o/\rho T$, and $\eta'_r = \eta'\rho_o T_o/\rho T$ in which the subscript o denotes a reference state). Using the Williams-Landel-Ferry (WLF) or other similar equations (see section 2.1.7 for more details), one can relate the shift factor a_T to the glass transition temperature (T_g), and flow activation energy (E) of a polymer, which are characteristic of the polymer's molecular structure.

It should be pointed out that the use of time-temperature superposition is meaningful as long as the morphology of the polymer remains the same over the temperature range of interest, thus it has been used primarily for homopolymers. However, in recent years time-temperature superposition has been applied to compatible polymer blends and microphase-sparated block copolymers. It should be mentioned that there is no theoretical guideline as to how the values of a_T for compatible polymer blends and multiphase polymer systems may be predicted from the WLF or any other equations. Thus, the values of a_T for multiphase polymer systems (e.g., block copolymers) are usually obtained by shifting the values of G' (or η') along the frequency ω axis empirically.

Arnold and Meier [1970] first studied the SBS block copolymer melts at temperatures ranging from 150 to 200 °C. The $\eta'(\omega,T)$ data were superimposed onto master curves for each copolymer sample. The shift factors for all five block copolymer samples fell on one of two lines when plotted as a_T *vs* T (or log a_T *vs* $1/T$). Using the Arrhenius relationship [equation (2.1-12)], they calculated the activation energies E, which were 38 and 19 kcal/mole for the two lines. They pointed out that the 38 kcal/mole activation energy (which was also same as the activation energy of pure homo-polystyrene at that particular reference temperature) corresponded to the semicontinuous PS morphology (cylinder or lamella) and the 19 kcal/mole (close to pure PB activation energy) activation energy corresponded to the dispersed PS morphology (PS sphere). A similar activation energy (37 kcal/mole) was reported by the Tschoegl group [Fesko and Tschoegl 1971] for a SBS triblock copolymer, while constructing a master curve at temperatures around T_g of the polystyrene phase. Although the data could be superposed without difficulty, a simple consideration of the nature of the retardation processes in two-phase systems (such as the SBS triblock copolymers at $T < T_s$ leads one to skepticism that valid master curves should result from simple translation of the measured viscoelastic responses along the logarithmic time or frequency axis. Such a translation, valid for thermorheologically simple materials, is predicated upon the assumption that all retardation times are equally affected by a change in temperature. A two-phase material would fulfill this requirement over the entire time scale only if the responses of both phases would be identical. This could not be true in general and would be unlikely in practice. Thus, the two-phase systems, being thermorheologically complex, would admit superposition by simple translation at most in regions of temperature and time or frequency over which the behavior is completely dominated by one or the other phase.

Gouinlock and Porter [1977] reported that a master curve for $\eta(\dot{\gamma})$ of a SBS melt over a temperature range that spanned the microphase-separation transition separated into two branches, one branch characterizing the non-Newtonian behavior of the SBS triblock copolymer (with 25% PS) and the other corresponding to the Newtonian response. The activation energy decreased from 46 kcal/mole at 80 °C to 17 kcal/mole at 170 °C (well above $T_s \cong 142$ °C). All activation energy data fell between E values of the constituent homopolymers, which indicated that the PS blocks altered the dynamic properties of the PB component (the continuous phase), and ultimately the dynamic properties of the whole material, at all temperatures examined (since the activation energy of homo-PB was almost a constant, 19 kcal/mol, over the temperature range). Futamura and Meinecke

[1977] also reported activation energy for SBS, SIS, SEBS and SEPS triblock copolymers in the same range (from 16 to 38 kcal/mole).

Han *et al.* took another approach. In order to determine the microphase separation temperature (also called order-disorder transition temperature), they [Han & Kim 1987 and 1993; Han *et al.* 1989 and 1990] plotted G' versus G'' logarithmically, instead of superimposing the viscoelastic functions. This log G' *vs* log G'' plot was first used in 1941 by Cole and Cole [1941] for a number of materials and thus is also called Cole-Cole plots. Han *et al.* observed that the log G' *vs* log G'' plots were virtually independent of temperature for single-phase homopolymers and compatible polymer blends in the molten state, but very sensitive to variation in the morphological state of heterogeneous polymer systems. The log G' *vs* log G'' plots for diblock copolymers investigated by Han *et al.* varied with temperature up to a certain critical temperature and then became virtually independent of temperature as the temperature increased further. Therefore, the critical temperature at which log G' – log G'' plots ceased to vary with temperature was determined as T_s.

Rosedale and Bates [1990] studied the poly(ethylenepropylene)-poly(ethylethylene) (PEP-PEE) diblock copolymers (with 55% PEP) and found that in the terminal zone ($\omega \rightarrow 0$), the reduced-variable plots of G_r' *vs* ω_r and G_r'' *vs* ω_r fell into two distinct categories: $G_r' \propto \omega_r^2$, $G_r'' \propto \omega_r$ for samples in the disordered state and $G_r' \propto G_r'' \propto \omega_r^{0.5}$ in the ordered state. A critical frequency $\omega_{r,c}$ was found, above which ($\omega_r > \omega_{r,c}$) each modulus, instead of being separated into the above two categories (ordered or disordered), superimposed satisfactorily and formed one master curve. Similar results were reported by Winter *et al* [1993] for a SIS triblock copolymer.

Some researchers had tried superimposing the rheological functions for the block copolymers, but little has been done to understand why it is possible to superimpose data for an apparently two-phase material. In this study, we investigated several triblock copolymers with different molecular weight, PS compositions and morphologies, with a new emphasis on the kinetics of the microstructure formation in various regimes of temperature.

7.2. Experimentals

7.2.1 Sample Characterization and Preparation

The triblock copolymer samples used in this study were commercial polymer products (under the trade name VECTOR styrenic block copolymers), provided by DEXCO Polymers of plaquemine, LA. The samples were characterized by DEXCO and the details are listed in Table 7.1. The molecular weight and molecular weight distribution were measured by DEXCO. Some samples (e.g. SIS-4111) were also tested in our lab using NMR (Nuclear Magnetic Resonance, not in Table 7.1). The melt index data were also provided by DEXCO.

The glass transition temperatures (T_g) of the constituent blocks were measured by DSC under a nitrogen blanket in this lab. T_g varied slightly depending on the heating or cooling rates. Here, $T_g^{PS} \cong 70$ °C, $T_g^{PB} \cong -90$ °C and $T_g^{PI} \cong -60$ °C at zero DSC scan rate (extrapolated). These values were taken as the peak values on DSC curves where the glass transition occurred (see Chapter 6). The peaks, either endothermic or exothermic depending on whether it was a heating or cooling run, usually covered a temperature range of up to 50 degrees. Later in this chapter, we will find that the T_g measured by rheology is usually higher than this peak value taken from DSC curves (e.g. for T_g^{PS}, it was found to be around 100 °C by rheology). This is because the reported DSC values are taken as the temperature at the peak of the transition but rheology detects the completion of the transition where the viscoelastic functions change abruptly.

Table 7.1: Sample Characterizations

Polymer	*Mw*	*Mw/M_n*	ϕ_{PS}	Morphology	Melt Index
	(kg/mol)		(%)		(g/10 min.)*
SIS-4111	125,000	≤1.06	18	PS sphere	12
SIS-4211	90,000	≤1.06	29	PS cylinder	13
SIS-4411-D	75,000	≤1.06	44	PS lamellae	40
SBS-8508	70,000	≤1.06	29	PS cylinder	12
SBS-6241-D	60,000	≤1.06	43	PS lamellae	23

* . 200 °C, 5 kg.

The block copolymer pellets were first pressed into discs of 25 mm in diameter and 2 mm in thickness in a compression-molding device at temperature around 170 °C for rheological tests. The compression molding was done either in air or in vacuum. Under either molding condition, the molding time was controlled to be under 2~3 minutes to avoid possible thermal damage. (The rheological results from samples molded under air and vacuum showed no apparent difference.) Avoidance of rheological artifacts (e.g., slip due to use of mold release compounds) is discussed in Appendix B. The sample disc was then further compressed in the RMS-800 at around 200 °C and the final gap between the parallel plates was set at around 1 mm. The excess sample at the platen rim was trimmed away.

7.2.2 Equipment and Experimental Procedure

The rheological instrument used in the project was the Rheometrics Mechanical Spectrometer RMS-800 (Rheometrics Scientific, Parsippany, NJ, USA). Parallel plates geometry was employed and nitrogen was used as purging gas throughout the test. The details of the RMS-800 instrument can be found in section 4.1.

For measuring the rheological properties, such as moduli G' & G'' and dynamic viscosities η' & η'', the sample disc in the rheometer was first heated to 200 °C and annealed for about 10 minutes, then cooled to the testing temperature. The high temperature was necessary for both releasing the stress that built up during the compression molding and setting the gap, and it is also important to soften the polymer at this high temperature so that it sticks to the surface of the plate (wets the platen surface). Strain sweep tests were performed at all testing temperatures in order to select a proper strain and frequency pair (i.e., low enough) so that the material's rheological response was well within the linear viscoelastic range. But at the same time, material stress had to be high enough so that the material response yielded large enough torque values for accurate RMS-800 results. The strain amplitude chosen for tests at all temperatures and frequencies (from 0.01 to 100 rad/s) was 1%.

7.3. Results and Discussion

Consider curves of $G'(\omega)$ measured at different temperatures and displayed on plots of log G' *vs* log ω. If a polymeric material is thermorheologically simple, the distance, log a_T, by which a given value of log $G'(\omega)$, at temperature T must be translated horizontally to fall onto the log $G'(\omega)$ curve at reference temperature T_R, is the same for all values of ω. This arises because, by the definition of a thermorheologically simple material, all retardation times, $\tau_i(T)$, where I = 1,2,3,…. , at temperature T bear a constant ratio, a_T, to the corresponding retardation times, $\tau_i(T_R)$, at the reference temperature T_R, i.e.,

$$\frac{\tau_i(T)}{\tau_i(T_R)} = a_T \qquad (7.3-1)$$

Hence, all data recorded at a given temperature form a segment of the total response or master curve and a simple translation of the segment along the log ω axis by the amount log a_T will result in superposition. If, however, the material is thermorheologically complex (i.e., a two-phase material such as block copolymer at $T<T_s$), equation 7.3-1 does not hold, and log a_T becomes a function of frequency in

addition to temperature. Consequently, shifts of different magnitude are required for each value of ω.

Though there are several empirical equations proposed to calculate a_T values for thermorheologically simple materials (see section 2.1.7), there is no theoretical guideline as to how the values of a_T for thermorheologically complex materials (multiphase polymer systems) may be obtained from these equations. Thus, the values of a_T for multiphase polymer systems (block copolymers in particular) are usually obtained by shifting the values of G' (or G'') obtained at one temperature along the frequency ω axis to merge into a master curve representing T_R. By shifting enough such curves one can define the entire master curve from its various segments. This empirical shifting has to meet the following criteria: (a) exact matching of the shapes of adjacent (nearby T) curves, (b) the same values of shift factor a_T must superpose all types of viscoelastic functions into their own master curves, and (c) the temperature dependence of a_T must have a reasonable form consistent with experience.

Figures 7.1 to 7.5 show reduced plots of tan δ, which by definition is a measure of the ratio of energy lost to energy stored in a cyclic deformation (tan $\delta = G''/G' = \eta'/\eta^{*}$). It is dimensionless and conveys no physical magnitude of the modulus or viscosity. The reference temperature T_{ref} chosen is usually related to the glass transition temperature, T_g.

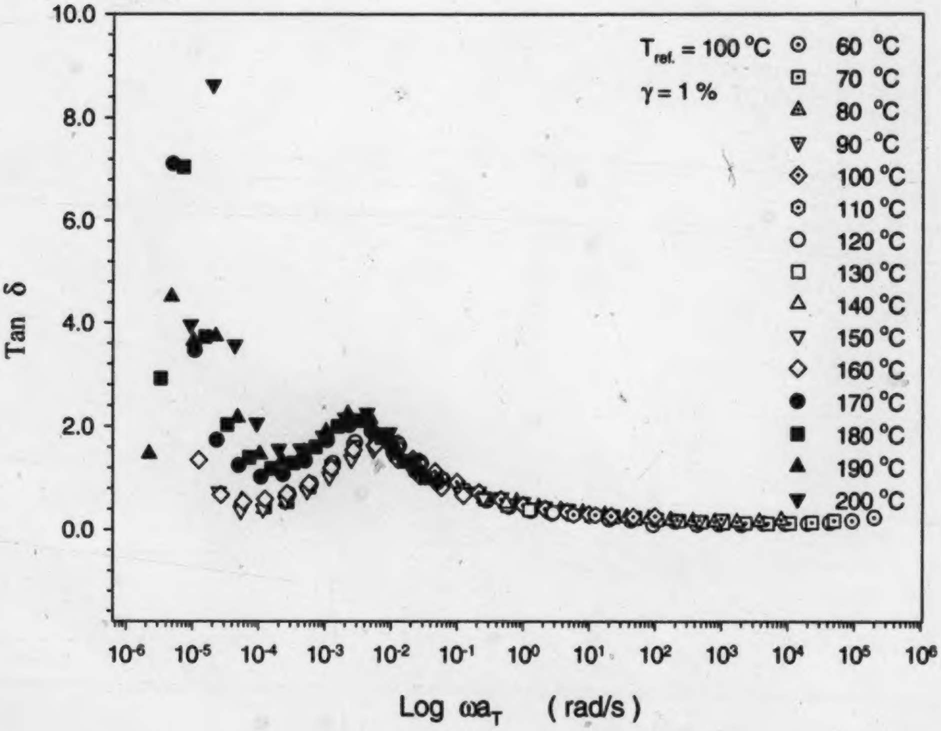

Figure 7.1: Reduced plot of tan δ for SIS-4111 (M_w = 125,000 g/mol, ϕ_{PS} = 18 %), at reference temperature 100 °C. Open symbols represent the data taken at $T \leq 160$ °C, and the filled symbols stand for data at $T \geq 170$ °C. T_s = 167 ± 2 °C.

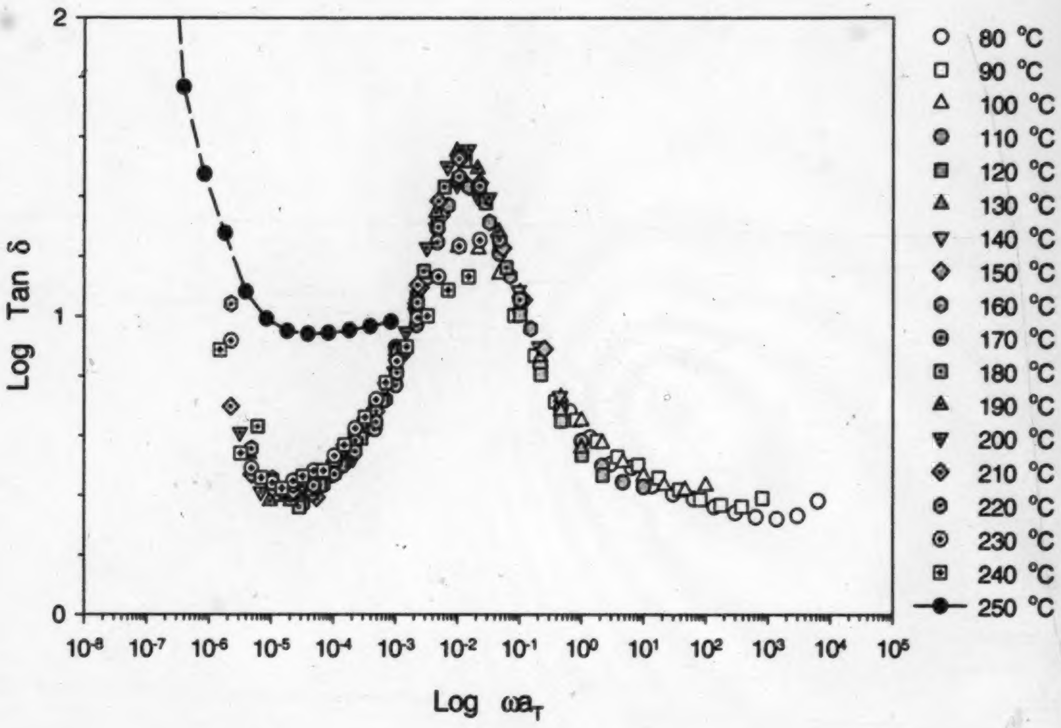

Figure 7.2: Reduced plot of tan δ for SBS-8508 (M_w = 70,000 g/mol, ϕ_{PS} = 29 %), at reference temperature 100 °C. Open symbols represent the data taken at $T \leq 100$ °C, the light-color filled symbols represent data at $100 < T \leq 240$ °C and the dark-color filled symbol stands for the data at $T = 250$ °C. $T_s \cong 242$ °C.

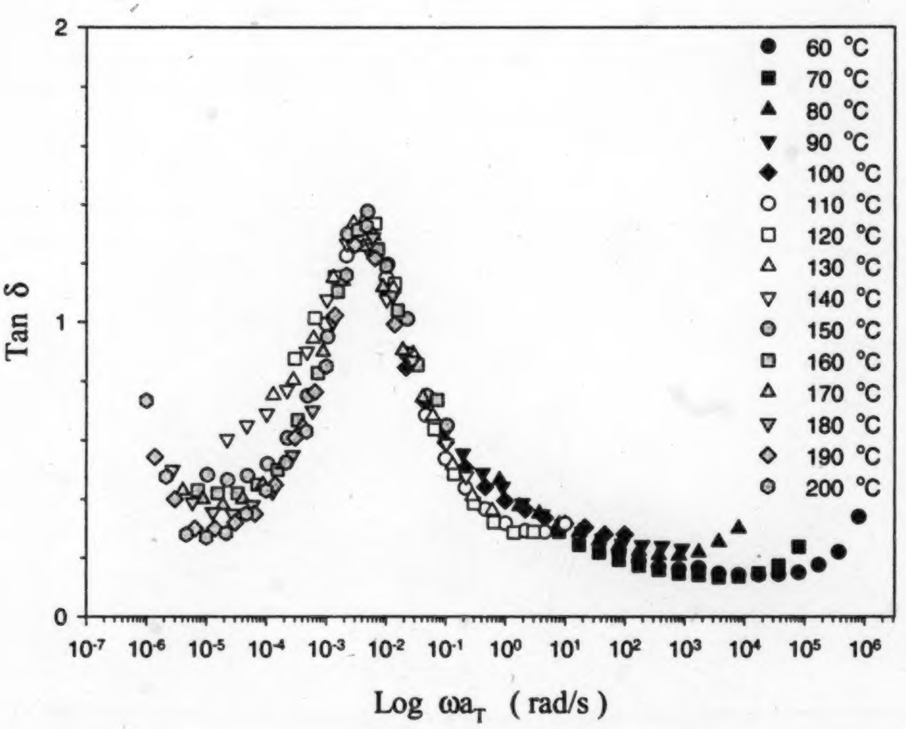

Figure 7.3: Reduced plot of tan δ for SIS-4211 (M_w = 90,000 g/mol, ϕ_{PS} = 29 %), at reference temperature 100 °C. Dark-color filled symbols represent the data at $T \leq 100$ °C, the open symbols represent the data at $100 < T \leq 140$ °C and the light-color filled symbols stand for the data at $T \geq 150$ °C.

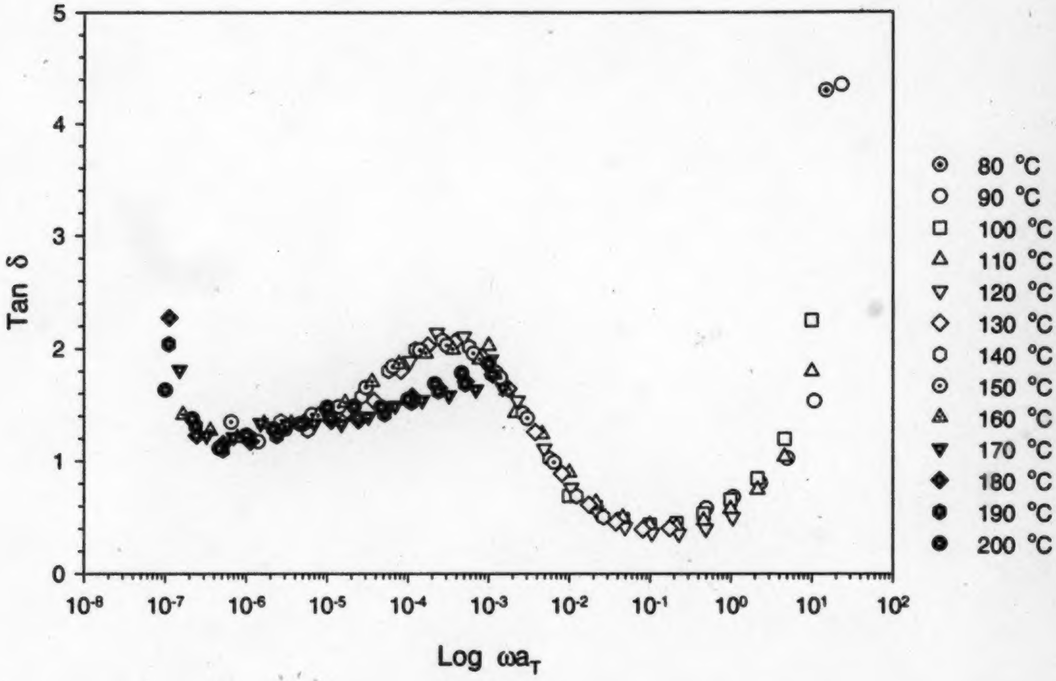

Figure 7.4: Reduced plot of tan δ for SIS-4411-D (M_w = 75,000 g/mol, ϕ_{PS} = 44%), at reference temperature 100 °C. Open symbols represent the data at $T \leq 160$ C, and the filled symbols stand for data at $T \geq 170$ °C.

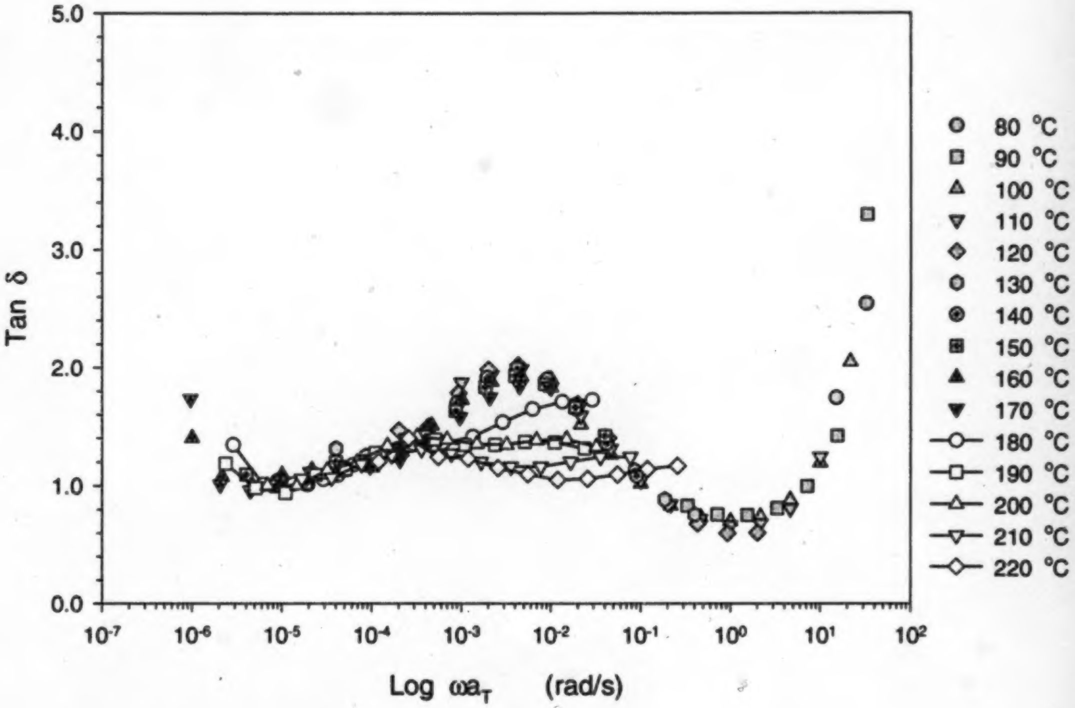

Figure 7.5: Reduced plot of tan δ for SBS-6241-D (M_w = 60,000 g/mol, ϕ_{PS} = 43%), at reference temperature 100 °C. Filled symbols represent the data at $T \leq 170$ °C, and the open symbols represent the data at $T \geq 180$ °C.

For block copolymers, however, T_g is not unique. Therefore, in this study we arbitrarily choose $T_{ref} = 100$ °C which is close to T_g^{PS}.

At low frequencies ($\omega \rightarrow 0$), tan δ is large for all the uncross-linked polymers and in fact becomes inversely proportional to the frequency. Because in this terminal zone, G'' is proportional to ω and G' to ω^2, so from G''/G' it is clear that tan δ is proportional to ω^{-1}. This ($G'' \propto \omega$ and $G' \propto \omega^2$) is also used by some researchers [Rosedale and Bates 1990, Han and Kim 1993] as a criterion to identify T_s for the block copolymers. In the disordered state ($T > T_s$) the block copolymers behave like uncross-linked amorphous polymers ($G'' \propto \omega$ and $G' \propto \omega^2$), but more like cross-linked polymers in the ordered state ($T < T_s$, and G'' is not proportional to ω and G' to ω^2). In fact, it was found that both G'' and G' are proportional to $\omega^{0.5}$, $G' \sim G'' \sim \omega^{0.5}$, in the ordered state ($T < T_s$) [Rosedale and Bates 1990].

This criterion is also used in this study to identify T_s for some of the samples. In the ordered state ($T < T_s$): $G' \sim G'' \sim \omega^{0.5}$ and tan δ has a finite value. But in the disordered state ($T > T_s$), tan δ has the tendency to go to infinity when $\omega \rightarrow 0$ (since tan δ is proportional to ω^{-1}). In figure 7.1 the tan δ data fall on one master curve at $T \leq 170$ °C, but fail to superimpose on to one curve at $T \geq 170$ °C. For this particular polymer (SIS-4111) we measured that $T_s = 167 \pm 2$ °C (see Chapter 5, Section 5.3.1). Tan δ data at $T \geq 167$ °C all have the tendency to go to infinity. The reason that tan δ curves are able to superimpose on to one master curve at $T < T_s$ is, we believe, that the polyisoprene

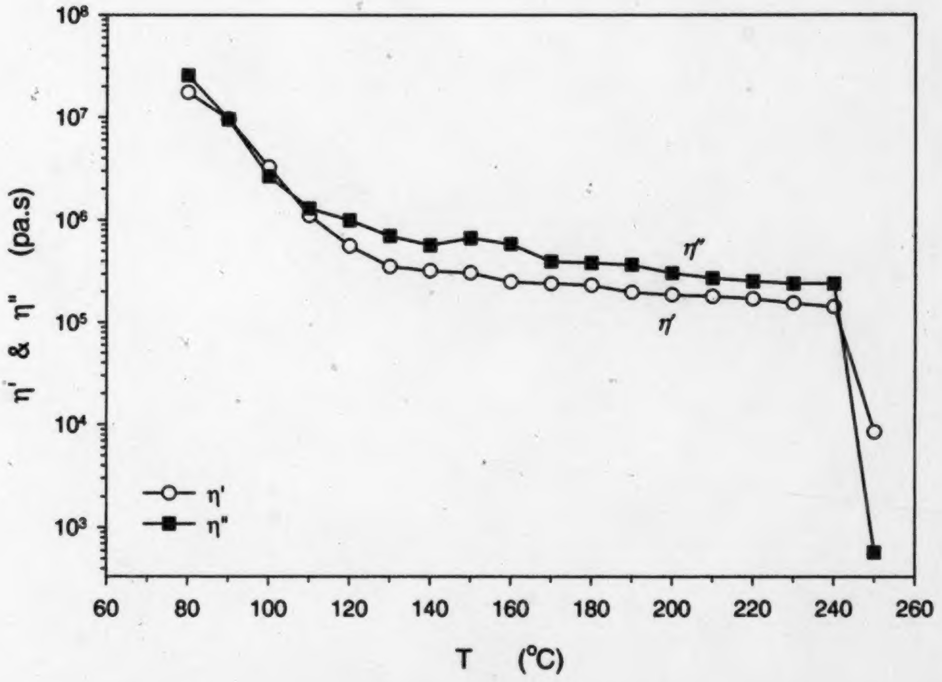

Figure 7.6: Frequency sweep test for SBS-8508. Open circular symbols are dynamic viscosity η', and the filled square symbols are η''. Both η' and η'' drop dramatically and cross over each other at around 242 °C. ω= 0.01 rad/s and γ^0 = 1%.

rubbery matrix phase (82%) dominates the rheological responses. This will be evident when we discuss the tan δ behavior at around T_g^{PS} in the later part of this chapter. On the other hand, failing to superimpose the data at $T > T_s$ is, we believe, due to the concentration fluctuation (see Chapter 5).

For sample SBS-8508, the viscosities η' and η'' are plotted as functions of temperature in Figure 7.6. Both functions drop dramatically above 240 °C, and cross over each other at around 242 °C. The η'', which is a measure of the energy stored in the sample, drops below the dynamic viscosity η' (which measures the energy dissipated in the sample) at $T > 240$ °C. In Figure 7.2, the tan δ also goes to infinity as $\omega \rightarrow 0$ above 240 °C. Thus, T_s is identified to be around 242 °C. This T_s also agrees well with the result predicted by the Leary-Williams (L-W) theory [Leary and Williams 1974, Henderson and Williams 1985, Spaans *et al.* 1999].

The L-W model [Leary and Williams 1970, 1973 and 1974] predicts spontaneous microphase separation upon cooling the polymer from its high-temperature state of homogeneity (or spontaneous re-mixing upon heating) will become possible if the free energy of mixing $\Delta G_m = \Delta H_m - T\Delta S_m$ goes to zero (where ΔH_m and ΔS_m are the corresponding enthalpy and entropy changes). Thus $T_s = \Delta H_m/\Delta S_m$. Most of the dependence of T_s on M and ϕ_{PS} lies within ΔH_m rather than ΔS_m, so evaluation of ΔH_m leads to the major understanding of $T_s(M, \phi_A)$ behavior for any given microstructural geometry.

The L-W theory uses regular solution theory to show [Leary and Williams 1973] that, to a good approximation, $\Delta H_m \propto M\phi_A\, \phi_B\, (\delta_A - \delta_B)^2$, where $\phi_A + \phi_B = 1$ and δ_i is the solubility parameter of either block components i (A or B). Since the model therefore predicts that $T_s \propto M$ *and* $T_s \propto \phi_A\, \phi_B = \phi_A\, (1 - \phi_A)$, the value of T_s for a present experimental case (labeled α) can be scaled from an earlier calculated one (or earlier experimental result, labeled β) by (with same constituent blocks):

$$T_s^{\alpha} = \frac{\overline{M}_n^{\alpha}[\phi_A^{\alpha}(1-\phi_A^{\alpha})]}{\overline{M}_n^{\beta}[\phi_A^{\beta}(1-\phi_A^{\beta})]} T_s^{\beta} \qquad (7.3-2)$$

However, the L-W model does imply that the scaling strategy can be used only for cases wherein the same microstructures prevail (dispersed PS spheres, or lamella etc.). This condition is determined largely by the magnitude of ϕ_A, so an approximately matching of this parameter between the experimental and model cases is necessary.

The T_s^{β} of a reference SBS sample (taken from published data [Leary and Williams 1974] with molecular weight M_w = 58,000 g/mol and ϕ_{PS} = 46.3%) is 515 K. With equation 7.3-2, we predict for SBS-8508 (M_w = 70,000 and ϕ_{PS} = 0.29) that $T_s^{\alpha} \cong$ 241.8 °C, which is very close to what measured by reduced tan δ plot (Figure 7.2) and frequency sweep result (Figure 7.6).

L-W model also extends the scaling strategy to include other block copolymers such as SIS [Henderson and Williams 1985], so that T_s can be estimated without employing the entire calculation scheme. In the lowest order of approximation, considering SIS and SBS copolymers with the same ϕ_{PS}, $T_s^{(0)}$ for the former can be estimated as

$$\frac{T_s^{(0)}(SIS)}{T_s(SBS)} = \frac{(\delta_S - \delta_I)^2 \overline{M}_{SIS}}{(\delta_S - \delta_B)^2 \overline{M}_{SBS}} \qquad (7.3-3)$$

where T_s(SBS) is taken from published results of detailed theoretical calculation or experimental data. However, this approximation to T_s(SIS) is too crude for most practical purposes and fails to reflect interphase information. A better estimation $T_s^{(1)}$ using the basic L-W theory was proposed [Henderson and Williams 1985], as represented by

$$T_s^{(1)}(SIS) = C_i T_s^{(0)}(SIS) \qquad (7.3-4)$$

where C_i is a coefficient that depends on which type of $\phi_{PS}(x)$ function in the interphase is used (x = coordinate measured across the interphase). For the copolymers with slightly different ϕ_{PS} such as the samples used in this study, we further incorporate the compositions into equation 7.3-3 as implied by Equation 7.3-2:

$$\frac{T_s^{(0)}(SIS)}{T_s(SBS)} = \frac{(\delta_S - \delta_I)^2 \overline{M}_{SIS} \phi_{PS} \phi_{PI}}{(\delta_S - \delta_B)^2 \overline{M}_{SBS} \phi_{PS} \phi_{PB}} \qquad (7.3-5)$$

Figure 7.3 shows the reduced plot of tan δ for sample SIS-4211. In the terminal zone where $\omega \rightarrow 0$, the data separates into two branches. One branch contains data at $T \leq$ 140 °C. The other branch consists of data at $T \geq 150$ °C. Failing to superimpose the data onto one master at 140-150 °C indicates a phase transition occurs at around 150 °C. The Leary-Williams scaling theory [Eq. 7.3-5] predicts T_s for this polymer to be around 160 °C, a little higher than the transition temperature measured by the reduced tan δ plot. The discrepancy could be due to the two samples having different interphase composition profiles $\phi_{PS}(x)$, which is not accommodated by the scaling ratio of Equation 7.3-5.

Figures 7.4 and 7.5 show the reduced plot of tan δ for SIS-4411-D and SBS-6241-D, respectively. In the terminal zone ($\omega \to 0$) the master curves break up above certain temperatures. For SIS-4411-D, at $T \geq 170$ °C the tan δ splits from the master curve and does not show a maximum at $\omega > 10^{-5}$. For SBS-6241-D at $T \geq 180$ °C, tan δ departs from the master curve and does not show the maximum at $\omega > 3 \times 10^{-4}$. These similar behaviors of tan δ only happened to the block copolymers with 44% PS content, which had the lamellar morphology. For samples with lower PS content, the master curves break up differently (Figures 7.1, 7.2 and 7.3). The Leary-Williams theory predicts that $T_s \cong 170$ °C for SIS-4411-D and $T_s \cong 258$ °C for SBS-6241-D. The theoretical result is close to the transition temperature measured by superimposing tan δ for SIS-4411-D but higher than the SBS-6241-D transition temperature.

In the transition zone ($10^{-4} < \omega < 10^{-1}$) between glasslike and rubberlike consistency, however, all loss tangent data go through a pronounced maximum regardless of the PS content and the molecular weight (Figure 7.1 ~7.5). It is of interest that at the high frequency end of the curve ($\omega \geq 10^{-1}$ rad/s) where the block copolymers are in the glassy state, the loss tangent behaves in accord with the PS content. At low PS (SIS-4111 with 18% PS and spherical morphology) tan δ data fall on one master curve above and below the PS glass transition temperature. At T_g^{PS} the PI matrix is in rubbery state and the PS phase transfers from rubbery to glassy. But the reduced plot of tan δ reflects no texture change at all. The success of superimposing the loss tangent indicates that the rheological behavior of this polymer (SIS-4111) is completely dominated by the PI phase. The small amount of PS spheres act like particle fillers which affect very little the rheological response of the PI matrix. This also explains why at $T_g^{PS} < T < T_s$, a two-phase system in nature, the rheological functions of these block copolymers can still be successfully superimposed.

At moderate PS content (SIS-4211 and SBS-8508, both with 29% PS and cylindrical morphology), tan δ at the high frequency end ($\omega > 10^{-1}$ rad/s) splits (Figures 7.2 and 7.3). The loss tangents at $T < T_g^{PS}$ (= 100 °C) fail to superimpose onto the existing master curve ($T_s > T > T_g^{PS}$). The glass transition of the PS phase is clearly shown on the reduced tan δ plot. In this case, the rheological response of these two block copolymers is not completely dominated by the rubbery (PI or PB) phase. The effect of the glassy PS cylindrical domains inside the rubbery matrix of the middle block is evident. Compared to SIS-4111 (18% PS and spherical PS morphology), it is understandable that for these two copolymers (29% PS and cylindrical PS morphology) the glassy PS cylinders (nominally of infinite length) among the rubbery matrix will affect the rheological properties more effectively than the PS spheres.

For SBS-6241-D and SIS-4411-D with two dimensions of semi-infinite extent (lamella PS phases), when the PS phases transform from rubbery to glassy we expect to see more prominent changes in the loss tangent curves. As shown in Figures 7.4 and 7.5, tan δ goes to a large value at the high frequency end ($\omega > 10^{-1}$ rad/s). Loss tangent is defined as the ratio of the energy lost to the energy stored in a cyclic deformation: tan $\delta = G''/G'$. For a rigid solid, such as glass, rubber and tightly cross-linked polymer, there would be no energy lost except the energy stored in the material during a cyclic deformation. However, for a liquid ($T > T_t$) there is only energy loss but no energy stored. So naturally, for liquid the loss tangent tends to go to infinity (as I used it to identify the homogeneous state), and tan δ tends to go to zero for solid. But in Figures 7.4 and 7.5, the loss tangent showed a rather large value. At $T < T_g^{PS}$, the two-dimensional PS microphases act like network joining points in the rubbery matrix (PI or PB phase) and the material behaves like a cross-linked polymer. The large amount of glassy PS phases (44%) also makes the sample more solid than rubber. So the high value of loss tangent indicates the possibility that slip between specimen and platen occurred during the oscillatory test at high frequency and large strain amplitude.

deGennes [1979b] believed that all polymer (melts) will slip on metal surface, as these large molecules can hardly wet the surface. We also found in some cases the polymer melt did slip during tests with the rheometer (Appendix B). For cross-linked solid materials (at $T < T_g^{PS}$), such as SIS-4411-D and SBS-6241-D, it is understandable that they slip on the metal platen surface during high frequency tests. Once the slip occurred, it gave the false response of a liquid, thus the tan δ would show a rather large value. This slip is mainly due to the presence and domination of large amount of glassy PS lamellar domains. Thus, the rheological function measured at around T_g^{PS} is very much dominated by the PS phase, even though it is the minority phase (~ 44%).

The slip that occurred among copolymers with high PS content is also evident in Figures 7.7 and 7.8. In Figure 7.7, the complex viscosity η^* ($\equiv [\eta'^2 + \eta''^2]^{1/2}$) for SBS-6241-D (44% PS) is plotted at different temperatures. Below the glass transition temperature of the PS phase ($\cong$ 100 °C), this material is in a solid state with planar glassy PS domains connected by the rubbery PB middle block. The complex viscosity for this kind of material should increase with decreasing temperature and show power-law ω-behavior. Instead, η^* at 70 ~90 °C (solid lines and light-color filled symbols) drops as ω increases and the value of η^* drops even below those (dotted line) at $T >> T_g^{PS}$. The frequency at which η^* drops increases with temperature, e.g. at 80 °C η^* drops at $\omega = 10^{-1}$ rad/s, but at 90 °C η^* drops at $\omega \cong 3$ rad/s. The more close to T_g^{PS}, slip only occurs at higher ω. This is also clear in Figure 7.8. Plotted dynamic viscosity η' as a function of temperature at different ω, η' drops at certain temperature below T_g^{PS}, instead of going up (e.g. power-law behavior for solid material such as this SBS should be at $T < T_g^{PS}$). When the frequency is higher, the slip occurs even at 90 °C (e.g. at 100 rad/s, it slips at all temperatures ≤ 90 °C). But at very low frequency (e.g. 0.01 rad/s), no slip seems to happen even at 70 °C. Similar behaviors were found for SIS-4411-D (44% PS), but not for other block copolymer samples.

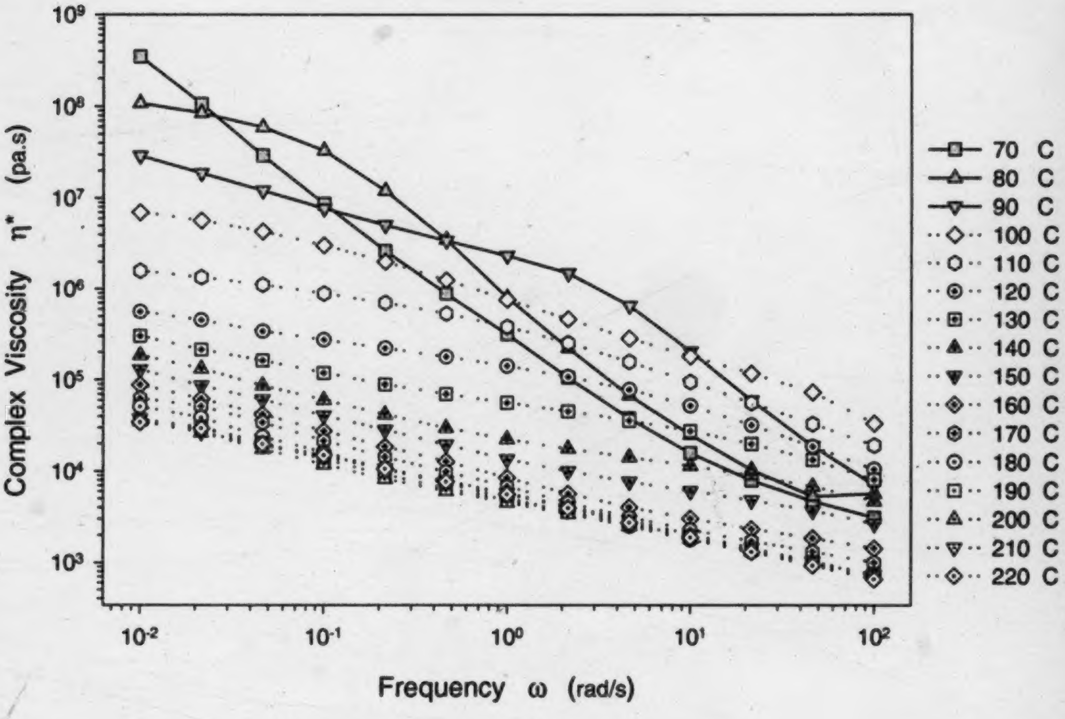

Figure 7.7: Frequency sweep tests for SBS-6241-D, with M_w = 60,000 g/mol and ϕ_{PS} = 43%. Complex viscosity $\eta^* \equiv (\eta'^2 + \eta''^2)^{1/2}$. Solid line represents η^* data at $T < T_g^{PS}$ and where slip occurs at high ω Dash line represents the η^* data at $T > T_g^{PS}$.

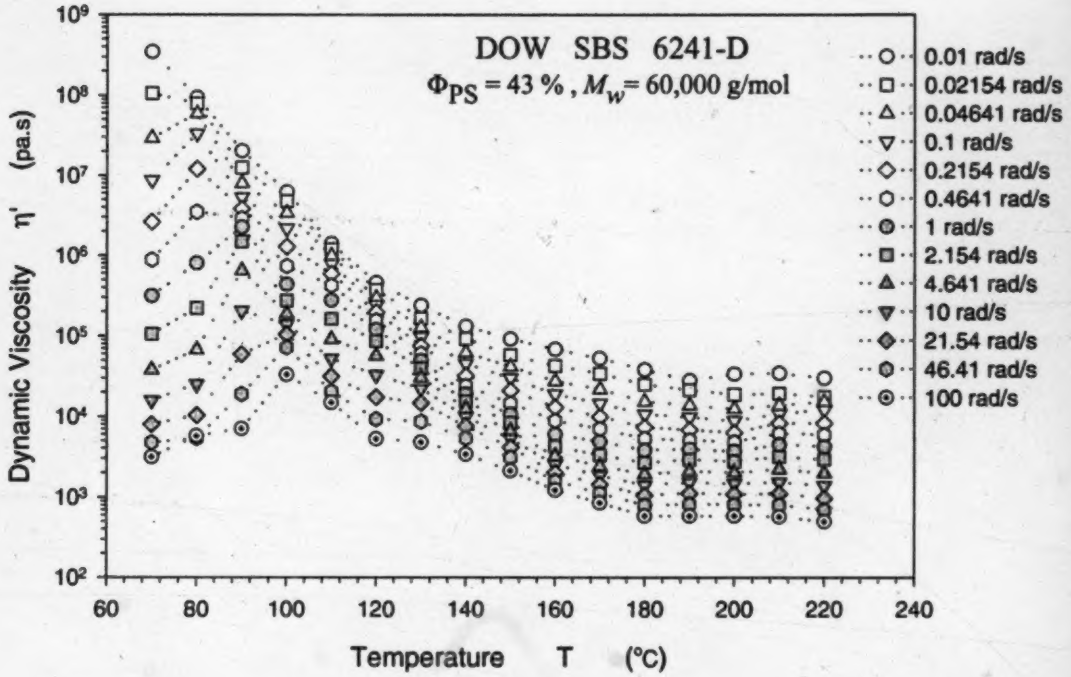

Figure 7.8 : Dynamic viscosity η' for SBS-6241-D at different oscillatory frequency ω. The data at $T < T_g^{PS} = 100$ °C show slip and for higher frequency the slip persists to higher temperature (e.g. at $\omega = 100$ rad/s, the slip occurs even at 100 °C; while at $\omega = 0.1$ rad/s, the slip only occurs at $T < 80$ °C). Also notice that at $T \geq 180$ °C, or $T > T_s$, the dynamic viscosity becomes a constant. The reason that instead of an abrupt drop of viscosity at T_s, as some block copolymers do (e.g. SIS-4111), the constant values of η' are probably due to the high content of PS.

The viscosity curves in Figure 7.7 were also superimposed using the same set of shifting factors for the loss tangent data, and the result is shown in Figure 7.9. The η^* data superposes onto a perfect master at $T \leq 170$ °C but fails at $T \geq 180$ °C where the η^* data depart slightly from the master curve. This temperature also agrees well with the $T_s \cong 170$ °C measured by the reduced plot of loss tangent (Figure 7.5). Unlike superimposing the tan δ (which were only shifted along the ω axis mostly), η^* were not only shifted along the ω axis, but also along the vertical-axis. The same set of shift factors a_T that superimposed the loss tangent data was used to shift η^* along the frequency. Another set of shifting factors b_T was used to shift η^* along the vertical-axis. Both vertical and horizontal shifting is empirical, according to the three criteria for superposition (see Chapter 2, Section 2.1.7). We did, however, employ a computer program developed by Gordon and Shaw [1994], to check our results. Although easy to use once mastered, it neglects most of the small deviations on the curves and forces the rheological functions onto a master curve. Even so, the computer generated master curve qualitatively agrees with our result well.

The shift factors were fit to one of the correlation equations developed (also see Chapter 2, Section 2.1.7). And the best results are obtained with the Arrhenius equation, which is claimed to be most useful for high temperatures:

$$\log a_T = B\left(\frac{1}{T} - \frac{1}{T_{ref.}}\right) \qquad (7.3-6)$$

or

$$\log a_T = A + \frac{E}{RT} \qquad (7.3-7)$$

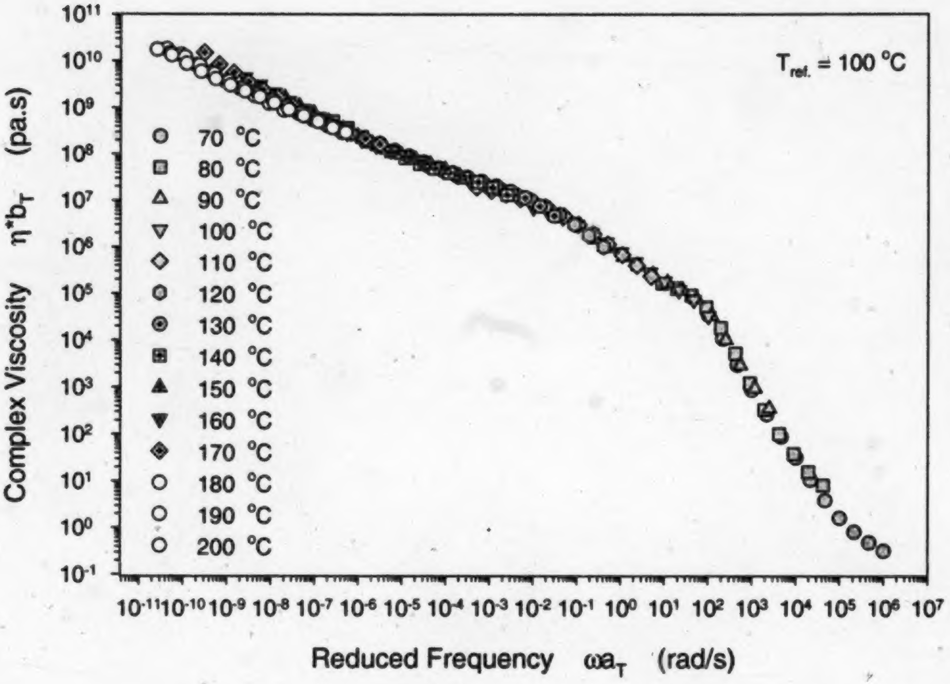

Figure 7.9: Reduced plot of complex viscosity for SBS-6241-D (43% PS, 60,000 g/mol molecular weight). The filled symbols represent the data at $T \leq$ 170 °C, and the open symbols represent data at $T \geq 180$ °C. The master curve splits at temperature between 170 ~ 180 °C, which indicts the MST. The first shoulder at $\omega = 10^2$ rad/s is due to slip between the sample disc and the metal surface of the rheometer.

where A and B are constants, T_{ref} is the reference temperature (100 °C), and E is the activation energy of the material. The temperature dependence of a_T and b_T that was correlated by equation 7.3-7 (for SBS-6241-D) is shown in Figure 7.10. Both shifting factors have unit values at the reference temperature ($T_{ref} = 100$ °C). At T_s, the two curves change slopes. From equation 7.3-7 the constant E, which is interpreted as activation energy for an elementary flow process, can be calculated. All activation energy data are listed in Table 7.2.

The shift factor b_T, however, does not have any particular physical meaning. For a simple fluid, it is often taken as $b_T = \eta_o(T)T_R\rho_R/\eta_o(T_R)T\rho$, where $\eta_o(T)$ is the Newtonian limiting viscosity at temperature T (or the reference temperature T_R) and ρ is the density at either temperature. For block copolymers, such as the samples we used in this study, it is usually not practical to measure η_o (if it ever exists). The ratio of ρ_R/ρ is ($\cong 1.0$). So we made vertical shift of the viscosity data empirically, matching the adjacent curves exactly.

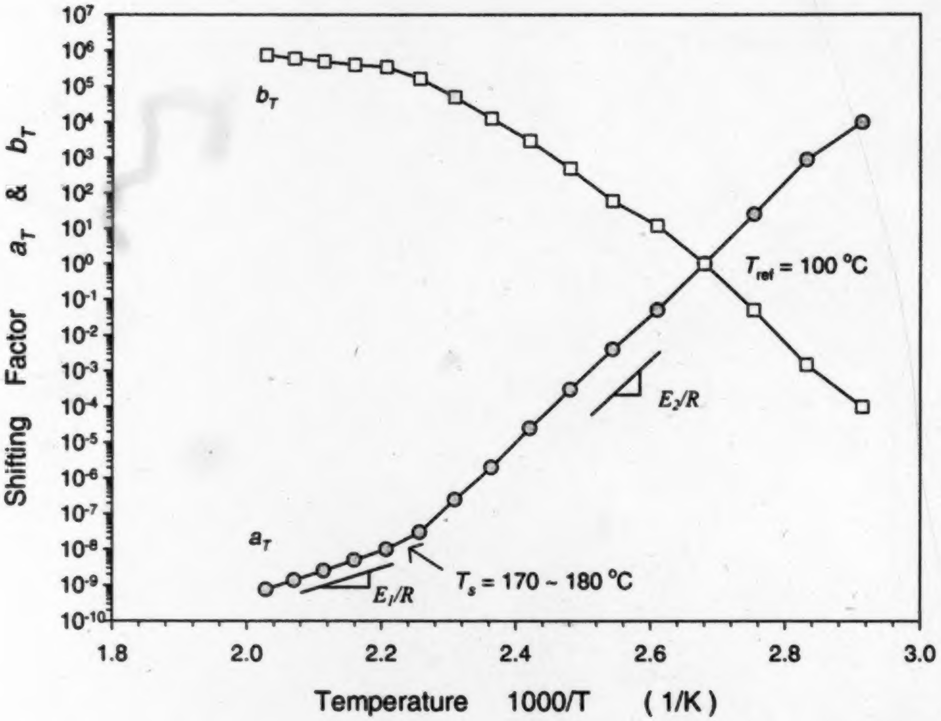

Figure 7.10 : Shifting factors a_T & b_T for SBS-6241-D. The filled symbols stand for a_T, and the open symbols stand for b_T. Both shifting factors have unit values at the reference temperature T_{ref} = 100 °C and both curves change slopes, which by Arrhenius equation is the activation energy E, around T_s. E_1 and E_2 correspond to the activation energy at temperatures above and below T_s, respectively.

Table 7.2 : Characterizing T_S and activation Energy E

#	GRADE	M_w kg/mol	PS wt %	Morphology PS	T_S °C	E_1 kcal/mol	E_2 kcal/mol
1.	SIS-4111	125	18%	sphere	~167	10.38	36.38
2.	SIS-4211	90	29%	cylinder	~145	28.96	55.41
3.	SIS-4411-D	75	44%	lamellae	~165	29.32	86.63
4.	SBS-8508	70	29%	cylinder	~242	12.15	39.97
5.	SBS-6241-D	60	43%	lamellae	~175	28.16	80.81
6.	PS		100%			39~43.2[1]	
7.	PB		0%			7.6[1]	
8.	PI		0%			~8[2]	

[1] The activation energy for the pure polystyrene and polybutadiene are taken from references [Arnold and Meier 1970] and [Futamura and Meinecke 1977]

[2] The activation energy for the pure polyisoprene is taken from reference [Kung *et al* 1985]

The reduced plots of complex viscosity η^* for all five block copolymer samples are shown in Figure 7.11, and the shift factors a_T are plotted in Figure 7.12. Plots of E_1 and E_2 appear in Figure 7.13.

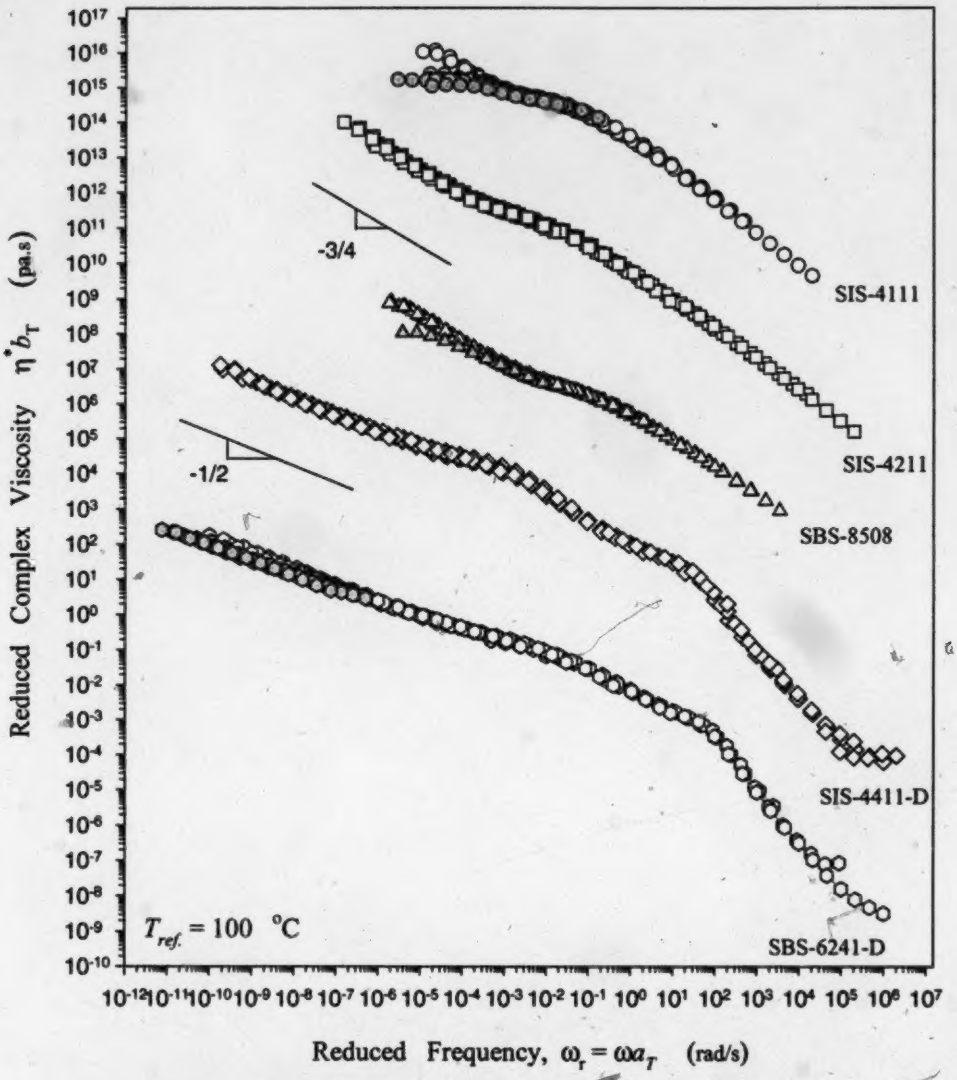

Figure 7.11: Reduced plot of viscosity, at 100 °C reference temperature, for five block copolymer samples: SIS-4111 (S/I=18/82), SIS-4211 (S/I=29/71), SBS-8508 (S/B=29/71), SIS-4411-D (S/I=44/56) and SBS-6241-D (S/B=43/57). Open symbols represent the data below T_s, and filled symbols represent data above T_s. At the terminal zone ($\omega \to 0$) the slope (for data at $T < T_s$) for samples with 43~44% PS is about $-\frac{1}{2}$, and around $-\frac{3}{4}$ for samples with 18% and 29% PS.

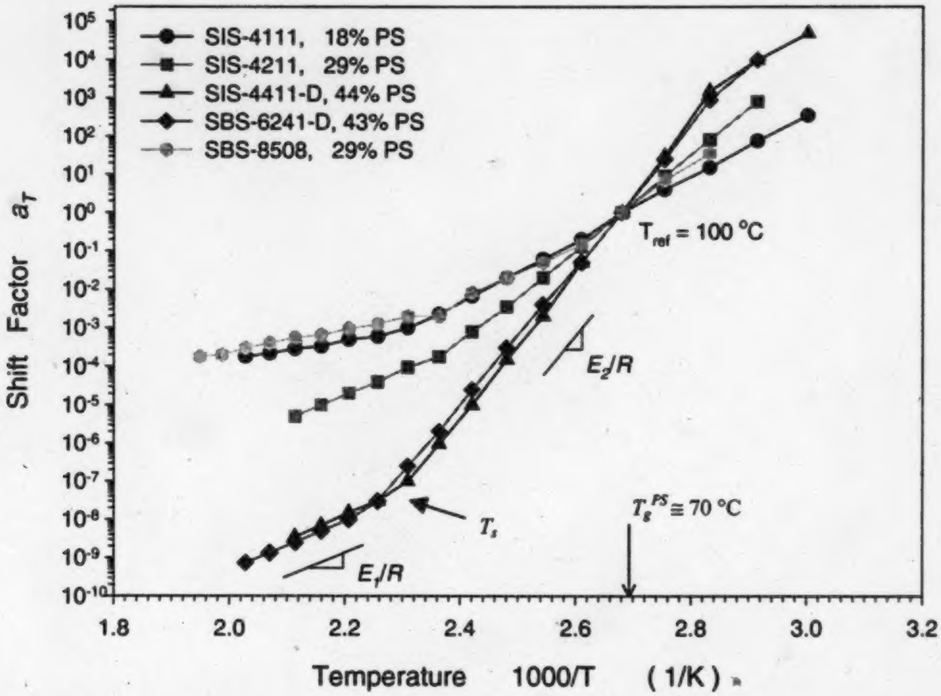

Figure 7.12 : Shift factor a_T for the block copolymer samples. The data were fit to the Arrhenius equation. All curves pass through the $a_T = 1$ point at the reference temperature (T_{ref} = 100 °C). The temperature at which the curve changes slope is defined as T_s. E_1 and E_2 are defined as the activation energies below and above the micro-phase separation temperature, respectively.

Three of the master curves show splits around T_s. For SIS-4111 and SBS-8508, the η^* curves at $T > T_s$ actually leveled, showing a constant limiting (Newtonian) viscosity which indicates the samples are truly in a homogeneous state. SIS-4411-D, however, shows only a minor deviation for η^* below and above T_s. Sample SIS-4211 and SBS-6241-D do not show even any deviation at T_s on the η^* master curves, although on the reduced plots of loss tangent the phase transition is clearly indicated. At this point, we are not sure what causes this difference. One explanation is that the fluctuation effects above T_s. Since the *MST* is a weak first order transition induced by concentration fluctuation, above T_s there exists large amplitude concentration fluctuation. When this concentration fluctuation develops into certain amplitude as T_s is approached, some rheological functions measured around T_s may not be sensitive enough to distinguish the difference between large amplitude composition fluctuation and ordered micro-structure. Rosedale and Bates [1990] also found for a PEP-PEE diblock copolymer that the G' function failed to superimpose from $T < T_s$ up to T_s+ 50 °C, which they attributed to strong composition fluctuation.

One common feature of these master curves in Figure 7.11 is they all show two shoulders, one at $\omega_r \approx 10^{-3} \sim 10^{-1}$ rad/s. This is also reported by Arnold and Meier [1970]. Another shoulder (more like a "knee") that appears only on the master curves of SIS-4411-D and SBS-6241-D is, as we discussed before, caused by the slip between the sample disc and the platen surface of the rheometer (not related to mold release agent). Despite this artifact, the superposition remains good, suggesting that the slippage itself reflects a fundamental property.

Rosedale and Bates [1990] studied PEP-PEE (polyethylenepropylene-polyethylethylene) diblock copolymers containing 55% (by volume) of PEP and found that below the *MST* both loss and storage modulus are functions of $\omega^{0.5}$ in the terminal zone ($G' \sim G'' \sim \omega^{0.5}$ or $\eta' \sim \eta'' \sim \omega^{-1/2}$, where $\eta' \equiv G''/\omega$ and $\eta'' \equiv G'/\omega$). In the present study, I also found $\eta^* \sim \omega^{-1/2}$ in the terminal zone for samples with lamella morphology (SBS-6241-D and SIS-4411-D in Figure 7.11). Both η' and η'' have the same slope ($\sim\omega^{-1/2}$) in the terminal zone. But for samples with cylindrical and spherical morphologies (SIS-4211, SBS-8508 with 29% PS and SIS-4111 with 18% PS), $\eta^* \sim \omega^{-3/4}$ (Figure 7.11, both $\eta' \sim \eta'' \sim \omega^{-3/4}$ also) at $\omega \rightarrow 0$. This leads to $G' \sim G'' \sim \omega^{1/4}$. Such a result has apparently not been reported before. It is tempting to assign such behavior to the intrinsic microstructural differences between the continuous (lamellar) and dispersed (cylindrical and spherical) geometries.

At $T < T_s$, the block copolymers are phase-separated and the polystyrene block congregated into micro-domains depending on the PS content: lamellae (40% ~ 60%), cylinder (20 ~40%) and sphere (10 ~20%). In the terminal zone the low frequency (or long-wavelength) shear deformations are a probe of long range structure because they correspond to the longest relaxation times that are related to long range cooperative motions. Thus, the rheological functions measured in this terminal region respond to different morphologies accordingly. As measures of the energy stored elastically (G') and the energy lost by viscous process (G''), both G' and G'' are more sensitive to frequency for lamella structures than for cylindrical and spherical microstructures. As was shown G'

$\sim G'' \sim \omega^{1/2}$ for SIS-4411-D; SBS-6241-D and $G' \sim G'' \sim \omega^{1/4}$ for SIS-4211; SBS-8508; SIS-4111.

The shift factors a_T for the five block copolymer samples are plotted *vs* $1/T$ in Figure 7.12. All a_T 's have the unit value at the reference temperature ($T_{ref} = 100$ °C). The data were fit to the Arrhenius equation (Eq. 7.3-7). The slopes of the curves are defined as E/R, where E is the activation energy for the elementary flow process of the molecules; values for E_1 and E_2 are listed in Table 7.2. E_1 and E_2 correspond to the activation energies at temperatures below and above *MST*. The temperature at which the slope of the curve changes from E_1 to E_2 is identified as T_s, for that particular sample. The activation energies for all samples are plotted *vs* ϕ_{PS} in Figure 7.13.

The activation energy of pure polystyrene is taken from Arnold and Meier [1970] and Futamura *et al* [1977]. E for polystyrene is evaluated for mono-disperse sample with $\overline{M} \cong 97{,}000 \sim 100{,}000$ g/mol molecular weight, within temperature range of 140 ~ 200 °C. And E for the pure polybutadiene is taken from Futamura and Meinecke [1977] for homo-polybutadiene with 83,000 g/mol molecular weight. Both homopolymer activation energies were evaluated at temperatures above their glass transition temperatures.

All activation energies E_1 (at $T > T_s$) represent disordered melts which should behave roughly like random copolymers of the same composition. Thus, it is consistent with this picture that these E_1 values lie somewhere between the activation energies of two homopolymer block components (PS and PB or PI). Though the relationship of

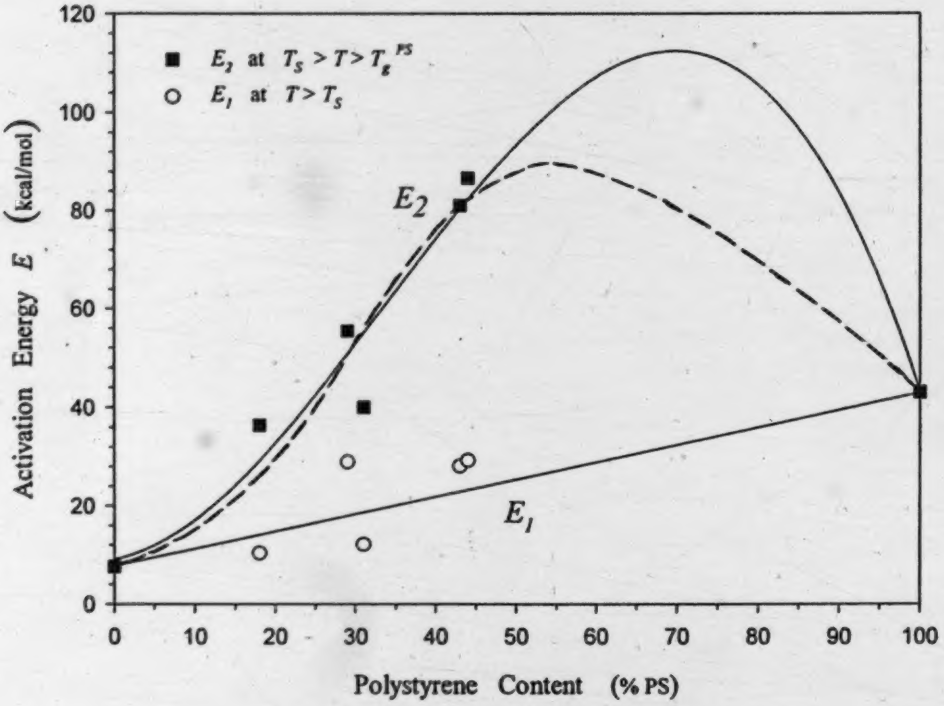

Figure 7.13: Plot of the activation energy as a function of the PS content. The open circular symbols represent E_1 and the filled square symbols represent E_2. E_1 and E_2 correspond to the activation energy at temperature below and above the micro-phase separation transition, which are taken from the slopes of the shift factor plot by the Arrhenius equation. Both solid and dash lines are regressions of the experimental data.

activation energy between the homo-polymers and E_1 for the block copolymers is not strictly linear-additive, E_1 does increase with the PS composition, Figure 7.13 shows that a linear $E_1(\phi_S)$ relationship is compatible with the somewhat scattered data, supporting the contention that the copolymer is disordered in the sense that PS and PB (or PI) segments are randomly intermingled as expected for fully miscible systems. This is because in the homogeneous disordered state, for the randomly mixed block copolymer molecules the activation energy for elementary flow process is a combination of the activation energy of both block components. The value will always be somewhere between those of the two constituent blocks. When the PS content increases, with its higher activation energy level the activation energy for the whole block copolymer will subsequently increase accordingly.

On the other hand, at $T < T_s$ the activation energy E_2 is much higher than either of the two block components in the intermediate range of PS composition. Two linear regression curves (solid line and dash line) was fitted to the data (filled square symbols). Though only seven data points are available (from the five block copolymer samples plus two homopolymers), the fitted curves do qualitatively reveal some of the morphological features of these block copolymers in the ordered state. The activation energies E_2 of block copolymers are between the activation energy of either of the individual components at $\phi_{PS} \leq 25\%$, but have much higher values at $\phi_{PS} > 25\%$ and reaches a maximum at 70% PS content (solid line).

The physical interpretation of this is quite obvious. At $\phi_{PS} \leq 25\%$, The polystyrene block forms either spherical or semi-continuous cylindrical micro-domains that are scattered throughout the matrix of rubbery middle block. The whole sample behaves as PI (or PB) melt, but with PS micro-domains acting as fillers. These PS fillers are connected with each other by the PI (or PB) block. The rheological and mechanical properties of the block copolymers, at this range of PS content, are mainly dominated by the PI (or PB) middle block. The flow properties (in small-strain oscillatory tests), as represented by the activation energies here, are mainly the properties of the middle rubbery block with the secondary influence of the scattered PS end block micro-domains. Thus, the activation energies E_2 at this range of PS content are somewhere between the activation energy of the middle block and the PS end block. But the activation energy would not abide by the linear additivity rule (as the activation energy of block copolymers at $T > T_s$ would do) since the middle blocks and the end blocks are not randomly mixed. These microphase separated block copolymers behaving like cross-linked polymers have higher activation energy (Figure 7.13, filled square symbols) than those of block copolymers in disordered state (Figure 7.13, open circular symbols).

At $25\% < \phi_{PS} < 100\%$, however, the E_2 are higher than either of the block components. E increases with ϕ_{PS} and reaches a maximum at about 70% PS, then decreases with ϕ_{PS} and eventually reduces to the activation energy of PS. The curve for E_2 at $\phi_{PS} > 50\%$ is only the regression curve fitting of the seven data available. It represents the activation energy at $50\% < \phi_{PS} < 100\%$ only qualitatively. Within the composition range of 25% ~ 70%, the block copolymers have the morphologies of two-dimensional PS cylinder and three-dimensional PS lamellae. The rheological properties are dominated by the microphase-separated (like "cross-linked") structure, rather than either the rubbery middle block or the PS domains. The samples are virtually solid-like and unable to flow. The Arrhenius model predicts that the viscosity is a function of both kinetic and activation energy, $\eta = Ae^{E/RT}$, where A is a constant, E and RT are the activation and Brownian energy respectively. At fixed temperature the flow property is proportional to the activation energy, exponentially. The activation energy, as an indication of the flow property (e.g. viscosity), should be higher than either of the middle rubber block or the end PS block. And it reaches a maximum at 70% PS content where the PS block is known to be the dominant phase.

Here, we used linear regression to fit the $E_2(\phi_{PS})$ experimental data, with a polynomial equation up to the third-order term (such as $y = a + bx + cx^2 + dx^3$). If we used a linear equation only up to the second-order term, then the activation energy exceeds the activation energy level of PS block at 19% PS content and reaches the maximum value around 50% PS content (dash line in Figure 7.13). (This coincides with the Leary-Williams model's prediction of enthalpy change where $\Delta H \propto \phi_A\phi_B$ which reaches a maximum at 50% composition). Although the actual PS content at which $E_{BC} > E_{PS}$ occurs and E_{BC} reaches a maximum is unknown, it is clear from the curve-fitting that $E_{BC} > E_{PS}$ occurs when the PS phase becomes continuous (at 19~25% PS content, where the PS domain changes from spheres to two-dimensional cylinders) and the maximum value is achieved when the PS domain becomes dominant (e.g. becoming the matrix of the material, at 50 ~ 70% PS content).

Leary-Williams model [Leary and Williams 1970 and 1974] predicted that the existence of the interphase had a profound impact on the rheological properties of block copolymers. When some macroscopic force is imposed on the sample then individual chains will also experience some local stress field. The total force on a chain will be the sum of frictional as well as interphase thermodynamics forces, $F = F^f + F^i$. Four terms were considered to contribute to the friction: drag on B segments moving through B matrix (F_{BB}^f), drag on A segments through A domain (F_{AA}^f), drag on A segments moving through B matrix (F_{AB}^f) and drag on each type of segment in the interphase with varying composition (F^{fi}). An interphase barrier force therefore exists which is the negative gradient of the chemical potential: $F_A^i = -\nabla \mu_A$. If the external force on the chain is less than F_A^i, then block pull-out will not be possible and no flow could occur (which would explain the absence of a limiting viscosity η_o at low $\dot{\gamma}$ for most of the block copolymers). This explains why at certain PS composition (25~100% in this study) the activation energy E_2 for block copolymers should be higher than either of the constituent homopolymers. At temperatures above their glass transition temperatures polystyrene and polybutadiene (or polyisoprene) are in the molten state with a Newtonian-limiting viscosity. But the block copolymer samples, at $T_g^{PB} < T_g^{PI} < T_g^{PS} < T < T_s$, are virtually flowless solids with rheological and mechanical properties of a cross-linked polymer. Thus, the activation energy (or the initial force) for the flow to occur for block copolymer must be higher than either PS or PB (or PI) melts.

7.4. Conclusions

Five triblock copolymer samples have been used in the study of time-temperature superposition. The rheological functions (e.g. tan δ, η', η'' and η^*) of the copolymers were superimposed on to a master curve at reference temperature of 100 °C. Though rheologically there is no strict rule on how to identify T_s, the master curves constructed did reveal the weak phase transition by splitting into two branches. The superposition of loss tangent and the complex viscosity show that rheological responses of copolymers are dominated by either the PS phase or the rubbery phase depending on the PS content, especially as the temperature approaches T_g^{PS}. In the low-ω terminal zone (at $T < T_s$), complex viscosity η^* (as well as the dynamic viscosity η' and η'') is proportional to $\omega^{-1/2}$ for copolymers with 44% PS composition ($G' \sim G'' \sim \omega^{1/2}$). For copolymers with 18% and 29% PS, $\eta' \sim \eta'' \sim \eta^* \sim \omega^{-3/4}$ ($G' \sim G'' \sim \omega^{1/4}$). The Arrhenius equation was used to correlate the empirical shifting factor a_T and the activation energy E for elementary flow process was calculated. E was found to be between the activation energy of those of the two block components at $T > T_s$, and roughly abided by the linear additivity rule. In the disordered state ($T < T_s$), the activation energy was fitted by a parabolic function of the PS composition. At low PS content (0 ~ 25%), E_{BC} increases with ϕ_{PS} between E_{PB} (or E_{PI}) and E_{PS}. At around 19~25% PS composition when the PS microdomains becomes continuous, E_{BC} exceeds E_{PS}, and reaches a maximum when polystyrene becomes the dominant phase (60 ~ 70% PS). This is also explained by the Leary-Williams model.

Chapter 8 Thermal Degradation of Block Copolymers

8.1. Introduction

As described in the previous chapters, we studied block copolymers extensively in a wide range of temperatures. In many cases the possibility of sample degradation (thermal or oxidative) had to be dealt with before any further investigation could be made. In this chapter, a collective result of those many experiments (both DSC and NMR results) is presented.

The main features of the degradation of polystyrene (PS) and polybutadiene (PB) have been known for many years, and the behavior of the binary blends of the homopolymers has also been studied [McNeill *et al* 1978]. That investigation revealed interesting stabilization effects on the degradation of PS when present in a blend with PB. The extent of these stabilization effects is greater in the copolymer (SB diblock copolymer) than in the blend [McNeill and Stevenson 1985]. The SB diblock copolymers are also found to be more stable than random copolymers of S and B monomers [Abu-Zeid and Youssef 1986]. When degraded separately, both polymers evolve volatile materials at appreciable rates at temperatures above 350 °C, in N_2 or in air.

Although styrene-butadiene copolymers are the most important and widely used synthetic rubber in the world, we have found only two publications on the thermal stability of these important materials. Both studies used SB diblock copolymers, which are of almost no practical importance. No study on SBS and SIS, the two most commercially useful triblock copolymers, has been found. In this report we have used DSC and NMR to investigate the thermal stability of the SBS and SIS copolymers, and the results were compared to the stability of the corresponding homopolymers.

8.2. Materials and Equipment

Three triblock copolymer samples were used in this study: one SBS copolymer and the other SIS copolymer. Both are commercial products (under the trade name VECTOR styrenic block copolymers), provided by DEXCO Polymers (of Plaquemine, LA). The sample characterizations are listed in Table 8.1.

Table 8.1: Sample Characterizations

Polymer	$\overline{M}_w$	$\overline{M}_w/\overline{M}_n$	ϕ_{PS}	Morphology	Melt Index
	(kg/mol)		(%)		(g/10 min.)*
SIS-4111	125,000	≤1.06	18	PS sphere	12
SBS-8508	70,000	≤1.06	29	PS cylinder	12
SIS-4411-D	75,000	≤1.06	44	PS lamellae	40
Polystyrene	105,000		100	---	--

* 200 °C, 5 kg.

The glass transition temperatures (T_g) of the constituent blocks were measured by DSC under a nitrogen blanket in this lab. T_g appears to vary slightly depending on the heating or cooling rates (see Figure 8.1). Here, $T_g^{PS} \cong 70$ °C, $T_g^{PB} \cong -90$ °C and $T_g^{PI} \cong -60$ °C. These values were taken as the peak values on DSC heating curves where the glass transition occurred.

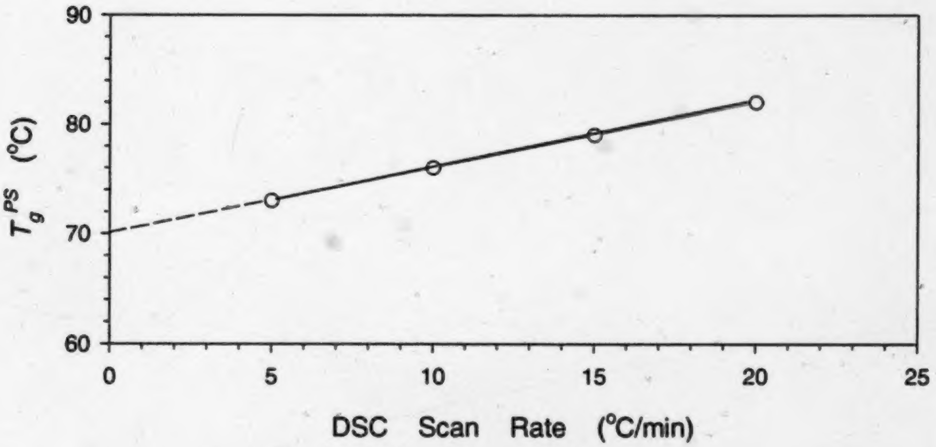

Figure 8.1: DSC heating scan of SIS-4111. The glass transition temperatures of the PS segments are measured at different scanning rate and extrapolated to zero scan rate.

Two instruments were used in this project. One was a Differential Scanning Calorimeter (DSC) and other was Nuclear Magnetic Resonance (NMR). The DSC tests were conducted in our lab and the NMR tests were done in the Department of Chemistry Analytical Lab. For DSC tests the block copolymer sample was weighed at 15~20 mg and loaded into a non-hermetic aluminum pan. The DSC tests were conducted either in an environment of nitrogen or air (i.e., presence of oxygen). One scanning rate was used during all DSC tests (5 °C/min heating). In NMR tests, the block copolymer sample was first dissolved $CHCl_3$ solvent. The solution was then subjected to the NMR tests.

8.3. Results and Discussion

8.3.1 DSC Study of Thermal Degradation of TriblockCopolymers

Very useful information can be obtained from thermal analysis curves of the high-temperature degradation of the block copolymers. Polymer degradation by thermal or thermo-oxidative reactions is generally accompanied by absorption or evolution of heat. Therefore, DSC is very useful in these studies.

Figures 8.2 to 8.4 shows the results of DSC scanning for the three block copolymer samples (SIS-4111, SBS-8508 and SIS-4411-D), both in the presence of oxygen (in air) or with nitrogen purging. The T_g^{PS} in the three plots are at around 70 °C. Figure 8.5 shows the DSC trace of a homopolystyrene in either air or N_2 (with T_g^{PS} = 100 ~110 °C, as expected for high molecular weight linear PS).

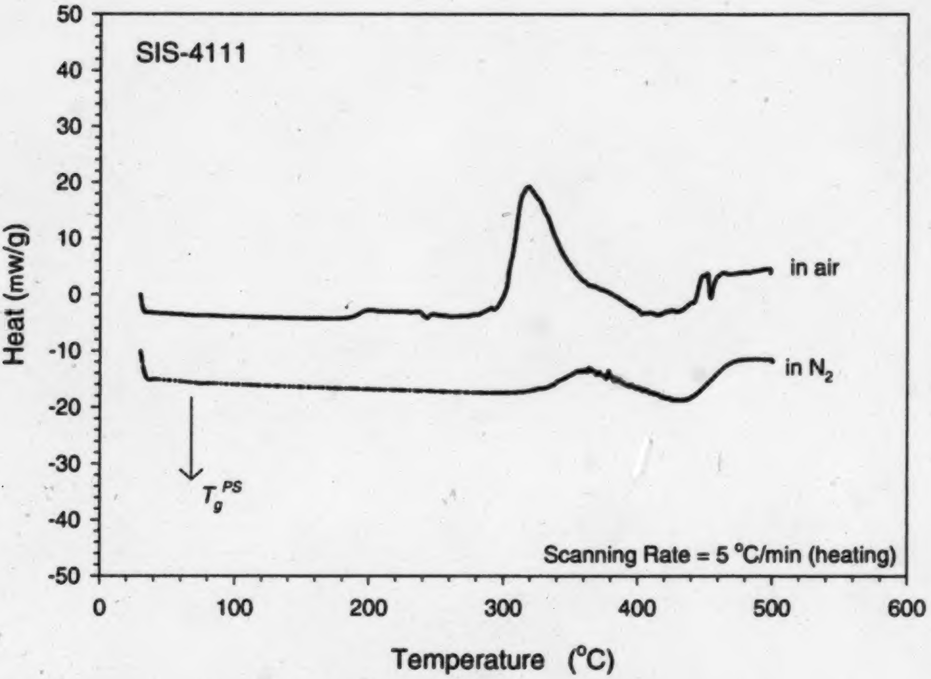

Figure 8.2: DSC scan of SIS-4111, at 5 °C/min heating. The sample has about 18% PS and 82% PI. The two curves have been shifted vertically to avoid overlapping.

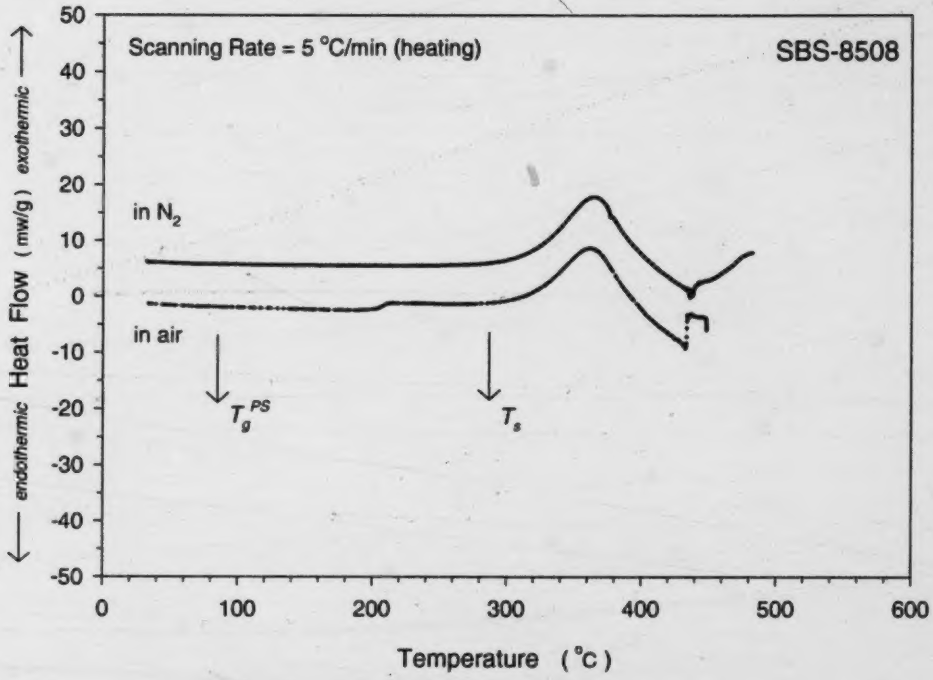

Figure 8.3: DSC scan of SBS-8508, at 5 °C/min heating. The sample has 29% PS and 71% PB. The two curves have been shifted vertically to avoid overlapping.

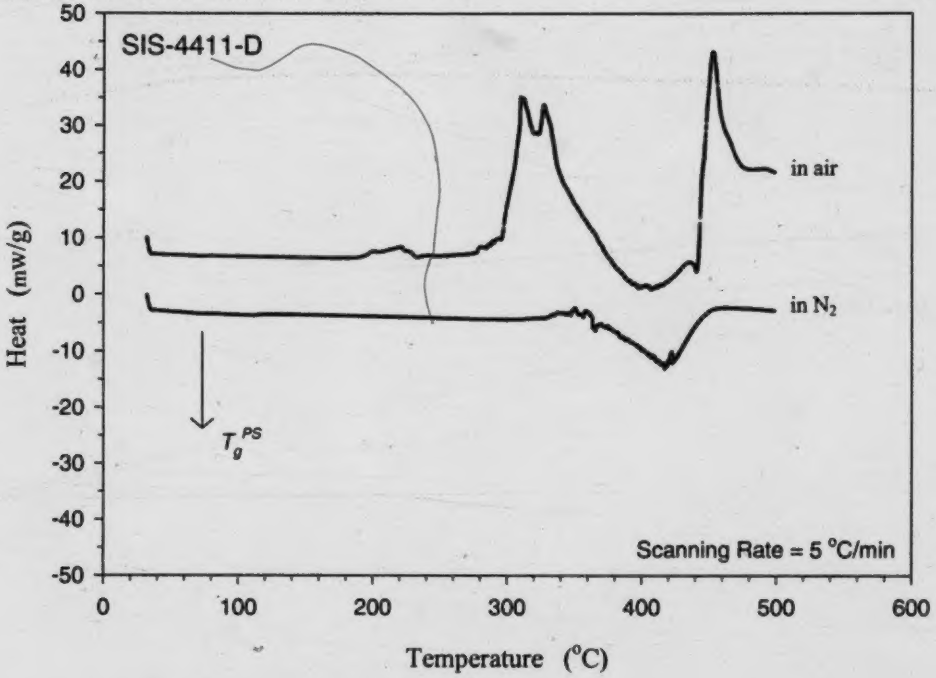

Figure 8.4: DSC scan of SIS-4411-D, at 5 °C/min heating. The sample has 44% PS and 54% PI. The two curves have been shifted vertically to avoid overlapping.

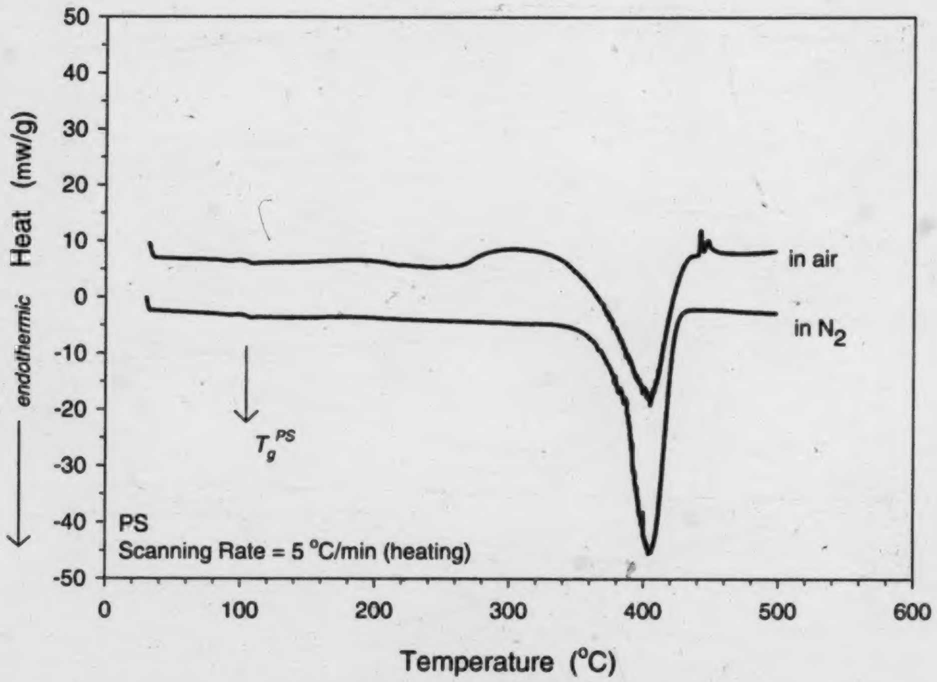

Figure 8.5: DSC scanning of homopolystyrene, at 5 °C/min heating. The two curves have been shifted vertically to avoid overlapping.

All three copolymer samples tested in air show a step increase in DSC trace at around 200 °C (except in Figure 8.4, in which it is a small exothermic peak). These changes on the DSC curves (step increase in Figure 8.2 and 8.3 and a small exothermic peak in Figure 8.4) are the result of oxidative degradation since they are not seen in N_2. A similar gentle exotherm is also found in Figure 8.5, for homo-PS tested in air. The oxidative degradation of homo-PS occurs at around 270 °C. Although we have no data on homo-PB and homo-PI, the copolymer oxidative degradations that occur at around 200 °C (in Figure 8.2 to 8.4) are the results of reaction between oxygen and the PB and PI blocks (most probably with the PB and PI double bonds). When the samples were tested in N_2, no such changes can be found and the copolymer samples (and PS) are stable up to 300 °C and above.

When the block copolymer is heated the first reaction to occur is cyclisation in the PB sections of the chains. McNeill *et al.* [1985] had reported that this cyclisation of PB chains occurred at 300-400 °C, for a diblock copolymer sample (an exothermic peak on DSC heating curve around 360 °C). This happens to our triblock copolymer samples as well. In Figures 8.2-8.4, these cyclisation reactions are represented by exothermic peaks at around 320-360 °C, both in air and N_2. These exothermic peaks are usually larger when sample was tested in air (with O_2) for the SIS copolymers (compared to the peaks when sample was tested in N_2, in Figure 8.2 and 8.4). In Figure 8.4, the PI chain cyclisation reaction is so trivial that the exthermic peak at 350 °C is very small (in N_2). For the SBS sample, in Figure 8.3 though, the exothermic peaks for PB chain cyclisation are almost the same in air and N_2. The difference may be caused by the chain structure.

The PB segment is a straight chain, with no bulky side groups to impede chain bond rotation. The cyclisation reaction will occur (such as open double bonds) whether with O_2 or N_2. The PI segment, however, is a straight chain with many side groups ($-CH_3$ and $-CH_2-CH_3$) right next to the double bonds. Thus, in N_2 these side groups may hinder the reactions between double bonds (which results in less cyclisation reactions), while with O_2 the oxygen free radicals ($RO\cdot$) may actually help the cyclisation reaction to occur. That is why the exothermic peaks on the "in air" curves are larger than that on the "in N_2" curves, for the SIS samples.

McNeill and Stevenson [1985] also reported that homo-PS had a single stage decomposition in the region of 400-420 °C. In Figure 8.5, we showed the homo-PS sample degraded at about 402 °C (an endothermic peak). The same endothermic peaks are found in Figures 8.2-8.4, both with O_2 and N_2. But for block copolymers, the degradation of the PS segments was shifted to higher temperatures. The endothermic peaks all appear at 430 °C. This agrees with what McNeill and Stevenson [1985] have reported for diblock copolymers, the presence of PB (or PI) stabilizes the PS segments in the block copolymer.

8.3.2 DSC and NMR Study of the Possible Degradation during Rheological Tests

Our main concern about the degradation is the possibility that the block copolymer samples degraded during the rheological tests, which were conducted at high temperatures and lasted a long time. The block copolymer samples have been tested in the rheometer for different lengths of time. Upon visual inspection of the sample at testing temperature, the copolymer sample looked like solid rubber after being tested rheologically at $T_g^{PS} < T < T_s$, but this solid rubber was easy to break. After being tested at $T_s < T < 260$ °C, the sample was liquid-like (very soft polymer melt immediately after the oven was open, but rubbery at room temperature). Above 260 °C, the tested sample was cross-linked, rubbery and impossible to break up. The DSC and NMR test results of the same sample are shown in Figures 8.6 to 8.8.

In Figure 8.6 are seen DSC results for SIS-4111 samples that had been in the RMS-800 for 6 to 10 hours (with N_2 purging). Curves 1, 2 and 3 are the DSC traces for SIS-4111 samples that have been tested rheologically for 6 to 10 hours at different temperatures. Curve 4 is the DSC trace of a fresh SIS-4111 sample. All four curves show the same glass transition temperature of undegraded PS and PI phases. No major difference could be found between these curves. The discontinuity at $T = 35$ °C for curves 1, 2 and 3 is due to different DSC heating procedures. The sample was first heated from 35 °C to 200 °C, then cooled to –100 °C (not shown), and finally heated back to 35 °C. The fresh sample, however, was heated from –100 °C up to 200 °C, continuously.

Figures 8.7 and 8.8 show the results of NMR tests. The NMR trace of a fresh SIS-4111 sample is shown in Figure 8.7. And a typical NMR result of a SIS-4111 sample that has been tested in the rheometer at 180 °C for 6 hours is shown in Figure 8.8 (the NMR results for samples tested at other temperatures are not shown, but are all similar to Figure 8.8).

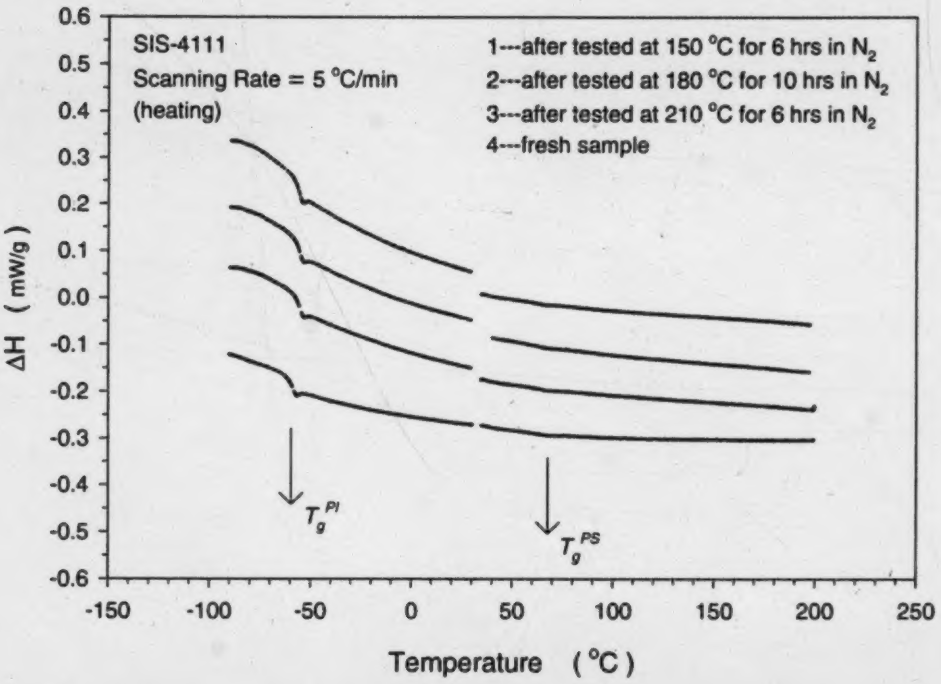

Figure 8.6: DSC scanning of SIS-4111, at 5 °C/min heating, after the samples have been tested in the rheometer for different lengths of time. For curves 1, 2 and 3, the samples were heated from 35 °C up to 200 °C, then cooled to –100 °C at the same rates, and finally heated up to 35 °C. Thus, the curves (1, 2, and 3) discontinue at T = 35 °C. The curves have been shifted vertically to avoid overlapping.

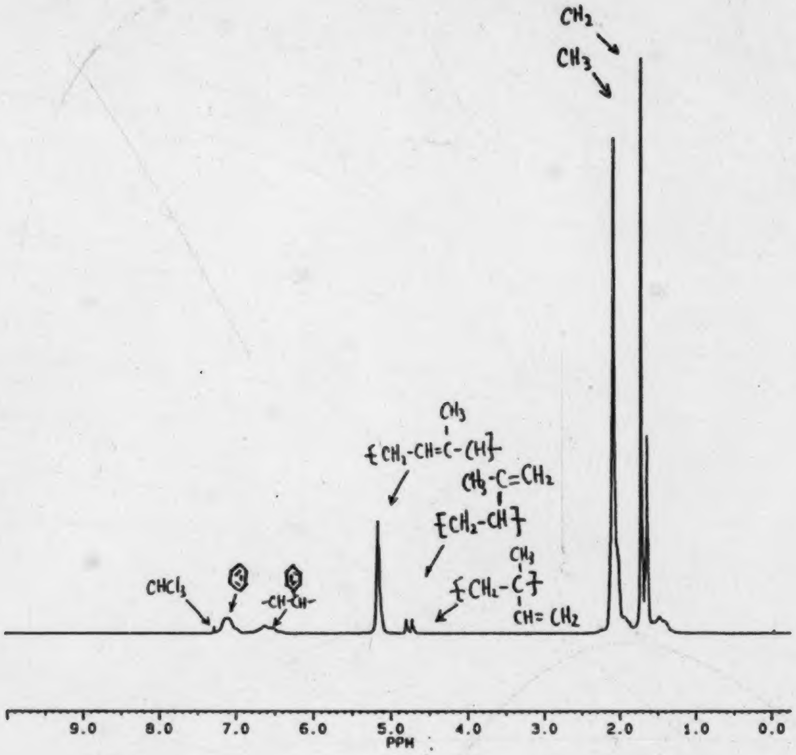

Figure 8.7: NMR trace of fresh SIS-4111 sample. Test was done in *$CHCl_3$* solvent.

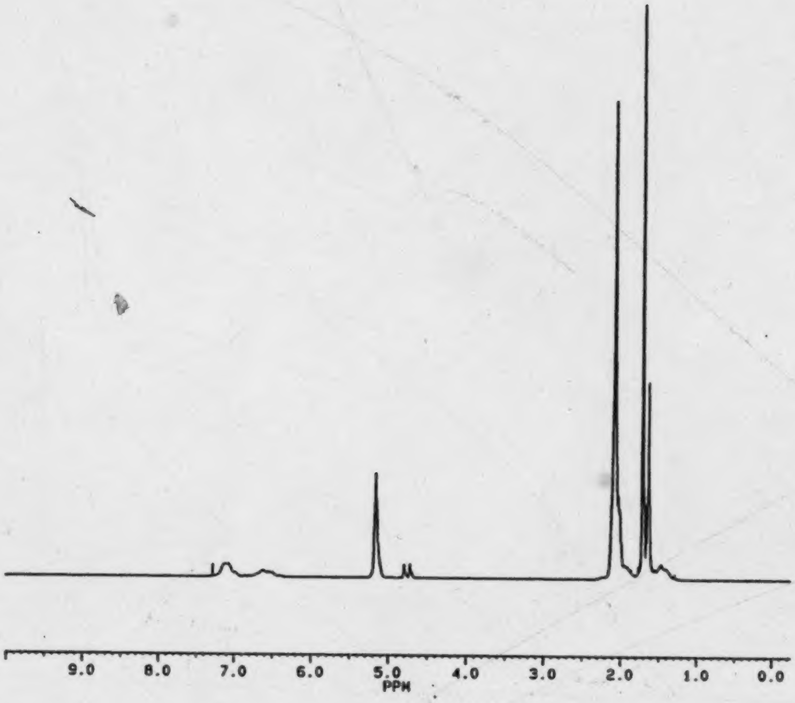

Figure 8.8: NMR trace of SIS-4111. The copolymer sample has been tested in rheometer at 180 °C for 6 hours. The sample was tested in *$CHCl_3$* solvent.

The peaks in Figure 8.7 and 8.8 represent various functional groups. Comparing the corresponding peaks in the two figures, we can see that the number of functional groups was not changed after the sample had been tested in the rheometer. No degradation has been found during the rheological tests.

8.4. Conclusions

The thermal stability of three triblock copolymers has been studied by DSC. With the presence of O_2, the butadiene (and isoprene) segments start to crosslink at about 200 °C and the styrene segments degrade at 275 °C. With or without the presence of O_2, the PB (and PI) segments decompose completely at around 360 °C. The PS segments, on the other hand, degrade at 430 °C. The existence of the rubbery sections in the block copolymer stabilize the PS. The decomposition temperature of the PS segments is elevated.

The possibility of thermal degradation during the rheological tests has also been studied, by DSC and NMR. No degradation has been found for the SIS sample that has been tested in the rheometer for several hours, at temperature up to 210 °C.

Chapter 9 Conclusions

This thesis consists of three major research projects and one minor one. Each project is independent and unique in terms of advancing the understanding of many properties of block copolymers.

In the first project we presented a rheological investigation of the ordering phenomena of an asymmetric styrene-isoprene-styrene (SIS) triblock copolymer around the microphase-separation temperature. A narrow temperature range right below the *MST* ($\Delta T = T_s - T \cong 10^{o} C$) was found within which the ordering process could be carefully studied. A three-stage growth pattern of storage modulus $G'(t)$ was observed, which resembled a nucleation and growth process. The ordering process was much slower at low temperatures than at temperatures near T_s. The process of forming the body-centered-cubic (bcc) lattice structure takes the majority of the time. The oscillatory shear flow used in $G'(\omega,t)$ measurements was found to have the effect of accelerating the ordering. The shearing movement in dynamic testing also caused composition fluctuation above T_s. For the two frequencies used in this study, the kinetics of microstructure formation below the *MST* was relatively insensitive to the frequency. But the composition fluctuation developed above the *MST* was very sensitive to the frequency. The effect of annealing has been also studied. Annealing the sample within 5 degrees below T_s showed that the time required for the ordering process was substantially shortened when the lower temperatures within this ΔT range were used, and the sample also showed higher values of rheological properties, which in turn indicated a larger degree of ordering.

In the second major project, the ordering process and the corresponding heat evolution of two triblock copolymers have been studied with the Differential Scanning Calorimeter (DSC). When the block copolymers were cooled from above T_s two distinct exothermic peaks were found, which corresponded to the glass transition of the rubber block and the microphase-separation transition. The heat associated with the glass transition was about the same at all cooling rates, but the broadness of the peak was found to be rate-dependent. The heat produced by the microphase-separation transition, however, varied dramatically depending on the cooling rate. This behavior, in turn, reflects the complication of the ordering mechanism. The microphase-separation occurs instantly upon cooling through T_s. But the growth of the long-range microstructure depends very much on the speed of cooling.

In the third major project, five triblock copolymer samples have been used in the study of time-temperature superposition. The rheological functions (e.g. tan δ, η', η'' and η^*) of the copolymers at various temperatures were superimposed onto a master curve at reference temperature of 100 °C. Though rheologically there is no strict rule on how to best identify T_s, the master curves did reveal the weak *MST* by splitting into two branches. The superposition of loss tangent δ and the complex viscosity η^* show that rheological responses of block copolymers are dominated by either the PS phase or the rubbery phase depending on the PS content, especially as the temperature approaches

T_g^{PS}. In the low-ω terminal zone (when $T < T_s$), complex viscosity η^* and the dynamic viscosities (η' and η'') are proportional to $\omega^{1/2}$ for copolymers with 44% PS composition and lamella microstructure (i.e., $G' \sim G'' \sim \omega^{1/2}$). For copolymers with 18% and 29% PS and corresponding dispersed microdomains of PS spheres or cylinders, $\eta' \sim \eta'' \sim \eta^* \sim \omega^{3/4}$ ($G' \sim G'' \sim \omega^{1/4}$). The Arrhenius equation was used to correlate the empirical shifting factor a_T and the activation energy E for an elementary flow process was calculated. E for $T > T_s$ was found to be between the activation energies of those homopolymers corresponding to the two block components and roughly abided by the linear additivity rule with variation of molecular composition. In the ordered state ($T < T_s$), the activation energy was a parabolic function of the PS composition. At low PS content (0 ~ 25%), E_{BC} increased with ϕ_{PS} between E_{PB} (or E_{PI}) and E_{PS}. In the range 19~25% PS composition, when the PS microdomains became continuous, E_{BC} exceeded E_{PS}, and reached a maximum when polystyrene became the dominant phase (60 to 70% PS). This is also explained by the Leary-Williams model.

In the last project, the thermal stability of three triblock copolymers has been studied by DSC. With the presence of O_2, the butadiene (and isoprene) segments started to crosslink at about 200 °C and the styrene segments degraded at 275 °C. With or without the presence of O_2, the PB (and PI) segments decomposed completely at around 360 °C. The PS segments, on the other hand, degraded at 430 °C. The presence of the rubbery sections in the block copolymer stabilized the PS. The decomposition temperature of the PS segments was thereby elevated. The possibility of thermal degradation during the rheological tests was also studied, by DSC and NMR. No degradation was found for the SIS sample that had been tested in the rheometer for several hours, at temperature up to 210 °C.

Appendix A Calibrations

A.1. Torque

Torque calibration on the RMS-800 transducer are done by hanging a known weight on a monofilament line which loops over a pulley to a 5 cm moment arm mounted on the transducer. The arrangement is shown in Figure A.1.

A 200 g weight (supplied with the rheometer calibration kit) should result in a 1000 g.cm ± 3% torque (according to manufacturer specifications). The torque values resulting from several weights were measured to determine the calibration and linearity of the transducer in the normal (or high-torque) range. These are shown in Table A.1. As a consequence of verification of the manufacturer's calibration (X), within the 3% tolerances specified, the RMS-800 values (X') for torque and related physical properties were used without any correction factors being applied.

Table A.1: Normal Torque Range Calibration

Weight (g)	Torque (g.cm)*	Error**
200	1001	+0.1%
100	504.4	+0.88%
50	252.7	+1.08%

* Average of three readings

** Error = $(X' - X) / X = \Delta X / X$

In order to determine the reliability of measured torque values below the quoted lower reliability limit of 2 g.cm a calibration was also performed with small weights.

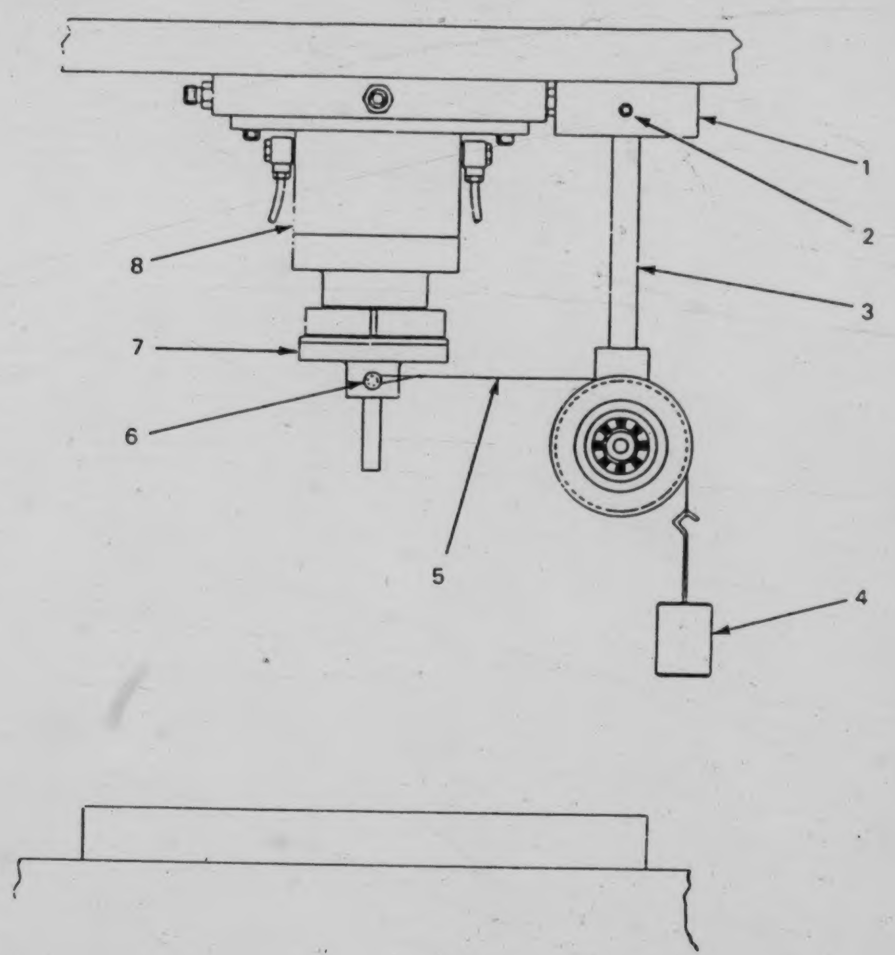

LEGEND

1. Pulley Mounting Bracket
2. Set Screw
3. Calibration Pulley
4. Weight
5. Monofilament Line
6. Moment Arm
7. Calibration Collar
8. Mid Range FRT

Figure A.1: Transducer calibration set-up.

Table A.2: Low Torque Range Calibration

weight (including ½ line)	0	510 mg*	210 mg*	60 mg
true torque (g.cm)	0	2.55	1.05	0.3
Indicated Torque (g.cm)	0.01400	2.65000	1.11000	0.41610
	0.00860	2.62000	1.09900	0.25990
	0.00422	2.62100	1.08300	0.37870
	0.01390	2.61900	1.07300	0.31520
	0.00741	2.61800	1.08600	0.47790
	0.00801	2.60700	1.06700	0.19390
	0.02500	2.59600	1.06200	0.19390
	0.00490	2.60800	1.06900	0.42610
	0.00067	2.60900	1.06700	0.32010
	0.00062	2.60300	1.05000	0.45950
	0.00339	2.61000	1.05800	0.22010
	0.01900	2.59100	1.06600	0.31520
	0.00342	2.58000	1.06600	0.47870
	0.01041	2.57500	1.06500	0.45640
		Statistical Analysis		
Mean	0.00883	2.60764	1.07293	0.35084
Standard Deviation	0.00725	0.01677	0.01701	0.10702

* Total of standard weights (500 or 200) plus monofilament line.

First, the zero was determined. With no weight or line on the moment arm (Figure A.1) many readings of the zero were taken to determine the average "zero" reading. Weights of 500 mg, 200 mg and 50 mg were then hung on the moment arm and many torque readings were recorded. At these low weights the weight of the monofilament line may have had a measurable effect on the reading. The weight of the line was 0.0205 g. Roughly half the line extends from the high point of the pulley wheel to the weight.

Therefore, only half the weight of the line was included in the calculation of total weight. The results are given in Table A.2 along with statistical analysis.

For the 510 mg and 210 mg weights, the mean indicated torque was 2.2% higher than the true torque (calculated from the weight and length of the moment arm). The standard deviation was almost 30%. Such high error and standard deviation throws into question the reliability of numerical results in this torque range (3×10^{-1} g.cm). However, since the mean indicated torque for the "zero" was one order of magnitude lower it can be concluded that RMS-800 torques in the range of 10^{-1} g.cm can be used with confidence.

A.2. Gap

The gap, or spacing between the surfaces of the platens in contact with the sample (H in Equation 4.1-1), must be known accurately in order to calculate the strain. A problem therefore arises because the platens expand and contract with temperature, thereby changing the gap. In order to account for this a calibration was performed to determine the change in gap with temperature.

The gap was first zeroed at room temperature by lowering the upper platen until a positive normal force was detected by the first deflection of the normal force analogue meter. The upper platen was then raised and the platens were heated a few degrees using the convection oven, allowing a 5 minutes thermal soak time after steady temperature had been reached. At the new temperature the upper platen was again lowered until the first deflection of the normal force analogue meter was detected. The gap reading then indicated the combined expansion of both platens and hence the decrease in the gap. The results are given in tabular form in Table A.3 and graphically in Figure A.2. This expansion of the platens decreases the true gap by the same amount. Therefore, if the gap is zero at some temperature T_1, then the true gap at T_2 can be obtained by subtracting the "gap" reading from Table A.2 or Figure A.2 at T_2 minus that at T_1 from the gap indicated by the dial gauge.

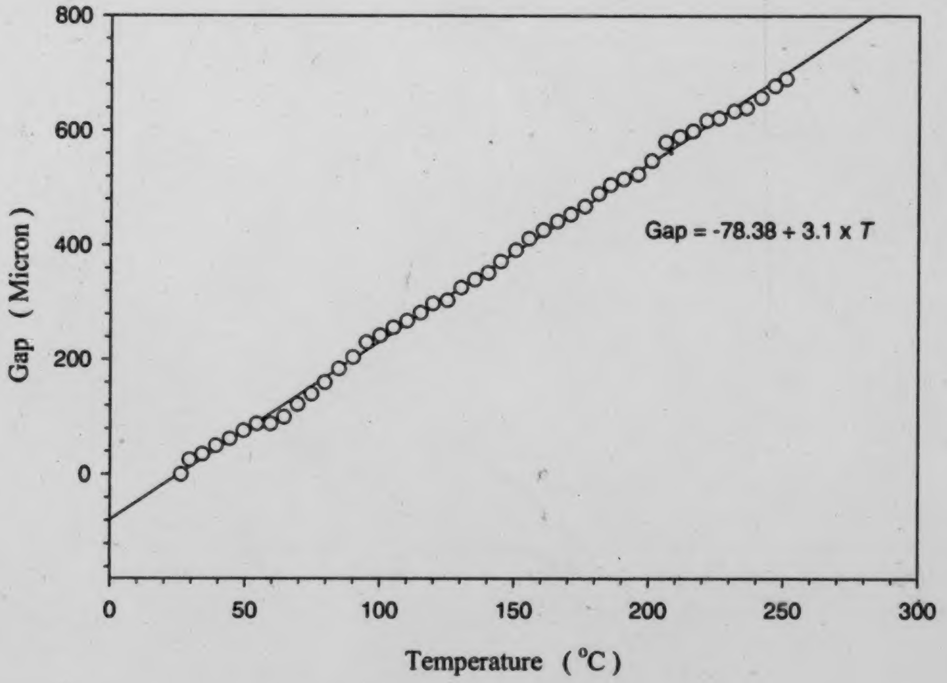

Figure A.2: Tool Expansion Calibration

Table A.3: Tool Expansion Calibration

Temperature (°C)	Gap (Microns)	Temperature (°C)	Gap (Microns)
26.3	0	140.3	352
29.4	25	144.9	372
34.2	35	150.5	392
39.2	50	155.5	412
44.3	62	160.7	427
49.4	76	165.9	442
54.4	88	170.9	454
59.4	88	176.1	468
64.4	100	181.2	490
69.5	122	185.6	506
74.6	140	190.6	516
79.6	160	195.8	524
84.8	184	200.9	548
90	204	206.2	580
95	230	211.2	590
100.1	242	216.2	600
105.1	256	221.3	618
110.1	268	226	622
115.1	282	231.5	634
119.8	298	236.2	640
125.1	304	241.6	658
130.3	326	246.6	678
135.3	340	250.8	690

A.3. Circulation Jacket

The circulation jacket was described in Section 4.1.9. A calibration was performed to dtermine sample temperature *vs.* tool (platen) temperature. A polydimethylsiloxane (silicone) fluid was loaded between the parallel platens with 2 mm gap and three thermocouples of diameter 0.020 inch were inserted at different points in the sample. One thermocouple was very close to one of the nitrogen ports in the furnace jacket. The thermocouples were read on a DVM and referenced to an ice point in a 1 L beaker of distilled water and ice made from distilled water, chilled overnight. The ice was replenished frequently to maintain the temperature within 0.2 °C of zero as read on a mercury thermometer with 0.1 °C divisions. It was found that silicone fluid temperatures at steady state never varied more than two tenths of a degree between the three thermocouples.

With the circulator set for minimum temperature (-30 °C) the nitrogen flow rate was gradually increased to achieve minimum sample temperature. It was found that a N_2 flow rate of 5 L per minute as measured on a Matheson 603 rotameter yielded the sample temperature closest to the temperature set point. At this N_2 flow rate the circulator temperature set point was gradually increased and both tool temperature and sample temperature were recorded. The results of this calibration are given in Table A.4 and in Figure A.3.

Table A.4: Circulation Jacket Temperature Calibration

Temperature (°C)					
Set Point	Tool	Sample	Set Point	Tool	Sample
-30	-24.6	-22.85	25	24.7	24.53
	-23.6	-22.06	30	29.4	28.65
-28	-23.3	-21.59	35	34.0	33.66
	-20.8	-19.11		38.4	38.13
	-19.3	-17.84	40	38.7	38.35
	-19.0	-17.62	45	43.4	43.06
	-18.8	-17.54		47.7	47.43
-23	-18.9	-17.52		48.1	47.82
	-14.5	-13.62		48.2	47.89
	-14.3	-13.32	50	48.3	47.82
-18	-14.4	-13.35	55	52.8	52.71
	-10.2	-9.49		57.2	57.10
-13	-9.9	-9.22		57.4	57.32
	-5.7	-5.32	60	57.6	57.37
	-5.4	-5.00	65	62.3	62.18
-8	-5.3	-4.90		66.8	66.87
	-0.8	-0.73	70	67.0	66.97
-3	-0.6	-0.61	75	71.7	71.83
0	2.0	2.02		76.3	76.54
	6.4	6.24	80	76.5	76.61
5	6.5	6.22		81.1	81.28
10	11.0	10.98	85	81.2	81.45
15	15.5	15.37	90	85.9	86.31
20	20.1	19.89		90.6	90.97
			95	90.7	91.12
				95.4	95.85
				95.5	

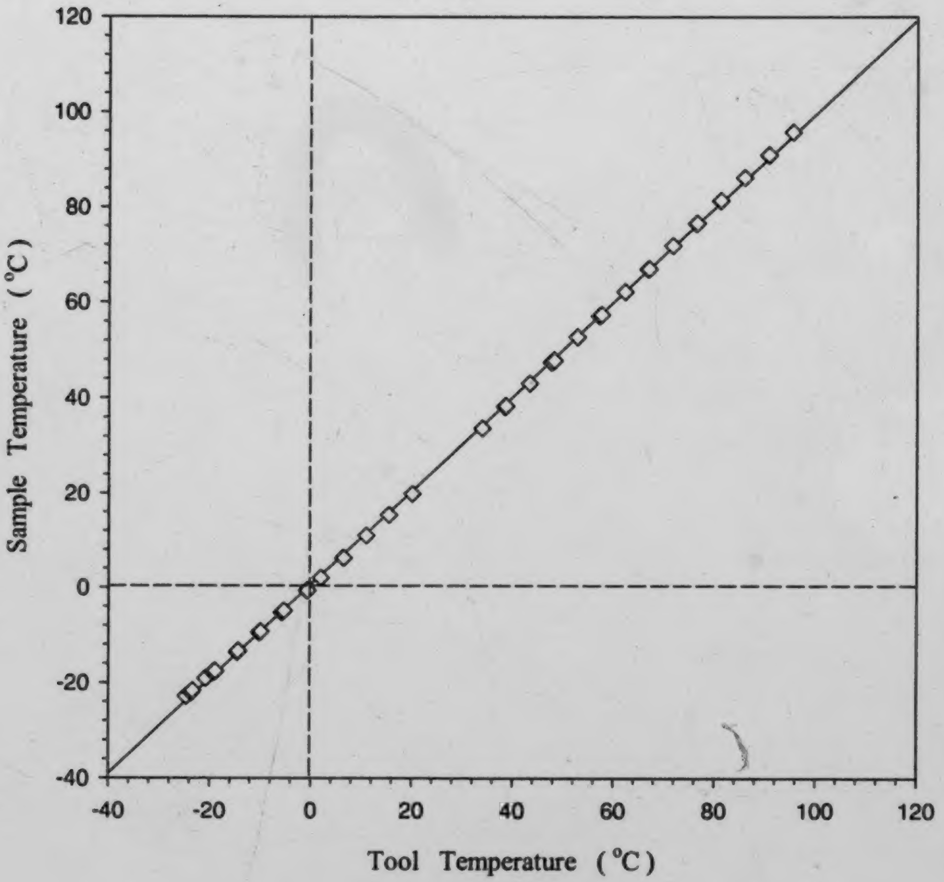

Figure A.3: Circulation Oven Temperature Calibration

Appendix B Effect of Mold Release Agent on the Rheological Test : Slip Effects

Rheological measurements on gels, concentrated suspensions, emulsions, foams and polymer melts at high stresses are often confounded by slip at solid boundaries with the result that the flow field, or kinematics, are unknown. From a theoretical point of view, it has been conjectured by de Gennes and Seances [1979] that a high-molecular-weight polymer melt flowing on a smooth, nonadsorbing solid surface should always slip for any shear rate.

There are two things bring us to pay attention to the slip problem in the block copolymer. First, most of the rheological tests of block copolymer are done between two smooth parallel plates of stainless steel. Secondly, because it is difficult to remove the sample disc from the mold during the sample preparation, sometime a liquid mold release agent (usually a silicone or terfluro products) is applied by spray onto the mold's metal surface before the polymer is melted for molding.

I used polyethylene (HDPE melts, which was thought to be a simple polymer fluid when melted) to investigate this problem. A series of dynamic tests were conducted. In Figure B.1, dynamic viscosity is plotted versus angular frequency. When a silicone-base mold release agent was used, the viscosities changed along with the gap between the upper and lower plates. The larger the gap, the lower the apparent viscosity, which

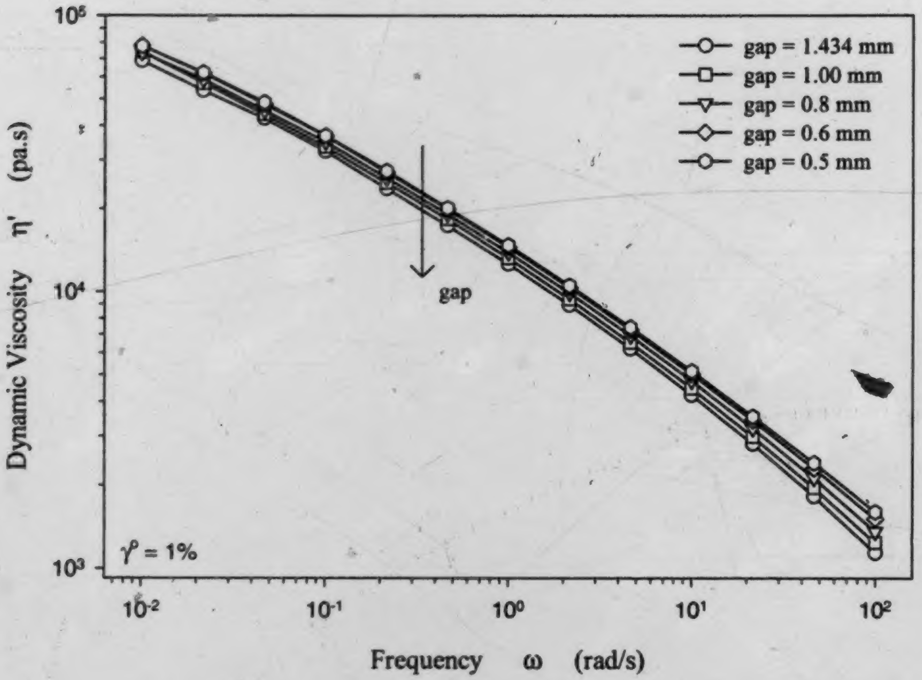

Figure B.1: Dynamic test of HDPE sample, at 150 °C with 1 % strain. The sample was molded with a silicone-based mold release agent. As the gap increases, the apparent viscosity decreases.

indicated the slip effect. Since viscosity is an intrinsic property of the material, it should not be a function of the gap spacing between the upper and lower platens.

In a steady unidirectional simple shear flow between parallel plates, the shear rate (when there is no slip at the boundary) is $\dot{\gamma} = \frac{V_x}{y}$, where V_x is the velocity at one boundary ($V_x = 0$ at the other) and y is the gap spacing between the platens. An analogous expression can be derived for rotational shear which is also oscillatory, describing the dynamic tests used in measuring η' and η^{*}. Since we are comparing the viscosity curves in Figure B.1 at constant frequency, thus $V_x (= r\omega)$ is fixed and shear rate is inversely proportional to the gap ($\dot{\gamma} \propto \frac{1}{y}$).

Viscosity is defined as $\eta \equiv \frac{\tau}{\dot{\gamma}}$, where τ is the shear stress. When we increase the gap y, $\dot{\gamma}$ decreases. For simple polymer material with a fixed value of viscosity, the shear stress should decrease as well to keep η constant (according to $\eta \equiv \frac{\tau}{\dot{\gamma}}$). As we see in Figure B.1 when the gap y increases, viscosity decreases. This means that the shear stress τ drops more than it should. This indicates the presence of some artifact, such as a boundary condition not being fulfilled. One possibility is that slip at the platen surface exists. Slip is usually caused by the shear stress between the two contacting (platen) surfaces. When τ between the two surface is greater than the slip stress τ_s ($\tau \geq \tau_s$), then slip occurs and the stress τ will drops to or below τ_s. Thus, the decreasing viscosity indicates that slip has occurred during the test.

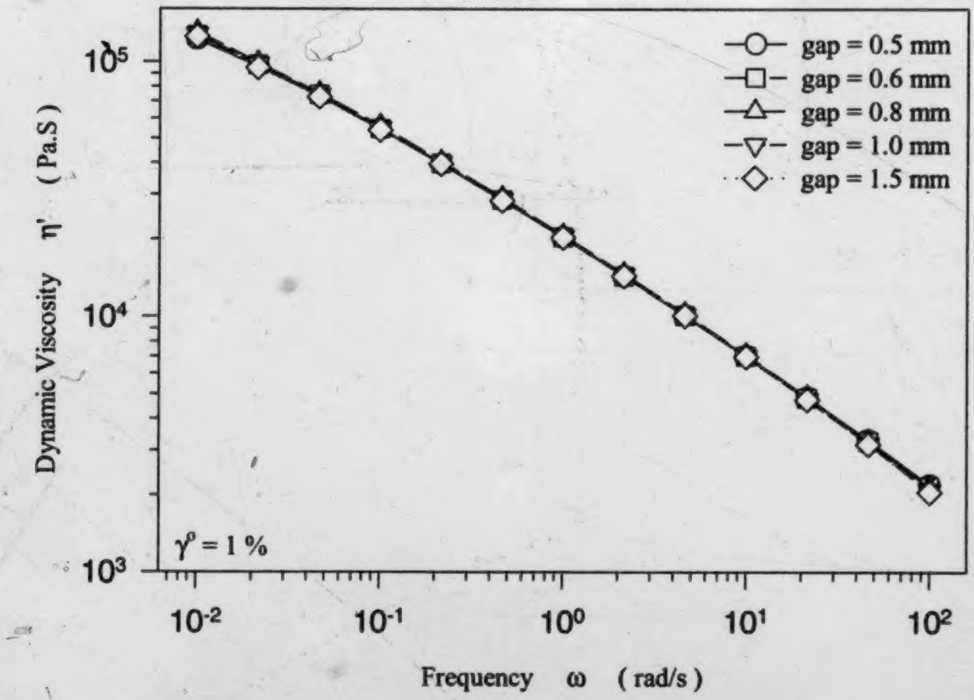

Figure B.2: Dynamic test of HDPE sample, at 150 °C and 1 % strain. The sample was molded with aluminum foil (no mold release agent). The viscosity does not change with increasing gap.

In Figure B.2, similar tests with the same range of gap spacing were made for the same HDPE samples, except, instead of mold release agent, aluminum foil was used to line the mold during the sample preparation. All viscosity data fall on one curve, as is expected, despite the changing gap. Apparently no slip during testing has occurred when aluminum foil was used during molding. Comparison of Figures B.1 and B.2 shows that apparent viscosities in Figure B.2 are approximately 20 % larger, meaning that τ was larger, indicating that the sample was adhering firmly to both plates, and the data in Figure B.1 appear lower only because of the artifact of slip.

We conducted steady shear tests on the same HDPE samples. The samples were all prepared using aluminum foil (no mold release agent). The results are shown in Figure B.3. The non-Newtonian viscosity decreases as the gap increases, especially at high shear rates. At low shear rate the viscosities are more or less the same, indicating almost no slip occurs. At high shear rates, however, the viscosities drop as the gap increases. When the shear rate is too high, slip occurs eventually, just as de Gennes has predicted.

Although the actual slip phenomenon is highly complex and beyond the scope of this study, I have found that slip between the polymer sample and the rheometer platens very likely occurs when the mold release agent is used during the sample preparation and when high shear rates are employed in the steady shear tests. Since then, we have abandoned all practice of using mold release agents during sample preparation, and also tried to avoid using high shear rates in all steady shear tests.

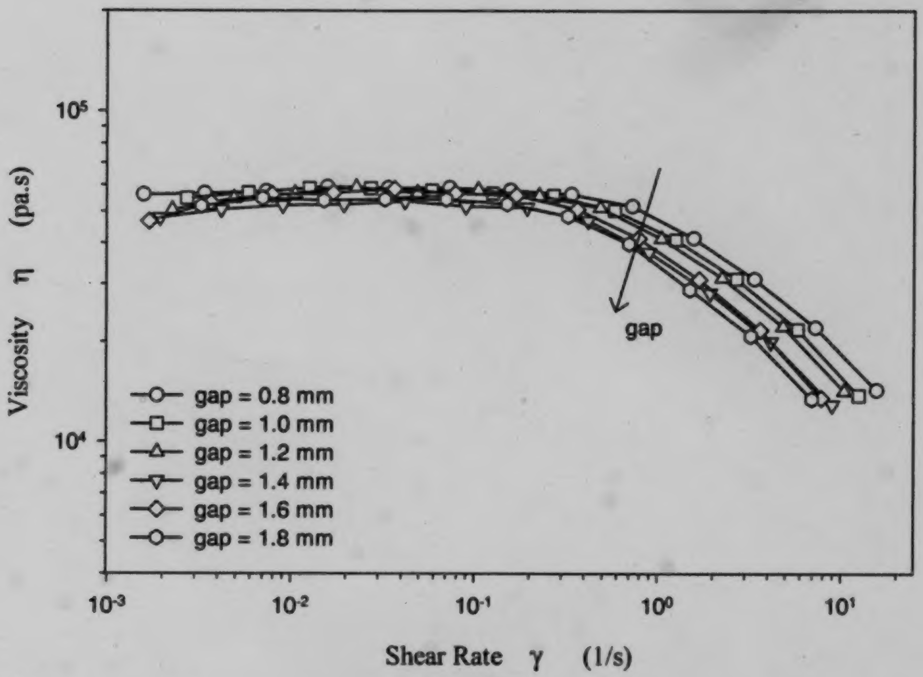

Figure B.3: Steady shear test of HDPE sample, at 150 °C. The viscosity decreases with increasing gap, especially at the high shear rate end.

Appendix C Determine the Cloud Point and Pour Point Temperature of Crude Oil by Rheology

Crude oil contains various amounts of dissolved wax, (paraffin wax, microcrystalline wax and/or petrolatum) that tends to separate from oil during cold weather. Wax deposition in petroleum reservoirs, process equipment and pipelines can occur when the crude oil is cooled below its cloud point temperature. The phase-transition behavior of this n-alkane system is analogous to those of other polymer systems, such as polyethylene and copolymers. Consequently, n-alkanes are a natural starting point for understanding organic crystallography and related phase transition of a number of polymer blend and solution systems.

In the oil (petroleum) industry, the cloud point temperature and the pour point temperature are usually measured by the standard ASTM methods. Upon fluid cooling, the temperature at which the oil sample changes from clear to cloudy is called cloud point temperature, manifesting that the wax has started to precipitate in the oil. When a standardized cup of oil is cooled below the cloud point, the tilting of the cup will cause the oil to flow out until a certain temperature is reached at which the oil can no longer pour out. This temperature is called the pour point temperature, manifesting the wax has formed a network structure. Some researchers [Ronningsen *et al* 1991 and Letoffe *et al* 1995] also used DSC (an alternative ASTM method for the cloud point temperature measurement) to measure the pour point temperature.

Nevertheless, depending on the amount of wax in the oil, sometimes it is difficult to measure the cloud point and pour point temperature with DSC, and the ASTM cup test for measuring the pour point is unsatisfactory because it is empirical and operator-dependent. We measured the dynamic viscosity of the cooling crude oil to show how a fundamental rheological test can be used to find the temperatures of these weak phase transitions more accurately.

More than 20 oil samples, with different wax content, were provided by DBR Research (Edmonton) and used in this project; here we show some of the results. DSC results are shown in Figure C.1. Oil sample no.1 was cooled from 80 °C. The wax content in this sample was very low. The cloud point temperature, in this case, cannot be measured directly from the DSC curve (but is marked for reference). A very broad curvature can be vaguely seen, from 15 to 30 °C. The peak point could be identified as the cloud point (~23 °C). But by DSC alone, it is hard to identify any cloud point. The pour point temperature is, however, measured to be 13 °C, which is at the beginning of the large exothermic peak that reflects the wax agglomeration process. Once this process starts, the oil will develop a network structure of wax and transform from liquid-like to solid-like (for $T < T_p$).

In Figure C.2, for the same sample, a dynamic test was conducted to measure the complex viscosity. Both frequency (1 rad/s) strain amplitude (1%) were low enough to ensure the test is well within the linear range, meaning the structure in the oil will not be damaged by the rotating plates.

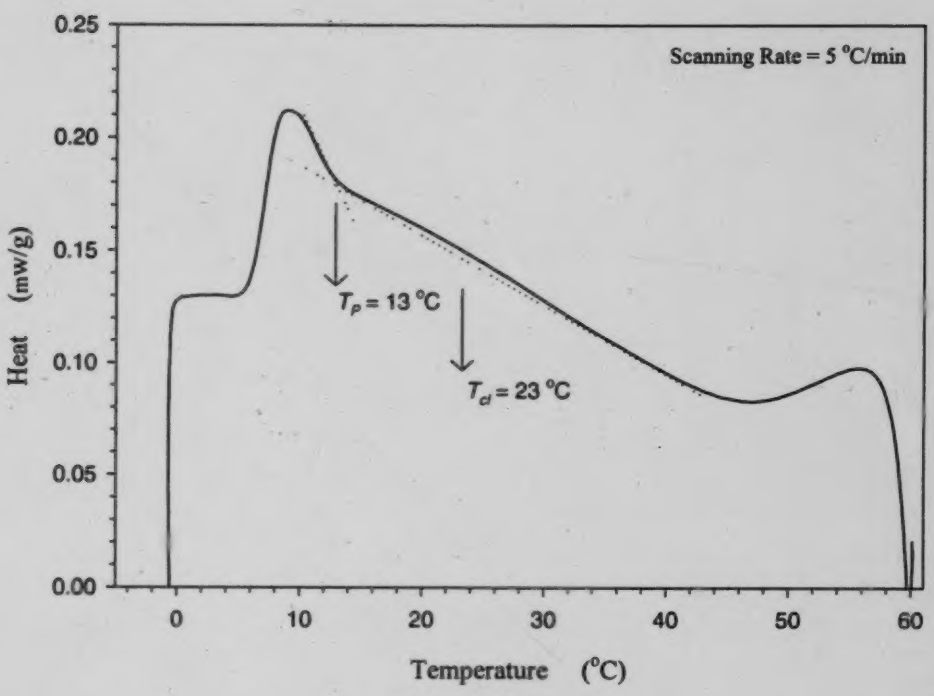

Figure C.1: DSC scan of oil sample No.1 (cooling curve). The pour point is 13 °C, and the cloud point could not be identified positively. The DSC scan rate is 5 °C/min.

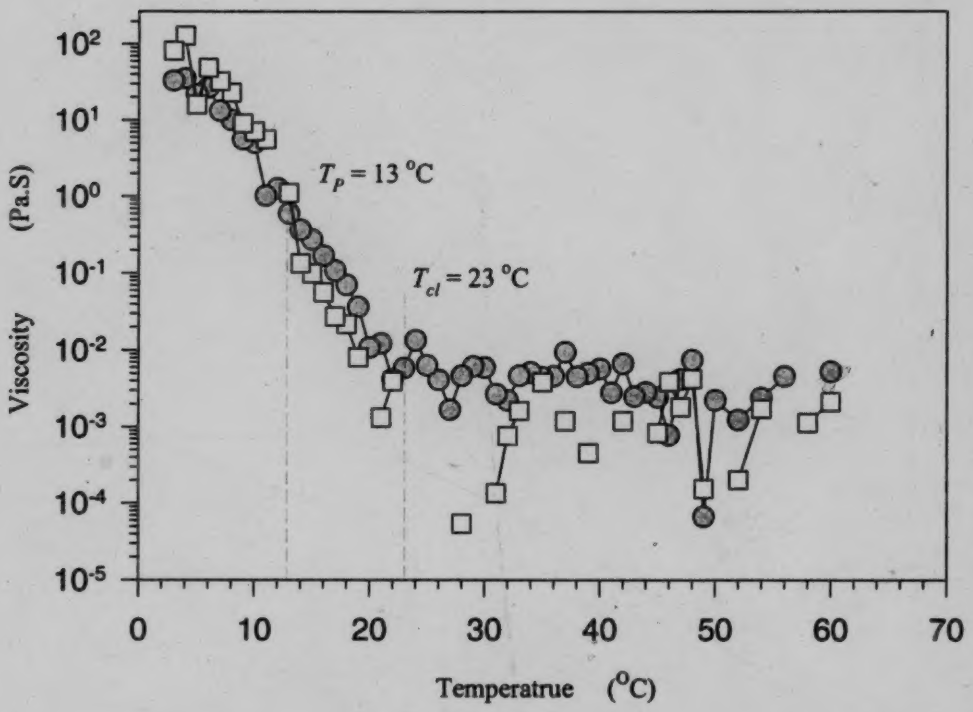

Figure C.2: Dynamic test of oil sample No.1 (cooling). The open square symbols are η'', and the filled circular symbols are η'. The test was done with ω = 1 rad/s, γ^{o} = 1%. The sample was cooled at about 5 °C/min.

According to Bird [1987], complex viscosity $\eta^*(\omega)$ is defined as:

$$\eta^* = \eta' - i\eta'' \qquad \text{(C-1)}$$

The real part η', the dynamic viscosity, may be thought of as the viscous contribution, associated with energy dissipation; the imaginary part η'', may be thought of as the elastic contribution, associated with energy storage. When $\eta' > \eta''$, means the material is liquid-like; when $\eta' < \eta''$, means the material is more solid-like. When η' and η'' are plotted *vs.* temperature on the same graph, the point where two curves cross each other seems to be a reasonable temperature to be identified as the temperature where phase transition occurs (such as T_p).

In Figure C.2, both η' and η'' curves are level at temperature above 23 °C, the viscosity measured is very low (almost same as the viscosity of water). Below 23 °C both curves start to curve up, the increasing of viscosity is a sign of the wax precipitation, thus we say the cloud point temperature is about 23 °C. By rheology, the cloud point is unarguably clear and measurable. The presence of dark color, as is common with petroleum, obscures the visual identification of cloudiness at T_c, but has no effect on rheology. At 13°C the two curves cross each other, showing the oil is transformed from a liquid-like state to a solid-like state, manifesting the wax in the oil starting to form a network structure, thus we say 13°C is the pour point temperature. The pour point identified in this way agrees well with the DSC result (Figure C.1).

Figure C.3 and Figure C.4 show similar results for oil sample No.2. This sample has a larger amount wax, which is shown on the DSC curve around 40 °C as a large

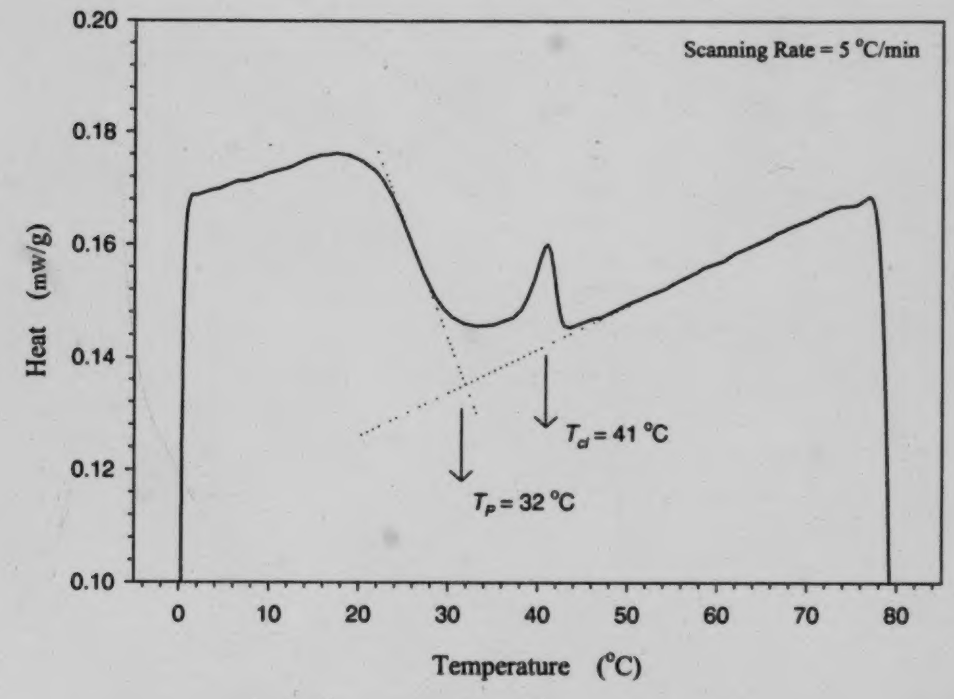

Figure C.3: DSC scan of oil sample No.2, with 5 °C/min cooling rate. The cloud point is 43 °C, and the pour point is 32 °C.

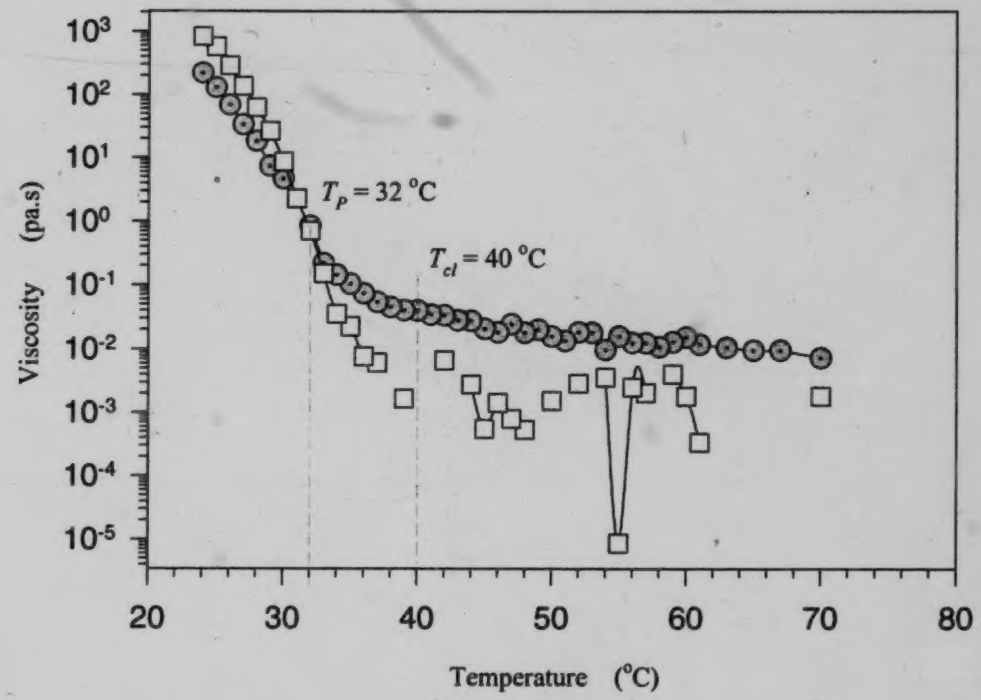

Figure C.4: Dynamic test of oil sample No.2, with $\omega = 1$ rad/s and $\gamma^0 = 1\%$. The filled circular symbols are η', and the open square symbols are η''. The sample was cooled at about 5 °C/min during the test.

exothermic peak when the wax precipitates from the oil. The cloud point is measured as the peak temperature (41 °C) when the majority of the wax precipitated. The pour point is, however, measured as the temperature at the beginning of the consolidation peak (32 °C), when the wax starts to develop network structure. In Figure C.4, the rheological measurements agree with the DSC results very well.

Rheology, thus, has been proven to be more accurate and useful in terms of measuring the weak phase transition, such as the pour point and the cloud point, when the heat associated to such a phase transition sometimes is too small for DSC to measure.

References

1. Abu-Zeid, M. E.; Youssef, Y. A; Abdul-Rasoul, F. A.; **Thermal Degradation of Butadiene-Styrene-Based Rubber** *Journal of Applied Polymer Science* **1986,** *31,* 1575.

2. Adams, J. L.; Quiram, D. J.; Graessley, W. W.; Register, R. A.; Marchand, G. R.; **Ordering Dynamics of Compositionally Asymmetric Styrene-Isoprene Block Copolymers** *Macromolecules* **1996,** *29,* 2929.

3. Aggarwal, S. L.; ed. **1970,** *Block Copolymers* New York: Plenum

4. Aggarwal, S. L.; *Polymer* **1976,** *17,* 938.

5. Allport, D. C. and Jones, W. H.; ed. **1973,** *Block Copolymers* New York: Wiley

6. Angelo, R. J.; Ikeda, R. M. and Wallach, M. L.; **Multiple Glass Transitions of Block Polymers** *Polymers* **1965,** *6,* 141.

7. Arnold, K. R. and Meier, D. J.; **A Rheological Characterization of SBS Block Copolymers** *J. Appl. Polym. Sci.* **1970,** *14,* 427.

8. Avrami, M.; *J. Chem. Phys.* **1939,** *7,* 1103. ; **1940,** *8,* 212. ; **1940,** *9,* 177.

9. Baer, M. *J. Polymer Sci.* **1964,** *A 2,* 417.

10. Bair, H. E.; *ASTM Spec. Tech. Publ.* **1994,** *STP 1249,* 60-81.

11. Balsara, N. P. and Hammouda, B. (a); *Phys. Rev. Lett.,* **1994,** *72,* 360.

12. Balsara, N. P.; Hammouda, B.; Kesani, P. K.; Jonnalagadda, S. V. and Straty, G. C. (b); *Macromolecules* **1994,** *27*, 2566.

13. Bates, F. S.; Cohen, R. E. and Berney, C. V.; *Macromolecules* **1982,** *15*, 584.

14. Bates, F. S.; Berney, C. V. and Cohen, R. E.; *Macromolecules* **1983,** *16*, 1101.

15. Bates, F. S.; **Block Copolymers near the Microphase Separation Transition 2: Linear Dynamics Mechanical Properties** *Macromolecules* **1984,** *17*, 2607.

16. Bates, F. S.; Bair, H. E. and Hartney, M. A.; *Macromolecules* **1984,** *17*, 1987.

17. Bates, F. S.; Rosedale, J. H.; Fredrickson, G. H. and Glinka, C. J.; **Fluctuation-Induced First-Order Transition of an Isotropic System to a Periodic State** *Phys. Rev. Lett.* **1988,** *61*, 2229.

18. Bates, F. S.; Rosedale, J. H.; Bair, H. E. and Russell, T. P. (a); *Macromolecules* **1989,** *22*, 2557.

19. Bates, F. S. and Wiltzius, P. (b); *J. Chem. Phys.* **1989,** *91*, 3258.

20. Bates, F. S. and Fredrickson, G. H. (a); **Block Copolymer Thermodynamics: Theory and Experiment** *Annual Review of Physical Chemistry* **1990,** *41*, 525.

21. Bates, F. S.; Rosedale, J. H. and Fredrickson, G. H. (b); *J. Chem. Phys.* **1990,** *92*, 6255.

22. Bianchi, V.; Pedemonte, E. and Torturro, A.; **Statistical Thermodynamics of Styrene-Butadiene Block Copolymers** *Journal of Polymer Science: Polymer Letters*, **1969,** *7*, 785-788.

23. Binder, K.; *Rep. Prog. Phys.* **1987,** *50,* 783; **Phase Transitions in Polymer Blends and Block Copolymer Melts: Some Recent Developments** *Advances in Polymer Science* **1994,** *112*, 181.

24. Bird, R. B.; Armstrong, R. C. and Hassager, O.; *Dynamics of Polymeric Liquids* vol. 1, 2nd Ed., John Wiley & Sons 1987,

25. Bishop, E. T. and Davidson, S.; **Network Characteristics of the thermoplastic Elastomers** *J. of Polym. Sci.: Part C,* **1969,** *26*, 59-79.

26. Bishop, E. T.; Holden, G. and Legge, N. R.; **Thermoplastic Elastomers** *J. of Polym. Sci.: Part C,* **1969,** *26*, 37-57.

27. Brazovskii, S. A.; *Soviet Phys. JETP* **1975,** *41*, 85.

28. Brunwin, D. M.; Fisher, E. and Henderson, J. F.; **Developments in Self-reinforced Elastomers** *J. of Polym. Sci.: Part C,* **1969,** *29*, 135-147.

29. Burke, J. J. and Weiss, V.; eds. **1973,** *Block and Graft Copolymers* New York: Syracuse Univ. Press

30. Canter, N. H.; *J. Polym. Sci., Part A-2,* **1968,** *6*, 155.

31. Choplin, A. A. L. and Prud'Homme, R. E.; **Rheology of Polystyrene/Poly(vinyl methyl ether) Blends near the Phase Transition** *Journal of Polymer Science: Part B: Polymer Physics* **1991,** *29*, 1573-1578.

32. Chung, C. I. and Gale, J. C. ; *Journal of Polymer Science , Polymer Physics edition* **1976,** *14*, 1149.

33. Chung, C. I. and Lin, M. I.; *J. Polym. Sci. Polym. Phys. Ed.* **1978,** *16*, 545.

34. Cohen, R. E. and Ramos, A. R.; *Macromolecules* **1979,** *12*, 131.

35. Cohen, R. E. and Wilfong, D. E.; *Macromolecules* **1982,** *15*, 370.

36. Collin, B.; Chatenay, D.; Coulon, G.; Ausserre, D.; Gallot, Y.; **Ordering of Copolymer Thin Films as Revealed by Atomic Force Microscopy** *Macromolecules* **1992,** *25*, 1621.

37. Cooper, S. L. and Tobolsky, A. V.; *Text. Res. J.* **Sept., 1966,** p.802

38. Couchman, P. R. and Karasz, F. E.; *Macromolecules* **1978,** *11*, 117.

39. Couchman, P. R.; *Macromolecules* **1980,** *13*, 1272.

40. de Gennes, P. G. (a); *Scaling Concepts in Polymer Physics* **1979,** Ithaca, Cornell Univ. Press.

41. de Gennes, P. G. (b); *Faraday Discuss. Chem. Soc.* **1979,** *68*, 96.

42. de Gennes, P. G. and Seances, C. R.; *Acad. Sci. Ser. B.* **1979,** *288*, 129.

43. de la Cruz, M. O.; *J. Chem. Phys.* **1989,** *90*, 1995.

44. Diamant, J.; Soong, D. S. and Williams, M. C.; **The Mechanical Properties of Styrene-Butadiene-Styrene (SBS) Triblock Copolymer Blends with Polystyrene (PS) and Styrene-Butadiene Copolymer (SBR)** *Polymer Engineering and Science* **1982,** *22*, 673-683

45. Diamant, J.; Soong, D. S. and Williams, M. C.; **Modeling the Viscoelastic Behavior of SBS Block Copolymer Solids** *Contemporary Topics in Polymer Science* **1984**, *4*, 599-627

46. Diamant, J. and Williams, M. C.; **Microstructural Influences on Volumetric Properties of Styrene-Butadiene-Styrene Block Copolymers** *Polymer Engineering and Science* **1986**, *26*, 525-533

47. Diamant, J.; Williams, M. C. and Soane, D. S.; **Microstructural Diagnosis of Block Copolymer Nonlinear Mechanical Properties I: Uniaxial Stress/Strain** *Polymer Engineering and Science* **1988**, *28*, 207-220

48. Diamant, J. and Williams, M. C. (a); **Microstructural Diagnosis of Block Copolymer Nonlinear Mechanical Properties II: Free Recovery from Large Tensile Deformations** *Polymer Engineering and Science* **1989**, *29*, 227-234

49. Diamant, J. and Williams, M. C. (b); **Microstructural Diagnosis of Block Copolymer Nonlinear Mechanical Properties. III: Cycling Tensile Tests** *Polymer Engineering and Science* **1989**, *29*, 235-243

50. *Encyclopedias of Polymer Science and Engineering*, 2nd Edition, **1989**

51. Estes, G. M.; Cooper, S. L. and Tobolsky, A. V.; *J. Macromol. Sci., Rev. Macromol. Chem.* **1970**, *4*, 313.

52. Ferry, J. D.; *Viscoelastic properties of Polymers.* Wiley, New York, **1980**, Chapt. 11.

53. Fesko, D. G. and Tschoegl, N. W.; **Time-Temperature Superposition in Thermorheologically Complex Materials** *Journal of Polymer Science: Part C*, **1971**, *35*, 51-69.

54. Flory, P. J.; *Journal of Physical Chemistry* **1942,** *10*, 51.

55. Floudas, G.; Pispas, S.; Hadjichristidis, N.; Pakula, T.; Erukhimovich, I.; **Microphase Separation in Star Block Copolymers of Styrene and Isoprene. Theory, Experiment, and Simulation** *Macromolecules* **1996,** *29*, 4142.

56. Fox, T. G.; *Bull. Am. Phys. Soc.* **1956,** *[2]1*, 123.

57. Fox, T. G.; Loshaek, S.; **Influence of Molecular Weight and Degree of Crosslinking on the Specific Volume and Glass Temperature of Polymers** *Journal of Polymer Science* **1955,** *15*, 371-390.

58. Fredrickson, G. H. and Helfand, E.; **Fluctuation Effects in the Theory of Microphase Separation in Block Copolymers** *J. Chem. Phys.* **1987,** *87*, 697.

59. Fredrickson, G. H. and Leibler, L.; *Macromolecules* **1989,** *22*, 1238

60. Fujimura, M.; Hashimoto, H.; Kurahashi, K. Hashimoto, T. and Kawai, H.; *Macromolecules* **1981,** *14*, 1196.

61. Futamura, Shingo and Meinecke, Eberhard A.; **Effect of Center Structure on the Physical and Rheological Properties ABA Block Copolymers. Part II: Rheological Properties** *Polymer Engineering and Science* **1977,** *12*, 563-569.

62. Goodman, I.; ed. **1982,** *Developments in Block Copolymers-1.* New York: Applied Sci.

63. Goodman, I.; ed. *Developments in Block Copolymers-2.* **1985,** New York: Applied Sci.

64. Gordon, G. V. and Shaw M. T.; *Computer Programs for Rheologists* **1994** Hanser,.

65. Gordon, M. and Taylor, J. S.; *Journal of Applied Chemistry* **1952,** *2*, 493.

66. Gouinlock, E. E. and Porter, R. S.; **Linear Dynamic Mechanical Properties of an SBS Block Copolymer** *Polymer Engineering and Science* **1977,** *17*, 535.

67. Gunton, J. D.; San Miguel, M. and Sahni, P. S.; *Phase Transitions and Critical Phenomena* ed. C. Domb and J. L. Lebowitz **1983,** *8*, 267. New York: Academic

68. Hadziioannou, G. and Skoulios, A. (a); *Macromolecules* **1982,** *15*, 258.

69. Hadziioannou, G.; Picot, C.; Skoulios, A.; Ionescu, M. –L.; Mathis, A. (b); *et al.* *Macromolecules* **1982,** *15*, 263.

70. Han, C. D.; Kim, J. and Kim, J. K.; **Rheological Technique for Determining the Order-Disorder Transition of Black Copolymers** *Journal of Polymer Science: Polymer Physics Ed.* **1987,** *25*, 1741.

71. Han, C. D.; Kim, J. and Kim, J. K.; **Determination of the Order-Disorder Transition Temperature of Block Copolymers** *Macromolecules* **1989,** *22*, 383.

72. Han, C. D.; Baek, D. M. and Kim, J. K.; **Effect of Microdomain Structure on the Order-Disorder Transition Temperature of Polystyrene-*block*-Polyisoprene-*block*-Polystyrene Copolymers** *Macromolecules* **1990,** *23*, 561-570.

73. Han, C. D. and Kim, J. K.; **On the use of Time-Temperature Superposition in Multicomponent/Multiphase Polymer Systems** *Polymer* **1993,** *34*, 2533-2539.

74. Han, J. H.; Feng, D.; Chin, C. F. and Han, C. D.; **Effects of Sample Preparation and Flow Geometry on the Rheological Behavior and Morphology of Microphase-Separated Block Copolymers: Comparison of Cone-and Plate and Capillary Data** *Polymer* **1995,** *36*, 155-167.

75. Hansen, Paula J. and Williams, Michael C.; **Yield Stress and Flow Measurements in ABA Block Copolymer Melts** *Polymer Engineering and Science* **1987**, *27*, 586-597

76. Hasegawa, H.; Tanaka, H.; Yamasaki, K. and Hashimoto, T.; *Macromolecules* **1987,** *20*, 1651.

77. Hasegawa, H.; Hashimoto, T.; **Self-Assembly and Morphology of Block Copolymer Systems** *Comprehensive Polymer Science : 2nd Supplement* **1996,** 497.

78. Hashimoto, T.; Nagatoshi, K.; Todo, A.; Hasegawa, H. and Kawai, H.; *Macromolecules* **1974,** *7*, 364.

79. Hashimoto, T.; Todo, A.; Itoi, H. and Kawai, H.; *Macromolecules* **1977,** *10*, 377.

80. Hashimoto, T.; Shibayama, M. and Kawai, H. (a); *Macromolecules* **1980,** *13*, 1237.

81. Hashimoto, T.; Fujimura, M. and Kawai, H. (b); *Macromolecules* **1980,** *13*, 1660.

82. Hashimoto, T.; Shibayama, M. and Kawai, H.; *Macromolecules* **1983,** *16*, 1093; 1427; 1434.

83. Hashimoto, T. Ijichi, Y. and Fetters, L. J.; *J. Chem. Phys.* **1988,** *89*, 2463.

84. Helfand, E and Wasserman, Z. R.; **Statistical Thermodynamics of Microdomain Structures in Block Copolymer Systems** *Polymer Engineering and Science* **1977,** *17*, 582-586.

85. Helfand, E. and Wasserman, Z. R. **Block Copolymer Theory** *Developments in Block Copolymers—1* **1982,** New York: Applied Sci., p.99

86. Henderson, C. P. and Williams, M. C.; **A Model for Triblock Copolymer Rheology** *Journal of Polymer Science: Polymer Letters Edition* **1979,** *17*, 257-261.

87. Henderson, C. P. and Williams, M. C. (a); **Influence of the Interphase on Block Copolymer Thermodynamics: Extension of the Leary Model** *Journal of Polymer Science: Polymer Physical Edition* **1985,** *23*, 1001-1029.

88. Henderson, C. P. and Williams, M. C. (b); **Asymmetric Composition Profiles in Block Copolymer Interphases: 1. Experimental Evidence** *Polymer* **1985,** *26*, 2021-2026.

89. Henderson, C. P. and Willians, M. C. (c); **Asymmetric Composition Profiles on Block Copolymer Interphases: 2. Thermodynamic model predictions and implications** *Polymer* **1985,** *26*, 2026-2038.

90. Holden, G.; Bishop, E. T. and Legge, N. R.; *Proc. Int. Rubber Conf., 5th*, **1967**

91. Holden, G.; Bishop, E. T. and Legge, N. R.; **Thermoplastic Elastomers** *J. Polym. Sci., Part C*, **1969**, *26*, 37.

92. Hong, K. M. and Noolandi, J.; *Macromolecules* **1983,** *16*, 1083.

93. Huggins, M. L.; *Journal of Physical Chemistry* **1941,** *9*, 440.

94. Hugenberger, G. S. and Williams, M. C.; **Complex Viscosity of Block Copolymer Solutions with Models of Microstructural Degradation** *Macromolecules* **1988,** *21*, 1773-1783

95. Ijichi, Y. Hashimoto, T. and Fetters, L. J.; *Macromolecules* **1989,** *22*, 2817.

96. Ikeda, R. M.; Wallach, M. L. and Angelo, R. J.; **Multiple Glass Transitions of Block Copolymers. II. Differential Scanning Calorimetry of Styrene-Diene Block Copolymers** in *Block Polymers (S.L. Aggarwal, ed.), Plenum, New York,* **1970, p43.**

97. Inoue, Takashi; Soen, Toshiichi; Hashimoto, Takeji and Kawai, Hiromichi; **Thermodynamic Interpretation of Domain Structure in Solvent-Cast Films of A-B Type Block Copolymers of Styrene and Isoprene** *Journal of Polymer Science: Part A-2,* **1969,** *37*, 1283-1302.

98. Iskandar, M. and Krause, S.; *Journal of Polymer Science: Polymer Physics Edition* **1981,** *19*, 1659.

99. Jackson, C. L.; Barnes, K. A.; Morrison, F. A.; Mays, J. W.; Nakatani, A. I. and Han, C. C.; **A Shear-induced Martensitic-like Transformation in a block Copolymer Melt** *Macromolecules* **1995,** *28*, 713-722.

100. Jian, T.; Anastasiadis, S. H.; Semenov, A. N.; Fytas, G.; Adachi, K.; Kotaka, T.; **Dynamics of Composition Fluctuations in Diblock Copolymer Solutions Far from and near to the Ordering Transition** *Macromolecules* **1994,** *27*, 4762.

101. Juliano, P. C.; *Ph.D. Thesis,* University of Akron, Akron, Ohio, **1968.**

102. Kaelble, D. H.; *Computer-Aided Design of Polymers and Composites* Marcel Dekker, New York, **1985,** pp. 145-147.

103. Kaelble, D. H.; Trans. Soc. Rheol. 1971, 15, 235.

104. Kaelble, D. H. and Cirlin, E. H.; *J. Polym. Sci., Polym. Symp.* **1973,** *43*, 131.

105. Koberstein, J. T. and Russell, T. P.; **Simultaneous SAXS-DSC Study of Multiple Endothermic Behavior in Polyether-Based Polyurethane Block Copolymers** *Macromolecules* **1986,** *19*, 714-720.

106. Kotaka, T. and White, J. L.; *Trans. Soc. Rheol.* **1973,** *17*, 587.

107. Krause, S.; **Microphase Separation in Block Copolymers: Zeroeth Approximation** *Journal of Polymer Science: Part A-2* **1969,** *7*, 249-252.

108. Krause, S.; Dunn, D. J.; Seyed-Mozzaffari, A. and Biswas, A. M.; **Microphase Separation in Diblock and Triblock Copolymers of Styrene and α-Methylstyrene** *Macromolecules* **1977,** *10*, 786.

109. Kraus, G.; Childers, C. W. and Gruver, J. T. (a); *J. Appl. Polym. Sci.* **1967,** *11*, 1581.

110. Kraus, G. and Gruver, J. T.(b); **Properties of Random and Block Copolymers of Butadiene and Styrene II: Melt Flow** *J. Appl. Polym. Sci.* **1967,** *11*, 2121.

111. Kraus, G.; Naylor, F. E. and Rollmann, K. W.; *J. Polym. Sci., Part A-2*, **1971,** *9*, 1839.

112. Kraus, G.; Rollmann, K. W. and Gardner, J. O.; *J. Polym. Sci., Polym. Phys. Ed.*, **1972,** *10*, 2061.

113. Leary, D. F. and Williams, M. C; **Statistical Thermodynamics of A-B-A Block Copolymers: I.** *Polymer Letters* **1970,** *8*, 335-340.

114. Leary, D. F. and Williams, M. C.; **Statistical Thermodynamics of A-B-A Block Copolymers: II.** *Journal of Polymer Science: Polymer Physics Edition* **1973,** *11*, 345-358.

115. Leary, D. F. and Williams, M. C.; **Statistical Thermodynamics of ABA Block Copolymers. III. Microstructural Transitions and Model Verification** *Journal of Polymer Science: Polymer Physics Edition* **1974,** *12*, 265-287.

116. LeGrand, D. G.; *Polymer Preprints of the American Chemical Society, Division of Polymer Chemistry* **1970,** *11*, 434.

117. Leibler, L.; **Theory of Microphase Separation in Block Copolymers** *Macromolecules* **1980,** *13*,1602.

118. Letoffe, J. M.; Claudy, P; Kok, M. V.; Garcin, M. and Volle, J. L.; *Fuel* **1995**, *74*, 810.

119. Leung, L. M. and Koberstein, J. T.; **DSC Annealing Study of Microphase Separation and Multiple Endothermic Behavior in Polyether-Based Polyurethane Block Copolymers** *Macromolecules* **1986,** *19*, 706-713.

120. Ma, S. K.; *Modern Theory of Critical Phenomena* **1976,** %Reading, Mass.: Benjamin-Cummings

121. MacKnight, W. J. and Karasz, F. E.; In *Comprehensive Polymer Science (S. L. Aggarwal, ed)* **1989,** *Vol. 7*, 111. Pergamon, Oxford.

122. Maecker, N. L.; Armentrout, D. N.; **Styrene Polymers: Degradation** *Encyclopedia of Polymer Science and Engineering, 2nd Edition* **1989,** *16*, 1.

123. Manthis, A.; Hadziioannou, G. and Skoulios, A.; **Unit Cell Deformation under elongational Stress of Oriented SIS Three-block Copolymers** *Polymer Engineering and Science* **1977,** *17*, 570-572.

124. Marker, L.; **Phase Equilibria and Transition Behavior of Block Copolymers--a Simple Model** *Polymer Preprints of the American Chemical Society, Division of Polymer Chemistry* **1969,** *10*, 524.

125. Mayes, A. M.; Olvera de la Cruz, M.; *J. Chem. Phys.* **1989,** *91*, 7228.

126. McGrath, J. E.; *Ph.D. Thesis, University of Akron, Akron, Ohio* **1967**.

127. McNeill, I. C.; Ackerman, L. and Gupta, S. N.; *Journal of Polymer Science, Polymer Chemistry Edition.* **1978,** *16*, 2169.

128. McNeill, I. C. and Stevenson, W. T. K.; **Thermal Degradation of Styrene-Butadiene Diblock Copolymer: Part 1-Characteristics of Polystyrene and Polybutadiene Degradation** *Polymer Degradation and Stability* **1985,** *10*, 247.

129. McNeill, I. C. and Stevenson, W. T. K.; **Thermal Degradation of Styrene-Butadiene Diblock Copolymer: Part 2-Characteristics and Mechanism of Degradation of the Copolymer** *Polymer Degradation and Stability* **1985,** *10*, 319-334.

130. Meier, D. J.; **Theory of Block Copolymers, I. Domain Formation in A-B Block Copolymers** *Journal of Polymer Science: Part C,* **1969,** *26*, 81-98.

131. Meier, D. J.; ed. *Block Copolymers: Science and Technology.* **1983**, New York: MMI Press / Harwood Academic Publ.

132. Meier, D. J.; **A Theory of the Domain and Interfacial Properties of Block Copolymers** In *Polymer Colloquy, Kyoto, Japan, September* **1997**

133. Merrett, F. M.; *Trans. Faraday Soc.* **1954,** *50*, 759.

134. Meyer, G. C. and Widmaier, J. M.; **Glass Transition Temperatures of ABA Poly(styrene-b-isoprene) Block Copolymers By Differential Scanning Calorimetry** *Journal of Polymer Science: Polymer Physics Edition* **1982,** *20*, 389-398.

135. Milner, S. T.; Witten, T. A. and Cates, M. E. (a); *Europhys. Lett.* **1988,** *5*, 413; *Macromolecules* **1988,** *21*, 2610.

136. Milner, S. T.; Witten, T. A. and Cates, M. E. (b); *Macromolecules* **1988,** *22*, 853.

137. Milner, S. T. and Witten, T. A. (c); *J. Phys. Paris* **1988,** *19,* 1951.

138. Minor, H. B.; Shaw, A. W. and Wilcoxen, C. H., Jr.; *US Patent 3,507,934 (Shell Oil Co.)* **1970.**

139. Miyamoto, T.; Kodama, K. and Shibayama, K.; **Structure and Properties of a Styrene-Butadiene-Styrene Block Copolymer** *Journal of Polymer Science: part A-2* **1970,** *8*, 2095-2103.

140. Mori, K.; Hasegawa, H. and Hashimoto, T.; *Polym. J.* **1985,** *17*, 799.

141. Morrison, F. A.; Winter, H. H.; Gronski, W. and Barnes, J. D.; **Effect of Unidirectional Shear on the Structure of Triblock Copolymers. 2. Polystyrene-Polyisoprene-Polystyrene** *Macromolecules* **1990,** *23*, 4200-4205.

142. Morrison, F. A.; Mays, J. W.; Nakatani, A.; Han, C. C.; **Flow-Induced Effects in a Microphase-separated Styrene-Butadiene-Styrene Triblock Copolymer** *Polymer Preprints* **1993,** *34*, 678.

143. Mutter, R.; Stuhn, B.; **Static and Kinetic Aspects of the Ordering Transition in Thin Films of Diblock Copolymers** *Macromolecules* **1995,** *28*, 5022.

144. Noshay, A. and McGrath, J. E.; *Block Copolymers-overview and critical survey* **1977**, Academic Press, NY, p187.

145. Owens, J. N.; Gancarz, I. S.; Koberstein, J. T. and Russell, T. P.; **Investigation of the Microphase Separation Transition in Low Molecular Weight Diblock Copolymers** *Macromolecules* **1989,** *22*, 3380.

146. Paul, D. R. and Barlow, J. W.; *MMI Press Symp. Ser.* **1982,** *2*,1.

147. Perahia, D.; Vacca, G.; Patel, S. S.; Dai, H. J.; Balsara, N. P.; **Annealing Effects and Signatures of the Order-Disorder Transition in Block Copolymer Cylinders** *Macromolecules* **1994,** *27*, 7645.

148. Pico, E. R. and Williams, M. C.; **Viscosity in the Phase Transition Region of Triblock Copolymer Systems** *Nature* **1976,** *259*, 388-389.

149. Pico, E. R. and Williams, M. C. (a);); **Thermodynamics of Plasticized Triblock Copolymers. I. Theory** *Journal of Polymer Science: Polymer Physics Edition* **1977,** *15*, 1585-1600.

150. Pico, E. R. and Williams, M. C. (b); **Thermodynamics of Plastic Triblock Copolymers. Part II: Model Verification by Light Transmittance and Rheology** *Polymer Engineering and Science* **1977,** *17*, 586-597

151. Pico, E. R. and Williams, M. C.; **Solvation and Phase Separation in ABA Block Copolymers** *Journal of Applied Polymer Science* **1978,** *22*, 445-457

152. Prest, W. M. and Porter, R. S.; **Rheological Properties of Poly(2,6-dimethylphenylene Oxide)-Polystyrene Blends** *Journal of Polymer Science: Part A-2*, **1972,** *10*, 1639-1655.

153. Ramos, A. R. And Cohen, R. E.; *Polym. Eng. Sci.* **1977,** *17*, 639.

154. Richards, R. W. and Thomas, J. L.; *Polymer* **1981,** *22*, 581.

155. RMS-800 Operating Instructions, *Rheometrics Inc.* 1986

156. Robeson, L. M.; Matzner M., Fetters, L. J. and McGrath J. E.; *Recent Advances in Polymer Blends, Grafts and Blocks,* ed. L. H. Sperling **1974,** p.281, New York: Plenum

157. Rodriguez, F.; **Principles of Polymer Systems** *3rd Edition*, **1989,** Hemisphere Publishing Co., P48.

158. Roe, R. J. Fishkis, M. and Chang, J. C.; *Macromolecules* **1981,** *14*, 1091.

159. Ronningsen, H. P.; Bjorndal, B.; Hansen, A. B. and Pedersen, W. B.; *Energy & Fuels* **1991,** *5*, 895.

160. Rosedale, J. H.; Bates, F. S.; **Rheology of Ordered and Disordered Symmetric Poly(ethylenepropylene)-Poly(ethylethylene) Diblock Copolymers** *Macromolecules* **1990,** *23*, 2329.

161. Rouse, P. E., Jr.; **A Theory of the Linear Viscoelastic Properties of Dilute Solution of Coiling Polymers** *Journal of Chemical Physics* **1953,** *21*, 1272-1280.

162. Russell, T. P.; Menelle, A.; Anastasiadis, S. H.; Satija, S. K.; Majkrzak, C. F.; **The Ordering of Thin Films of Symmetric Diblock Copolymers** *Progress in Colloid & Polymer Science* **1993,** *91*, 97.

163. Schlick, S. and Levy, M. *J. Phys. Chem.* **1960,** *64*, 883.

164. Schuler, M.; Stuhn, B.; **Dynamics of Structure Formation at the Microphase Separation Transition in Diblock Copolymers** *Macromolecules* **1993,** *26*, 112.

165. Semenov, A. N.; *Soviet Phys. JETP* **1985,** *61*, 733.

166. Semenov, A. N.; *Macromolecules* **1989,** *22*, 2849.

167. Shen, M.; Soong, D. and Hansen, D. R.; **Viscoelastic Properties of Homogeneous Block Copolymers** *Polymer Engineering and Science* **1977,** *17*, 560-562.

168. Shull, K. R.; Kramer, E. J.; Bates, F. S.; Rosedale, J. H.; **Self-Diffusion of Symmetric Diblock Copolymer melts near the Ordering Transition** *Macromolecules* **1991,** *24*, 1383.

169. Smith, T. L. and Dickie, R. A.; **Viscoelastic and Ultimate Tensile properties of Styrene-Butadiene-Styrene Block Copolymers** *J. Polym. Sci., Part C*; **1967,** *26*, 163.

170. Spaans, R. D.; Muhammad, M. and Williams, M. C.; **Probing the Interfacial Region of Microphase-Separated Block Copolymers by Differential Scanning Calorimetry** *Journal of Polymer Science: Physics Edition*, **1999.**

171. Spontak, R. J. and Williams, M. C. and Schooley, C. N.; **Morphology of Bulk SBS Block Copolymers Prepared by Wet Cryo-ultramicrotomy** *Journal of Materials Science* **1986,** *21*, 3173-3178.

172. Spontak, R. J.; Soong, D. S. and Williams, M. C.; **Modeling the Viscoelastic Behavior of SBS Block Copolymer Solids** *Contemporary Topics in Polymer Science* **1984,** *4*, 599-627

173. Spontak, R. J. and Williams, M. C. (a); **Microstructural Response of SiIm and SBS Block Copolymers to Heat Treatment** *Polymer Journal* **1988,** *20*, 649-471.

174. Spontak, R. J. and Williams, M. C. (b); **Three-dimensional Study of Cylindrical Morphology in a Styrene-Butadiene-Styrene Block Copolymer** *Polymer* **1988,** *29*, 387.

175. Spontak, R. J.; Williams, M. C. and Agard, D. A. (c); **Interphase Composition Profile in SB/SBS Block Copolymers, Measured with Electron Microscopy, and Microstructural Implications** *Macromolecules* **1988,** *21*, 1377.

176. Spontak, R. J. and Williams, M. C.; **Microstructural and Bulk Characterization of Two Poly(siloxane-imide) Multiblock Copolymers** *Journal of Applied Polymer Science* **1989,** *38*, 1607-1640

177. Spontak, R. J. and Williams, M. C.; **Thermodynamics of Tapered Styrene-Butadiene Block Copolymers** *Journal of Macromolecular Science-Physics B* **1989,** *28*, 1-24.

178. Spontak, R. J. and Williams, M. C.; **Prediction of Microstructures for Polydisperse Block Copolymers, using Continuous Thermodynamics** *Journal of Polymer Science: Polymer Physics* **1990,** *28*, 1379-1407.

179. Szwarc, M.; Levy, M. and Milkovich, R.; *J. Am. Chem. Soc.* **1956,** *78*, 2656.

180. TA Instruments DSC 2910 Operating Manual

181. Takenaka, M.; Kung, L.; Ying, Q.; Chu, B.; Peiffer, D.; **Synchrotron Small-Angle X-ray Scattering of Slow Spinodal Decomposition in a Block Copolymer** *Macromolecules* **1995,** *28*, 2700.

182. Tamura, S.; Murakami, K.; Kuwazoe, H.; .; **Isothermal Degradation of cis-1,4-Polyisoprene Vulcanizates** *Journal of Applied Polymer Science* **1983,** *28*, 3467.

183. Tanaka, H.; Hashimoto, T.; **Stability Limits for Macro- and Microphase Transitions and Compatibilizing Effects in Mixtures of A-B Block Polymers with Corresponding Homopolymers** *Polymer Communications* **1988,** *29*, 212.

184. Thomas, E. L.; Alward, D. B.;Kinning, D. J.; Handlin, D. L. and Fetters, L. J.; *Macromolecules* **1986,** *19*, 2197.

185. Tobolsky, A. V.; Andrews, R. D.; **Systems Manifesting Superposed Elastic and Viscous Behavior** *Journal of Chemical Physics* **1943,** *13*, 3-27.

186. Todo, A.; Uno, H.; Miyoshi, K. ; Hashimoto, T. and Kawai, H.; *Polym. Eng. Sci.* **1977,** *17*, 527.

187. Toledano, J. –C. and Toledano, P.; *The Landau Theory of Phase Transition* **1987,** Teaneck, NJ: World Scientific

188. Vogt, S.; Anastasiadis, S. H.; Fytas, G.; Fischer, E. W.; **Dynamics of Composition Fluctuations in Diblock Copolymer Melts above the Ordering Transition** *Macromolecules* **1994,** *27*, 4335.

189. Wang, Wei Yan and Williams, Michael C.; *American Institute of Chemical Engineers (AIChE) annual meeting*, Miami, USA, Nov. **1998**

190. Weissenberg, K.; **The Testing of Materials by Means of the Rheogoniometer** W. P. Griffith & Sons Ltd., London, 1966.

191. Widmaier, J. J. and Meyer, G. C.; *J. Polym. Sci. Polym. Phys. Ed.* **1980,** *18*, 2217.

192. Williams, M. L.; Landel, R. F.; Ferry, J. D.; **The Temperature Dependence of Relaxation Mechanisms in Amorphous Polymers and Other Glass-Forming Liquids** *Journal of America Chemical Society* **1955,** *77*, 3701-3707.

193. Winey, K. I.; Patel, S. S.; Larson, R. G. and Watanabe, H.; **Interdependence of Shear Deformations and Block Copolymer Morphology** *Macromolecules* **1993,** *26*, 2542-2549.

194. Winter, H. H.; Scott, D. B.; Gronski, W.; Okamoto, S. and Hashimoto, T.; **Ordering by Flow near the Disorder-Order Transition of a Triblock Copolymer Styrene-Isoprene-Styrene** *Macromolecules* **1993,** *26*, 7236.

195. Wong, G. C. L.; Commandeur, J.; Fischer, H.; de Jeu, W. H.; .; **Oriential Wetting in Hybrid Liquid Crystalline Block Copolymers** *Physical Review Letters* **1996,** *77*, 5221.

196. Xie, R.; Yang, B.; Jiang, B.; Zhang, Q.; Xu, Y.; **Rheology studies on the Phase Behavior of Two-Phase Polymer Systems** *Acta Polymerica Sinica* **1994,** *2*, 134.

197. Yamaoka, I. and Kimura, M.; **Effects of Morphology on Mechanical Properties of a SBS Triblock Copolymer** *Polymer* **1993,** *34*, 4399-4409.

198. Yano, S.; **Changes in the Dynamic Modulus during Thermal Degradation of Polyisoprene Vulcanizates** *Rubber Chemistry and Technology* **1980,** *53*, 944.